

SLENDER CONCRETE DEEP BEAMS :  
BEHAVIOUR, SERVICEABILITY AND STRENGTH

A thesis presented for the degree of  
Doctor of Philosophy  
in the University of Newcastle upon Tyne

by

MOHAMED CHEMROUK, Ingenieur d'Etat, M.Sc.

NEWCASTLE UNIVERSITY LIBRARY

-----  
088 22920 9  
-----

THESIS L3409

Department of Civil Engineering,  
University of Newcastle upon Tyne,  
England.

October, 1988.

## ACKNOWLEDGEMENTS

The work described in this thesis was carried out in the Civil Engineering Department of the University of Newcastle upon Tyne.

The author is sincerely grateful to Professor F. K. Kong, head of the structures division, for his expert guidance and supervision of this work. His valuable comments and advice throughout the study have been very helpful.

The author would also like to take this opportunity to express his appreciation and thankfulness to all those who, in some way or another, have helped in this research. In particular, special thanks and recognition are due to :

Professor M. B. Pescod, O.B.E., Head of Department, for extending the facilities of the Civil Engineering Department for the experimental work to be carried out.

The Algerian government for sponsoring the author to pursue this research.

The technical staff of the Department, in particular G. Stacey, J. Allen, E. Armstrong and K. Scholefield.

Finally, the author is most thankful and owes much to his wife Naima, herself a doctoral research student and at the same time a mother to our son Ouassim, for her constant encouragement and moral support throughout this study. It is to the two of them that this thesis is dedicated.

## ABSTRACT

Reinforced concrete deep beams have useful applications in construction. However, their design is not yet covered by the British Standard BS 8110: 1985 which explicitly states that "for the design of deep beams, reference should be made to specialist literature".

A selection of literature on deep beams is considered. First, the major works that have led to design recommendations are reviewed. Then, the current major codes and manuals covering deep beams, namely the CIRIA Guide, the European CEB-FIP model code, the American ACI(318-83) (revised 1986) code and the Canadian CAN3-A22.3-MB4 code are outlined; worked examples are given in order to illustrate their practical applications and compare their different approaches to deep beam design. The purpose of this literature review was to define the deep beam problem and identify the major questions still remaining unanswered together with the limitations of the present design documents on the subject.

The nature of diagonal cracking in slender deep beams has recently raised a question as to the application of the shear-strength equation in cl.3.4.2 of the CIRIA Deep Beam Guide. The effectiveness of web reinforcement on serviceability and strength of deep beams in general is also an area where strong disagreement exists. A testing programme, consisting of 15 beams of height/thickness ratios ranging from 20 to 50 and grouped in 3 different series, was performed to provide information on these two areas. The main variables were the height/thickness ratio and the quantity and arrangement of web steel. The beams were tested under concentrically applied two point-loads. Based on the test results and observations, modifications are given for the CIRIA equation and other formulae derived from stocky deep beam tests to be used in slender ones for analysis and design purposes. A new formula is also proposed for the prediction of the ultimate shear capacity.

The stability of deep beams is another area which has received less attention in the past by researchers and designers who often avoided the problem by opting for stocky sections. To quote from the CIRIA Guide "as a possible criterion of failure, buckling can not be disregarded". However, information on such topic is very scarce in the literature. Currently, the only documents that provide design guidelines for buckling are the CIRIA Guide and the Portland Cement Association Design Aid, both of which are based on theoretical studies and engineering judgement. An experimental testing programme, consisting of 7 large scale beam-panels

with height/thickness ratios in the range of 20 to 70 and a constant span/depth ratio of 1.0, provided buckling data against which the reliability of the two design documents was assessed. These tests confirmed that both documents offer a safe buckling design with the CIRIA Guide being too conservative.

Although deep beams are frequently continuous over several spans, very little published data exist for such beams. For this purpose, 12 two-span continuous concrete deep beams with span/depth ratios less than 1.0 and having different quantities and arrangements of web reinforcement were tested under two point-loads. The specimens were heavily instrumented to obtain as much information as possible about the behaviour of the beams at each stage of loading. Applied loads and reactions were among the measurements made and enabled the actual bending moment distribution to be determined and compared to that of corresponding continuous shallow beams. Based on the test results and observations and in the light of other published work, recommendations are given for the bearing, shear and flexural design of continuous deep beams.

## CONTENTS

1 INTRODUCTION AND OVERVIEW OF PREVIOUS RESEARCH ON DEEP BEAMS . . . . .	1
1.1 GENERAL . . . . .	1
1.2 RESEARCH OBJECTIVES . . . . .	3
1.3 THESIS OUTLINE . . . . .	4
1.4 OVERVIEW OF THE PREVIOUS WORK . . . . .	6
1.4.1 GENERAL BACKGROUND . . . . .	6
1.4.2 MAJOR DEEP BEAM LITERATURE . . . . .	8
2 DESIGN OF REINFORCED CONCRETE DEEP BEAMS - USE OF NATIONAL CODES AND MANUALS - . . . . .	24
2.1 INTRODUCTION . . . . .	24
2.2 KONG et al RECOMMENDATIONS . . . . .	25
2.3 CIRIA DEEP BEAM DESIGN . . . . .	30
2.4 CEP-FIP RECOMMENDATIONS FOR DEEP BEAMS . . . . .	38
2.5 CANADIAN CODE PROVISIONS FOR DEEP BEAMS . . . . .	42
2.6 AMERICAN CODE PROVISIONS FOR DEEP BEAMS . . . . .	47
2.7 DISCUSSION . . . . .	55
3 DIAGONAL CRACKING OF SLENDER CONCRETE DEEP BEAMS . . . . .	57
3.1 INTRODUCTION . . . . .	57
3.2 EXPERIMENTAL PROGRAMME . . . . .	58
3.2.1 DESCRIPTION OF THE TEST SPECIMENS . . . . .	58

3.2.2	BEAM NOTATION	61
3.2.3	MATERIALS	62
3.2.3.1	The concrete	62
3.2.3.2	The reinforcement	63
3.2.4	CASTING AND CURING	63
3.2.5	TESTING	63
3.3	DISCUSSION OF THE TEST RESULTS ON DIAGONAL CRACKING	65
3.3.1	CRACK DEVELOPMENT AND CRACKS PATTERNS	65
3.3.1.3	Flexural Cracks	65
3.3.1.4	Inclined Cracks	67
3.3.1.5	Diagonal Cracks	68
3.3.2	STRAIN MEASUREMENTS	70
3.3.3	FAILURE MODES	71
3.3.4	DIAGONAL CRACKING LOADS	72
3.4	APPLICATION OF THE CIRIA SHEAR EQUATION TO SLENDER DEEP BEAMS	76
3.5	MOHR CIRCLE ANALYSIS	79

#### 4 WEB REINFORCEMENT EFFECTIVENESS AND ULTIMATE STRENGTH OF SLENDER

	CONCRETE DEEP BEAMS	83
4.1	INTRODUCTION	83
4.2	PRESENTATION AND DISCUSSION OF THE TEST RESULTS ON WEB REINFORCEMENT EFFECTS	85
4.2.1	CRACKING OF THE BEAMS AND CRACK WIDTHS	85
4.2.2	IN-PLANE DEFLECTIONS	89
4.2.3	OUT-OF-PLANE DEFLECTIONS	90

4.2.4	ULTIMATE LOADS . . . . .	92
4.3	ULTIMATE LOAD BEHAVIOUR OF CONCRETE DEEP BEAMS . . . . .	95
4.4	ULTIMATE LOAD PREDICTION OF DEEP BEAMS . . . . .	100
4.4.1	EXISTING FORMULAE . . . . .	100
4.4.2	PROPOSED FORMULA . . . . .	102
5	INSTABILITY OF SLENDER DEEP BEAM-PANELS - COMPARISON OF TEST	
	RESULTS WITH EXISTING DESIGN AIDS . . . . .	107
5.1	INTRODUCTION . . . . .	107
5.2	THE BUCKLING PROBLEM . . . . .	108
5.2.1	COLUMN BUCKLING . . . . .	108
5.2.2	PLATE BUCKLING . . . . .	111
5.3	CURRENT DESIGN PRACTICE FOR THE BUCKLING OF SLENDER DEEP	
	BEAM-PANELS . . . . .	113
5.3.1	CIRIA GUIDE PROCEDURE . . . . .	113
5.3.2	PORTLAND CEMENT ASSOCIATION DESIGN AID . . . . .	117
5.4	TESTING PROGRAMME . . . . .	120
5.5	TEST RESULTS . . . . .	123
5.5.1	CRACKS PATTERNS AND FAILURE MODES . . . . .	123
5.5.2	ULTIMATE LOADS . . . . .	125
5.5.3	LATERAL DEFLECTIONS . . . . .	125
5.6	PREDICTION OF THE BUCKLING STRENGTH . . . . .	127
5.6.1	CIRIA GUIDE METHOD . . . . .	127
5.6.2	PORTLAND CEMENT ASSOCIATION METHOD . . . . .	129
5.7	CONCLUSION . . . . .	132

6 CONTINUOUS DEEP BEAMS - EXPERIMENTAL PROGRAMME-	134
6.1 INTRODUCTION	134
6.2 DETAILS OF THE TEST SPECIMENS	136
6.3 BEAM NOTATION	138
6.4 MATERIALS	138
6.4.1 CEMENT	138
6.4.2 AGGREGATES	139
6.4.3 STEEL	140
6.5 CONCRETE DETAILS	140
6.5.1 MIX DESIGN	140
6.5.2 CONCRETE STRENGTH	141
6.5.3 STRESS-STRAIN RELATIONSHIP	143
6.6 BEAM MANUFACTURE	144
6.6.1 FORMWORK	144
6.6.2 CASTING	145
6.6.3 CURING	146
6.7 TEST RIG	146
6.7.1 GENERAL ARRANGEMENT OF THE TEST RIG	146
6.7.2 LOADING SYSTEM	147
6.7.3 LOAD AND SUPPORT BEARINGS	148
6.8 INSTRUMENTATION	150
6.8.1 DISPLACEMENT MEASUREMENTS	150
6.8.2 STRAIN MEASUREMENTS	151
6.8.3 CRACK WIDTH MEASUREMENTS	153
6.8.4 REACTION MEASUREMENTS	154
6.8.5 DATA LOGGING EQUIPMENT	154

6.9	PREPARATION AND TESTING OF THE BEAMS . . . . .	155
7	CONTINUOUS DEEP BEAMS - BEHAVIOUR UNDER LOAD AND TEST RESULTS - .	158
7.1	INTRODUCTION . . . . .	158
7.2	FORMATION OF CRACKS AND CAUSES OF FAILURE . . . . .	158
7.3	CONTROL OF CRACKS . . . . .	176
7.4	MEASURED LOADS . . . . .	177
7.4.1	DIAGONAL CRACKING LOADS . . . . .	177
7.4.2	ULTIMATE LOADS . . . . .	178
7.5	SETTLEMENT AT SUPPORTS . . . . .	179
7.6	REACTIONS AT SUPPORTS AND BENDING MOMENTS . . . . .	180
7.6.1	REACTIONS AT SUPPORTS . . . . .	180
7.6.2	BENDING MOMENTS . . . . .	182
7.7	STRAINS AND STRESSES . . . . .	183
7.7.1	STRAINS . . . . .	183
7.7.2	STRESSES . . . . .	187
7.8	DEFLECTIONS . . . . .	190
7.8.1	OUT-OF-PLANE DEFLECTIONS . . . . .	190
7.8.2	IN-PLANE DEFLECTIONS . . . . .	191
8	CONTINUOUS DEEP BEAMS - INTERPRETATION OF TEST RESULTS AND DESIGN	
	RECOMMENDATIONS - . . . . .	192
8.1	INTRODUCTION . . . . .	192
8.2	SETTLEMENT EFFECT ON CONTINUOUS DEEP BEAMS . . . . .	193
8.3	REACTIONS AND BENDING MOMENT DISTRIBUTION . . . . .	194
8.4	FLEXURAL DESIGN AND DETAILING OF MAIN STEEL . . . . .	197

8.5	SHEAR CONSIDERATIONS . . . . .	201
8.6	BEARING CAPACITY . . . . .	205
9	GENERAL CONCLUSIONS AND SUGGESTIONS FOR FURTHER RESEARCH . . . .	208
9.1	GENERAL CONCLUSIONS . . . . .	208
9.1.1	SINGLE SPAN DEEP BEAMS . . . . .	208
9.1.2	CONTINUOUS DEEP BEAMS . . . . .	213
9.2	SUGGESTIONS FOR FURTHER RESEARCH . . . . .	215
	REFERENCES . . . . .	218
	APPENDIX A : PREDICTION OF BUCKLING STRENGTHS . . . . .	227
	TABLES . . . . .	241
	FIGURES AND PLATES . . . . .	254

## LIST OF TABLES, FIGURES AND PLATES

Tables, Figures and Plates are presented at the back of this thesis in the following order :

TABLES	Pg. No.
Table 3.1: Properties of simply supported deep beams tested . . . . .	241
Table 3.2: Failure modes, total ultimate loads, flexural cracking loads, inclined cracking loads, diagonal cracking loads, and 0.3mm crack width loads . . . . .	242
Table 3.3: Position of initiation of diagonal cracking . . . . .	243
Table 3.4: Length and inclination of diagonal cracks . . . . .	244
Table 3.5: Diagonal cracking loads of single span deep beams - measured and predicted - . . . . .	245
Table 3.6: Shear strength values of single span deep beams - measured and predicted - . . . . .	246
Table 4.1: Ultimate loads of single span deep beams - measured and predicted - . . . . .	247
Table 5.1: Buckling loads - measured and predicted - . . . . .	248
Table 6.1: Properties of continuous deep beams tested . . . . .	249
Table 6.2: Steel Properties . . . . .	249
Table 7.1: Failure modes, total ultimate loads, flexural cracking loads, diagonal cracking loads and the serviceability limit state of cracking loads - continuous deep beams - . . . . .	250
Table 7.2: Reactions at supports at or close to ultimate - measured ones compared to those calculated according to shallow beam theory - . . . . .	251
Table 7.3: Bending moments at or close to ultimate - measured and calculated - . . . . .	251
Table 8.1: Shear strengths at ultimate - continuous deep beams - . . . . .	252

Table 8.2: Shear strengths at ultimate - single span deep beams - . . . . .	252
Table 8.3: Bearing stresses at loading points - beams which failed by proper concrete crushing - . . . . .	253
Table 8.4: Bearing stresses at loading points - beams where concrete crushing was precipitated by diagonal cracking - . . . . .	253

**FIGURES**

Figure 1.1: Cracks patterns of an ordinary beam . . . . .	254
Figure 1.2: The tied-arch of De paiva and Siess [40] . . . . .	254
Figure 1.3: Shear capacity of web reinforcement, Crist [38] a) Forces along inclined crack plane b) Forces in web reinforcement along inclined crack plane . . . . .	254
Figure 1.4: Meaning of symbols in equation 1.15 . . . . .	255
Figure 1.5: The lower-bound truss model of Kumar [78] . . . . .	255
Figure 2.1: Design example - geometry and loading - . . . . .	256
Figure 2.2: Reinforcement detailing - Kong et al recommendations [70] design example - . . . . .	256
Figure 2.3: Dimensions of a deep beam - CIRIA Guide [85] - . . . . .	257
Figure 2.4: Reinforcement detailing - CIRIA Guide design example - . . . . .	257
Figure 2.5: Reinforcement detailing - CEB-FIP [33] design example - . . . . .	258
Figure 2.6: Deep beam truss model according to the Canadian code [23] . . . . .	258
Figure 2.7: Reinforcement detailing - Canadian code design example - . . . . .	259
Figure 2.8: Effectiveness factors for vertical and horizontal web reinforcement - ACI code [1] - . . . . .	259
Figure 2.9: Reinforcement detailing - ACI code design example - . . . . .	259

Figure 3.1: Details of test beams  
a) Dimensions of test beams - series CA, CC  
b) Loading scheme  
c) Dimensions of test beams - series F . . . . . 260

Figure 3.2: Reinforcement detailing - series CA, CC beams . . . . . 261

Figure 3.3: Arrangement of LVDT's and strain transducers  
- series CA, CC beams - . . . . . 262

Figure 3.4: Cracks patterns at failure  
- series CA, CC, F beams - . . . . . 263

Figure 3.5: Typical sequence of cracking in a deep beam . . . . . 265

Figure 3.6: Representation of a diagonal crack  
- dotted line for stocky deep beams,  
full line for slender deep beams - . . . . . 265

Figure 3.7: Comparison of measured diagonal cracking load  
with predicted one - author's tests on slender  
deep beams - . . . . . 266

Figure 3.8: Comparison of measured diagonal cracking load  
with predicted one - Robins [94] tests on  
stocky deep beams - . . . . . 266

Figure 3.9: Typical strains in the inclined load path . . . . . 267

Figure 3.10: Longitudinal strain distribution at mid-span  
sections - series CA beams:  $L/h = 1.4$  . . . . . 268

Figure 3.10: contd. Longitudinal strain distribution at mid-span  
sections - series CC beams:  $L/h = 1.4$  . . . . . 269

Figure 3.10: contd. Longitudinal strain distribution at mid-span  
sections - series CB beams (chapter 5):  $L/h = 1.0$  . . . . . 270

Figure 3.11: Relation between tensile splitting strength of  
concrete  $f_t$  and compressive strength  $f_{cu}$  . . . . . 271

Figure 3.12: Variation of safety factor  $f$  with  $h/b$  ratio . . . . . 271

Figure 3.13: Explanation of diagonal cracking nature in  
slender deep beams using Mohr circle  
a) Section 1 assumed not to deflect laterally under  
compressive axial loads  
b) Section 1' bound to deflect laterally under  
compressive axial loads  
c) Stress-state of small element in section 1  
d) Stress-state of corresponding element in  
section 1'

e) Mohr circle representation . . . . .	272
Figure 4.1: Load against maximum crack width . . . . .	273
Figure 4.1: contd. Load against maximum crack width . . . . .	274
Figure 4.2: Load against vertical deflection . . . . .	275
Figure 4.2: contd. Load against vertical deflection . . . . .	276
Figure 4.3: Lateral deflections - series CC beams . . . . .	277
Figure 4.3: contd. Lateral deflections - series CC beams . . . . .	278
Figure 4.4: Typical strain measurements at level of main tensile steel . . . . .	279
Figure 4.5: Compressive strain distribution at sections perpendicular to the load path . . . . .	281
Figure 4.5: contd. Compressive strain distributon at sections perpendicular to the load path . . . . .	282
Figure 4.6: Truss model of a deep beam proposed by Kotsovos [76] a) One point-load b) Two point-loads . . . . .	283
Figure 4.7: Typical flexural failure (CIRIA Guide [85]) . . . . .	283
Figure 4.8: Rotational motion of the end portion of the beam clearly visible at failure . . . . .	284
Figure 4.9: Ultimate loads - measured and predicted - series CA, CC, F beams . . . . .	285
Figure 4.10: Derivation of equation 4.11 . . . . .	285
Figure 5.1: Details of test beams - series CB a) Dimensions of test beams b) Loading scheme . . . . .	286
Figure 5.2: Reinforcement details - series CB beams . . . . .	286
Figure 5.3: Cracks patterns at failure - series CB beams . . . . .	287
Figure 5.3: contd. Cracks patterns at failure - series CB beams . . . . .	288
Figure 5.4: Buckling load against h/b ratio . . . . .	288
Figure 5.5: Buckling load against lateral deflection at mid-height - series CB beams . . . . .	288

Figure 5.6: Lateral deflection profiles - series CB beams . . . . .	289
Figure 5.6: contd. Lateral deflection profiles - series CB beams . . . . .	290
Figure 5.6: contd. lateral deflection profiles - series CB beams . . . . .	291
Figure 5.6: contd. lateral deflection profiles - series CB beams . . . . .	292
Figure 5.7: PCA design table A1 interpolated - Load capacity coefficient against $e/b$ - . . . . .	293
Figure 5.8: Buckling loads - measured against predicted - . . . . .	293
Figure 6.1: Details and loading scheme of continuous deep beams . . . . .	294
Figure 6.2: Reinforcement detailing for continuous beams . . . . .	294
Figure 6.2: contd. Reinforcement detailing for continuous beams . . . . .	295
Figure 6.2: contd. Reinforcement detailing for continuous beams . . . . .	296
Figure 6.3: Grading curve of aggregates . . . . .	297
Figure 6.4a: Speedy moisture tester . . . . .	297
Figure 6.4b: Reliability of the speedy moisture tester . . . . .	297
Figure 6.5: Development of tensile strength of concrete $f_t$ with age (high strength concrete) . . . . .	298
Figure 6.6: Relation between cube and cylinder compressive strengths of concrete (high strength concrete) . . . . .	298
Figure 6.7: Stress-strain curves for concrete . . . . .	299
Figure 6.8: Details of the small formwork . . . . .	299
Figure 6.9: A beam being demolded from the big formwork . . . . .	300
Figure 6.10: A beam being cured with the control specimens . . . . .	300
Figure 6.11: Comparison of two concrete curing methods . . . . .	301
Figure 6.12: Testing rig arrangement . . . . .	301
Figure 6.13: Schematic representation of the loading system . . . . .	302

Figure 6.14: Typical calibration graph of the jacks . . . . .	302
Figure 6.15: Bearing details	
a) at loading points	
b) at support points . . . . .	303
Figure 6.16: Locations of lateral displacement and strain measurements in continuous beams . . . . .	304
Figure 6.17: Interior support - reaction and settlement measurements -	
a) dial gauges monitoring settlement and load cell monitoring reaction	
b) calibration of load cell . . . . .	305
Figure 6.18: A demountable strain transducer	
a) Details and dimensions	
b) Fixed on concrete surface in 45-degree-rosette	
c) Calibration with extensometer	
d) Typical calibration graph . . . . .	306
Figure 7.1: Cracks patterns - continuous deep beams . . . . .	307
Figure 7.2: Load against maximum crack width	
a) series CD beams . . . . .	309
b) series CE beams . . . . .	310
Figure 7.3: Settlement at supports . . . . .	311
Figure 7.4: Load against settlement	
a) series CD beams . . . . .	312
b) series CE beams . . . . .	313
Figure 7.5: Reactions at supports - series CD beams . . . . .	314
Figure 7.5: contd. Reactions at supports - series CE beams . . . . .	315
Figure 7.6: Bending moment distribution - continuous deep beams . . . . .	316
Figure 7.6: contd. Bending moment distribution - continuous deep beams . . . . .	317
Figure 7.7: Typical compressive strain distribution at sections perpendicular to the load path . . . . .	318
Figure 7.7: contd. Typical compressive strain distribution at sections perpendicular to the load path . . . . .	319
Figure 7.8: Typical compressive strain distribution along the load path . . . . .	320

Figure 7.9: Load against maximum compressive strain within the load path . . . . .	321
Figure 7.9: contd. Load against maximum compressive strain within the load path . . . . .	322
Figure 7.10: Typical tensile strain distribution within the load path before diagonal cracking . . . . .	323
Figure 7.11: Strains along the longitudinal reinforcement at bottom and top - series CD beams . . . . .	324
Figure 7.11: contd. Strains along the longitudinal reinforcement at bottom and top - series CE beams . . . . .	325
Figure 7.12: Longitudinal strain distribution above interior support at 400 kN - series CD beams . . . . .	326
Figure 7.12: contd. Longitudinal strain distribution above interior support at 400 kN - series CE beams . . . . .	327
Figure 7.13: Longitudinal strain distribution at mid-span sections - series CD beams . . . . .	328
Figure 7.14: Typical vertical strain distribution above interior support . . . . .	329
Figure 7.15: Load against maximum compressive stress within the load path . . . . .	330
Figure 7.15: contd. Load against maximum compressive stress within the load path . . . . .	331
Figure 7.16: Load against vertical deflection - series CD beams . . . . .	329
Figure 8.1: Flow of forces in the moderately deep beams of Rogowsky et al [96] [97] ( $2 < L/h < 5$ ) . . . . .	332
Figure 8.2: Flow of forces in the author's beams ( $L/h < 1$ ) . . . . .	332
Figure A.1: Interaction diagram of beam CB-40-0.182 . . . . .	333

**PLATES**

Plate 3.1: Front view of a beam in the testing rig - loading arrangement - . . . . .	334
Plate 3.2: Side view of a beam in the testing rig - instrumentation on the back - . . . . .	335

Plate 3.3: Typical shear failure of a deep beam - splitting along a diagonal crack and spalling of concrete - . . .	336
Plate 5.1: Typical ductile buckling failure	
a) Front view	
b) Side view . . . . .	337
Plate 6.1: Continuous deep beams in the rig ready for testing	
a) series CD beam	
b) series CE beam . . . . .	338
Plate 6.2: The data logging system and the load control unit . . .	339
Plate 7.1: Typical cracks development with load . . . . .	340
Plate 7.2: Types of failure of the continuous deep beams tested	
a) Typical shear-bearing failure (bearing failure precipitated by diagonal cracking)	
b) Typical proper bearing failure . . . . .	341

## NOTATIONS

Unless otherwise defined, the meanings of the symbols used are as follows :

A	Area of reinforcement crossing the diagonal crack (fig.1.4)
A <sub>h</sub>	Area of horizontal web reinforcement
A <sub>v</sub>	Area of vertical web reinforcement
A <sub>s</sub>	Area of main longitudinal reinforcement
A <sub>w</sub>	Area of typical web reinforcement
A <sub>n</sub>	Area of reinforcement perpendicular to a diagonal crack
a	Shear-span (shear arm)
b	Thickness of a deep beam section. In Equ 5.5 and 5.6, b refers to the plate width. In Equ 5.3, b refers to the smaller dimension of the column section.
b <sub>1</sub>	Unit width of a beam-panel
C	Width of bearing. C also refers to the compression force of the horizontal concrete strut (fig.2.6)
C <sub>1</sub>	Empirical coefficient equal to 1.4 for normal weight concrete and 1.0 for lightweight concrete.
C <sub>2</sub>	Empirical coefficient equal to 130 N/mm <sup>2</sup> for plain round bars and 300 N/mm <sup>2</sup> for deformed bars.
d	Effective depth of a section, taken as the distance from the extreme compression fibre to the centroid of the longitudinal tension reinforcement
e	Load eccentricity
e <sub>2</sub>	Eccentricity at the top (at loading points)
e <sub>1</sub>	Eccentricity at the bottom (at reaction points)
e <sub>add</sub>	Additional lateral deflection due to slenderness effect
E	Modulus of elasticity
E <sub>t</sub>	Tangent modulus (section 5.3.1)
EI	Flexural stiffness
EI'	Flexural stiffness of the equivalent panel (chapter 5 and appendix A)
f	Safety factor (Equ 3.7)
f' <sub>c</sub>	Compressive strength of a concrete cylinder
f <sub>cr</sub>	Critical stress (Equ 5.5 and 5.6)
f <sub>cu</sub>	Compressive strength of a concrete cube (characteristic strength of concrete)
f <sub>2</sub>	Maximum stress in the concrete strut (section 2.5)
f <sub>max</sub>	Maximum allowable crushing strength of concrete (section 2.5)
f <sub>t</sub>	Tensile splitting strength of concrete
f <sub>y</sub>	Yield stress of the reinforcement

$h$	Depth of a deep beam section. In Equ 5.2 and 5.3, $h$ refers to the depth of a column section. In Equ 5.6, $h$ refers to a plate width
$h_a$	Active height of a deep beam section as defined in the CIRIA Guide (section 2.3, fig.2.3)
$h_e$	Effective height as defined in chapter 5 and Appendix A
$I$	Second moment of area
$K$	Buckling coefficient as in section 5.3.1 and in Appendix A. In section 5.3.2, $K$ is an effective depth factor.
$L$	Span length of a deep beam
$L_e$	Effective length (chapter 5 and Appendix A)
$L_o$	Clear-span length, measured between faces of supports
$M$	Bending moment at a section
$M_u$	Design bending moment
$M_r$	Moment of resistance
$M_i$	Initial moment as in clause 3.8.3.2 of BS 8110 (Appendix A)
$M_{add}$	Additional moment due to slenderness effect (section 5.3.1 and Appendix A)
$M_1, M_2$	Modification factors for the critical stresses due to interaction effects (section 5.3.1 and Appendix A)
$N$	Compressive axial load
$N_h$	Average equivalent horizontal stress (section 5.3.1 and appendix A)
$N_v$	Average equivalent vertical stress (section 5.3.1 and Appendix A)
$N_{hcr}$	Critical horizontal stress (section 5.3.1 and Appendix A)
$N_{vcr}$	Critical vertical stress (section 5.3.1 and Appendix A)
$p$	Percentage of steel
$p_s$	Percentage of main tensile steel (section 4.4.2)
$p_h$	Percentage of horizontal web steel (section 4.4.2)
$p_v$	Percentage of vertical web steel (section 4.4.2)
$R$	Reduction factor to allow for the early appearance of diagonal crack (Equ 3.4, 3.6, 4.3)
$R'_h$	Stress ratio = $N_h/N_{hcr}$ (section 5.3.1 and Appendix A)
$R'_v$	Stress ratio = $N_v/N_{vcr}$ (section 5.3.1 and Appendix A)
$R'_s$	Stress ratio = $\tau/\tau'_{cr}$
$s$	Spacing of web reinforcement
$s_v$	Spacing of vertical web reinforcement
$s_h$	Spacing of horizontal web reinforcement
$t$	Plate thickness (section 5.2.2)
$T$	Tension force (section 2.5, fig.2.6)

V	Shear force
V <sub>u</sub>	Design shear force
V <sub>n</sub>	Nominal shear force
V <sub>c</sub>	Shear force resisted by concrete
V <sub>s</sub>	Shear force resisted by steel
v	Shear stress
v <sub>u</sub>	Design shear stress
v <sub>c</sub>	Shear stress resisted by steel
x	Clear-shear-span, distance between the inside face of a support block and the outside face of a load block
x <sub>e</sub>	Effective shear-span (Equ 2.8)
x <sub>crit</sub>	Critical section
Y	Depth at which a web bar intersects a diagonal crack (Equ 1.15, fig.1.4)
α	Angle between the diagonal crack and the bar intersecting it
β	= a/h. β also refers to a coefficient which depends on the type of reinforcement (Equ 2.9)
β <sub>1</sub>	Stress block depth factor, (section 2.6)
γ <sub>f</sub>	Partial safety factor for loading
γ <sub>m</sub>	Partial safety factor for material
δ	Moment magnification factor taking account of the slenderness effect (Equ 5.4)
ε <sub>1</sub>	Principal tensile strain
ε <sub>2</sub>	Principal compressive strain
ε <sub>x</sub>	Longitudinal strain, tensile when positive. In section 7.7.2 ε <sub>x</sub> refers to the measured strain in x direction
ε <sub>y</sub>	Measured strain in y direction
ε <sub>cu</sub>	Ultimate concrete strain (= 0.0035 in BS 8110)
θ	Angle of inclination of the inclined strut (fig.2.6)
θ <sub>1</sub>	Angle of inclination of a diagonal crack : stocky deep beam (fig.3.6)
θ <sub>2</sub>	Angle of inclination of a diagonal crack : slender deep beam (fig.3.6)
θ <sub>3</sub>	Angle defined in fig.3.6
θ <sub>m</sub>	Measured angle of inclination of diagonal cracks (table 3.4)
σ <sub>c</sub>	Compressive stress (fig.3.13, section 3.5)
σ <sub>th</sub>	Tensile stress due to in-plane bending (fig.3.13, section 3.5)
σ <sub>pc</sub>	Principal compressive stress (fig.3.13, section 3.5)
σ <sub>pt</sub>	Principal tensile stress (fig.3.13, section 3.5)
σ <sub>x</sub>	Stress in x direction
σ <sub>y</sub>	Stress in y direction
φ	Load capacity coefficient (chapter 5 and Appendix A)

$\Phi$	Strength reduction factor, defined in cl.9.3.2 of ACI code
$\Phi_c$	Material resistance factor = 0.6 for concrete, given in the Canadian code
$\Phi_s$	Material resistance factor = 0.85 for steel, given in the Canadian code
$\eta$	Load capacity reduction coefficient, taking account of isolated footings (section 5.3.2 and Appendix A)
$\lambda$	Coefficient accounting for the type of concrete (Equ 2.13)
$\lambda_1 \lambda_2$	Coefficients defined in section 2.3, Equ 2.8
$\nu$	Poisson's ratio for concrete
$\tau$	Average equivalent shear stress (section 5.3.1 and Appendix A)
$\tau_{cr}$	Critical shear stress (section 5.3.1 and Appendix A)

## CHAPTER ONE

### INTRODUCTION AND OVERVIEW OF PREVIOUS RESEARCH ON DEEP BEAMS

#### 1.1 GENERAL

A beam having a depth greater than normal in relation to its span is called a deep beam. Although an exact definition of deep beams is yet to be agreed on universally [1] [33], it is widely accepted that deep beam action occurs at span/depth ratios less than about 2.5.

Deep beams are used in multi-storey buildings as transfer girders to provide column offsets or as panel-beams supporting the floors and spanning between end columns. They also have useful applications in other civil engineering works such as rectangular tanks and bins, foundation walls and recently [102] [103] in offshore gravity type concrete structures. The tilt-up construction is another area where deep panel-beams span between isolated footings such as pile caps and support the roof of an industrial building. The behaviour of deep beams is significantly different from that of beams of more normal proportions and require special consideration in analysis, design and reinforcement detailing. Such difference in behaviour is still not yet fully understood, and it is only comparatively recently that design recommendations were given in official documents.

In the U.K, the current practice is based on recommendations put forward in CIRIA Guide [85] and, to date, there is no British code of practice for deep beam design. Other international recommendations are given in the European CEB-FIP [33], the American code ACI(318-83) (revised 1986) [1] and the Canadian code CAN3-A22.3-M84 (1984) [23].

However, the complexity of the problem is so great that, as yet, no adequate analytical or practical solution has been developed and consequently the design methods proposed in these documents are semi-empirical and not comprehensive enough to cover the range of reinforced concrete deep beams in application in practice. Recently [61], there was some concern that the CIRIA Guide [85], considered as the most detailed document on the subject, may not always be safe for the shear design of slender deep beams. Buckling is a possible design criterion [53] [58] for deep beams and is covered only in the CIRIA Guide [85]. However, due to lack of experimental data, the CIRIA design procedure for buckling had to be based on theoretical studies and engineering judgement.

Although deep beams have been studied by a number of researchers over the last 20 years, continuous deep beams have not been extensively investigated. Existing knowledge in this area is very scarce and design procedures stem from elastic analysis or are extrapolated from test results on simple span beams.

## 1.2 RESEARCH OBJECTIVES

The purpose of this study is to present more information on areas not satisfactorily covered by existing design documents and give further clarifications where conflicting opinions have been given by previous researchers. In particular, it is specifically attempted to:

1. Investigate clearly the nature of diagonal cracking in slender deep beams and the consequence of using the CIRIA design method [85] for shear. Suggested modifications are given for such method to be used for shear design of slender deep beams.
2. Assess the effect of web reinforcement in deep beams in general. The parameters considered are the type of arrangement, the quantity of web steel and the shear-span/depth ratio
3. Calibrate existing design methods for buckling of slender concrete deep beams (namely the Portland Cement Association method [88] and the CIRIA method [85]) against test data, and assess their usefulness as design documents. This is achieved by comparing measured experimental buckling loads with those predicted by the two design methods. To calculate the CIRIA buckling loads, an analytical method is developed by the author, jointly with others, and is presented in internal technical reports [59] [60].
4. Investigate and present more information on the ultimate strength behaviour of continuous deep beams with particular attention devoted to the following :
  - a. Crack formation and development of crack width
  - b. Strain development

- c. Vertical and lateral deflections
  - d. Web reinforcement influence on the cracks, deflections and ultimate strengths
  - e. Mechanism of 'flow of forces' and distribution of reactions at supports
5. Develop design guidelines and hints for continuous deep beams.

### 1.3 THESIS OUTLINE

This work started with an overview of the major literature which has a direct bearing on the existing design documents for deep beams. This is presented in section 1.4 of this chapter. Its purpose is to trace the different parameters studied and the range of interest of each parameter, and critically examine the findings with a view of identifying eventual defects. This would also help in determining areas which require further investigation. In chapter 2, the existing deep beam design guidelines given in the four major documents, namely the CIRIA Guide [85], the CEB-FIP model code [33], the Canadian code [23] and the ACI(318-83) (revised 1986) code [1] are reviewed. Design examples are given to illustrate their practical applications and outline their different approaches to the problem.

In chapter 3, an experimental programme is designed to give more information on the nature of diagonal cracking in slender deep beams. Based on the test results, a suggested modification to the CIRIA shear

design procedure is proposed so that it can be safely used for slender deep beams. The test results of the experimental programme described in chapter 3 were also used to assess the effectiveness of web reinforcement in deep beams. This is presented in chapter 4 which also outlines the general behaviour of single span deep beams. In this chapter, the author proposes a formula for predicting the ultimate load of a deep beam failing in shear and compares it to existing ones.

Chapter 5 deals with the problem of buckling encountered in slender deep beams. An experimental programme is designed to give buckling data against which two existing design methods are assessed.

In chapter 6, the experimental programme for continuous deep beams is described. It includes details of the test beams, the concrete mix design, the fabrication and curing of the specimens, the loading system, the instrumentation and the test procedure. In chapter 7, the behaviour of the continuous deep beams under load is described and the test results are presented and discussed which include cracks patterns, modes of failure, crack widths, diagonal cracking loads, ultimate loads, settlement of supports, reactions and bending moment distribution, concrete strains and stresses, deflections. Chapter 8 includes a further discussion and interpretation of the test results on continuous deep beams. Recommendations for their design are presented.

Chapter 9 summarizes the principal findings of this study and gives some suggestions for further research work.

## 1.4 OVERVIEW OF THE PREVIOUS WORK

### 1.4.1 GENERAL BACKGROUND

A substantial amount of analytical and experimental work has been carried out on shear in reinforced concrete. Nevertheless, no generally accepted approach has been developed for the design of reinforced and prestressed concrete members subject to shear. This is reflected by the different codes and technical documents in existence over the world and their markedly different content, underlining the diversity of opinions on the structural behaviour of concrete. The degree of diversity in the interpretation of a particular structural action can be inversely related to the fundamental knowledge of the action. For example, a comparison of the design methods for the behaviour of reinforced concrete in bending shows minor differences in approach which reflects the designer's excellent knowledge of behaviour under such action as compared to that of shear. Thus, shear in general is a controversial topic in structural concrete [57] [4] [74] [75] [109] [50] [83] [24] and no single theory is capable of explaining all aspects of behaviour under such action.

The earliest theories led to the conclusion that the shear stress on a section of a beam was constant below the neutral axis at  $V/bz$  (  $b$  is the beam width and  $z$  the lever arm ) and varied parabolically to zero at the compression face above the neutral axis. To this day, this conclusion is still not fully justified, though, so far, its use has led to safe design. Nevertheless, it is widely agreed among researchers [4] [57]

[109] that the shear force is resisted by the combined action of the shear  $V_{cz}$  in the uncracked compression zone, the shear force  $V_d$  from the dowel action of the longitudinal reinforcement and the shear  $V_a$  due to aggregates interlock, that is :

$$V = V_{cz} + V_d + V_a \quad 1.1$$

The contribution of the different components is, however, not clearly quantified and difficult to predict. The absence of a generally accepted approach for shear design stems perhaps from the difficulty in unifying these three actions under a single rational theory.

It is recognized [4] [46] [57] [110] that the failure mode of a reinforced concrete beam is strongly dependent on the shear-span/depth ratio  $a/h$ . Many other parameters have been observed to be significant, of which the steel ratio and the concrete strength are most important.

- Typically, for  $6 > a/h > 2.5$  the failure crack pattern of a beam that failed in shear is shown in fig.1.1a. The failure crack develops from a normal flexural crack and extends rapidly to the load point. At the same time, a split develops along the main reinforcement towards the support.
- For  $a/h < 2.5$ , a typical shear failure of such beams is shown in fig.1.1b. A diagonal crack develops independently in the shear span and is straighter. It forms as a result of the splitting action of the compression force that is transmitted directly from the loading point to the support.

The two kinds of behaviour are described [4] [46] [51] as 'beam action' in the former case and 'arch action' in the latter case. In the beam action, the ultimate load is sensibly the same as the diagonal cracking load. An arch action, however, is an additional method for transmitting the load to the support, and the ultimate load is much higher than the diagonal cracking load.

Deep beams are usually associated with the arch action and, hence, have a considerable strength reserve beyond diagonal cracking. Such arch action, and thus the 'tied arch' that can form, depends on the method of load application.

#### 1.4.2 MAJOR DEEP BEAM LITERATURE

Much of the early work on deep beams was based on elastic analysis. Dishinger [42] was probably the first researcher to have started it and obtained stress distribution for continuous deep beams. His analysis illustrated clearly that, in an elastic deep beam, the distribution of bending stresses deviates completely from linearity. The Portland Cement Association used Dishinger's elastic solution to give design guidelines for reinforced concrete deep beams [89]. Since then, there has been several other elastic solutions for deep beams [9] [10] [26] [48] [112]. A thorough survey of literature on the early elastic work is reported in references [5] [28]. Generally, the methods used were Fourier - series solutions, the method of finite differences, and photoelastic techniques. Recently, with the spread of the computer use, the finite element

analysis became the pioneering elastic solution for deep beams [44] [85] [94].

All of these solutions, the finite element analysis included, assume an isotropic homogeneous material which obeys Hooke's law and, thus, are not valid after cracking has occurred in the beam. Nevertheless, they highlighted the differences between shallow beams and deep beams in that the usual hypothesis that plane sections before bending remain plane after bending does not hold for the latter. Consequently, the flexural stresses are not linearly distributed and there may be more than one neutral axis as found in the present tests (fig.3.10). The vertical and shear strains are large compared to the bending ones and therefore make a significant contribution to the total deformation than is the case for shallow beams. A state of high biaxial stresses over the supports and under concentrated loads exists in deep beams.

Design methods [26] [89] [112], based on working stresses and consistent with the then service load requirements as design criteria, were proposed.

The move from service load requirements to ultimate strength has meant that these methods can no longer be relied on for design and analysis. Instead, the research should be directed towards the ultimate load behaviour for which the elastic analysis could only predict the location and orientation of the cracks.

Leonhardt and Walther [80] were among the first to have initiated such turn in research by conducting ultimate load tests on reinforced concrete deep beams. Their work forms the basis of the current CEB-FIP international recommendations for the design of concrete deep beams [33]. It consisted of 13 beams tested to destruction; 9 of which were simply supported with span/depth ratio of 1, 2 were on continuous supports and 2 indirectly loaded.

Five of the single span beams were uniformly loaded on the top and 4 tested under uniform bottom loads. It was found that, while <sup>an</sup> elastic solution provides a good description of the deep beam behaviour before cracking, the stresses measured after cracking differed significantly from the theoretical elastic stresses. In particular, the actual tensile stresses in the reinforcement were much smaller than those values predicted from <sup>the</sup> elastic solution. Furthermore, strain measurements on concrete and steel indicated that all of the test beams developed a marked 'tied arch' action, that is a truss frame having inclined concrete as compression members and main steel as tension ones. They noted that stresses in the tension reinforcement decreased much less towards the end supports than the bending moments, implying that the steel acted as a tension tie with approximately constant force from one end of the beam to the other. On this basis, the authors recommended that the flexural reinforcement be carried through to the support without curtailment. Failure at the support regions at lower loads was observed in beams with bent-up bars which were not effective in resisting shear forces and would only weaken the tension chord. Leonhardt and Walther [80] suggested that

the main reinforcement should be distributed over a depth of  $0.2 h$  and be adequately anchored at the supports and that this could be best achieved by horizontal hooks. In their view, unfavorable action could result from vertical hooks and contributes towards crushing of concrete at supports. Beams having light main reinforcement (  $0.134\%$  ) failed in flexure. When the main steel ratio was increased to  $0.268\%$ , failure changed to either crushing at the support or failure of the inclined concrete strut. For beams loaded at the bottom, they suggested the use of hanger bars at least over a depth equal to the span so that the arching cracks resulting from the relatively high vertical stresses could be restrained.

In deep continuous beams, Leonhardt and Walther found that the bending moment distribution and reactions at supports differ completely from those of ordinary beams. Shear deformation reduces interior support moments ( and reactions ) and increases the mid-span moments ( and end reactions ).

The authors concluded that, in general, shear and shear reinforcement are not the main concern in deep beams since the principal compressive stresses are always critical near the bearing and thus dictate the upper limit of the carrying capacity for such beams.

De paiva and Siess [40] were another pair of researchers who have initiated the ultimate deep beam behaviour. They conducted a series of tests on deep beams in the transition range; the span/depth ratios,  $l/h$ , varied between 2 and 4. The beams were tested under static two

point-loads giving shear/span ratios,  $a/h$ , ranging from 0.67 to 1.33. The main reinforcement consisted of straight bars anchored at the supports. Web reinforcement, where used, consisted of either vertical or inclined stirrups. All the beams exhibited a tied arch behaviour after the diagonal cracks had developed (see fig.1.2). Such behaviour was confirmed from strain measurement along the tension reinforcement and along the top of the beam. The tied arch action was suggested earlier by Kani [50] to explain the behaviour of ordinary beams loaded close to the supports ( fig.1.1b ).

De paiva and Siess [40] found that the web reinforcement had no effect on the formation of inclined cracks and seemed to have little effect on the ultimate strength of the beams. The failure modes of the specimens depended mainly on the amount of main reinforcement and changed from flexure to flexure-shear as the percentage of tensile steel was increased from 0.83 % to 2.56 %. The concrete strength was found to have more influence on beams failing in shear. An empirical equation, taking into account the effects of  $f'_c$ ,  $p$ , and  $a/h$ , cylinder compressive strength, percentage of tensile steel and shear-span/depth ratio respectively, was proposed for the prediction of the ultimate shear strength. However, such equation had a limited application since almost half ( 9 out of 19 ) the specimens failed in flexure. This makes the sample of shear failure rather small and leads to question of confidence in using it. Also, the small size of the specimens tested ( span of 610 mm, depth from 178 mm to 330 mm) may have introduced scale effects. Indeed, Chana [25] showed that the shear strength tends to increase as the specimen size decreases.

To sum up, De paiva and Siess work had a great impact on deep beam research in that it served as a basis on which to build on for many researchers.

At the beginning of the seventies, an important contribution to ultimate load behaviour was made by Crist [38] who conducted a series of static tests on nine large scale deep beams with span/depth ratios ranging between 1.6 and 3.8. Web reinforcement, where present, consisted of an orthogonal pattern of steel and the beams were loaded with 7 point-loads to simulate a uniformly distributed load. The observed behaviour of the specimens was similar to that already described in De paiva and Siess tests [40], with the beams that had web reinforcement failing essentially in flexure and those without web reinforcement failing in shear.

Using the lower boundaries of the test data, Crist developed equations for the shear strength of deep beams which form the basis of the actual ACI code recommendations for deep beams [1]. For this reason, it is felt important to review the derivation of such formulae. It starts with the premise that the total shear capacity is made of a concrete contribution plus a web steel contribution; that is :

$$V_u = V_c + V_s \quad 1.2$$

The critical section is assumed to occur at the middle of the diagonal crack. For uniformly distributed load, such section, defined from the centre line of the support, is given as :

$$x_{crit} = 0.2 L \quad \text{with } L/d < 5$$

where L is the span length and d the effective depth.

The shear capacity of the concrete, that is the concrete contribution, is assumed to be :

$$V_C = \left( 3.5 - \frac{4}{3} \frac{M}{V d} \right) \left( 1.9 \sqrt{f'_c} + 2500 \frac{V}{M} \rho d \right) b d \quad 1.3$$

Where M is the bending moment at the critical section

V is the shear force at the critical section

$f'_c$  is the cylinder compressive strength of concrete

$\rho$  is the main steel ratio

The second term on the right hand-side member represents the inclined cracking load of an ordinary beam [1], while the first term reflects the reserve shear capacity of deep beams beyond diagonal cracking.  $V_C$  is subject to the following restrictions :

$$V_C < 6 \sqrt{f'_c} b d \quad 1.4$$

$$1 < \left( 3.5 - \frac{4}{3} \frac{M}{V d} \right) < 2.5$$

The shear capacity of the web reinforcement, that is the web steel contribution, was developed from shear friction along the inclined crack as illustrated in fig.1.3a

From shear friction analogy, fig.1.3a

$$S = F_N \tan \Phi \quad 1.5$$

Where  $F_N$  is the normal force on the inclined crack

$\tan \Phi$  is the apparent coefficient of friction

S is the shear force along the crack

According to Crist [38],  $F_n$  is produced by tension in the reinforcement which results from crack widening as slip occurs.

The vertical component of the shear along the crack is

$$V_s = S \sin\theta \quad 1.6$$

Assuming yielding of the web reinforcement at ultimate gives

$$F_v = A_v f_y \quad 1.7$$

From fig.1.3b, we have :

$$\Sigma(F'_n) = \Sigma(F_v) \sin(\alpha+\theta) \quad 1.8$$

and

$$F_n = \Sigma(F'_n) = \Sigma(F_v) \sin(\alpha+\theta) \quad 1.9$$

Therefore

$$V_s = \Sigma(F_v) \sin(\alpha+\theta) \tan\phi \sin\theta \quad 1.10$$

For uniformly spaced horizontal and vertical web bars, equation 1.10 becomes :

$$V_s = f_y d \tan\phi \left( \frac{A_v}{s_v} \cos^2\theta + \frac{A_h}{s_h} \sin^2\theta \right) \quad 1.11$$

where  $A_v$  is the area of vertical web reinforcement within a spacing  $s_v$

$A_h$  is the area of horizontal web reinforcement within a spacing  $s_h$ .

Crist [38] developed a lower bound crack inclination from his test data as :

$$\cos^2\theta = 1/12 ( 1 + L_o/d ) \quad 1.12$$

where  $L_0$  is the clear span.

Substituting this into equation 1.11 gives:

$$V_s = f_y d \tan \Phi \left( \frac{A_v}{s_v} \frac{1}{12} (1 + L_0/d) + \frac{A_h}{s_h} \frac{1}{12} (11 - L_0/d) \right) \quad 1.13$$

Crist [38] originally suggested a value of 1.5 for the coefficient of friction  $\tan \Phi$ . It will be shown in chapter 2 that the ACI code uses a coefficient of 1.0 to err on the side of safety. Finally, Crist imposes the following restriction on the total shear capacity of the beam,

$$V_u < 8 \sqrt{f'_c} b d \quad 1.14$$

In the shear friction analogy, any bar crossing the inclined crack should be considered, without making the difference as to whether the bar is meant for shear or for flexure. Crist, however, seems to make such difference in his model and ignores the effect of the main tensile steel acting as shear friction reinforcement. Also his model considers web reinforcement as equally effective at any location down the depth, so long as it intersects the inclined crack.

To date, the most extensive experimental work on the behaviour of reinforced concrete deep beams is that carried out under the direction of Kong [63] [64] [65] [66] [68] [69] [70]. It was initiated at the university of Nottingham, followed on at Cambridge university and is going on at Newcastle university [58] [61].

The early work was related to the strength and behaviour of stocky deep beams without web openings [63] [64] [65] [66] [68] [69] [70], and was extensively used in the production of the Constructional Industry Research and Information Association (CIRIA) Guide [85] published in 1977. Tests on 135 beams made of normal and lightweight concrete were performed. The span/depth ratios ranged between 1.0 and 3 and the clear-shear-span/depth ratios ranged between 0.23 and 0.7. The beams were tested under two point-loads applied at the top. Of eight arrangements of web reinforcement used, inclined bars were found to be the most effective in controlling crack widths and vertical deflections and in increasing the ultimate shear strength of both normal and lightweight concrete beams. The other types of web reinforcement depended on the geometry of the beams. For deeper beams, horizontal bars at close spacing near the soffit were the next most effective. When the span/depth ratio increased, the effectiveness of horizontal bars diminished and that of vertical bars increased to become more effective at  $L/h$  of 3.

From these tests, the authors were able to confirm that the clear-shear-span/depth ratio was a more important parameter than the span/depth ratio. With few exceptions, the cracks patterns and modes of failure of all the tested beams were similar despite the differences in web reinforcement and geometric and loading properties. A typical behaviour was this: on loading, the first cracks to form were flexural cracks in the central region of the beams. At higher loads, further cracks formed near the supports and propagated upward towards the loading

points. These cracks which formed at, or close to, the beam soffit were harmless unless the main reinforcement was light. When the load reached 70 to 90 % of ultimate, a new type of diagonal cracks suddenly appeared in the shear-span at a distance of about  $h/3$  from the soffit. These diagonal cracks were often accompanied by a rather loud noise. On further increase in load, a diagonal crack would split the beam approximately along the line joining the loading and support bearing blocks. Failure of the inclined strut by crushing of concrete between two diagonal cracks was reported in very few cases. Another type of failure involved the propagation of the diagonal crack into the compression zone at the loading or support bearing block, followed by concrete crushing. From the numerous tests, Kong et al [68] made the following observations:

1. The ultimate shear strength of a deep beam is made of a concrete contribution plus a steel contribution. It increases with a decrease in  $x/h$ , the clear-shear-span/depth ratio.
2. The diagonal crack which forms in the shear-span is akin to the splitting of a concrete cylinder. Where stiff load bearing blocks are used, the diagonal crack is approximately the line joining the inside face of the support to the outside face of the loading block. That is an angle of inclination of  $\cot^{-1}(x/h)$ .
3. The angle of intersection of a bar with the diagonal crack is important. The more nearly a bar is perpendicular to the diagonal crack, the more efficient it is in resisting shear.
4. After the diagonal crack has formed, the end portion of a beam tends to rotate about the nearest loading point. Thus, the ability of a

bar to restrain such rotation increases with the depth at which it intersects the diagonal crack.

5. The main longitudinal reinforcement helps to restrain the growth of the diagonal crack and, thus, has a major contribution to the shear capacity.

These useful test observations, together with the failure modes described previously, led the authors to come up with a semi-empirical equation for the ultimate shear strength of deep beams and was later adopted in section 3.4 of the CIRIA Guide [85]. However, the equation is valid for top loaded deep beams only and is as follows :

Shear strength = concrete contribution + steel contribution

$$V = C_1 \left(1 - 0.35 \frac{x}{h}\right) f_t bh + C_2 \frac{n}{\sum A} \frac{y}{h} \sin^2 \alpha \quad 1.15$$

where  $C_1$  is a coefficient equal to 1.4 for normal weight concrete and 1.0 for lightweight concrete.

$C_2$  is a coefficient equal to 130 N/mm<sup>2</sup> for plain round bars and 300 N/mm<sup>2</sup> for deformed bars.

$f_t$  is the cylinder splitting tensile strength of concrete; where  $f_t$  is not available, it may be estimated from the cube strength  $f_{cu}$  as  $f_t = 0.5 \sqrt{f_{cu}}$ .

$A$  is a typical web bar that crosses the diagonal crack. For the purpose of this equation, the main longitudinal bars are also considered as web bars (see fig.1.4).

$y$  is the depth at which the web bar intersects the critical diagonal crack (dotted line in fig.1.4)

$\alpha$  angle between the bar being considered and the diagonal crack,  $0 < \alpha < \pi/2$

$n$  is the total number of bars, including the longitudinal bars, that intersect the critical diagonal crack.

Tests on reinforced concrete deep beams with web openings have also been conducted by Kong and his associates Sharp, Kubick, Beaumont and Appleton [71] [72] [73]. Their work gives a clear visualization of the effect of openings on the ultimate strength of deep beams. They presented a simple structural idealization of the normally complex load transfer mechanism and modified equation 1.15 accordingly so that it can take account of a rectangular opening. More recently, research began at Cambridge university on the strength and stability of slender concrete deep beams [47] and is now being continued at Newcastle university [114] [108] where the first test results have just been made public [58] [61]. It became clear [53] [61] that existing design documents [85] could be unsafe for the shear design of slender deep beams.

Recently, Rogowsky, MacGregor, and Ong [96] have conducted tests at the university of Alberta on 7 single span deep beams and 17 two-span continuous deep beams, each span being 2000 mm in length. The shear-span/depth ratios ranged from 1 to 2.5. Various arrangements and amount of web reinforcement were used, including no web reinforcement, minimum and maximum horizontal web reinforcement and minimum and maximum vertical web reinforcement. The beams were loaded and supported through column stubs cast monolithically with the beams. Such loading and supporting system could be considered as the most realistic one reported in the literature. The loads were applied at the top centre of each span.

These 17 continuous beams together with the two beams tested by Leonhardt and Walther [80] represent the only test data available on continuous deep beams. In addition to the usual measurements made for single span beams, the authors monitored the support reactions; these were reported earlier by Leonhardt and Walther to differ completely from those of ordinary continuous beams. All the beams tested failed in shear by crushing of the concrete in the inclined compression struts. Horizontal web reinforcement was found to be ineffective. In contrast, vertical stirrups when used in sufficient number increased the strength of the beam and improved the ductility. The test specimens behaved essentially as 'trusses' or 'tied arches' after the formation of diagonal cracks. The authors concluded that the current design recommendations, based on tests on simply supported deep beams, are not realistic; they do not attempt to predict the strength of the tied arch which form after diagonal cracking. When compared with test results, the ACI code [1] was found unfit for the design of continuous deep beams. Design recommendations, based on plastic truss models of behaviour, were put forward by the authors for both simple and continuous deep beams [97]. These will be discussed in more details in chapters 7 and 8.

Solutions using plastic truss models have been presented elsewhere [78] [82] and form the basis of the current Canadian recommendations for the design of concrete deep beams [23]. However, as stated by Kong and Chalton [55], plastic concepts and the fundamental theorems have often been misunderstood by engineers and used wrongly. Indeed, the truss model (fig.1.5) used by Kumar [78] to obtain a theoretical lower bound on

the collapse load does not satisfy the equilibrium condition and consequently, as reported by Kong and Kubičk [79], his solution can not be a lower bound one.

Kubičk [77] presented a truss model which satisfied both the yield and equilibrium conditions. However, his model could not reflect all the possible failure modes which are likely to occur in deep beams. It does not recognize the diagonal splitting failure, most commonly encountered in deep beams, and deals only with flexure and bearing failures. In the truss model proposed by the Canadian code recommendations [23], the problem in a typical deep beam is one of excessive compressive stresses in the bearings and concrete struts [31] [32]. Yielding of the main steel can also be catered for. However, from the present author's experimental programme and from other investigators [64] [69] [93] [77], these failures occur only rarely and the main problem of deep beams is diagonal splitting for which a lower bound solution based on a truss model has proved to be unsafe [77].

In summary, the elastic analysis cannot predict the ultimate behaviour of reinforced concrete deep beams. Laboratory tests are valuable tools for such purpose. Numerous investigations have been carried out through ultimate load tests. Those which have found their way into design codes or technical documents or served as basis for others have been reviewed. The significant findings of the works reviewed are as follows :

1. deep beams sustain a considerable strength beyond diagonal cracking. Such strength is due to tied-arch action which develops after

inclined cracking.

2. The concrete quality is important for beams failing in shear.
3. The main reinforcement, as tension chord of the tied-arch, should not be weakened by cut-offs and should be well anchored at supports. It contributes considerably towards the shear capacity of a deep beam by restraining the diagonal cracks.
4. There is strong disagreement about the effectiveness of web reinforcement particularly horizontal one. Nevertheless, web reinforcement was found not to affect the diagonal cracking load.
5. The behaviour of a deep beam is strongly dependent on the shear-span/depth ratio. The span/depth ratio is of a lesser importance.
6. The reactions and moment distributions in continuous deep beams could be different from those in ordinary beams.

## CHAPTER TWO

### DESIGN OF REINFORCED CONCRETE DEEP BEAMS - USE OF NATIONAL CODES AND MANUALS -

#### 2.1 INTRODUCTION

The design of reinforced concrete deep beams is not covered by CP 110 : 1972 [36] nor by the new BS 8110 : 1985 [16], section 3.4.1.1 of which explicitly states that 'for the design of deep beams, reference should be made to specialist literature'. The new Eurocode [45] (still in the draft stage) for concrete structures does not include deep beams; it simply refers to the CEB-FIP : 1978 model code [33] which is one of the main design documents for such structural members. The other design documents are the American code ACI(318-83) (revised 1986) [1], the CIRIA Guide : 1977 [85] and the Canadian code CAN-A23.3-M84 : 1984 [23]. Another technical document based on elastic analysis but still in use is that published by the Portland Cement Association : Design of Deep Girders [89]. Based on an extensive on-going research work, Kong and associates [70] proposed some recommendations for the design of concrete deep beams.

Of these documents, the PCA report [89] does not deal with the behaviour of the beam at ultimate and will not be reviewed here. Interested readers can consult reference [70] which clearly shows that such method is rather conservative and out of date. The CIRIA design

guide could be considered as the most comprehensive and technically advanced document on the subject.

A review of the different approaches to deep beam problem adopted in the above mentioned design documents is given, illustrated with design applications. For the sake of comparison, the same design case is considered in all the methods.

## 2.2 KONG ET AL RECOMMENDATIONS

These design recommendations, which apply to beams loaded on top only, are based on <sup>an</sup> extensive on-going research programme [63] [64] [65] [66] [68] [70]. At first they were proposed for deep beams having clear-shear-span/depth ratios between 0.23 and 0.7. Recent tests [58] together with those carried out by the author and described in chapter 3 of this thesis showed that these recommendations could satisfactorily be extended to deep beams having clear-shear-span/depth ratios ranging from 0.0 to 0.7.

### a) Flexural design :

The design bending moment  $M_u$  should not exceed

$$M_u = z A_s f_y / \gamma_m \quad 2.1$$

where  $\gamma_m$  is the material safety factor for steel, usually taken as 1.15

$z$  is the lever arm, assumed to be  $0.6h$  for  $L/h > 1$

and  $0.6L$  for  $L/h < 1$

The lever arm expressions result in a conservative flexural design since a finite element analysis [95] revealed that  $z$  could exceed these values. However, the authors justified the use of the lever arm expressions by arguing that, according to the design method, the main reinforcement forms an integral part of the shear reinforcement as will be shown later in the design application. Therefore, an excess in flexural steel would help improving the shear strength.

b) Shear design

The design method is based on equation 1.15 which Kong et al [68] developed from their research work. Such equation is rewritten below :

$$Q_{ult} = C_1 \left(1 - 0.35 \frac{x}{h}\right) f_t bh + C_2 \Sigma A \frac{y}{h} \sin^2 \alpha \quad 2.2$$

where the notations are exactly those used in equation 1.15 and defined in fig.1.4.

Equation 2.2 predicts the collapse load. When used for design, a lower bound limit of 75 % (derived from tests by Kong et al [70]) should be adopted. In addition, the partial safety factors should be used. For design purpose, equation 2.2 becomes :

$$Q = 0.75 C_1 \left(1 - 0.35 \frac{x}{h}\right) \frac{f_t}{\gamma_m} bh + 0.75 \frac{C_2}{\gamma_m} \Sigma A \frac{y}{h} \sin^2 \alpha \quad 2.3$$

where  $\gamma_m = 1.5$  for concrete and 1.15 for steel. However, since  $f_t$  is proportional to  $\sqrt{f_{cu}}$ , it could be reasonable to take  $\gamma_m = \sqrt{1.5}$  for concrete.

When using this design method, the total steel contribution, that is the

contribution given by the second term on the right hand side of equation 2.3, should be at least 20 % of the design shear force and that the web steel proper should contribute at least 25 % of that total steel contribution.

#### Design Example Using Kong et al Recommendations

The idealized loading and geometry of a deep beam, carrying two columns on top, are as shown in fig.2.1, where  $Q/2$  is the column load plus an allowance for a distributed load including the self weight of the beam. The total applied load  $Q = 7600$  kN. Design the reinforcement and the beam thickness, given  $f_{cu} = 40$  N/mm<sup>2</sup>,  $f_y = 460$  N/mm<sup>2</sup>,  $f_t = 3.2$  N/mm<sup>2</sup>.

From fig.2.1: span/depth ratio  $L/h = 6300/3500 = 1.8 < 3$   
 clear-shear-span/depth  $x/h = (2000 - 500)/3500 = 0.43 < 0.7$   
 Both ratios are in the ranges required; hence, the design method applies.

- Flexural strength :

$$\text{Lever arm } z = 0.6h = 2100 \text{ mm}$$

$$\text{Design bending moment } M_u = \gamma_f \frac{Q}{2} \times 2000$$

where  $\gamma_f$  is the partial safety factor for dead and live loads.

$\gamma_f = 1.4$  will be adequate for this design.

$$\text{Ultimate moment of resistance } M_r = z A_s f_y / \gamma_m$$

Equating the two moments gives :

$$1.4 \times 3800 \times 10^3 \times 2000 = 2100 \times 3500 \times A_s \times 460/1.15$$

$$A_s = 12666.7 \text{ mm}^2.$$

Provide 16 No.32 mm diameter bars in 4 layers of 4 bars each (12867.9 mm<sup>2</sup>).

- Shear strength :

Consider equation 2.3; the shear resistance of the concrete is given by the first term of that equation, namely:

$$0.75 C_1 (1 - 0.35 \frac{x}{h}) \frac{f_t}{\gamma_m} bh$$

$$0.75 \times 1.4 (1 - 0.35 \times 0.43) \frac{3.2}{1.5} \times 3500 \times b = 6660.08 b$$

The beam thickness can be chosen so that the concrete resists more than 60 % of the design shear force  $V_U$

$$V_U = \gamma_f Q/2 = 1.4 \times 3800 = 5320 \text{ kN}$$

$$6660.08 b = 0.6 \times 5320 \times 10^3$$

$$b = 480 \text{ mm.}$$

Calculate the shear resistance of the beam with the main bars only :

$$Q_1 = 0.75 \times 1.4 (1 - 0.35 \times 0.43) \frac{3.2}{1.5} \times 480 \times 3500$$

$$+ 0.75 \times \frac{300}{1.15} \times 12867.9 \times \frac{Y}{3500} \times 0.84$$

An average value of  $Y = 3200 \text{ mm}$  is adequate for this design.

This will yield :

$$Q_1 = (3196.8 + 1927.1) \text{ kN} = 5123.9 \text{ kN}$$

This shows that the main reinforcement resists a high proportion of the shear force and thus is important for bending as well as shear according to Kong et al [70].

The shear force to be resisted by the web steel is given by:

$$5320 - 5123.9 = 196.1 \text{ kN}$$

The total steel contribution to the shear strength

$$5320 - 3196.8 = 2123.2 \text{ kN} > 0.2 V_U = 1064 \text{ kN}$$

The web steel should contribute at least 25 % of the total steel contribution, that is  $0.25 \times 2123.3 = 530.8 \text{ kN} > 196.1 \text{ kN}$ . Thus, the quantity of web steel is to be calculated on the basis of the minimum contribution value 530.8 kN as below

$$530.8 \times 10^3 = 195 \times \Sigma A_w \frac{Y}{3500} \sin^2 \alpha$$

Kong et al recommend the use of horizontal bars nearer to the bottom of the beam. Assuming an average value of  $Y = 0.65h$  for design purpose

$$530.8 \times 10^3 = 195 \times A_w \times \frac{0.65 \times 3500}{3500} \times 0.84$$

$$\text{total web steel } A_w = 4985.4 \text{ mm}^2$$

Provide 26 No.16 mm diameter bars ( $5227.6 \text{ mm}^2$ ) horizontally in both faces (13 in each face). Kong et al recommend [70] to use additional reinforcement such as U-bars near the supports where concrete is expected to be highly stressed.

The detailing is shown in fig.2.2.

### 2.3 CIRIA DEEP BEAM DESIGN

the CIRIA Guide [85] applies to beams having span/depth ratios of less than 2.0 for simple span beams and less than 2.5 for continuous span beams. It should be used in conjunction with the British code CP 110 : 1972 [36]. However, the author sees no reason for it not to be used in conjunction with the new BS 8110 : 1985 [16] which supersedes the former code. The Guide defines an effective span and height as follows (see fig.2.3) :

$$L = L_0 + (\text{lesser of } C_1/2 \text{ or } 0.1L_0) + (\text{lesser of } C_2/2 \text{ or } 0.1L_0)$$

$$h_a = h \text{ or } L \text{ whichever is the smaller}$$

the Guide limits the active height  $h_a$  to a depth equal to the span and considers the excess height above the span as not playing any part in carrying the load.

Effective support width  $C_1$  (or  $C_2$ ) = the smaller of actual length or  $0.2L_0$

#### (1)- SIMPLE RULES

Apply to uniformly loaded deep beams over two or more supports

##### a) Flexural strength

The Guide recommends that where  $L/h_a > 1.5$ , it is necessary to check that the applied moment does not exceed the capacity of the concrete section :

$$M_u < 0.12 f_{cu} b h_a^2 \quad 2.4$$

where  $f_{cu}$  is the concrete cube compressive strength

$b$  is the beam width

If  $L/h_a < 1.5$ , this checking is unnecessary.

The area of the main longitudinal steel is given by :

$$A_s > M_u / (0.87 f_y z) \quad 2.5$$

where the lever arm  $z$  is to be taken as  $(0.2L + 0.4h_a)$  for single span beams and  $(0.2L + 0.3h_a)$  for multiple span beams.

The reinforcement so provided should extend from one support to the other without reduction and should be distributed over a depth of  $0.2h_a$ . The bars should be anchored to develop 80 % of the maximum ultimate force beyond the face of the support. A proper anchorage contributes to the confinement of concrete at the supports and improves the bearing strength.

#### b) Shear strength

(i) Bottom-loaded beams : The shear force should satisfy the following condition

$$V < 0.75 b h_a v_u \quad 2.6$$

where  $v_u$  is the maximum value of shear stress, taken from table 6 of CP110 for normal weight concrete or table 26 for lightweight aggregates concrete.

If the above condition is not satisfied, the geometry or loading of the beam should be changed. Hanger bars should be provided in both faces to resist the bottom loads at a design stress of  $0.87f_y$ . Horizontal web reinforcement should be provided over the lower half of the beam depth  $h_a$  and over a length of span  $0.4h_a$  from the face of support. The area of this reinforcement should be at least 0.8 times the area of hanger steel per unit length.

(ii) Top-loaded beams : The shear force should not exceed the concrete capacity limits below

$$V < 2 (bh_a^2/x_e) v_c \quad \text{for } h_a/b < 4$$

$$V < 1.2 (bh_a^2/x_e) v_c \quad \text{for } h_a/b > 4 \quad 2.7$$

$$V < bh_a v_c$$

The effective clear-shear-span  $x_e$  is taken as  $L/4$  for uniformly distributed loading;  $v_c$  is the ultimate concrete shear stress taken from table 5 and 25 of CP 110 for normal weight concrete and lightweight aggregates concrete respectively.

If conditions 2.7 are not satisfied, the geometry or loading of the beam should be changed.

A nominal quantity of web reinforcement not less than that required for a wall under clauses 3.11 and 5.5 of CP 110, consisting of horizontal and vertical bars in each face, should be provided. The vertical bars should be anchored around the main longitudinal bars; the horizontal web bars should be anchored as links around the vertical bars at the ends of the beam.

#### c) Bearing strength

For deeper beams ( $l/h < 1.5$ ), the bearing capacity is the governing design criterion, particularly for those having shorter shear spans. Under the simple rules, the bearing stress should not exceed  $0.4 f_{cu}$ .

#### d) Crack control

The minimum percentage of reinforcement in a deep beam should comply with

the requirements of clause 3.11 and 5.5 of CP 110. The maximum bar spacing is limited to 250 mm. In a tension zone, the proportion of the total steel area related to the local concrete area in which it is embedded should not be less than  $(0.52\sqrt{f_{cu}})/0.87f_y$ . This implies that after cracking, the full tensile strength of concrete is carried by the reinforcement stressed at  $0.87f_y$ . The maximum crack width is limited to 0.3 mm in<sup>a</sup> normal environment and 0.1 mm in<sup>an</sup> aggressive environment. To control these limits, bar spacings given in tables 2 and 3 of the CIRIA Guide [85] should not be exceeded.

## (2)- SUPPLEMENTARY RULES

The supplementary rules are to be used in conjunction with the simple rules. They cover the design of deep beams in general, including those under concentrated loads, indirect loading and indirectly supported. For clarity, only the design of deep beams under top loading will be reviewed. For flexural design, the simple rules, reviewed previously, apply without modification.

### a) Shear strength

The ultimate shear capacity of a deep beam loaded at the top is given by :

$$V/bh_a < \lambda_1 \left(1 - 0.35 \frac{x_e}{h_a}\right) \sqrt{f_{cu}} + \lambda_2 \frac{n}{\Sigma} \frac{100 A_y \sin^2 \alpha}{bh_a^2}$$

2.8

Where  $\lambda_1 = 0.44$  for normal weight concrete and 0.32 for lightweight aggregates concrete

$\lambda_2 = 1.95 \text{ N/mm}^2$  for deformed bars and  $0.85 \text{ N/mm}^2$  for plain round ones

b is the beam width and  $h_a$  the active height.

A, Y,  $\alpha$  and n are similar symbols as those defined in equation 1.15 and fig.1.4.

The effective clear-shear-span  $x_e$  is taken as :

- The clear-shear-span x (see fig.1.4) for a load which contributes more than 50 % of the total shear force at support.
- L/4 for uniformly distributed load over the whole span
- The weighted average of clear-shear-spans where more than one load acts and none contributes more than 50 % of the shear force at the support. The weighted average is calculated as  $\Sigma(V_r x_r)/\Sigma V_r$ , where  $V_r$  is an individual shear force and  $x_r$  its clear-shear-span,  $V = \Sigma V_r$ .

For an orthogonal pattern of web reinforcement, the Guide presents equation 2.8 in a simplified form as below

$$V/bh_a = \lambda_1 v_x + \beta(v_{ms} + v_{wh} + v_{wv}) \quad 2.9$$

Where  $\lambda_1$  is as in equation 2.8,  $\beta = 1.0$  for deformed bars and 0.4 for plain round bars;  $v_x$  is the concrete shear stress parameter which depends on  $f_{cu}$  and  $x_e/h_a$  and is presented in a tabulated form;  $v_{ms}$  is the longitudinal steel shear stress parameter which depends on  $x_e/h_a$  and the main steel ratio and is presented in a tabulated form;  $v_{wh}$  ( $v_{wv}$ ) is the horizontal (vertical) web reinforcement shear stress parameter which depends on the horizontal (vertical) web steel ratio and  $x_e/h_a$  and is presented in a tabulated form in the CIRIA

Guide [85].

The ultimate shear capacity is subject to the following condition

$$V/bh_a < 1.3 \lambda_1 \sqrt{f_{cu}} \quad 2.10$$

where  $\lambda_1$  is as defined in equation 2.9

The Guide suggests that the total steel contribution to the shear strength of the beam should not be less than  $0.2V$ . Reinforcement which is not within the height  $h_a$  is to be ignored.

b) Bearing strength

The bearing stress limit of  $0.4f_{cu}$  under the simple rules may be increased to  $0.6f_{cu}$  and  $0.8f_{cu}$  at end supports and at internal supports for continuous beams respectively, provided that the concrete is adequately confined at the support zones. A proper anchorage of the main reinforcement helps to confine the concrete. The CIRIA Guide gives detailing requirements in clause 3.4.3 for additional<sup>o</sup> confining reinforcement. Under concentrated loads, the bearing stress may be limited to  $0.8f_{cu}$  provided that adequate confining reinforcement is present.

**Design Example Using the CIRIA Guide:**

Design the reinforcement and the beam thickness for the deep beam shown in fig.2.1.

- Geometry :

$$\text{span/depth ratio } L/h = 6300/3500 = 1.8 < 2$$

The CIRIA Guide rules are applicable

$$\text{Effective span } L = 6300 \text{ mm}$$

$$\text{Active height } h_a = 3500 \text{ mm}$$

$$\text{Effective support width } C = C_1 = C_2 = 500 \text{ mm} < 0.2 L_0 = 1160 \text{ mm}$$

- Loading :

$$\begin{aligned} \text{Design bending moment } M_u &= \gamma_f \times Q/2 \times 2000 \\ &= 1.4 \times 3800 \times 2000 \\ &= 1.064 \times 10^7 \text{ kN.mm} \end{aligned}$$

$$\text{Design shear force } V_u = \gamma_f \times Q/2 = 5320 \text{ kN}$$

Two concentrated loads act on the beam; hence, the supplementary rules apply.

- Flexural strength :

$$L/h_a = 1.8 > 1.5$$

equation 2.4 needs to be checked to ensure that the strength of the concrete in compression due to bending is adequate.

$$M_u < 0.12 f_{cu} b h_a^2 = 0.12 \times 40 \times b \times 3500^2$$

$$b > 1.064 \times 10^{10} / 5.88 \times 10^7 = 180.9 \text{ mm.}$$

Provided that the beam thickness is higher than 180.9 mm, the strength of the concrete in compression due to bending will be adequate.

$$\text{The lever arm } z = 0.2L + 0.4h_a = 2660 \text{ mm.}$$

From equation 2.5, the tensile reinforcement area is

$$A_s > 1.064 \times 10^{10} / (0.87 \times 460 \times 2660) = 9995.00 \text{ mm}^2$$

Provide 21 No.25 mm diameter deformed bars (10311 mm<sup>2</sup>). The

reinforcement is arranged in 7 layers of 3 bars each, extending from support to support without curtailment and distributed over a depth of  $0.2h_a = 700$  mm.

- Shear strength :

the beam supports two concentrated loads applied at the top;  
consider an orthogonal pattern of web reinforcement.

From equation 2.9

$$V/bh_a = \lambda_1 v_x + \beta(v_{ms} + v_{wh} + v_{wv})$$

where  $\lambda_1 = 0.44$ ,  $\beta = 1$  (considering deformed bars)

$$x_e/h_a = (2000 - 500) / 3500 = 0.43$$

A reasonable value of the beam thickness may be determined from the maximum shear capacity condition (equation 2.10) :

$$V_u/bh_a < 1.3 \lambda_1 \sqrt{f_{cu}}$$

$$b > 5320 \times 10^3 / (1.3 \times 0.44 \times 6.32 \times 3500) = 420.3 \text{ mm}$$

take  $b = 450$  mm

Main steel ratio  $p = 10311 / 450 \times 3500 = 0.65$  %

From the CIRIA Guide, table 4 :  $v_x = 5.37$  N/mm<sup>2</sup>

From the CIRIA Guide, table 6 :  $v_{ms} = 1.07$  N/mm<sup>2</sup>

Consider a nominal quantity of web reinforcement of 0.25 % each way, horizontally and vertically, consisting of 12 mm bars near each face at 200 mm spacing. From the CIRIA Guide, tables 7 and 8 :  $v_{wh} = 0.21$  N/mm<sup>2</sup>,  $v_{wv} = 0.015$  N/mm<sup>2</sup>

The total shear capacity is :

$$\begin{aligned} V &= (0.44 \times 5.37 + 1 \times 1.07 + 1 \times 0.21 + 1 \times 0.015) \times 450 \times 3500 \\ &= 5761.0 \text{ kN} > 5320 \text{ kN} \end{aligned}$$

The steel contribution is :

$$(1 \times 1.07 + 1 \times 0.21 + 1 \times 0.015) \times 450 \times 3500 = 2039.6 \text{ kN}$$

$$0.2 V_U = 0.2 \times 5320 = 1064 \text{ kN} < 2039.6 \text{ kN}$$

- Bearing capacity :

Assuming adequate confinement of the concrete at the support regions, the bearing capacity can be increased to  $0.6f_{cu}$ .

$$\text{Bearing stress } f_b = V_U/bC = 5320 \times 10^3 / (450 \times 500) = 23.6 \text{ N/mm}^2$$

$$0.6f_{cu} = 0.6 \times 40 = 24 \text{ N/mm}^2 > f_b = 23.6 \text{ N/mm}^2$$

The reinforcement detailing is shown in fig.2.4.

#### 2.4 CEB-FIP RECOMMENDATIONS FOR DEEP BEAMS

The draft Eurocode No.2 : 1984 'common unified rules for concrete structures' [45] (still in draft form) does not have any guidelines concerning the design of reinforced concrete deep beams. It refers to the CEB-FIP : 1978 model code [33] for the design of these structural elements.

According to the CEB-FIP recommendations, a deep beam should have a span/depth ratio  $L/h$  less than 2 for simply supported deep beams and less than 2.5 for continuous ones. For single span beams, the area of the main longitudinal reinforcement should be calculated as for normal beams using the largest bending moment in the span and a lever arm  $z$  taken as :

$$z = 0.2 (L + 2h) \quad \text{for } 1 < L/h < 2$$

$$z = 0.6L \quad \text{for } L/h < 1$$

These two expressions show that in deep beams the lever arm varies at a lower rate with the depth  $h$ . When the depth exceeds the span, the lever arm becomes independent of the beam depth. The main longitudinal reinforcement so calculated should extend without curtailment from one support to the other and be adequately anchored at the ends. Vertical hooks cause the development of cracks in the anchorage zone and, thus, should be avoided. The required steel should be distributed uniformly over a depth of  $(0.25h - 0.05L)$  from the soffit of the beam. The CEB-FIP code recommends the use of small diameter bars which are more efficient in limiting the width and development of cracks under service loads and facilitate the anchorage at the supports.

For continuous deep beams, the lever arm  $z$  is taken as :

$$z = 0.2 (L + 1.5h) \quad \text{for } 1 < L/h < 2.5$$

$$z = 0.5L \quad \text{for } L/h < 1$$

The main longitudinal steel in the span should be detailed as for simply supported beams. Over the support, half the steel should extend across the full length of the adjacent span; the remaining half is stopped at  $0.4L$  or  $0.4h$ , whichever is smaller, from the face of the support.

The design shear force should not exceed the lesser of

$$(0.10 bh f'_c) / \gamma_m \quad \text{and} \quad (0.10 bL f'_c) / \gamma_m \quad 2.11$$

where  $b$  is the width,  $h$  the beam depth,  $f'_c$  the characteristic cylinder strength of concrete and  $\gamma_m$  a partial safety factor

for material.

The web reinforcement is provided in the form of a light mesh of orthogonal reinforcement consisting of vertical stirrups and horizontal bars placed near each face and surrounding the extreme vertical bars. The web steel ratio should be in the range of 0.25 % in each direction near each face for smooth round bars and 0.20 % for high bond bars. Additional bars should be provided near the supports, particularly in the horizontal direction.

The aim of the web reinforcement is mainly to limit the crack widths which may be caused by the principal tensile stresses. In addition to the orthogonal mesh of reinforcement, for beams loaded at the bottom edge vertical stirrups are required to transmit the load into the upper portion of the beam.

#### Design Example Using the CEB-FIP Recommendations

Consider again the beam in fig.2.1; design the reinforcement and the beam thickness.

From fig.2.1,  $L/h = 1.8 < 2$

CEB-FIP recommendations apply.

- Flexural strength :

$$\text{Lever } z = 0.2 (6300 + 2 \times 3500) = 2660 \text{ mm}$$

$$\text{Design bending moment } M_u = \gamma_f \times Q/2 \times 2000$$

$$\text{Moment of resistance } M_r = f_y / \gamma_m \times A_s \times z$$

Equating the two bending moments gives :

$$A_s = \frac{1.4 \times 3800 \times 10^3 \times 2000 \times 1.15}{460 \times 2660}$$

The longitudinal steel area  $A_s = 10000 \text{ mm}^2$

Provide 21 No.25 mm diameter bars ( $10311 \text{ mm}^2$ ).

The reinforcement is detailed in 7 layers of 3 bars each, extending from support to support without curtailment and distributed over a depth of  $(0.25h - 0.05L) = 560 \text{ mm}$  from the soffit.

- Shear strength :

The design shear force  $V_u = \gamma_f \times Q/2 < 0.10 bh f'_c / \gamma_m$

with  $f'_c$  taken as  $0.8f_{cu} = 32 \text{ N/mm}^2$

$$1.4 \times 3800 < 0.1 \times b \times 3500 \times 32/1.5$$

$$b > 712.5 \text{ mm}$$

take  $b = 715 \text{ mm}$

Web reinforcement :

Consider a bar spacing of 200 mm, say, the required area for each bar :

$$A_w = 0.2 \% \times b \times s = (0.2 \times 715 \times 200)/100 = 286 \text{ mm}^2$$

Provide an orthogonal mesh of 20 mm diameter deformed bars at 200 mm centre to centre near each face ( $A_v = A_h = 314 \text{ mm}^2$ ).

Near the supports the spacing is reduced to 100 mm.

The detailing is shown in fig.2.5.

## 2.5 CANADIAN CODE PROVISIONS FOR DEEP BEAMS

The Canadian CAN3-A23.3-M84 : 1984 code [23] provisions for deep beams are based on a truss model consisting of compression struts and tension tie as in fig.2.6.

Unless special confining reinforcement is provided, the concrete compressive stresses in the nodal zones, defined as the regions where the struts and tie meet (fig.2.6), should not exceed :

- $0.85 \phi_c f'_c$  in nodal zones bounded by compressive struts and bearing areas.
- $0.75 \phi_c f'_c$  in nodal zones anchoring one tension tie.
- $0.60 \phi_c f'_c$  in nodal zones anchoring tension ties in more than one direction

where  $\phi_c$  is a material resistance factor = 0.6 for concrete,

$f'_c$  is the cylinder compressive strength of concrete.

The nodal zone stress limit conditions together with the equilibrium condition determine the geometry of the truss such as the depth of the nodal zones and the forces acting on the struts and tie. The main tension tie reinforcement is determined from the tensile tie force. These reinforcing bars should be effectively anchored to transfer the required tension to the lower nodal zones of the truss to ensure equilibrium. The code, then, requires the checking of the compressive struts against possible crushing of concrete as below :

$$f_2 < f_{2\max}$$

2.12

where  $f_2$  is the maximum stress in the concrete strut  
 $f_{2max}$  is the diagonal crushing strength of the concrete, given by :

$$f_{2max} = \lambda \phi_c f'_c / (0.8 + 170 \epsilon_1) \quad 2.13$$

where  $\lambda$  is a modification factor to take account of the type  
of concrete,  $\lambda = 1.0$  for normal weight concrete

$\epsilon_1$  is the principal tensile strain, crossing the strut

Equation 2.13 takes account of the fact that the existence of a large  
principal tensile strain reduces considerably the ability of concrete to  
resist compressive stresses.

For design purpose,  $\epsilon_1$  may be computed from :

$$\epsilon_1 = \epsilon_x + (\epsilon_x + 0.002) / \tan^2 \theta \quad 2.14$$

where  $\epsilon_x$  is the longitudinal strain

$\theta$  is the angle of inclination of the diagonal compressive  
stresses to the longitudinal axis of the member (fig.2.6).

The code requires the use of a minimum area of  $0.002 b_s v$  for  
vertical web reinforcement in the form of stirrups, with a spacing not  
exceeding  $d/5$  nor 300 mm, and  $0.002 b_s h$  for horizontal web bars near  
each face with a spacing not exceeding  $d/3$  nor 300 mm. The function of  
this web reinforcement is mainly to control diagonal cracking and ensure  
ductility of the beam.

Design Example Using the Canadian code :

Design the deep beam in fig.2.1 to carry the two concentrated loads.

- Geometry :

The upper nodal zones are bounded by compressive struts and bearing areas; the permissible nodal zone stress is :

$$0.85 \phi_c f'_c = 0.85 \times 0.6 \times 4640 = 2366.4 \text{ psi} = 16.32 \text{ N/mm}^2$$

The bearing stress at the upper nodal zone is :

$$1.25 \times 3800 \times 10^3 / (500 \times b) < 16.32 \text{ N/mm}^2$$

$$b > 1.25 \times 3800 \times 10^3 / (500 \times 16.32)$$

$$b > 582 \text{ mm}$$

where '1.25' represents the dead load factor in the Canadian code [23].

The upper nodal zone depth "a" is such that :

$$C/ba < 0.85 \phi_c f'_c$$

$$a > C / (0.85 b \phi_c f'_c) \quad 2.15$$

where C is the compressive force in the horizontal strut.

The lower nodal zones anchor a tension tie; hence, the maximum nodal stress allowed for is :

$$0.75 \phi_c f'_c = 0.75 \times 0.6 \times 4640 = 2088 \text{ psi} = 14.4 \text{ N/mm}^2$$

The bearing stress at the lower nodal zone is :

$$1.25 \times 3800 \times 10^3 / (500 \times b) < 14.4 \text{ N/mm}^2$$

$$b > 659.7 \text{ mm}$$

take  $b = 660$  mm

The lower nodal zone depth "a'" is such that :

$$T/(bxa') < 0.75 \phi_c f'_c$$

$$a' > T / (0.75 b \phi_c f'_c) \quad 2.16$$

For the equilibrium of the truss to be achieved, C and T should be equal. Dividing equation 2.15 by equation 2.16 and rearranging gives :

$$a' = (0.85/0.75) a \quad 2.17$$

From the equilibrium of the truss, fig.2.6, taking moment about the reaction point :

$$C (h - a/2) - T a'/2 = 1.25 \times 3800 \times 2000 \quad 2.18$$

Substituting equations 2.15, 2.16 and 2.17 into equation 2.18 and rearranging gives :

$$a^2 - 3286.3 a + 828.2 \times 10^3 = 0$$

hence,  $a = 275$  mm

$$a' = 311 \text{ mm}$$

- Flexural strength :

$$T = C = 0.85 \phi_c f'_c ab = 0.85 \times 0.6 \times 32 \times 275 \times 660 = 2962 \text{ kN}$$

$$\begin{aligned} A_s &= T / (\phi_s f_y) = 2962 \times 10^3 / 0.85 \times 460 \\ &= 7575.4 \text{ mm}^2 \end{aligned}$$

where  $\phi_s$  is the material reduction factor for steel, taken as 0.85 in the Canadian code [23].

Provide 16 No.25 mm diameter bars, distributed in 4 layers of 4 bars each ( $7858.9 \text{ mm}^2$ ). Horizontal hooks are to be used to provide the necessary anchorage length for the tensile steel.

- Check for crushing of concrete at the compression struts :

(i) The compressive stress in the horizontal strut :

$$f_2 = C/ab = 2962 \times 10^3 / (275 \times 660) = 16.32 \text{ N/mm}^2$$

since the transverse tensile strain  $\epsilon_1 = 0$  (no steel crossing the strut) the maximum compressive stress allowed is :

$$f_{2\max} = \phi_c f'_c = 0.6 \times 32 = 19.2 \text{ N/mm}^2 > 16.32 \text{ N/mm}^2$$

(ii) The compressive stress in the inclined strut :

The compressive force is (fig.2.6) :  $1.25 \times 3800 / \sin 58 = 5601 \text{ kN}$

\* The compressive stress at the top is :

$$f_2 = 5601 \times 10^3 / (660 \times 570.6) = 14.9 \text{ N/mm}^2$$

Since no tension tie crosses this region,  $f_{2\max} = 19.2 \text{ N/mm}^2$

\* The compressive stress at the bottom of this strut is :

$$f_2 = 5601 \times 10^3 / (660 \times 588.8) = 14.4 \text{ N/mm}^2$$

This region is crossed by a tension tie ( main steel ) and thus, the limiting stress is reduced by the effect of the transverse strain  $\epsilon_1$ . Assuming an average strain of the tension tie bars of  $\epsilon_x = 0.001$  (half the yield strain ) and considering equation 2.14 :

$$\epsilon_1 = 0.001 + (0.001 + 0.002) / \tan^2(58) = 0.00217$$

from equation 2.13 :

$$\begin{aligned} f_{2\max} &= 0.6 \times 32 / (0.8 + 170 \times 0.00217) \\ &= 16.4 \text{ N/mm}^2 > 14.4 \text{ N/mm}^2 \end{aligned}$$

- Web reinforcement :

The code requires a minimum area of 0.002 bs horizontally and vertically. Considering 12 mm diameter bars;  $A_w = 226.2 \text{ mm}^2$

$$s = 226.2 / (0.002 \times 660) = 171.4 \text{ mm}$$

s should be smaller than  $d/5$  or 300 mm for vertical bars and  $d/3$  or 300 mm for horizontal bars.

Use 12 mm diameter bars at 160 mm spacing horizontally and vertically near each face. The detailing is shown in fig.2.7.

## 2.6 AMERICAN CODE PROVISIONS FOR DEEP BEAMS

For flexure, the ACI(318-83) (revised 1986) code [1] defines deep beams as structural members having a span/depth ratio of  $5/4$  for simply supported beams and  $5/2$  for continuous ones. The code does not give detailed guidelines for flexural design of deep beams. It is simply suggested to consider the non-linear distribution of strains and the possibility of lateral buckling. In the commentary to the code [2], the designer is advised to consult other documents such as [26] [89] when designing a deep beam for flexure.

Contrary to the CEB-FIP model code [33], the emphasis of the American code is on shear design, because it is argued that the strength of deep beams is more likely to be controlled by shear. According to ACI(318-83) (revised 1986), the shear provisions can be applied to beams loaded at the top and for which  $L_0/d$  is less than 5, where  $L_0$  is the clear span and  $d$  the effective depth of the concrete section.

A critical section for shear is defined by the code as that half-way between the load and the face of support for concentrated load and that

at  $0.45L_0$  from the face of support for uniformly distributed load.

The design is based on :

$$V_u < \Phi V_n \quad 2.19$$

where  $V_u$  is the design shear force at the critical section

$V_n$  is the nominal shear strength

$\Phi$  is the capacity reduction factor for shear.

and

$$V_n = V_c + V_s \quad 2.20$$

where  $V_c$  is the shear strength provided by concrete

$V_s$  is the shear strength provided by steel

The nominal shear strength  $V_n$  should not exceed the following :

$$V_n < 8 \sqrt{f'_c} b d \quad \text{for } L_0/d < 2 \quad 2.21$$

$$V_n < 2/3 (10 + L_0/d) \sqrt{f'_c} b d \quad \text{for } 2 < L_0/d < 5$$

where  $f'_c$  is the concrete cylinder compressive strength

$b$  is the beam width.

The shear provided by concrete is calculated from :

$$V_c = (3.5 - 2.5 \frac{M_u}{V_u d}) (1.9 \sqrt{f'_c} + 2500 p \frac{V_u d}{M_u}) b d \quad 2.22$$

where  $M_u$  is the design bending moment at the critical section

$V_u$  is the design shear force at the critical section

$p$  is the ratio of the main steel area to the area of the concrete section ( $p = A_s/bd$ )

The second term on the right hand side member of equation 2.22 is the concrete shear strength for normal beams, given in ACI(318-83) (revised 1986) [1]. The first term on the right hand side member is a multiplier to allow for strength increase in deep beams, subject to the restrictions below :

$$(3.5 - 2.5 \frac{M_u}{V_u d}) < 2.5$$

and

2.23

$$V_c < 6 \sqrt{f'_c} bd$$

In the case where  $V_u$  exceeds  $\Phi V_c$ , shear reinforcement in the form of an orthogonal mesh must be provided to carry the excess shear. The contribution of shear reinforcement,  $V_s$ , is given by:

$$V_s = \left[ \frac{A_v}{s_v} \left( \frac{1 + L_o/d}{12} \right) + \frac{A_h}{s_h} \left( \frac{11 - L_o/d}{12} \right) \right] f_y d \quad 2.24$$

Combining between equations 2.19 , 2.20 and 2.24 gives:

$$\frac{A_v}{s_v} \left( \frac{1 + L_o/d}{12} \right) + \frac{A_h}{s_h} \left( \frac{11 - L_o/d}{12} \right) = \frac{V_u - \Phi V_c}{f_y d} \quad 2.25$$

where  $A_v$  is the area of vertical web reinforcement within a spacing  $s_v$ .

$A_h$  is the area of horizontal web reinforcement within a spacing  $s_h$ .

$f_y$  is the yield strength of the web steel.

In the case where  $V_U$  is less than  $\Phi V_C$ , an orthogonal mesh of web reinforcement should be provided with the area of vertical web steel not less than  $0.0015 bs_v$  and that of horizontal steel not less than  $0.0025 bs_h$ . In any case,  $s_v$  should not exceed  $d/5$  or 18 inches, whichever is less;  $s_h$  is limited to the lesser of  $d/3$  or 18 inches.

In equation 2.25, the coefficients in parenthesis represent weighting factors for the relative effectiveness of the vertical and horizontal web reinforcement; fig.2.8 shows the variation of such factors with  $L_0/d$ . It can be seen from fig.2.8 that the ACI code [1] considers horizontal web reinforcement as more effective than vertical one. From equal effectiveness at a clear-span/effective-depth ratio of 5, considered by the American code as the limit of deep beam action, horizontal bars become more effective as  $L_0/d$  decreases while the effectiveness of vertical bars diminishes to an absolute minimum.

The revised edition of the American code contains a special clause dealing with continuous deep beams. For loads applied at the sides or from the bottom of a beam, the design for shear should be the same as for ordinary members.

#### Design Example Using the American code

Consider the beam in fig.2.1, design the reinforcement and the beam thickness. The imperial units version of the ACI code [1] has been considered throughout this thesis and conversions into SI units, wherever

necessary, were made.

- Flexural strength :

$$L/h = 6300/3500 = 1.8 > 5/4$$

The flexural reinforcement is to be designed using ordinary beam equations.

$$\begin{aligned} \text{Design bending moment } M_u &= 1.4 \times 3800 \times 10^3 \times 2000 \\ &= 1.064 \times 10^{10} \text{ N.mm} \end{aligned}$$

Allowing for multiple layers of large bars as main tensile reinforcement, the effective depth is taken as

$$d = (3500 - 250) \text{ mm , say,}$$

Assuming a trial stress block depth  $a = 500$  mm and considering clause 10.3.1 of the commentary to the code [2] :

$$A_s = \frac{M_u}{\phi f_y (d - a/2)} = \frac{1.064 \times 10^{10}}{0.90 \times 460 (3250 - 250)} = 8566.8 \text{ N/mm}^2$$

Check the initial assumption of 'a' [2] :

$$a = \frac{A_s f_y}{0.85 f'_c b}$$

where  $b$ , beam width, = 515 mm (to be checked from shear considerations)

$$a = \frac{8566.8 \times 460}{0.85 \times 32 \times 515} = 281.3 \text{ mm}$$

After four iterations, the stress block depth  $a = 270.9$  mm, giving  $A_s = 8251.7$  mm<sup>2</sup>.

Provide 18 No.25 mm diameter deformed bars in 3 layers of 6 bars each (8835 mm<sup>2</sup>).

Calculate the balanced steel ratio  $p_b$

$$p_b = 0.85 \beta_1 \frac{f'_c}{f_y} \times \frac{87000}{(87000 + f_y)}$$

where  $f'_c = 32 \text{ N/mm}^2 = 4640 \text{ psi}$ ;

$\beta_1$  is the stress block dept factor, from cl.10.2.7.1

of the code [1]:  $\beta_1 = 0.85 - (640/1000) \times 0.05 = 0.818$

$f_y = 460 \text{ N/mm}^2 = 66700 \text{ psi}$

the balanced steel ratio  $p_b = 0.0274$ .

The maximum steel ratio permitted by ACI code is :

$$p_{max} = 0.75 p_b = 0.75 \times 0.0274 = 0.0205.$$

The actual steel ratio is  $p = 8835.75 / (515 \times 3250)$

$$= 0.0053 < 0.0205.$$

The minimum steel ratio allowed by ACI code is :

$$p_{min} = 200 / f_y = 200 / 66700 = 0.003 < 0.0053$$

The actual steel ratio provided is well below the maximum and above the minimum allowed by ACI(318-83) (revised 1986) code [1].

- Shear strength :

$$L/d = (6300 - 500) / 3250 = 1.78 < 5$$

Hence, the ACI code shear provisions for deep beams apply.

The critical section for shear is at  $0.5(2000 - 250) = 875 \text{ mm}$  from

the face of support or at  $(875 + 250) = 1125$  mm from its centre line.

Design shear force at the critical section :

$$V_U = 1.4 \times 3800 = 5320 \text{ kN}$$

Bending moment at the critical section :

$$M_U = 1.4 \times 3800 \times 1125 = 5985 \times 10^3 \text{ kN.mm}$$

Equation 2.19 together with equation 2.21 give :

$$b > (V_U / \Phi) \left( \frac{1}{8 \sqrt{f'_c} d} \right) = \frac{5320 \times 10^3}{0.85 \times 8 \times 0.47 \times 3250} = 512 \text{ mm}$$

take  $b = 515$  mm

The ratio  $M_U / (V_U d) = 5985 \times 10^6 / (5320 \times 10^3 \times 3250) = 0.346$

$$\left( 3.5 - 2.5 \frac{M_U}{V_U d} \right) = 2.63 > 2.5$$

take 2.5

From equation 2.22:

$$v_c = v_c / bd = 2.5 \left[ 1.9 \times 68.12 + 2500 \times 0.0053 \times \frac{5320 \times 3250}{5985 \times 10^3} \right]$$

$$v_c = 419.3 \text{ psi} = 2.89 \text{ N/mm}^2$$

This exceeds the limiting value of  $6 \sqrt{f'_c} = 408.7$  psi

$$= 2.82 \text{ N/mm}^2,$$

take  $v_c = 408.7$  psi = 2.82 N/mm<sup>2</sup>.

The design shear stress  $v_u = V_U / bd = 5320 \times 10^3 / (515 \times 3250)$

$$= 3.18 \text{ N/mm}^2$$

$$\Phi v_c = 0.85 \times 2.82 < v_u = 3.18 \text{ N/mm}^2$$

Hence, web reinforcement must be provided in accordance with equation 2.25.

$$\frac{A_v}{s_v} \left( \frac{1 + 1.78}{12} \right) + \frac{A_h}{s_h} \left( \frac{11 - 1.78}{12} \right) = \frac{3.18 - 0.85 \times 2.82}{0.85 \times 460}$$

which simplifies to

$$0.23 \frac{A_v}{s_v} + 0.77 \frac{A_h}{s_h} = 1.03$$

It is clear from this equation that according to ACI code [1], vertical web bars are less effective than horizontal ones particularly for deeper beams. Using the minimum requirements for  $A_v$  and choosing 12 mm diameter deformed bars :

$$A_v = 113.1 \times 2 = 226.2 \text{ mm}^2$$

the spacing is :

$$s_v = 226.2 / (0.0015 \times 515) = 292.8 \text{ mm}$$

$s_v$  should be smaller than  $d/5 = 650 \text{ mm}$  or 18 inches (457.2 mm), take 12 mm diameter vertical bars spaced at 290 mm, near each face.

For horizontal web bars:

$$A_h/s_h = (1.03 - 0.18)/0.77 = 1.10$$

Choosing 16 mm diameter bars, gives :

$$A_h = 201.06 \times 2 = 412.12 \text{ mm}^2.$$

$$s_h = A_h/1.10 = 359 \text{ mm}$$

$s_h$  should be smaller than  $d/3 = 1083 \text{ mm}$  or 18 inches (457.2 mm).

take 16 mm diameter horizontal bars at 300 mm spacing,

near each face. The detailing is shown in fig.2.9.

## 2.7 DISCUSSION

The review of the major deep beam design documents in use throughout the world reveals further that the deep beam problem is as yet not clearly understood.

The CEB-FIP recommendations, based on Leonhardt and Walther's experimental work [80], make emphasis on flexural design and do not give specific guidance on how to determine the web reinforcement. In contrast, the ACI code provisions, based on the work of Crist [38], centre on shear design and refer to other documents for calculating the main reinforcement. The CIRIA Guide considers the findings of a number of researchers, of which the experimental works of Leonhardt and Walther [80] and of Kong et al [63] [64] [65] [66] [68] are the most used. It deals with both flexural and shear design of deep beams falling within specific ranges for certain parameters. The Canadian code, however, adopted the diagonal compression strut analogy [31] [32] and reduces the problem of a deep beam design mainly to that of excessive concrete stresses in the struts. Flexural reinforcement forming the tension tie is calculated from a 'truss' equilibrium. Of these documents, the CIRIA Guide is perhaps the most detailed and comprehensive one, though still irrational for shear.

In conclusion, while flexural design of deep beams shows minor differences in approach, significant variations of the semi-empirically based shear design exist. This will continue to be the case in the

absence of a logical physical shear theory which implements all the possible failure modes.

## CHAPTER THREE

### DIAGONAL CRACKING OF SLENDER CONCRETE DEEP BEAMS

#### 3.1 INTRODUCTION

The expected advance in material technology and the expanding need for higher strength in compression have contributed to the development of high strength concrete [3]. Improvement in the placing, compaction and finishing techniques have resulted in lower water/cement ratios. In addition to this, the recent development of superplasticisers [15] [27] made the achievement of high concrete strengths possible. Consequently, slender elements are increasingly used in the construction industry such as columns, shear walls and deep beams in high rise buildings. Offshore construction is another field where very slender deep beams have been used [102] [103].

Although a substantial library work exists on deep beams in general [63] [64] [65] [66] [68] [92] [100], there is a need for a better understanding of the behaviour of slender deep beams. A recent comparison of the observed behaviour of slender deep beams [58] with that of stocky deep beams has revealed a significant difference; namely the major diagonal cracks <sup>c</sup> in slender deep beams make a smaller angle of inclination with the horizontal than one would expect the diagonal cracks in the stocky deep beams [68] [70] [100]. This observation has important implications in deep beam design and in the application of the CIRIA

shear-strength equation [85] (equation 2.8 in this thesis).

To provide more information on the diagonal cracking of slender deep beams and their design implications, a series of tests was carried out on concrete deep beams. The main parameter considered for this purpose was the slenderness ratio (height/thickness ratio). The experimental programme was also intended for investigating the effects of parameters such as the quantity and arrangement of web steel, the concrete strength and the shear-span/depth ratio on the serviceability and strength of slender deep beams. This will be discussed in chapter 4.

## 3.2 EXPERIMENTAL PROGRAMME

### 3.2.1 DESCRIPTION OF THE TEST SPECIMENS

The test specimens consisted of 15 slender concrete deep beams divided into 3 series : CA, CC, F.

Series CA (fig.3.1a, table 3.1) : consisted of 5 beams made of high strength concrete and having a height  $h$  1000 mm, an overall length 1700 mm and a simple span  $L$  1400 mm, giving a span/depth ratio of 1.4. The thickness varied from 40 mm to 20 mm to give slenderness ratios (height/thickness ratios) ranging from 25 to 50. The shear-span/depth ratio was 0.4 and the clear-shear-span/depth ratio 0.17 (table 3.1, fig.3.1a). The web reinforcement consisted of a rectangular mesh of 5 mm hard drawn wires spaced at 200 mm vertically and horizontally . The main

reinforcement consisted of three deformed bars placed near the bottom of the beams (fig.3.2); previous investigations [64] [65] have shown that such arrangement of the main tension reinforcement could substantially increase the shear strength of the beams. Depending on the beams thicknesses (table 3.1), 12 mm or 16 mm bar size was used. To prevent premature failure at the loading and reaction points, the beams were tapered locally and reinforcement cages of 230 x 230 mm, consisting of 2 x 2 x 25 mm welded wire mesh, were used at these points. As can be seen from table 3.1, the main parameter considered in this series of beams is the slenderness ratio  $h/b$ .

Series CC ( fig.3.1a, table 3.1 ) : consisted of 6 beams made of moderately high strength concrete and were geometrically identical to series CA beams except that the thickness was kept constant at 30 mm, giving a constant slenderness ratio of 33. As stated previously, the aim of this series was to investigate the nature of diagonal cracking as well as the effectiveness of web reinforcement which will be discussed in chapter 4. The web reinforcement of series CC consisted of 8 mm deformed bars as these are the most likely type of reinforcement to be used in practice for structures of this kind [14] [39]. The quantity and arrangement of the steel varied as in fig.3.2 and table 3.1 and will be discussed in details in chapter 4. The main reinforcement for all the beams consisted of 3 deformed bars of 12 mm diameter, placed near the bottom. Reinforcement cages similar to those used in series CA beams were used to prevent bearing failure.

Series F (table 3.1, fig.3.1c ) : consisted of 4 beams of moderately high strength concrete, identical to those in the continuous deep beam programme which will be discussed in chapters 6 and 7. The 4 beams were of height  $h$  960 mm and thickness 47 mm, giving a slenderness ratio  $h/b$  of 20. Two overall lengths were used, 2000 mm and 1600 mm, giving spans of 1720 mm and 1320 mm respectively. For more details, see chapter 6. For reasons explained in chapter 4, section 4.1, the web reinforcement consisted of 6 mm diameter plain round bars in two layers. The arrangement and quantity of the steel are as in fig.6.2 and table 3.1. The main reinforcement consisted of three deformed bars of 12 mm near the bottom . The main parameters considered for this series were the arrangement of the web steel and the clear-shear-span/depth ratio which varied from 0.21 to 0.0. It is to be noted that, due to the test rig restrictions, the clear-shear-span/depth ratio could not be isolated from the span/depth ratio and changing the former meant changing the latter as well. However, from previous investigations [66] [77], the effect of the clear-shear-span/depth ratio on the diagonal cracking and ultimate strength of deep beams is more important than the span/depth ratio. Series F beams were tested in collaboration with an M.Sc student [8] and were primarily aimed at providing a comparison with the strength and behaviour of continuous deep beams in chapters 6, 7 and 8.

### 3.2.2 BEAM NOTATION

Except for series F specimens, all the beams are identified by a letter C followed by letters A or C. The first letter, C, indicates that the beam was cast and tested solely by the author. The second letter indicates the order in which the series was cast and the geometric properties of the beam. Series F beams were the last to be cast and tested in collaboration with an M.Sc student to complement the author's work. After the series letter, the notation changes according to what the main parameter to be investigated is.

- In series CA beams, the slenderness ratio  $h/b$  is given after the first hyphen and the eccentricity/thickness ratio is given after the second hyphen. CA-25-0.0 refers to a beam of series CA having an  $h/b$  ratio of 25 and being loaded concentrically ( $e/b = 0.0$ ).

- In series CC, the quantity of web reinforcement used is given after the hyphen and the letter after the slash indicates the type of arrangement. Letters V for vertical, H for horizontal, and O for orthogonal, were used. '0.0' indicates that no web reinforcement was used. CC-0.79/V refers to a beam of series CC with 0.79 % of web steel in the form of vertical bars. Similarly, CC-0.0 indicates a beam of series CC without web reinforcement.

- In series F, the clear-shear-span/depth ratio is given after the first hyphen. After the second hyphen, the quantity and type of

arrangement of web steel are given. F-0.0-0.5/H refers to a beam of series F, tested with a clear-shear-span/depth ratio of zero and had 0.5 % of web steel in the form of horizontal bars.

### 3.2.3 MATERIALS

#### 3.2.3.1 The concrete

The concrete used for series CC and F beams is the same as that used for the manufacture of continuous deep beams in chapter 6. Details of the ingredients and mixing procedure will be given in section 6.5.1 of chapter 6.

Due to the slenderness of the specimens, the concrete used for series CA beams was of higher strength. The mix was achieved by trial and adjustments and had the following properties:

- 7-day cube strength of  $70 \text{ N/mm}^2$
- Water/cement ratio of 0.35
- Aggregates/cement ratio of 2.3
- Rapid hardening Portland cement was used
- The aggregates consisted of sand of 5 mm maximum size.

Further details are given in chapter 6, section 6.4.2.

- Melment L10 superplasticiser to improve the workability of the concrete.

The concrete strength at the day of testing is given in table 3.1. The cube strength  $f_{cu}$  and the tensile strength  $f_t$  were determined from an average of three cubes each in accordance with BS 1881 : 1983 [17] [18]. The cylinder compressive strength  $f'_c$  was deduced from the cube strength  $f_{cu}$  using equation 6.2. as explained in section 6.5.2. A typical stress-strain curve for this type of concrete, determined from cylinder tests, is given in fig.6.7. More details about the stress-strain characteristics are given in chapter 6, section 6.5.3.

#### 3.2.3.2 The reinforcement

The properties of the reinforcing bars used in all the beams are given in table 6.2 .

#### 3.2.4 CASTING AND CURING

The procedure of casting and curing of the test specimens is similar to that described in the continuous deep beam programme in chapter 6, sections 6.6.2 and 6.6.3.

#### 3.2.5 TESTING

The beams were simply supported and tested under two point-loads (fig.3.1, plates 3.1 and 3.2). Special bearing blocks (fig.6.15) allowed for the longitudinal translation and both in-plane and out-of-plane rotations. They also helped to restrain the concrete against local

crushing at the bearing zones. Loads were applied concentrically, as shown in the loading scheme of fig.3.1b.

Lateral displacements were measured at discrete positions (fig.3.3) using 15 LVDT transducers and data logger. Concrete strains were measured with demountable strain transducers [35], 36 per beam, on the back face and with demec gauges on the front face (fig.3.3). More details on the instrumentation used in the testing is given in chapter 6. To facilitate crack observation, the beams were cast in smooth formwork, whitewashed before testing and a 100 mm square grid was marked on each face (plates 3.1) so that cracks could be accurately located.

The testing procedure and equipment used will be described in chapter 6. Typically, the preparation and setting up of a beam for testing took three to four days and the testing itself took one day. During testing, safety was a primary concern; in addition to potential dangers caused by tests of this kind, premature buckling collapse is a common feature of slender deep beams [58]. As a precaution, an additional LVDT transducer was used as a deflection limit detector to cut-off the load immediately the vertical deflection exceeded a preset limit.

### 3.3 DISCUSSION OF THE TEST RESULTS ON DIAGONAL CRACKING

#### 3.3.1 CRACK DEVELOPMENT AND CRACKS PATTERNS

The cracks patterns at failure of the beams, together with the load at which each crack was first observed and the extent of the crack at that load are shown in fig.3.4. Those cracks which were believed to be the cause of failure are marked boldly and cross-hatchings indicate crushing of concrete, in some cases as a result of severe spalling. Because very few test data are available on slender deep beams, their cracking behaviour, as observed in the present tests, will be described with reference to that of stocky deep beams as explained in the literature [63] [64] [66] [100] [91]. Three main types of cracks were observed, fig.3.5;

1. Flexural cracks
2. Inclined cracks, initiating from the soffit of the beam in the vicinity of the supports
3. Diagonal cracks

Each type of crack will be discussed in detail.

##### 3.3.1.3 Flexural Cracks

On loading, the first cracks to form were flexural cracks in the region of maximum bending moment (fig.3.5, crack [1]). The flexural cracking load was typically 10 to 20 % of the measured ultimate load (table 3.2) and was somewhat lower than that of stocky deep beams of a

comparable span/depth ratio which could vary between 20 and 40 % [100]. This is expected since elastic analysis shows that for a given slender section of thickness  $b$  and depth  $h$ , the stress in the maximum bending region is given by :

$$\sigma_{\text{slender}} = M/Z \quad 3.1$$

where  $M$  is the bending moment and  $Z$  the section modulus.

For a stocky section having a thickness of  $kb$  ( $k$  a coefficient ranging from 2 to 5), a similar depth  $h$  and subject to the same bending moment, the stress will be :

$$\sigma_{\text{stocky}} = M/kZ = \sigma_{\text{slender}}/k \quad 3.2$$

Thus elastic analysis informs us that the flexural cracks should be expected to form earlier in slender sections .

The cracks were in general very narrow. Typically, their width was 0.02 mm when first formed and reached a maximum of 0.1 mm as the load was increased further. When vertical bars were present, vertical cracks formed along their positions (CC-0.79/V, CC-1.93/V) probably as a result of the slenderness of the beams and the small concrete cover ( crack [2] in fig.3.5 ). Their width reached as high as 0.3 mm ( CC-0.79/V, CC-1.93/V ) and then tended to close up as the diagonal cracks developed wider. Although some beams (CA-40-0.0, CA-33-0.0, CA-25-0.0, F-0.21-0.5/h) reached their full flexural capacity (table 3.6), no flexural failure occurred in the tests. This suggests that the flexural capacity given by equation 2.5 is a conservative one. This is because

the lever arm used in such equation and given by  $(0.2L + 0.4h)$  is based on elastic analysis [33] [85].

In general, the main reinforcement had just started to yield when the beams failed (1800 to 2000  $\mu s$ ) and in-plane deflections were below 4 mm (fig.4.2).

#### 3.3.1.4 Inclined Cracks

As the load was further increased, inclined cracks would form near the inside faces of the supports and propagate upwards and inwards (fig.3.5, crack [3]). These cracks, which have the common property of initiating at or very near the soffit of the beam and without cracking noise, tended to be quite harmless except for the beams without web reinforcement (CC-0.0) or with vertical web reinforcement only (CC-0.79/V, CC-1.93/V, F-0.21-0.5/V) where their width exceeded 0.3 mm before formation of diagonal cracks. They usually stayed very narrow at the level of the main tension reinforcement but widened above that level revealing the effectiveness of the main steel in restraining shear cracks. After the formation of the diagonal cracks, they too tended to close up and, in general, cracks initiating from the soffit of the beam hardly ever became critical. Only in two cases did the fractural failure occur along them (F-0.21-0.5/V, CC-0.0). In beams with smallest clear-shear-span/depth ratio, the formation of these cracks was delayed ( F-0.0-0.5/V, F-0.0-0.5/H ).

Inclined cracks form probably as a result of combined action between in-plane shear forces and bending moments.

#### 3.3.1.5 Diagonal Cracks

On further loading, diagonal cracks (fig.3.5, crack [4]) would form suddenly with a fairly loud cracking noise which could be easily heard within 10 m radius, particularly in beams of high strength concrete (series CA beams). The cracking phenomenon could be explained by this, when the limiting tensile strength of the concrete is reached in any of the shear spans as a result of increased shear in these regions, diagonal splitting occurs. From observation, the nature of splitting is similar to that of a split cylinder test. This diagonal cracking initiated not at the soffit but within the depth of the beam. During the testing, particular attention was devoted to observing where in the beam these cracks initiate first. However, due to the suddenness of their formation, the positions could only be limited in the form of small approximate intervals which were then projected vertically and horizontally such as those given in table 3.3. Crack widths were always maximum within these intervals. From table 3.3 two common intervals for all the beams for vertical and horizontal positions of initiation of the diagonal cracks can be deduced :

(0.35 to 0.45) h	vertically	
( x/2 to face of support )		horizontally

Where x is the clear-shear-span measured from the outside edge of the

loading point.

It is thus, tempting to consider the position defined by the centres of the two intervals, namely that at  $0.4h$  from the soffit of the beam and half-way between mid-shear-span and support face, as the most probable position where diagonal cracks initiate.

These cracks tended to be quite long at formation,  $0.6h$  to  $0.9h$  (see table 3.4), and propagated very little at subsequent loading. The diagonal cracking load, defined in these tests as the load at which the first diagonal crack formed, ranged from 30 to 60 % of the ultimate load (table 3.2). In most cases the first diagonal crack became the critical one and caused splitting of the beam. In all these respects, diagonal cracking in slender and stocky deep beams are similar. However, a significant difference was observed in these tests (table 3.4) in that the major diagonal cracks in slender deep beams were more inclined to the horizontal than those of stocky deep beams as reported in literature [52] [64] [68] [69] [77] [92] and formed somewhat at a lower load. With reference to fig.3.6, the critical diagonal crack in a stocky deep beam can be represented by the dotted line joining the inside edge of the bearing block at the support to the outside edge of that at the loading point [85], making an angle  $\theta_1$  with the horizontal. By comparison, the diagonal cracks in slender deep beams generally made a smaller angle of inclination with the horizontal, and can more accurately be represented by the full line in fig.3.6, making an angle  $\theta_2$  with the horizontal. The test results for 3 different shear-spans presented in table 3.4 show that the measured angles of inclination of the diagonal cracks,  $\theta_m$ , for

all the test beams are closer to  $\theta_2$  angles than  $\theta_1$  or  $\theta_3$  (defined by the chain dotted line in fig.3.6). This observation has important implications in deep beam design and in the application of the shear-strength equation in clause 3.4.2 of the CIRIA Guide [85].

### 3.3.2 STRAIN MEASUREMENTS

Strain measurements taken on the concrete surface in the 'inclined concrete strut' or notional load path (see fig.3.3) reveal that :

- Perpendicular to the load path, the strains were tensile as in fig.3.9. The maximum values always occurred in the lower half of the beam depth and were in the order of 100 to 200  $\mu\text{s}$  before diagonal cracking developed.
- Parallel to the load path (along line AB in fig.3.9), the strains were compressive. The maximum values were always below 1000  $\mu\text{s}$  before diagonal cracking. After diagonal cracking, these strains increased at a relatively faster rate; at 70 % of ultimate loads, the maximum compressive strains reached 2000  $\mu\text{s}$ .

This state of strains is similar to that in a standard concrete splitting test.

Longitudinal strain distributions at mid-span sections of the beams are shown in fig.3.10. It can be seen from that figure that strain distribution in deep beams is far from linearity and even more so as the span/depth ratio decreases. Moreover, fig.3.10 reveals that, in deep beams, there can be more than one neutral axis. However, the region of

maximum tensile stresses due to bending is always the one near the beam soffit. Compressive stresses due to bending may not be a problem in deep beams, particularly for deeper ones as in CB beams in fig.3.10.

### 3.3.3 FAILURE MODES

Based on tests observations on stocky deep beams, Kong et al [64] identified 4 failure modes as follows :

Mode 1: penetration of a diagonal crack into the compression zone at the loading or support region, resulting in immediate crushing failure of concrete there.

Mode 2: splitting of the beam into two by a diagonal crack.

Mode 3: crushing of the strut-like portion of the concrete between two diagonal cracks.

Mode 4: crushing of the concrete at a load or support bearing block.

Most of the beams in table 3.1 failed in mode 2, namely, by splitting along a diagonal crack and severe spalling of concrete (fig.3.4). Mode 3 occurred only in one beam, CC-1.98/H and mode 1 occurred in two beams, CA-50-0.0 and CA-29-0.0. None of the beams failed in mode 4 due to the special precautions taken by tapering the bearing zones and using additional reinforcement there. It will be shown in chapter 7 though, that, for enhanced shear and flexural capacities, this type of failure could be frequent. It was observed, however, that beams with vertical bars only exhibited a new type of failure characterised by crushing of concrete, initiated by bond failure, along a vertical bar within the

shear-span (CC-0.79/V, CC-1.93/V, F-0.0-0.5/V). This will be discussed further in chapter 4 when comparing the web reinforcement effectiveness.

Broadly, The failure modes (fig.3.4) are similar to those of stocky deep beams described by Kong et al [64] and elsewhere [91] [93] [100] and diagonal cracking appears to be the main cause of shear failure of slender deep beams.

### 3.3.4 DIAGONAL CRACKING LOADS

Since shear failure is characterised mostly by diagonal cracking, it is important to determine the load at which the concrete in the shear span first splits. In ordinary beams without shear reinforcement, this load represents the shear capacity of the beam [16]. In deep beams, however, the shear capacity could be more than twice that load [101] even when web reinforcement is not present. Table 3.5 gives the measured diagonal cracking loads for all the tested beams. In general, the beams had great strength reserve beyond diagonal cracking.

Considering equation 1.15, the first term of that equation is a semi-empirical expression of the capacity of the concrete in the shear span, that is:

$$V_{cr} = C_1 \left( 1 - 0.35 \frac{x}{h} \right) f_t bh \quad 3.3$$

It is argued [52] that when this capacity is reached the 'concrete strut'

between the loading and supporting points fails in a splitting mode, resulting in the formation of a diagonal crack. Using expression 3.3, the diagonal cracking loads of the test beams were calculated and compared with the measured values (see table 3.5 and fig.3.7). It can be seen from fig.3.7 and table 3.5 that the above expression greatly overestimates the diagonal cracking loads. This is because equation 3.3 is based on stocky deep beam tests; fig.3.8 shows that for such beams the prediction is more accurate.

An attempt was made by the author to modify the above equation to reflect the main behavioural differences between stocky and slender beams observed during the tests; namely, the diagonal cracks are more inclined to the horizontal and appear earlier in slender deep beams. From measurement of angle of inclination of the diagonal cracking (table 3.4), it is clearly shown that  $\theta_1$ , the angle considered for stocky deep beams (inclination of dotted line in fig.3.6) is higher than  $\theta_m$  and that  $\theta_2$  (inclination of the full line in fig.3.6) is closer to the measured angle  $\theta_m$ . Since the inclination of the diagonal crack seems to follow more closely the trend of  $\theta_2$ , the full line in fig.3.6, it would be more reliable to modify equation 3.3 accordingly by replacing the clear-shear-span  $x/h$  with the shear-span  $a/h$  (fig.3.1). The second difference in behaviour is the early appearance of the diagonal cracks in slender deep beams (30 to 60 % of ultimate loads as in table 3.2) as compared to stocky deep beams (50 to 90 % of ultimate load). Hence, for application to slender deep beams, the following modified expression is proposed for estimating the diagonal cracking load :

$$V_{CR} = R C_1 \left( 1 - 0.35 \frac{a}{h} \right) 0.52 \sqrt{f_{CU}} bh \quad 3.4$$

where R is a reduction factor reflecting the early appearance of diagonal cracks. R was determined from the present tests as 0.75.

It is to be noted that the tensile splitting strength of concrete  $f_t$  in equation 3.3 has been replaced by  $0.52\sqrt{f_{CU}}$  in equation 3.4 as used in the CIRIA Guide [85] and confirmed by tests in the present experimental work (fig.3.11). This is because the author believes that the risk involved in assessing the compressive strength of concrete is much less than that associated with the determination of the splitting strength. It is often difficult to ensure that the loading strips are exactly in the middle of the cube or cylinder and that the cube or cylinder itself is exactly in the middle of the loading plate of the testing machine. Hence the splitting cylinder strength obtained indirectly from compressive strength may be more reliable than obtained directly from tests.

Equation 3.4 was used to compute the diagonal cracking loads for all the test beams. The results given in table 3.5 and fig.3.7 show that a good prediction is obtained by the modified equation with a mean ratio of the measured cracking load to the predicted one of 1.04 .

Diagonal cracking loads have also been calculated using ACI(318-83) (revised 1986) code [1] and are presented in table 3.5 and fig.3.7.

Comparing the computed inclined cracking loads according to ACI code as given in table 3.5 and fig.3.7 with the measured ones reveals that the mathematical model used in reference [1] greatly underestimates inclined cracking strength of slender and, no doubt, of stocky deep beams. The average values are :

$$(P_{cr})_{aci} = 0.44 P_{crm}$$

where  $(P_{cr})_{aci}$  is the cracking load predicted by ACI code

$P_{crm}$  is the measured cracking load from tests.

This is because the mathematical model used is simply that used for ordinary beams, namely

$$V_{cr} = [1.9 \sqrt{f'_c} + 2500 p \frac{V d}{M}] bd \quad 3.5$$

where  $M$  and  $V$  are the moment and shear respectively at the critical section as defined in chapter 2, section 2.6.

ACI code assumes that diagonal cracking occurs at the same nominal shear stress as for ordinary beams but shear stress carried by the concrete is greater than the shear causing diagonal cracking.

The present tests (series CC and F beams) showed that web reinforcement had very little or no effect on the diagonal cracking load as reported by previous investigators on stocky deep beams [40]. This explains why both equations 3.4 and 3.5 are independent of the effect of web reinforcement.

### 3.4 APPLICATION OF THE CIRIA SHEAR EQUATION TO SLENDER DEEP BEAMS

Section 3.4.2 of the CIRIA Guide [85] states that the ultimate shear capacity of a deep beam loaded at the top is given by equation 2.8, that is :

$$v/bh_a = \lambda_1 \left(1 - 0.35 \frac{x_e}{h_a}\right) \sqrt{f_{cu}} + \lambda_2 \Sigma \frac{100 A Y \sin^2 \alpha}{bh_a^2}$$

3.6

where the notation are as defined in equation 2.8 and fig.1.4. For the purpose of the discussion here, it is sufficient to note that  $x_e/h_a$  is the effective clear-shear-span/depth ratio of the beam,  $Y$  is the depth from the top of the beam at which a reinforcing bar intersects the critical diagonal crack and that  $\alpha$  is the angle between a reinforcement bar and the critical diagonal crack, defined as the dotted line in fig.3.6 here.

The CIRIA equation, being based on tests on stocky deep beams, assumes that in a shear failure the critical diagonal crack may be represented by the dotted line in fig.3.6. However, as explained in the previous section, the critical diagonal crack in a slender deep beam should be represented by the full line rather than the dotted line in that figure. Since the shear capacity depends on the inclination of the diagonal crack, this implies that equation 3.6, which is primarily intended for stocky deep beams and for which it should give a factor of safety of about 2, will tend to overestimate the shear capacity and reduce the

safety factor when applied to slender deep beams. Indeed, the test results show that the safety factor could be very low (1.21 for beam CC-1.98/h, 1.10 for beams CC-1.93/V and 1.08 for beam CB-25-0.182) or even unsafe for design (beam F-0.0-0.5/V had a safety factor of 0.95).

For the same type of concrete, the same arrangement of web reinforcement and the same geometric and loading configurations such as the case of series CA beams, the safety factor decreases linearly as the slenderness ratio  $h/b$  increases (see table 3.6, fig.3.12). Such trend is expressed by the following equation, developed from the test results of series CA beams :

$$f = -0.0156 (h/b - 20) + 1.87 \quad 3.7$$

where  $f$  = safety factor =  $\frac{\text{measured ultimate load}}{\text{CIRIA design strength}}$

$h/b$  is the slenderness ratio

The average safety factor for all the beams is only 1.39 which is relatively low for a brittle and catastrophic shear failures such as those observed in the present tests.

To be applied to slender deep beams, equation 3.6 should be modified to reflect the difference in behaviour between stocky and slender deep beams as in the previous section, that is :

- (i)  $x_e/h_a$  should be taken as  $a/h$  (fig.3.6)
- (ii) a reduction factor  $R$  of 0.75 should be used with the first term on the right hand side of equation 3.6

(iii) The angle  $\alpha$  and the depth  $Y$  should be measured from the full line in fig.3.6 and not from the dotted line.

The modified CIRIA design equation for shear becomes :

$$V/bh_a = R \lambda_1 \left(1 - 0.35 \frac{a}{h}\right) \sqrt{f_{cu}} + \lambda_2 \Sigma \frac{100 A Y \sin^2 \alpha}{bh_a^2}$$

3.8

with  $R = 0.75$

Equation 3.8 was used to calculate the shear strength capacity for all the beams tested and the results are given in table 3.6. It can be seen from table 3.6 that the modified equation increases the mean safety factor to 1.81 with a standard deviation of 0.31, which is closer to what is expected for a shear failure.

The CIRIA Guide explicitly states that equation 3.6 is intended to apply over a range of 0.23 to 0.7 for  $x_e/h_a$  ( $x/h$  for the test beams). This was due to the lack of experimental data when such equation was developed. In the present tests the  $x/h$  ratio was reduced to zero (table 3.1, beams F-0.0-0.5/V, F-0.0-0.5/H). The results in table 3.6 and elsewhere [58] show that it is reasonable to extend the range of application of the CIRIA equation from 0.0 to 0.7 for  $x_e/h_a$ .

The shear strength capacities of the test beams were also calculated according to ACI code [1] which is the only document, other than the CIRIA Guide [85], making emphasis on the beam capacity to resist shear.

The results are shown in table 3.6 and reveal that the American code is reasonably safe for the shear design of slender deep beams. The average safety factor for all the beams is 2.13 with a relatively higher standard deviation of 0.42 and thus more scattered results compared to the modified CIRIA equation (equation 3.8).

### 3.5 MOHR CIRCLE ANALYSIS

As stated previously, the main difference between the behaviour of stocky and slender deep beams is the nature of diagonal cracking. The interaction between in-plane shear and out-of-plane bending is believed to be the factor influencing the diagonal cracks in appearing earlier and being more inclined to the horizontal in thin deep beams compared to stocky ones.

Due to the relatively high  $h/b$  ratio, slender deep beams deflect laterally when subject to compressive in-plane loads; even when these loads are applied concentrically as in the case of the present test beams. This lateral deflection in turn affects diagonal cracking. Maximum out-of-plane deflections recorded were 2.7 mm for series CA beams and 1.75 mm for series F beams. Those of series CC beams are presented as profiles in fig.4.3 where the maximum lateral deflection reached 4.25 mm before failure (beam CC-1.96/0). It is to be noted, however, that except beam CC-1.96/0, none of the other beams of this experimental programme failed as a result of excessive lateral deflection, though, this type of failure can not be disregarded (see chapter 5).

In this section, an attempt is made to explain the interaction between in-plane shear and out-of-plane bending and its resulting effect, using Mohr circle. Consider a section of slender deep beam (section 1, fig.3.13a) and assume that such section does not deflect laterally under compressive axial loading . Hence, the lateral bending moment of this 'ideal' section is negligible or null. This is similar to a stocky section behaviour. A small element just below mid-depth of face A of this section (fig.3.13a) will have a state of stress as shown in fig.3.13c where :

$\sigma_c$  = compressive axial stress =  $P/A$

$\sigma_{th}$  = tensile stress due to in-plane bending

$\sigma_{pt}$  = principal tensile stress, causing diagonal cracking

$\sigma_{pc}$  = principal compressive stress, parallel to the diagonal crack

$\tau$  = shear stress

$\theta$  = is the angle between the horizontal axis and the diagonal crack.

A real slender section of similar geometric and loading properties (section 1', fig.3.13b) is bound to deflect laterally even if the loading is applied concentrically, because of slenderness effect. The resulting maximum out-of-plane bending moment is at mid-depth and can be calculated from :

$$M_{add} = P e_{add} \quad 3.9$$

where  $P$  is the applied axial load and  $e_{add}$  the lateral deflection at mid-depth. Consequently, a small element of section 1' at the same position as that of section 1 and belonging to the face which is assumed

to be convex on loading (face A' in fig.3.13b) will have the state of stress shown in fig.3.13d where :

$$\sigma'_c = \text{compressive axial stress} = P/A - (M_{\text{add}} Y)/I$$

$$\sigma'_{th} = \sigma_{th} = \text{tensile stress due to in-plane bending}$$

$$\sigma'_{pc} = \text{principal compressive stress parallel to the diagonal crack}$$

$$\sigma'_{pt} = \text{principal tensile stress causing diagonal cracking}$$

$$\tau' = \tau = \text{shear stress}$$

$$\theta' = \text{angle between the horizontal axis and the diagonal crack}$$

The Mohr circle representation of the state of stress for these two elements is shown in fig.3.13e where the full line represents that of section 1 and the dotted line that of section 1'. It can be clearly seen from that figure that the angle  $2\theta'$  is smaller than  $2\theta$  which implies that at the same loading the angle of inclination of the diagonal crack is smaller for the section susceptible to out-of-plane deflection ( $\theta' < \theta$ ). The same figure shows that the principal tensile stress for the section susceptible to lateral deflection,  $\sigma'_{pt}$ , is higher than that of the section without lateral deflection,  $\sigma_{pt}$ , and hence the slender section is more likely to exhibit diagonal cracking earlier.

The Mohr circle representation reveals that, in slender deep beams, diagonal cracks are more inclined to the horizontal than in stocky ones and should be expected to form earlier. This supports the observations made by the author on the slender deep beams tested.

It can be expected from fig.3.13e that, under eccentrically applied loading and thus higher lateral deflection, the diagonal cracks will form even earlier and will be more inclined to the horizontal than for the case of beams loaded concentrically. Indeed observations from recent tests [114] confirm this and the diagonal cracking load was found to depend on the eccentricity/thickness ratio  $e/b$ .

## CHAPTER FOUR

### WEB REINFORCEMENT EFFECTIVENESS AND ULTIMATE STRENGTH OF SLENDER CONCRETE DEEP BEAMS

#### 4.1 INTRODUCTION

A literature survey on reinforced concrete deep beams shows that little is known about their behaviour and strength as influenced by web reinforcement and that available information is rather scattered or conflicting.

To the author's knowledge, since the publication of the CIRIA Guide [85] in 1977, the only major work made public on the effects of different types of web reinforcement on ultimate shear strength and behaviour of top loaded deep beams is that of Smith and Vantsiotis [100] [101]. However, no reference was made to the CIRIA Guide in that work, and the American ACI (318-77) was the major design document considered for comparison with test results.

The design recommendations given in the CIRIA Guide assume that the effectiveness of vertical web reinforcement decreases with the clear-shear-span/depth ratio,  $x/h$ . This was based on earlier work by Kong et al [63] [64] [65] where the minimum value of  $x/h$  used was 0.23. Recently, as the present work was being undertaken, one of the co-authors of the CIRIA Guide [14] [39] emphasised the need for more research on the

effect of horizontal web bars on top loaded deep beams as a test evidence for both the CIRIA Deep Beam Guide [85] and the American ACI code provisions for deep beam design [1].

The experimental programme described in chapter 3 was designed to provide information on both the nature of diagonal cracking and the effect of web reinforcement on simply supported slender concrete deep beams. The former point has been dealt with in chapter 3. In this chapter, the effect of web reinforcement on concrete deep beams in general, and on slender deep beams in particular, will be investigated. Beams of series CC and F (10 beams in all) were designed to have different arrangements and quantities of web reinforcement. In addition, in series F beams the clear-shear-span/depth ratio was varied to provide information on the relation between  $x/h$  and the type of web reinforcement.

Full description of the test beams and loading conditions are given in chapter 3. High yield deformed bars of 8 mm diameter were used as web reinforcement in series CC beams. This is because it is thought [14] [39] that this type of bars are more likely to be used in practice. However, due to the slenderness of the concrete sections used, the cover was not enough and cracks were observed along the bars on demolding the beams. Consequently, plain round bars of smaller diameter, 6 mm, were used in subsequent beams. The reinforcement patterns used are shown in figs.3.2 and 6.2

It was thought more appropriate to use a lower strength of concrete than that used in series CA beams so that the web steel effect could be better investigated. A concrete mix giving compressive strengths between 55 and 60 N/mm<sup>2</sup> after 28 days was used.

## 4.2 PRESENTATION AND DISCUSSION OF THE TEST RESULTS ON WEB REINFORCEMENT EFFECTS

### 4.2.1 CRACKING OF THE BEAMS AND CRACK WIDTHS

At each load increment, usually 25 kN applied by each jack, cracks were marked on the beam together with the load at which the cracks occurred. Crack widths were then measured using a battery operated hand microscope with 40 times magnification. Fig.4.1 shows the maximum crack width plotted against the total applied load. The loads at which the first diagonal crack occurred are also shown.

Series CC beam have the same geometric and loading properties; namely a span/depth ratio of 1.4 and a clear-shear-span/depth ratio of 0.17. The main parameters which varied were the arrangement and quantity of web steel. It can be seen from fig.4.1b that the maximum crack widths were smallest in beams CC-1.98/H and CC-0.82/H which both had horizontal web bars. Although the maximum crack width in beam CC-0.0, which had no web reinforcement, was generally larger than in any other beam, particularly after diagonal cracking, it can be seen that this was not true for beam CC-0.79/V and to a lesser extent beam CC-1.93/V (fig.4.1b). This shows

the inefficiency of vertical web bars used in the two beams. Despite that the quantity of web steel was more than doubled from beam CC-0.79/V (0.79 %) to beam CC-1.93/V (1.93 %), the ability to limit crack width was not improved. Typical values of crack widths at 300 kN were : 0.72 mm in beam CC-0.0 ; 0.82 mm in beam CC-0.79/V ; 0.64 mm in beam CC-1.93/V ; 0.4 mm in beam CC-0.82/H ; and 0.2 mm in beam CC-1.98/H. The maximum crack width of 0.3 mm imposed by BS 8110 [16] for serviceability limit state was exceeded in all the beams at 300 kN except where closely spaced horizontal bars were used (beam CC-1.98/H); for that beam the 0.3 mm limit was reached at 400 kN. Table 3.2 shows the load at which the serviceability limit state of cracking was reached for all the beams.

A close examination of fig.4.1b reveals that, for beams CC-0.0, CC-0.79/V, CC-1.93/V, that is beams without web reinforcement, with 0.79 % and with 1.93 % vertical web bars respectively, the load-maximum crack width curves show two stages of behaviour:

- An initial linear portion with a relatively steep slope before diagonal cracking,
- A second portion with a reduced slope, indicating a relatively increased rate of crack width with the load after diagonal cracking.

For beams CC-0.82/H and CC-1.98/H, with 0.82 % and 1.98 % of horizontal bars respectively, the load-maximum crack width curves exhibited only the first stage of behaviour described above with a steeper slope before and after diagonal cracking. Beam CC-1.98/H with closely spaced horizontal bars had the smallest rate of increase of crack width with load.

Due to an existing crack along the position of a horizontal bar, beam CC-1.96/0 with orthogonal reinforcement failed prematurely by buckling at a load at which the diagonal crack formed and thus, it was not possible to assess the effectiveness of such type of web reinforcement after diagonal cracking. However, before diagonal cracking, the slope of the curve load-maximum crack width was steeper than in beams with vertical bars and orthogonal bars are more effective in controlling crack width than vertical ones.

Slender deep beams present the additional risk of buckling as compared to stocky ones. This will be discussed in more details in section 4.2.3 and in chapter 5.

In series F beams, it was further attempted to assess the effectiveness of web reinforcement with changing geometric and loading properties while keeping the web steel ratio constant at 0.5 %. However, due to test rig restrictions, it was not possible to achieve considerable variations in both the clear-shear-span/depth ratio and span/depth ratio (varied from 0.21 to 0.0 and 1.79 to 1.38 respectively). For the same geometric and loading properties of  $x/h$  of 0.21 and  $L/h$  of 1.79, horizontal web bars were more effective. The 0.3 mm serviceability limit state of cracking was reached at 170 kN in beam F-0.21-0.5/V (with vertical web bars) as compared to 250 kN in a similar beam with the same amount of horizontal web bars, F-0.21-0.5/H. When both  $x/h$  and  $L/h$  were reduced, the load-maximum crack width curves (fig.4.1c) revealed a sharp distinct behaviour. Beam F-0.0-0.5/H with horizontal bars had approximately the same slope as beam F-0.21-0.5/H. However, beam

F-0.0-0.5/V with vertical bars had the flatest slope and smallest diagonal crack as compared to the others. This reveals the adverse effect of vertical web reinforcement on cracks control as the clear-shear-span/depth ratio decreases. The serviceability limit state for cracking was reached at 250 kN in beam F-0.0-0.5/H as compared to 200 kN in beam F-0.0-0.5/V.

In general, the flexural cracks, which never reached the preset limit of 0.3 mm, were narrower and shorter in beams with horizontal web steel.

The present tests (table 3.2, fig.4.1) clearly demonstrate that, for deep beams with shorter shear-spans, vertical web reinforcement is ineffective in restraining the diagonal cracking and could even have an adverse effect on both crack control and diagonal cracking load, no matter how much steel is used. Horizontal bars prove very effective in controlling diagonal cracking, particularly when closely spaced.

The argument concerning the effectiveness of web reinforcement is based on slender deep beam tests. Since diagonal cracks are more inclined to the horizontal in slender than in stocky deep beams, the present argument is deemed to err on the safe side for stocky deep beams where horizontal bars will be more nearly perpendicular to diagonal cracks, an ideal arrangement for a web bar to be fully effective [7] [64] [65] [66] [92].

#### 4.2.2 IN-PLANE DEFLECTIONS

Vertical deflections were measured at mid-span of the beams, using LVDT transducer attached to an operating unit controlling the load (see chapter 6 where full description of the equipment used in the testing programme is given). The plots of the total applied loads against vertical displacements of all the beams described in chapter 3 are shown in fig.4.2. The supports, made of concrete blocks, were assumed rigid enough for the settlement to be ignored in the simple span deep beam tests and, consequently, no allowances for supports settlements were made in plotting the load-vertical displacement curves of fig.4.2.

In general, the deflection varied linearly with the load and reached only 3 to 4 mm at ultimate. In series CC, beams with horizontal web reinforcement had smaller deflections than those with vertical or orthogonal bars (fig.4.2b). Fig.4.2b shows that beam CC-0.0, having no web reinforcement, is the only one to exhibit two linear portions:

- An initial linear portion up to 400 kN
- A relatively flat second portion from 400 kN onward, where the deflection would increase at a faster rate with the load.

The behaviour of such beam was similar to the moderately deep beams tested by De paiva and Siess [40]. The deflection was, at any load, higher in the beam without web reinforcement and highest at ultimate (4.5 mm). The plots of series F beams (fig.4.2c) show that, at corresponding load levels and for the same geometric and loading properties, beams with horizontal web reinforcement had smaller

deflections than those with vertical web bars.

On examining the plots for all the beams considered in the experimental programme (fig.4.2), it can be concluded that, for deep beams of this kind, in-plane deflection and, thus, the serviceability limit state of deflection, is not a problem. Indeed, with the exception of CC-0.0, all the beams exhibited only one stage (linear) behaviour up to ultimate as compared to the two-stage (bilinear) behaviour reported by De paiva and Siess [40] for moderately deep beams.

#### 4.2.3 OUT-OF-PLANE DEFLECTIONS

Under axial compressive loads, slender deep beams are more likely to deflect laterally, particularly when the applied loads are slightly eccentric as will be revealed in chapter 5.

A number of parameters such as the height/thickness ratio  $h/b$ , the eccentricity/thickness ratio  $e/b$ , the concrete strength and the arrangement of web reinforcement affect the out-of-plane deflection. The present tests have shown that beams with height/thickness ratio as high as 50 (beam CA-50-0.0 in table 3.1) can be tested satisfactorily without the lateral deflection getting high enough to cause premature buckling collapse. This type of failure and the main parameters affecting it directly, namely,  $h/b$  ratio and  $e/b$  ratio, will be discussed in details in chapter 5. In this section it is attempted to discuss the arrangement of web reinforcement which limits best the out-of-plane deflection. This

parameter is reflected in series CC beams which have a common slenderness ratio  $h/b$  of 33, and are thus more likely to deflect, and different types of web reinforcement arrangement. Although series F beams had different web reinforcement arrangements, their lateral deflections were very small (less than 1.75 mm at ultimate) due to their relatively small slenderness ratio  $h/b$  of 20.

Fig.4.3 shows the lateral deflection profiles for series CC beams. It can be seen from that figure that where vertical reinforcement was present, the out-of-plane deflection was smaller. The maximum deflection at ultimate was 0.84 mm in beam CC-0.79/V and 1.65 mm in beam CC-1.93/V. Beams with horizontal web bars exhibited larger deflections; 4.0 mm was recorded before failure in beam CC-0.82/H and 4.15 mm at ultimate in beam CC-1.98/H. These were in the same order as that of the beam without web reinforcement, CC-0.0, where the deflection was 3.5 mm just prior to failure. Following this, it can be concluded that vertical reinforcement is more effective in controlling excessive lateral deflection, a purpose for which horizontal bars were not effective.

From fig.4.3, it can be seen that the lateral deflection profiles for beam CC-1.96/0 are almost uniform over the three sections and present the highest out-of-plane deflection; this was due to an existing horizontal crack before the test along the position of a bar. On loading, the beam deflected steadily up to buckling collapse at a relatively low load (see table 3.2). This highlights the danger resulting from imperfections in construction and their adverse consequences, particularly in slender

sections such as thin deep beams, and calls for a need of higher safety factors when designing them.

#### 4.2.4 ULTIMATE LOADS

Table 3.2 shows the ultimate loads for all the beams described in chapter 3. However, for the purpose of assessing the effect of web reinforcement, concentration will be on series CC and F beams only. An examination of the concrete strengths  $f_{cu}$  and  $f_t$  for the two series of beams taken separately shows that the differences were very small (table 3.1) to be counted for the increase in strength and consequently, any strength variation was logically assumed to be due to web reinforcement effect.

In general, beams with horizontal web steel had the highest ultimate loads, though the strength increase was only a limited one. In series CC, the beam without web reinforcement (CC-0.0) failed at the same load as that with 0.79 % of vertical web bars. The only difference being that failure in the former was more brittle with more damage to the concrete than in the latter. When the amount of vertical web steel was increased from 0.79 % to 1.93 %, an adverse effect on the strength was observed; beam CC-1.93/V failed at 350 kN, with a strength decrease of 22 %. The concrete spalled along two adjacent web bars within the shear span, starting at either ends and joining at mid-depth (see fig.3.4). In contrast, with 0.82 % of horizontal web bars, the strength was 7 % higher than for the beam without web reinforcement and for that with the same

amount of vertical bars. When the quantity of horizontal bars was further increased by more than twice, the strength further increased by 4 %. This suggests that, although horizontal bars improve the ultimate strength of deep beams with shorter shear-spans, the strength increase is only a limited one. Thus, even when using the best arrangement of web steel, using higher quantity of web steel does not guarantee a substantial increase in strength. This is similar to the finding of Kong et al [65] [66] who argued that there is an optimum web reinforcement ratio above which no strength improvement is achieved. The estimation of such optimum needs further investigation.

In series F beams, with the same geometric and loading properties, beam F-0.21-0.5/H with horizontal bars failed at 8 % higher load than F-0.21-0.5/V with vertical bars. When the shear span decreases, previous investigators [66] [81] [85] [100] argued that the ultimate shear strength increases. The present tests show that, when horizontal steel formed the web reinforcement, the ultimate load increased with a decrease in the clear-shear-span/depth ratio. An increase of 20 % in strength was achieved as  $x/h$  was decreased from 0.21 to 0.0. In contrast, when the web reinforcement consisted of vertical bars, the ultimate strength decreased with the clear-shear-span/depth ratio; 21 % of strength decrease was recorded as  $x/h$  decreased from 0.21 to 0.0 and failure was by splitting along a vertical bar.

According to Kong et al [65] [66] and from the present tests on continuous deep beams (chapters 6, 7 and 8), a web bar is most effective

when it is more nearly perpendicular to a diagonal crack, which is approximately parallel to the line joining the loading and support points (fig.3.6). Following this argument, it can be said that when such line forms an angle of 45 degrees with the horizontal, vertical and horizontal bars become equally effective. This situation corresponds to a shear-span/depth ratio  $a/h$  of 1.0. For values of  $a/h$  higher than 1.0, the angle of the line joining the support to the reaction points with horizontal bars is smaller than 45 degrees and that with vertical bars is higher than 45 degrees and thus, vertical bars are likely to be more effective. For values of  $a/h$  smaller than 1.0, the situation is reversed and horizontal bars become more effective.

Following this argument and in the light of previous experimental evidence [65] [66] and the present tests, it can be concluded that vertical bars are not suitable as shear reinforcement for deep beams with shear-span/depth ratios less than 1.0. Horizontal bars should instead be used. It is recommended, however, that more tests be carried out so that the 'limit of effectiveness' of the two types of web reinforcement could be clearly defined.

### 4.3 ULTIMATE LOAD BEHAVIOUR OF CONCRETE DEEP BEAMS

Since the move from elastic to ultimate load behaviour in the mid-sixties by De paiva and Siess [40] and Leonhardt and Walther [80], a number of experimental investigations have been carried out on deep beams. The most important ones are those of Ramakrishnan and Anantanarayana [91], Crist [38], Kong et al [63 to 73], Smith and Vantsiotis [100], Rogowsky et al [96] and Subedi et al [104]. Some of these works have led to the design guidelines and recommendations described in chapter 2. However, there are still differences in opinions regarding deep beam behaviour and these are reflected in the different design methods adopted in the 4 major design documents [85] [33] [23] [1].

From the author's experimental observations on slender deep beams and in the light of other test evidence on stocky deep beams, it is attempted to describe the ultimate behaviour of deep beams in general.

- On loading, the first cracks to appear are flexural cracks in the region of maximum bending moment. They form quietly, grow slowly in length and spread uniformly over the span as the load is increased (see fig.3.4).

- On further increase in load (30 to 50 % of ultimate in stocky deep beams, 20 to 30 % in slender ones), inclined cracks form at the support regions at or very near the beam soffit. Usually these cracks extend upward towards the top centre and are harmless, except in beams without web reinforcement.

- At higher loads (50 to 90 % of ultimate in stocky deep beams, 30 to 60 % in slender ones), distinctive diagonal cracks develop, running from support to load point. The formation of these cracks is usually sudden, complete and accompanied by a loud noise. According to a number of researchers [47] [52] [91], the splitting action of these cracks is similar to that in a standard concrete cylinder or cube test. Observations from the present tests agree with this analogy. Owing to the sudden formation of these cracks, their exact position of initiation is difficult to spot. However, the literature tends to converge around the central region of the shear span. Crack widths were also reported [98] to be widest at that part of the beam. Similar observations were made by the author from the present tests with the exact position of initiation of the diagonal cracking centred around  $0.4h$ ,  $h$  being the beam depth.

In the absence of a rational method, a number of researchers [47] [68] [91] have used the split-cylinder analogy as a possible approach to determine the ultimate strength of a deep beam.

Compared to ordinary beams, deep beams have a marked strength reserve beyond diagonal cracking. The ultimate shear capacity is sometimes more than twice the diagonal cracking load ( table 3.2 ). This strength reserve could be explained by the fact that after diagonal cracking, a redistribution of the internal stresses occurs, resulting in the formation of a 'tied-arch' or 'truss' with the tensile reinforcement acting as a tension tie and the concrete parallel to the cracks as an

arch rib. The arching action seems to be more pronounced in beams having smaller shear-span/depth ratios. Inclined concrete compressive struts between the loading and support points were clearly defined by the diagonal cracks in the beams tested by the author (see fig.3.4). The uniformly distributed flexural cracks at the bottom part of the beams suggests that this region becomes equally stressed from one support to the other after diagonal cracking, reflecting a tie action. Such observation is supported by strain measurements along the tensile region where, as shown in fig.4.4, the strains at the supports increase rapidly after diagonal cracking.

Kong and Sharp [71] have used the term 'notional load path' to refer to the lines joining the bearing block at the support to that at the loading and stated that the load is transmitted to the support mainly through that path. This idea is shared by many investigators [40] [91] [97] [100] who, from observations on crack patterns, believe that after diagonal cracking a deep beam is structurally converted into a truss or a tied arch with the inclined struts as the compression members and the tensile steel as the tension tie.

In series F of the simple span beams and series CD and CE of the continuous beam tests, the author attempted to highlight such physical model or so called tied arch through strain measurements parallel to the inclined struts at three different transverse sections and along the tensile reinforcement. It can be seen from fig.4.5 which gives the strains at different positions from the centre of the strut after

diagonal cracking, that the strains are higher within the strut with a maximum peak at the centre. Outside the strut, the strains are small and even smaller at positions farthest from the centre of the strut. Fig.4.4 shows that before diagonal cracking, the steel strain is highest at mid-span region where the bending moment is maximum (between the two point-loads). At the faces of supports the strains are relatively small. After diagonal cracking, the strain distribution along the tensile region is almost uniform and in some cases strains are higher near the supports where the bending moment is close to null. The strain measurements in fig.4.4 and fig.4.5 clearly reveal that the 'truss' or 'tied arch' model is a valid structural idealization of a deep beam behaviour after diagonal cracking.

It is obvious that the type of tied arch or truss that can form depends on the method of load application as can be seen from fig.4.6 which illustrates two physical models of deep beams proposed by Kotsovos [76]. The slope of the inclined strut, approximately equal to  $h/a$ , would change according to the load application. From the present tests, the width of these inclined struts could reasonably be taken as the width defined by the bearing plates plus  $0.05h$  on either side (figs.4.5 and 4.6) that is :

$$w = C \sin\theta + 0.1h \qquad 4.1$$

where  $C$  is the bearing length

$\theta$  is the angle of inclination of the inclined strut

A proper failure of a deep beam, that is excluding any premature failure such as buckling in slender deep beams, crushing at the bearing or anchorage failure, is related to the failure of the truss or tied arch described above. A flexural failure occurs when the tensile reinforcement forming the 'tie' is very low and is characterised by rupture of the tension tie or crushing of the concrete rib in compression at the 'crown'. This type of failure (fig.4.7) could be frequent in moderately deep beams or when the tensile reinforcement is light as observed by De paiva and Siess [40] and Leonhardt and Walther [80] respectively. A shear failure takes place through the destruction of the inclined strut in one of the following ways :

- Splitting of the beam along the inclined strut, sometimes followed by a destruction of the concrete.
- Crushing of the concrete in the inclined strut.
- Crushing of the concrete at the compression zone at the loading or support regions after a diagonal crack has penetrated deeply into that zone.

Most of the shear failures reported in the literature fit in one of these three failure modes, although other descriptions have been used.

In the present tests, the end portion of the beam outside the diagonal cracks (outside the inclined struts) tended to rotate about the nearest loading point. Such rotational motion which was observed earlier by other investigators [47] [77], was clearly visible at failure (see fig.4.8). Before failure, this rotational movement was restrained mainly by the tensile reinforcement at the level of the supports, explaining

further the high tensile strains recorded there after diagonal cracking. This also emphasises the importance of the tensile steel in resisting shear and highlights the increase in effectiveness of a web bar with the depth as reported earlier [47] [64] and reflected in the CIRIA design equation for shear (equation 2.8). This is in contrast with the ACI code [1] where the web reinforcement is assumed equally effective down the beam depth and the main tensile steel contribution to shear is only indirectly considered in equation 2.22 through the use of the steel ratio  $p$ .

#### 4.4 ULTIMATE LOAD PREDICTION OF DEEP BEAMS

##### 4.4.1 EXISTING FORMULAE

Although numerous equations have been proposed [40] [41] [78] [91] [103] [107] for the ultimate strength prediction of deep beams failing in shear, only two have gained acceptance and found their ways into design documents. These are the formula of Crist [38], currently used in the American code [1], and of Kong et al [68] used in the CIRIA Guide. The CIRIA shear equation as used in chapter 2 (equation 2.8) is a lower bound one and uses safety factors and thus gives design values rather than ultimate ones as in table 3.6. For ultimate values of shear strength, the original Kong et al [68] expression, namely equation 1.15 is used, that is :

$$Q_{ult} = C_1 \left(1 - 0.35 \frac{x}{h}\right) f_t b h + C_2 \Sigma \frac{A_y \sin^2 \alpha}{h} \quad 4.2$$

where all the symbols are as explained in equation 1.15.

The ultimate load is given by :

$$P_1 = 2 Q_{ult}$$

The first term on the right hand side of equation 4.2 represents the diagonal cracking load and has been dealt with in chapter 3. The second term represents the strength reserve beyond diagonal cracking. The ultimate loads for all the beams described in chapter 3 were calculated from equations 4.2 and are presented in table 4.1. In the same table, the measured ultimate loads are given. It can be seen from table 4.1 and fig.4.9 that equation 4.2, developed for stocky deep beams, overestimates the ultimate load of slender deep beams. The reason for this is the nature of diagonal cracking in slender deep beams, being more inclined to the horizontal and appearing earlier as compared to those in stocky deep beams. This has been discussed in chapter 3.

Following the modifications proposed in chapter 3 by the author (as in equations 3.4 and 3.8), the ultimate load of a slender deep beam can be computed from :-

$$P_2 = 2 Q_{ult}$$

where  $Q_{ult}$  is given by

$$Q_{ult} = R C_1 \left( 1 - 0.35 \frac{a}{h} \right) 0.52 \sqrt{f_{cu}} bh + C_2 \Sigma \frac{A Y \sin^2 \alpha}{h}$$

4.3

Using equation 4.3, the ultimate loads for all the beams of chapter 3

were calculated and are given in table 4.1. It can be seen from the same table and from fig.4.9 that the above modified equation agrees better with the test results; the average measured/predicted ratio was 1.12.

The ultimate loads were also calculated using the ACI code [1] which, as mentioned, is based on Crist work [38]; equations 2.19 to 2.25 have been used. As a design document, the American code gives design values for the shear strength such as those presented in table 3.6. For ultimate load purpose, the reduction factor  $\phi$  is omitted and the ultimate load is given by :

$$P_3 = 2 V_n \quad 4.4$$

where  $V_n$  is the nominal shear strength as given by equation 2.20. The computed ultimate loads using the ACI code are presented in table 4.1. It can be seen from the same table and from fig.4.9 that, in general, ACI code [1] is very conservative; the average measured/predicted ratio is 1.81.

#### 4.4.2 PROPOSED FORMULA

The literature and the present tests reveal that diagonal splitting is the main type of failure of deep beams and that the splitting action is similar to that in a standard splitting test of a concrete cylinder. Such analogy is used to derive a formula for the ultimate shear strength of deep beams.

From the tests, it was observed (chapter 3) that the inclination of the diagonal cracks is best represented by the line joining the centre of the support block to that of the load bearing block (full line in fig.3.6). Consider a portion of a beam, such as shown in fig.4.10a. The load  $Q$  can be resolved in the direction of the line joining the centres of the load and support points, giving  $Q/\sin\theta$ , and horizontally, giving  $Q\cot\theta$  (see fig.4.10a). The component  $Q\cot\theta$  causes the bending effect and aggravates the rotational motion of the end portion of the beam after diagonal cracking as noticed during the tests. The component  $Q/\sin\theta$  causes the splitting. An idealised concrete cylinder of diameter  $h$  (fig.4.10a) is assumed to be split in the process. Strain measurements from the present tests (fig.3.9) and from the tests by Kubick [77] have shown that the strains along the line joining the centres of the load and support points, dotted line in fig.4.10a, are compressive and those perpendicular to that line are tensile. This suggests that the state of stress of a small element in the idealized concrete cylinder, fig.4.10a, is similar to that of a corresponding element in a real concrete cylinder having the same geometric properties.

For such cylinder, the splitting tensile stress [57] is given by :

$$f_t = \frac{F}{\pi/2 bh} \quad 4.5$$

where  $F$  is the splitting force

$b$  is the length of the cylinder and  $h$  its diameter

$(\pi/2 bh)$  represents the effective area of concrete

resisting the splitting force  $F$ .

In fig.4.10a, the splitting force is  $F = Q/\sin\theta$ , hence :

$$f_t = \frac{Q/\sin\theta}{\pi/2 bh} \quad 4.6$$

If a bar crosses the diagonal crack, as in fig.4.10b, it will contribute to the concrete resistance against splitting, whether it being a main tensile reinforcement or a web bar. Such contribution depends on the angle of the bar with the diagonal crack. Experimental evidence from previous investigators [7] [64] [65] [92] and in chapter 7 of this thesis shows that a web bar is most effective when it is perpendicular to the crack. Consider a total area of steel,  $A_n$ , normal to the direction of the crack and assume that, just before splitting, the tensile strains (strains perpendicular to the crack) in the concrete and in the steel are equal (strain compatibility). The equivalent effective area of concrete resisting the splitting action will be :

$$\pi/2 bh - A_n + \alpha_e A_n$$

and the tensile stress becomes :

$$f_t = \frac{Q/\sin\theta}{\pi/2 bh + (\alpha_e - 1)A_n} \quad 4.7$$

where  $\alpha_e$  is a modular ratio, given by  $E_s/E_c$ .

BS 8110 [16] recommends to use a value of 15 for  $\alpha_e$ .

For the particular case of vertical web bars of total area  $A_v$ , horizontal web bars of total area  $A_h$  and main longitudinal steel of total area  $A_s$ ,  $A_n$  can be obtained by resolving  $A_v$ ,  $A_h$ , and  $A_s$

in a direction perpendicular to the diagonal crack (fig.4.10b); only bars crossing that line should be considered, that is :

$$A_n = (A_h + A_s) \sin \theta + A_v \cos \theta \quad 4.8$$

with  $A_h = p_h bh$

$$A_s = p_s bh$$

$$A_v = p_v ab = p_v \beta bh$$

where  $p_s$ ,  $p_h$ ,  $p_v$  are the steel ratios for flexural reinforcement, horizontal web reinforcement and vertical web reinforcement respectively, and  $\beta = a/h$ .

From fig.4.10 :

$$\sin \theta = h / \sqrt{(a^2 + h^2)} = 1 / \sqrt{(1 + \beta^2)}$$

$$\cos \theta = a / \sqrt{(a^2 + h^2)} = \beta / \sqrt{(\beta^2 + 1)}$$

After substitution and rearrangement, equation 4.7 becomes :

$$Q = \frac{f_t bh}{(1 + \beta^2)} [\pi/2 \sqrt{(1 + \beta^2)} + (\alpha_e - 1)(p_s + p_h + \beta^2 p_v)] \quad 4.10$$

Following the argument in chapter 3, section 3.3.4, the tensile splitting strength of the concrete,  $f_t$ , is replaced by  $0.52\sqrt{f_{cu}}$  (see fig.3.9); equation 4.10 becomes then :

$$Q = \frac{0.52 \sqrt{f_{cu}} bh}{(1 + \beta^2)} [\pi/2 \sqrt{(1 + \beta^2)} + (\alpha_e - 1)(p_s + p_h + \beta^2 p_v)] \quad 4.11$$

which represents the ultimate shear strength. The ultimate

load for beams failing in diagonal splitting shear is :

$$P_4 = 2 Q$$

Equation 4.11 was used to calculate the ultimate loads for the test beams. As can be seen from table 4.1 and from fig.4.9, the prediction is satisfactory with a similar degree of accuracy as the modified Kong et al equation (equation 4.3). It errs on the safe side because the steel contribution towards the shear resistance is computed on a modular ratio basis. Compared to ACI method [1], which is very conservative, and to equation 4.2 (the original Kong et al [68] equation) which overestimates the ultimate loads of slender deep beams, both the modified Kong et al equation and the proposed equation gave better predictions with measured/predicted ratios of 1.12 and 1.10 respectively.

Equation 4.11 can be used for design purpose, provided :

- A lower bound expression for the splitting tensile strength of concrete,  $f_t$ , is used as in fig.3.11, namely  $f_t = 0.4\sqrt{f_{cu}}$ .  
Such lower bound value was obtained from test data.
- A safety factor for material is used; BS 8110 [16] recommends a value of 1.25 for shear.

## CHAPTER FIVE

### INSTABILITY OF SLENDER DEEP BEAM-PANELS - COMPARISON OF TEST RESULTS WITH EXISTING DESIGN AIDS

#### 5.1 INTRODUCTION

In the past, researchers and designers alike have always avoided the buckling problem in deep beams by opting for stocky sections. The tests described in chapter 3 have revealed that buckling is a possible design criterion, particularly for the more slender sections. Of the current design documents [1] [33] [23], only the CIRIA Guide [85] gives design guidelines for the buckling strength of deep reinforced concrete beams. It is stated [85], however, that in the absence of experimental evidence, such recommendations were based on theoretical studies and engineering judgement.

In the late seventies, the development of the tilt-up method of construction highlighted the need for a buckling design procedure to deal with the slender load bearing panels. The Portland Cement Association responded to the building industry's need and came up with a buckling design aid for tilt-up load-bearing walls [88], based on numerical analysis on column models.

Until recently [58], neither of the two buckling design procedures could be compared against experimental data. However, due to the nature

of the specimens, the recent tests reported by Kong et al [58] provided a direct assessment to the CIRIA Guide [85] only which, not surprisingly, was found very conservative.

As a follow-up research programme, the present author carried out buckling tests on 7 slender deep beam-panels with height/thickness ratios,  $h/b$ , varying from 20 to 70. The test specimens were designed to model the conditions set up in the PCA Design Aid [88] as closely as possible so that a direct assessment of its usefulness as a design document could be provided and a comparison with the broader CIRIA procedure be made.

Before the testing programme and results are presented, the buckling problem is discussed with reference to columns and plates and an overview of the two deep beam buckling design procedures is given.

## 5.2 THE BUCKLING PROBLEM

### 5.2.1 COLUMN BUCKLING

Strictly speaking, the term buckling refers to a process in which a structure moves from a neutral or unstable equilibrium to another equilibrium state which may or may not be stable [58]. Under longitudinal loads, a slender column deflects essentially in a uniaxial curvature. The Euler formula for the elastic critical buckling load of a slender column is the earliest engineering design formula that is still

in use today. It takes the form :

$$P_{cri} = \pi^2 EI / L_e^2 \quad 5.1$$

Where  $P_{cri}$  is the critical axial load necessary to bend the column

$EI$  is the column stiffness

$L_e$  is the effective column length (height)

For the application of the above formula, the column is assumed perfectly straight, made of homogeneous elastic material. In real structures, imperfections are always present and columns are not perfectly elastic.

Several researchers have taken up the early Euler work and extended it to inelastic buckling behaviour by modifying the elastic modulus  $E$ . Concepts such as the 'tangent modulus load' and the 'double modulus load' have been introduced and are well documented and explained in most modern textbooks on stability [111] [6]. Interested readers can consult reference [49] where a thorough historic review of column buckling theory is given.

In design, buckling failure is used more loosely to refer to failure with pronounced out-of-plane deformation. The need for simple design procedures led to the development of what is known as the 'additional moment concept', first used in the 1970 edition of the CEB-FIP code [34] and extended later into the British practice [16] [36]. This concept enables a slender column to be designed as a short column taking into account an additional bending moment due to out-of-plane deflection.

The additional moment concept consists broadly of estimating the maximum lateral deflection of the column subjected to axial load, using mathematical models. Then the additional bending moment is calculated as the axial load times (x) the estimated maximum lateral deflection. In the British practice, the mathematical model used for the lateral deflection is that developed by Cranston [37], namely

$$e_{add} = \frac{h}{1750} \left( \frac{L_e}{h} \right)^2 \left( 1 - 0.0035 \frac{L_e}{h} \right) \quad 5.2$$

Where  $e_{add}$  is the lateral deflection due to slenderness

$L_e$  is the effective column height (length)

$h$  is the depth of the column section

The recent BS 8110 [16] approximates equation 5.2 to

$$e_{add} = \frac{1}{2000} \left( \frac{L_e}{b} \right)^2 h = \beta_a h \quad 5.3$$

Where  $b$  is the smaller dimension of the column section.

The American practice [1], uses a magnification factor to amplify the design moment of the column. The magnification factor itself depends directly on the critical Euler load as follows :

$$\delta = \frac{C_m}{1 - P_u / \Phi P_{cri}} > 1 \quad 5.4$$

Where  $C_m = 0.6 + 0.4(M_1/M_2) > 0.4$

$M_1$  and  $M_2$  are the smaller and higher factored end moments

$\Phi$  strength reduction factor

$P_u$  is the factored axial load at a given eccentricity

$$P_{Cri} = \pi^2 EI / L_e^2$$

The main draw-back of this method is the effect of creep and cracking and the non-linearity of concrete, making the estimation of the EI value rather difficult.

### 5.2.2 PLATE BUCKLING

Usually, a plate is restrained on all four edges, and thus, when subjected to compressive loads, is more likely to buckle in a biaxial curvature. Early work was concerned with the buckling of plates made of homogeneous isotropic material. The bulk of it was carried out by Timoshenko and is presented in many textbooks [111] [6].

The critical stress of a plate subjected to different loading and boundary conditions was presented as :

$$f_{cr} = k \frac{\pi^2 E}{12 (1 - \nu^2)} \frac{1}{(b/t)^2} \quad 5.5$$

Where  $k$  is plate buckling coefficient, depends on the type of

loading, the aspect ratio  $a/b$ , and the boundary conditions

$b$  is the plate width

$t$  is the plate thickness

$E$  is the modulus of elasticity

$\nu$  is the Poisson's ratio

Subsequent researchers [99] concluded that, at buckling the collapse of plates is prevented by the restraints along the unloaded edges and thus, unlike columns, they continue to carry some post-buckling loads.

Von Korman, Sechler and Donnell [113] proposed an 'effective width' approach to explain the behaviour of a plate at ultimate conditions. According to them, the load acting on the full width of a plate is carried on two narrow strips along the unloaded edges. Failure is assumed to occur when these two strips reach yield. They suggested an expression to calculate the effective width and used equation 5.5 to estimate the yield stress of the plate.

Work on the buckling of reinforced concrete plates is relatively scarce. The tests carried out by Ernst et al [43] and Swartz et al [105] [106] are probably the most important works on reinforced concrete plates available in the literature. Generally the plates buckled in a biaxial curvature at stresses lower than the concrete cylinder compressive strength  $f'_c$  and showed no or very little post buckling strength. Swartz et al [105] proposed the following formula to estimate the concrete stress at the onset of buckling for simply supported plates :

$$f_{cr} = 0.425 f'_c B [-B + (4+B^2)^{0.5}] \quad 5.6$$

$$\text{Where } B = \frac{\pi^2}{6 \epsilon_0 (1-p)} (1/r + r)^2 (t/b)^2$$

Where  $r = h/b$  if  $h/b < 1$  and  $r = 1$  if  $h/b > 1$

$h$  = plate length,  $b$  = plate width,  $t$  = plate thickness

$p$  = total steel ratio

$f'_c$  = compressive strength of concrete cylinder

$\epsilon_0$  = peak strain at peak concrete stress.

It is interesting to note that in Swartz et al [105] plate buckling tests, the height/thickness ratios varied between 77.0 and 128.0 and thus equation 5.6, based on such high h/b ratios, could be thought of as not practical.

### 5.3 CURRENT DESIGN PRACTICE FOR THE BUCKLING OF SLENDER DEEP BEAM-PANELS

The current major documents for the buckling design of slender deep beam-panels are the CIRIA Guide [85] and the Portland Cement Association Design Aid [88]. The buckling procedures given in these documents will be reviewed very briefly.

#### 5.3.1 CIRIA GUIDE PROCEDURE

In the absence of experimental data, the CIRIA buckling procedure [85] had to be based on theoretical studies. Its aim is essentially to ensure a safe design for deep beam panels to avoid buckling. Elastic stress distribution is used and can be obtained from Appendix A of the Guide or from other specific elastic analysis such as the finite element method.

According to the CIRIA Guide, when a deep beam can not be defined as a short braced wall (clause 3.8.1.1 of CP 110 or 1.2.4 of BS 8110), the slenderness effect should be taken into account. An assumption, that a

deep beam is made up of an assembly of unit width column strips spanning vertically and horizontally, is considered and consequently the additional moment concept approach is used. The emphasis, however, is on the determination of the effective height and length of the deep beam-panel. Once these values are determined, the usual design procedure for a slender column is used, namely :

$$M_t = M_i + M_{add} \quad 5.7$$

Where  $M_i$  is the initial end moment

$M_{add}$  is the additional moment caused by slenderness effect,  $M_{add} = N e_{add}$

Where  $N$  is the maximum axial-load/unit-width, determined from elastic stress distribution given in Appendix A of the Guide or from other specific elastic analysis such as the finite element method.

$e_{add}$  is the additional eccentricity, given by the above equations 5.2 and 5.3 according to CP 110 [36] and BS 8110 [16] respectively.

The effective height (or length) to be used in the additional eccentricity expressions (equations 5.2 and 5.3) is determined according to three methods, namely :

- 1- The supplementary rules
- 2- The single-panel method
- 3- the two-panel method

For the supplementary rules to be used, the following conditions should be satisfied :

- The beam panel is adequately braced and rectangular in shape
- At least two opposite edges of the beam panel are laterally restrained
- The average shear stress ( $V/bh_a$ ) is less than 50 % of average vertical or horizontal axial compressive stress, whichever is greater.

When these conditions are fulfilled,  $h_e$  may be taken as

- For panels with all four edges restrained,  $h_e$  is taken as 1.1 x the shortest distance between centres of parallel lateral restraints
- For panels with one or two opposite edges free,  $h_e$  is taken as 1.5 x the distance between centres of parallel lateral restraints
- For panels with both rotational and lateral movements restrained,  $h_e$  is taken as the clear distance between restraints.

Where the above conditions are not satisfied, or where a more rigorous estimate of the effective height and length of the panel is required, then the single panel method or the two panel method, given in Appendix C of the Guide, should be used. The procedure starts by defining a rectangular equivalent panel having either free or simply supported edges and subjected to equivalent vertical, horizontal and shear stresses ( $N_v, N_h, \tau$ ) as in fig.123 of CIRIA Guide. The equivalent stresses to be used depend on whether the single panel method or the two panel method is to be considered. More details about the choice of the equivalent stresses is given in references [59] [60] [62] and in Appendix A of this thesis.

Average values of the elastic critical stresses are given in the Guide (figs.124 to 128) for vertical, horizontal and shear stresses,  $N'_{vcr}$ ,  $N'_{hcr}$  and  $\tau'_{cr}$  respectively, as functions of the flexural rigidity  $EI'$  and the panel dimensions; these take the form of :

$$N'_{vcr} = \frac{K \pi^2 EI'}{a^2} ; \quad N'_{hcr} = \frac{k \pi^2 EI'}{a^2} ; \quad \tau'_{cr} = \frac{4.7 \pi^2 EI'}{b^2} \quad 5.8$$

From this, stress ratios are calculated :

$$R'_{v} = \frac{N_v}{N'_{vcr}} ; \quad R'_{h} = \frac{N_h}{N'_{hcr}} ; \quad R'_s = \frac{\tau}{\tau'_{cr}} \quad 5.9$$

The procedure introduces new stress ratios  $R'_1$ ,  $R'_2$ ,  $R''_2$  where the suffix '1' and '2' refer to the direct stress parallel to the long edge and short edge, respectively, of the panel, that is

$$R'_1 = R'_h ; \quad R'_2 = R'_v ; \quad R''_2 = R'_2/M'_2$$

Where  $M'_2$  is a modification factor to eliminate the effect of the shear stress on the critical stress parallel to the short edge.

Using  $R'_1$  and  $R''_2$ , the effect of a direct stress of one direction on the critical stress of the other direction is estimated by modification factors  $M_1$  and  $M_2$  from interaction diagrams given in fig.130 of the Guide. the modified critical stresses become, then,

$$\begin{aligned} N_{vcr} &= \pi^2 EI'/h_e^2 = M_2 N'_{vcr} \\ N_{hcr} &= \pi^2 EI'/L_e^2 = M_1 N'_{hcr} \end{aligned} \quad 5.10$$

The effective height  $h_e$  and length  $L_e$  are determined from

equation 5.10 as follows:

$$h_e^2 = \frac{\pi^2 EI'}{M_2 N'_{vcr}} \qquad L_e^2 = \frac{\pi^2 EI'}{M_1 N'_{hcr}} \qquad 5.11$$

In the single panel method the equivalent applied stresses selected are upper bound values and should be used to analyse the cross-section. For the two panel method the effective height  $h_e$  and length  $L_e$  are determined separately from two panels differing in equivalent loading only. The effective height  $h_e$  is determined from the first panel for which the equivalent load consists of an upper bound horizontal stress and a lower bound vertical stress. The effective length  $L_e$  is determined from the second panel, having a lower bound horizontal stress and an upper bound vertical stress. In contrast to the single panel method, the actual stresses are used to analyse the cross-section, resulting in a more rational distribution of steel. The CIRIA Guide [85] buckling procedure is illustrated in more details with design examples in references [59] [60] [62] and in Appendix A of this thesis.

### 5.3.2 PORTLAND CEMENT ASSOCIATION DESIGN AID

According to the American practice [90], lateral buckling is likely to be a problem for deep beams having height/thickness ratios of more than 25. Despite this, no specific guidance is given in ACI(318-83) (revised 1986) [1] regarding their buckling design. However, a PCA Design Aid for tilt-up load-bearing walls [88] enables the buckling check to be carried

out for slender deep beam-panels, having height/thickness ratios between 20 and 50.

The PCA Design Aid was originally intended for the tilt-up method of construction to deal with reinforced concrete wall panels under uniformly distributed eccentric load applied at the top and continuous concentric reaction at the support.

The web reinforcement considered consists of one central layer or two symmetric layers of vertical bars. Horizontal reinforcement, though recommended for use, is not considered in the analysis. The method, which assumes that the vertical edges are not restrained, uses a column model to calculate the load capacity according to a numerical integration procedure by Pfang and Siess [86] [87] and Newmark [84]. For design purposes, load capacity coefficients are presented in tabulated forms for different geometric and loading configurations.

The load carrying capacity is given by :

$$P = \phi b_1 b f'_c \quad 5.12$$

Where  $\phi$  is the load capacity coefficient given in dimensionless form in Appendix A of the PCA Design Aid

$b_1$  is a unit width of the panel

$b$  is the thickness of the panel

$f'_c$  is the cylinder compressive strength of concrete

Where the wall panel rests on isolated footings instead of continuous ones, which reflects the case of deep beams, the PCA method assumes that the load is to be transferred to the footings through relatively narrow column-like strips. This will result in a reduction of the load capacity which is taken into account as follows :

$$\eta = \frac{P_{cri}}{P_{crc}}$$

Where  $\eta$  is the load capacity reduction coefficient  $< 1$

$P_{cri}$  is the buckling load of the strip element of a panel on an isolated footing of specific dimensions, determined from an elastic analysis or a tangent modulus approach (both described in [111]).

$P_{crc}$  is the buckling load of a strip element of a panel on a continuous support, taken as :

$$P_{crc} = \pi^2 E_t I / (kL_u)^2$$

Where  $E_t$  is the tangent modulus

$I$  is the moment of inertia of the section

$k$  is the effective length factor

$L_u$  is the unsupported height of the panel.

For design purpose,  $\eta$  is presented in a graphical form in the PCA Design Aid. The load capacity of a slender beam-panel resting on isolated footings becomes :

$$P_{isol} = \eta (\phi b_1 b f'_c) = \eta P_{cont} \quad 5.13$$

Concentrated loads are assumed distributed over an effective width of the panel as defined in section 14.2.4 of ACI(318-83) (revised 1986) [1], namely the smaller of :

- a. centre to centre distance between loads
- b. width of bearing plus four times the wall thickness.

In addition, the PCA design method takes account of transverse loads such as the lateral pressure due to wind. It is, however, limited to concrete having cylinder compressive strength less than 4000 psi ( $28 \text{ N/mm}^2$ ).

#### 5.4 TESTING PROGRAMME

The test specimens (fig.5.1a) consisted of 7 slender reinforced concrete deep beams of height  $h$  1400 mm, overall length 1700 mm, and simple span  $L$  1400 mm giving a span/depth ratio of 1.0. The thickness varied from 70 mm to 20 mm, giving height/thickness ratios  $h/b$  ranging from 20 to 70. The upper end of the range is believed to be among the highest  $h/b$  ever tested in beam-panels. The PCA Design Aid [88] does not recommend slenderness ratios higher than 50; to quote from it 'slenderness ratio higher than 50 is not recommended because of lack of supporting experimental evidence'.

The main reinforcement was so designed as to avoid flexural failure and consisted of high yield deformed bars of either 10 mm or 12 mm size used in numbers of 3 or 6, depending on the beam thickness (see fig.5.2, table 3.1). The web reinforcement used followed one of the patterns adopted in the PCA Design Aid, namely, a central layer of vertical bars

restrained by horizontal ones. It consisted of 6 mm diameter plain round bars at various spacings to achieve a steel ratio of 0.5 % both vertically and horizontally (fig.5.2). In addition, reinforcement cages were used at the loading and support regions to avoid concrete crushing there. The properties of the steel used are given in table 6.2 .

Due to the concrete strength limitation of the PCA design method, a concrete mix (water/cement ratio of 0.7 and aggregates/cement ratio of 5.0), giving lower strengths, was used. The average cube crushing strength was  $24 \text{ N/mm}^2$  at 7 days and  $41 \text{ N/mm}^2$  at the day of testing. The cylinder compressive strength  $f'_c$  was deduced from the cube strength using equation 6.2. Table 3.1 gives the concrete strength properties for all the beams.

Strictly speaking, the design tables given in the PCA Design Aid are meant for panels of practical scale with thicknesses ranging between 140 mm and 241 mm and load-eccentricities between 25 mm and 210 mm. It is obviously difficult to test such specimens in a laboratory. However, following recent tests by Kong et al [58], the buckling strength depends more on the eccentricity/thickness ratio  $e/b$  and, with it being dimensionless, is more convenient to describe the buckling behaviour of a deep beam. Consequently, a load-eccentricity/thickness ratio  $e/b$  of 0.182, corresponding to an eccentricity of 1.0 inch and a thickness of 5.5 inches in the PCA document, was used to model the present test specimens. The beams were tested under two point-eccentric-loads and rested on two simple supports (plate 3.1) with concentric reactions as

shown by the loading scheme in fig.5.1b. The shear-span/depth ratio and the clear-shear-span/depth ratio were 0.29 and 0.12 respectively (table 3.1).

Displacement transducers (described in chapter 6, section 6.8.1) placed in 3 columns of 5 each, were used to measure the lateral deflection above the two supports and at mid-span (see fig.3.3a). In addition, due to the sudden nature of buckling, two dial gauges were placed on the back to signal an impending collapse (plate 3.2). This safety precaution proved very useful in giving warning of buckling danger. Strains were monitored by strain transducers (described in section 6.8.2) placed in various positions on the back face of the beam, as shown in fig.3.3a (see plate 3.2). On the front face, the strains were measured at each increment by mechanical demec gauges at locations shown in fig.3.3b. The hand measurements were usually stopped as soon as buckling danger was felt (lateral deflections exceeding 4 mm).

This series of beams is indicated by a letter B which comes after the author's initial C. After the first hyphen the slenderness ratio  $h/b$  is given and the load-eccentricity/thickness ratio is given after the second hyphen.

## 5.5 TEST RESULTS

### 5.5.1 CRACKS PATTERNS AND FAILURE MODES

Fig.5.3 shows the cracks patterns at failure of the beams. The general trend of the cracks development is similar to that described in chapter 3 for the beams under concentric loading, with the diagonal cracks being the widest at formation and most harmful. With the beams having the same load-eccentricity/thickness ratio  $e/b$ , the failure mode depended mainly on the slenderness ratio  $h/b$ .

a)- For  $h/b$  ratio greater than 25, failure was by buckling. The beams split horizontally approximately along mid-depth section; Plate 5.1 shows a ductile buckling failure. Horizontal cracks appeared simultaneously with failure and thus could not be used as a warning sign for collapse. The buckling strength was about 30 % greater than the diagonal cracking load for beams with  $h/b$  ratios of 30 and 35 (CB-30-0.182, CB-35-0.182), 20 % greater for those with  $h/b$  ratios of 40 and 50 (CB-40-0.182, CB-50-0.182) and that with  $h/b$  ratio of 70 (CB-70-0.182) buckled just after the formation of the first flexural cracks.

b)- For  $h/b$  ratios smaller than (including) 25, the beams failed either in shear (CB-25-0.182) or at the bearing (CB-20-0.182). However, the lateral displacement profiles shown in fig.5.6 indicate that even beam CB-25-0.182 was on the verge of buckling; its maximum lateral deflection just prior to failure was similar to those in beams which

failed by buckling. Consequently, beam CB-25-0.182 is assumed to have reached its ultimate shear as well as buckling strengths. In contrast, beam CB-20-0.182 had not yet reached its ultimate buckling strength when it failed. The bearing failure was probably caused by the primary moment at the loading points. The load was applied through a relatively high eccentricity of 13 mm. At ultimate, the offset load caused the bearing plates to rotate, resulting in concrete spalling and crushing. In practice, the local effect of the primary moment  $P_e$  could be dealt with by proper detailing.

The failure modes were in agreement with the recommendations of the American practice [90]. However, test by Kong et al [58] showed that beams with slenderness ratios as low as 25 and  $e/b$  ratios as low as 0.1 can fail by buckling. This is believed to be due to the quality of concrete used. High strength concrete such as the one used by Kong et al [58] and by the author in series CA beams improves the shear capacity (table 3.2). Consequently, a small eccentricity causes a premature failure by buckling which is less dependent on concrete strength than shear. A low strength concrete, such as the one considered in the PCA Design Aid and used by the author in series CB beams, does not improve the shear capacity and, thus, the specimens may fail in shear or by local crushing at the bearings.

### 5.5.2 ULTIMATE LOADS

Table 5.1 shows the measured ultimate loads of the 7 beams. The ultimate loads estimated from the modified Kong et al equation for shear (equation 4.3) are given in the same table. It can be seen that the beams buckled at loads lower than the ultimate capacities, particularly for higher  $h/b$  ratios. Fig.5.4 shows that, for a constant  $e/b$  ratio, the buckling strength is very much dependent on the slenderness ratio; it decreased sharply as the  $h/b$  ratio increased. The same figure shows that beam CB-40-0.182 had a distinctly low buckling load which was probably due to an experimental error in setting the load-eccentricity. This highlights the need for a higher safety factor in design against buckling, particularly that laboratory conditions can hardly be achieved in practice.

### 5.5.3 LATERAL DEFLECTIONS

Lateral deflections for all the beams were recorded over each support and at mid-span section; the displacement profiles of those sections are shown in fig.5.6 . The maximum deflection often occurred at mid-depth, over one of the supports. At mid-span, the lateral deflection was always maximum at the unrestrained bottom edge and minimum at the restrained top edge. Such restraint was ensured by the relatively closely spaced loading jacks as compared to the widely spaced supports at the bottom.

In general, the deflections were very small until just before failure (see fig.5.6, last load increment) where the beams would creep rapidly towards buckling collapse. This was illustrated by two dial gauges placed on the back. The maximum deflection recorded was 7.6 mm (CB-40-0.182) just prior to failure. To a naked eye, these displacements are not evident and the beam-panel may appear to be straight. Such is the imminent buckling danger without visible warnings.

Curves, load versus maximum lateral displacement at mid-height, were plotted and are shown in fig.5.5. These curves indicate three stages of behaviour :

1. An initial stage where the lateral deflections are relatively small
2. A second stage with increased rate of change of deflection with load
3. A third stage where, following a small increase in load, the deflection would increase continuously until failure. Indeed, just prior to failure, the specimen would creep very fast towards collapse.

Stage 3 behaviour was mainly exhibited by the very slender deep beams (CB-40-0.182, CB-50-0.182, CB-70-0.182 in fig.5.5) for which stages 1 and 2 were relatively short. Beam CB-20-0.182, having the smallest  $h/b$  of 20, did not reach stage three and failed at the bearing while still in stage 2 behaviour. It can be concluded that, for slenderness ratios of 20 or less, buckling may not be the main concern.

## 5.6 PREDICTION OF THE BUCKLING STRENGTH

The buckling loads of the beam panels tested were predicted, using the CIRIA Guide [85] and the PCA Design Aid [88]. These predicted loads were compared to the measured ones to assess the usefulness of the two methods.

### 5.6.1 CIRIA GUIDE METHOD

Strictly speaking, the CIRIA guidelines are intended for designing the reinforcement against buckling and are not directly applicable for predicting ultimate buckling strengths. However, the author, jointly with others, have presented a way of adapting these guidelines to predict the ultimate buckling loads for deep beams (Appendix A). The procedure is clearly explained with illustrative examples in references [59] [60].

Load-moment interaction diagrams are required for the beams. These were constructed in accordance with the 'notes on the derivation of design charts' given in Appendix A of BS 8110 : part 3, using the actual properties of the beams. In practice, the standard column charts in BS 8110 : part 3 could be used. As reviewed previously, three methods are given in the CIRIA Guide, namely :

- The supplementary rules
- The single Panel method
- The two panel method

It is stated that the CIRIA Guide should be used in conjunction with CP 110 : 1972 [36]. However, since this was superseded by BS 8110 : 1985 [16], it is felt more appropriate to use it in conjunction with BS 8110. The CIRIA buckling procedure uses elastic stress distribution; Appendix A of the Guide gives stress distribution for different geometric and loading configurations. Stress distribution from other elastic analysis such as the finite element method can also be used. For the present case, the elastic stress distribution of the beams was taken from fig.57 of the CIRIA Guide.

As mentioned previously, the CIRIA procedure emphasises on the determination of the effective height  $h_e$  which, for series CB test beams (fig.5.1), was 2100 mm from supplementary rules, 1500 mm from the single panel method and 1790 mm from the two panel method (see Appendix A where detailed calculations are carried out for beam CB-40-0.182). In table 5.1, the factors of safety provided by the three methods are indicated by  $R_{sr}$ ,  $R_{sp}$ ,  $R_{tp}$ , where

$$R = \frac{\text{measured buckling load}}{\text{predicted buckling load}}$$

The particular method used to predict the load is indicated by a subscript to R, namely :

$R_{sr}$  : supplementary rules

$R_{sp}$  : single panel method

$R_{tp}$  : two panel method

The following observations can be made :

(i) The three CIRIA methods are conservative, with mean safety factors of  $R_{SR} = 41.1$ ;  $R_{SP} = 19.1$ ;  $R_{TP} = 7.3$ . Comparatively, the two panel method gave the most realistic results. Table 5.1 shows that both the supplementary rules and the single panel method are unduly conservative. It can be argued that, due to the nature of buckling, often sudden, catastrophic and unpredictable, and the rare occurrence in practice of very slender elements, factors of safety such as those achieved by the two panel method could be acceptable. In this matter, Kong et al [58] have argued that the fact that a method is too conservative for some very slender deep beams should not rule out its use.

(ii) For the three methods, the degree of conservatism increases as the  $h/b$  ratio increases. This is inhibited in the additional moment concept which, as pointed out by Cranston [37], yields conservative results for high slenderness ratios.

(iii) For practical design, the two panel method should be used. For the specimens having  $h/b$  ratios between 25 and 40, such method gave a mean safety factor of 5, which is not considered as high for buckling failure. Both the supplementary rules and the single panel method, though easier to use, need more refinement.

#### 5.6.2 PORTLAND CEMENT ASSOCIATION METHOD

To a certain extent, the test specimens were designed to fulfil the requirements of the PCA Design Aid [88]. The material properties and the loading arrangement followed closely those in the PCA document. The section properties, however, were smaller than those covered by the

method. It is believed [58] that the slenderness ratio  $h/b$  and the eccentricity/thickness ratio  $e/b$  are the most important parameters affecting the buckling behaviour. Indeed, a close examination of the PCA design tables reveals that, for the same eccentricity/thickness ratio and the same steel ratio, the load capacity factors are independent of the panel thickness or the eccentricity and depend only on the  $h/b$  ratio. An example for  $e/b = 0.5$  and steel ratio of 0.25 is given below:

b (mm)	e (mm)	(height/thickness) h/b				
		20	30	40	50	
140	70.0	0.110	0.051	0.030	0.017	(table A1)
165	82.5	0.110	0.050	0.026	0.018	(table A5)
190	95.0	0.110	0.054	0.030	0.010	(table A9)

Following this, the use of the PCA method to the present beam-panels seems to be justified. The  $e/b$  ratio of 0.182 adopted in the tests corresponds to table A1 of the PCA Design Aid, which is presented here in a graphical form (fig.5.7).

The reduction factor  $\eta$ , accounting for the isolated footings, was determined from fig.7 of the PCA Design Aid [88] as 0.73. From section 5.3.2 of this chapter, the concentrated loads were considered distributed over an effective width taken as:

$$2 (C + 4b)$$

Where  $C$  is the bearing width = 230 mm in the present tests

$b$  is the beam thickness

hence, for the test beam-panels in table 3.1, the PCA buckling loads are given by :

$$P_{pca} = 0.73 \times 2(230 + 4b) \phi b f'_c \quad 5.14$$

with  $\phi$ , the load capacity coefficient, taken from fig.5.7.

The calculation process is detailed for beam CB-40-0.182 in Appendix A. Table 5.1 shows the ratios of measured buckling loads to the predicted PCA buckling loads; this is indicated by a subscript pca to R. It can be seen from table 5.1 and fig.5.8 that, compared to the CIRIA methods, the PCA method gives a safe and better prediction of the buckling strength and is easier to use. The mean safety factor was 2.76. However, the use of such method is limited by the material properties (concrete strength  $f'_c < 4000$  psi, reinforcement yield strength  $< 60000$  psi), a steel ratio between 0.15 and 0.75, and the loading arrangement (eccentricity at the loads only as in fig.5.1b). Moreover, it considers that the load capacity of a panel having slenderness ratio  $h/b$  higher than 50 is negligible. The present tests, together with those of Kong et al [58], reveal that beam-panels with slenderness ratios as high as 70 (table 3.1, beam CB-70-0.182) and 67 [58] have sensible buckling strengths which should not be neglected in practical design.

In contrast, the CIRIA methods cope with wider ranges for such parameters. The two panel method, though relatively more conservative, could be considered as more suitable for practical use than the PCA method. Of course, for the particular case of tilt-up construction, the latter would be more convenient.

## 5.7 CONCLUSION

For the same load-eccentricity/thickness ratio  $e/b$ , the failure mode is strongly dependent on the slenderness ratio  $h/b$ . Where  $h/b$  was higher than 25 the test beams failed by buckling with a significant reduction in the failure load. For  $h/b$  equal or smaller than 25, failure was other than by buckling. However, the displacement profiles showed a significant lateral deflection for the two beams which did not fail by buckling, indicating that their buckling strength was not much higher, particularly beam CB-25-0.182.

The buckling recommendations in both the CIRIA Guide [85] and the PCA Design Aid [88] were found to be safe. However, for slenderness ratios of around 20, the latter may not be safe, though shear or bearing may be the governing design criterion for such cases.

In general, the buckling loads were better predicted by the PCA method. The disadvantage of this method is that its use is limited as discussed in section 5.6.2. Among the three methods given in the CIRIA Guide, the two panel method is the most realistic, though still conservative for higher  $h/b$  ratios.

The tests showed that buckling failures are in general sudden, catastrophic and difficult to predict. Safety should, then, be the primary aim of a buckling design. For such purpose, it is advisable to use the two panel method of the CIRIA Guide. Where the PCA method is

applicable, an easier and less conservative design would be achieved.

## CHAPTER SIX

### CONTINUOUS DEEP BEAMS - EXPERIMENTAL PROGRAMME-

#### 6.1 INTRODUCTION

Tests on reinforced concrete deep beams are very few compared to the thousand on ordinary beams reported in the literature. It is relatively difficult and rather expensive to carry out tests on large beams in general. The difficulty and the cost involved in testing slender deep beams (discussed in chapter 3) and continuous deep beams are even greater. Damage to equipment and injury to personnel are common factors associated with the tests. Probably for this reason experimental data on continuous deep beams is very scarce, despite that they are more likely to occur in practice than single span beams.

Current design procedures [1] [33] [23] [85] are empirically based on data from single span deep beams and, as a result, could be inadequate for continuous ones [96]. In 1966, Leonhardt and Walther [80] reported tests on two continuous beams with span/depth ratio of 0.9. Recently, 17 continuous beams having span/depth ratios ranging between 2 and 5 were tested in Canada by Rogowsky, MacGregor and Ong [96]. It is believed that these 19 tests represent most of the experimental data available in the literature on continuous concrete deep beams. This highlights the need for more laboratory tests in order to investigate their ultimate load behaviour, where knowledge is still very limited as compared to

elastic behaviour on which more work exists [42] [29] [13] [89].

In this direction, 12 reinforced concrete continuous deep beams were tested to destruction by the present author, using a relatively heavy instrumentation to obtain as much information as possible on the behaviour of the beams at each stage of loading. In addition, 4 similar single span beams were tested in collaboration with an M.Sc student [8] for comparison purposes. These 4 beams form series F and are described in chapter 3. The main parameters considered in this continuous deep beam programme are the effectiveness of the arrangement of web reinforcement, since conflicting opinions on this matter are numerous [96] [64] [65] [100], and the influence of the shear-span/depth ratio.

This study is a part of a long term research programme [53] initiated in the early seventies in the U.K under the direction of Kong [63]. In this chapter, the author's experimental programme on continuous beams is described. However, because of the same procedure used in the making of the beams and the same testing equipment and instrumentation, details given in this chapter hold for the single span deep beam programme in chapters 3 and 5.

## 6.2 DETAILS OF THE TEST SPECIMENS

The test specimens consisted of 12 two-span deep beams, divided into two series, CD and CE, according to geometric considerations (see table 6.1, fig.6.1).

Series CD consisted of 7 beams of height  $h$  960 mm, overall length 2000 mm and span length  $L$  860 mm, giving a span/depth ratio of 0.9. The thickness was constant at 47 mm, giving a height/thickness ratio of around 20 so that the slenderness effect could be at minimum. The shear-span ' $a$ ' and the clear-shear-span ' $x$ ' were kept constant for series CD beams at 430 mm and 200 mm respectively, giving a shear-span/depth ratio  $a/h$  and a clear-shear-span/depth ratio  $x/h$  of 0.45 and 0.21 respectively (fig.6.1, table 6.1).

Series CE consisted of 5 beams of height  $h$  960 mm, overall length 1600 mm and span length  $L$  660 mm, giving a span/depth ratio of 0.69. The thickness was similar to that of series CD beams, 47 mm, and the shear-span ' $a$ ' and the clear-shear-span ' $x$ ' were reduced to 230 mm and 0.0 mm respectively, giving  $a/h$  and  $x/h$  of 0.24 and 0.0 respectively. This is believed to be among the smallest shear-spans ever tested in deep beams.

The beams were tested under two point-loads applied at the top as in fig.6.1 and plate 6.1. The main reinforcement for the maximum positive moments, that is in the spans, consisted of three deformed bars of 12 mm diameter placed close to the soffit and arranged in three layers at 30 mm

spacings. These bars extended from one end of the beam to the other and were left free of anchor plates at both ends. According to conventional elastic analysis of an ordinary two-span beam, the negative moment over the interior support is higher than that at span and was resisted by similar three deformed bars of 12 mm size. These bars were placed at the top in accordance with a normal beam detailing and 2/3 of them were extended to both ends (see fig.6.2).

Various arrangements of web reinforcement were used, including no web reinforcement, minimum and maximum vertical bars, minimum and maximum horizontal bars and minimum and maximum inclined bars, of 6 mm diameter plain round bars for both series. Additional bars were used at the support and loading regions where the concrete is expected to be highly stressed. These consisted of a single layer of a reinforcing cage of 6 mm size bars. In addition, two lifting loops were cast on either ends of each beam to facilitate handling of the beams with an overhead travelling crane. They also helped in securing the beams in the test rig before and after testing. Details of the reinforcement are shown in fig.6.2

The concrete used in making the beams was of moderately high strength, similar to that used in series CC and F of the single span deep beam programme. Details of the mix properties and concrete strengths are given in section 6.5.

### 6.3 BEAM NOTATION

In all the beam notations, the first letter C is of no important significance; it refers to the author's initial and indicates that such beams were cast and tested by him. This is followed by a letter D for continuous deep beams with higher shear-span/depth ratio and a letter E for continuous deep beams with smaller shear-span/depth ratio. After the hyphen, the percentage of web steel is given. The type of arrangement of web reinforcement is indicated after the slash by a letter V for vertical, H for horizontal and I for inclined. For beams without web reinforcement, the number 0.0 follows the hyphen.

For example, CD-0.5/V refers to a continuous deep beam tested with a clear-shear-span/depth ratio of 0.21 and having 0.5 % of vertical bars as web reinforcement. CE-1.0/H refers to a continuous deep beam tested with a clear-shear-span/depth ratio of 0.0 and having 1.0 % of horizontal bars as web reinforcement. CD-0.0 refers to a continuous beam tested with a clear-shear-span/depth ratio of 0.21 and having no web reinforcement.

### 6.4 MATERIALS

#### 6.4.1 CEMENT

Ferrocete rapid hardening Portland cement, conforming to BS 12 :1978 [20] was used in the manufacture of all the beams. This choice was mainly due to the necessity for a quick reuse of the formwork. The cement was supplied by Blue Circle Group in bags of 50 kg and was kept in

a dry place, away from any moisture which might affect its properties.

#### 6.4.2 AGGREGATES

The aggregates consisted of zone-M sand, with 5 mm maximum size, brought from Caistron quarry. The grading of the aggregates was determined by sieve analysis in accordance with BS 882 : 1983 [21] and is shown in fig.6.3.

The sand-based aggregates were used with continuous grading without sieving or grading them. Immediately before mixing, an excess amount of wet sand was spread on the floor and mixed thoroughly for moisture uniformity. The moisture content was then determined using a 'speedy moisture tester' (fig.6.4a). Mixing formulae taking into account the instant moisture content would then be used to determine the mixing proportions. In addition to this, samples would be taken to the oven for 24 hours to determine the oven-dry moisture content and, hence, check the reliability of the 'speedy moisture tester'. It was found that on average, the oven-dry moisture content was 1.42 % higher (see fig.6.4b). This was thought reliable considering the water absorption for an oven-dry aggregates, which would normally be counted for by up to 2.0% allowance.

### 6.4.3 STEEL

High yield deformed bars were used as main reinforcement throughout the test (for both simply supported deep beams and continuous deep beams). Plain round mild steel bars were used as web reinforcement in continuous deep beams and in some simple span beams (series CB and F). High yield deformed bars and hard drawn wires were also used as web reinforcement in the simply supported deep beams (series CC and CA respectively). The yield and ultimate stresses for the steel bars used were determined from tensile tests on bar specimens in accordance with BS 18 : part 2 : 1971 [22] and are given in table 6.2.

## 6.5 CONCRETE DETAILS

### 6.5.1 MIX DESIGN

The concrete mix was usually established from a set of trial mixes after a target strength was set. Three concrete mixes were used throughout the tests described in this thesis, namely, high strength concrete mix (series CA beams), moderately high strength concrete mix (series CC, F, CD, CE beams) and lower strength concrete mix (series CB beams).

The moderately high strength concrete mix was used in the continuous deep beams and consisted of the following properties:

- water/cement ratio of 0.55

- aggregates/cement ratio of 3.5
- a superplasticiser to achieve an acceptable workability. Melment L10, classified as category A superplasticiser [27] was used for this purpose. 25 ml superplasticiser per kg of cement was found to give satisfactory results without causing grout bleeding.

This concrete mix resulted in a 7-day cube strength of 46 N/mm<sup>2</sup>

### 6.5.2 CONCRETE STRENGTH

The strength properties of the concrete at the day of testing for each beam are given in table 6.1. The concrete compressive strength  $f_{cu}$  and the tensile strength  $f_t$  were determined from an average of three (100x100x100) mm cubes each. BS 1881 : part 117 : 1983 [18] allows the determination of the splitting tensile strength from cubes, using the formula

$$f_t = 2F / (\pi l d) \quad 6.1$$

where F is the maximum load applied to the cube

l is the length of the specimen

d is the cross sectional dimension of the specimen

$(\pi/2) \times l d$  represents the effective area resisting

the splitting action.

The author carried out tensile splitting tests on (150x300) mm concrete cylinders and (100x100x100) mm concrete cubes cast from the same high strength concrete mix. The concrete specimens (cylinders and cubes) were tested simultaneously at various ages. The results are shown in

fig.6.5, which gives the concrete splitting tensile strength development with age for the two methods (cylinder splitting and cube splitting). Fig.6.5 shows that about 90% of the tensile strength is achieved at an early age (within 7 days) and is the same for the two methods during that period. After 28 days, the average difference between the two testing methods was less than 7 % of the concrete cylinder splitting strength. This experimental data endorses BS 1881 : part 117 [18] in suggesting that the results of splitting tests on cubes and cylinders are practically the same.

The cylinder compressive strength  $f'_c$ , when needed, was calculated from the cube strength  $f_{cu}$ , using the following equation :

$$f'_c = 0.80 f_{cu} \qquad 6.2$$

This relationship was determined from control tests on 10 (100x100x100) mm cubes and 10 (100x200) mm cylinders carried out by the author and from similar tests by Garcia [47]. In the author's tests, the cylinders were capped with mortar according to BS 1881: part 110: [19]. The results were used to plot the ( $f'_c - f_{cu}$ ) graph shown in fig.6.6 and establish the above relationship.

### 6.5.3 STRESS-STRAIN RELATIONSHIP

The stress-strain characteristics under uniaxial compression for the three types of concrete were determined from 100x200 mm cylinders, capped with mortar according to BS 1881: 1983 [19]. Four TML type PL-30-11 strain gauges with 30 mm gauge length were fixed to the concrete surface, two longitudinally and two transversally, and connected to a 'strain bridge' data logger which would display the reading in microstrain. The load was continuously applied by a digital Avery Denison compression machine which operates in load control only. Consequently, only the ascending portions of the stress-strain curves were determined and are shown in fig.6.7 for the three types of concrete used in the experimental work.

The average values for the modulus of elasticity for the three types of concrete were 31 kN/mm<sup>2</sup>, 28 kN/mm<sup>2</sup>, 24 kN/mm<sup>2</sup> for high strength concrete, moderately high strength concrete and low strength concrete respectively. It can be seen that, although the difference in compressive strength was very high from one type of concrete to the other (average values are 94 N/mm<sup>2</sup>, 58 N/mm<sup>2</sup> and 41 N/mm<sup>2</sup>), the elastic modulus E did not change much. From this, it can be concluded that E does not rise in proportion to strength and hence existing expressions [1] might overestimate the modulus of elasticity for high strength concrete as pointed out in reference [3].

Readings from the transversal strain gauges helped in determining the Poisson's ratio. Average values are 0.23 for high strength concrete and 0.20 for both moderately high and low strength concrete.

## 6.6 BEAM MANUFACTURE

### 6.6.1 FORMWORK

Two sets of formwork with different sizes were used for casting the beams in upright positions so that a close tolerance on their thicknesses could be achieved. Geometric imperfections are not desirable in structural forms in general, and particularly in laboratory tests such as these. The formwork needed to be stiff, carefully designed against lateral deflection from the wet concrete pressure which could produce barrel shaped beams, and allow for close control of the beam dimensions.

Both formworks consisted of two panels fixed to timber whalings and studs stiffened by a rigid steel frames. On one side the frame was welded to the base to hold the formwork in an upright position. The other side could be moved to vary the thickness of the beam and to allow for fixing of the reinforcement and demolding. The base of the formwork was welded to the floor. The surface of the formwork was made of varnished plywood sheets in order to achieve a smooth finish. The thickness of the beams was achieved by end and bottom timber closures accurately cut to the required value. Depending on the size of the formwork, either one or two Dynapac external vibrator type ER02 were

bolted to the steel frame to compact the concrete. Fig.6.8 shows the details of the small formwork and fig.6.9 shows the process of demolding a beam from the big formwork.

#### 6.6.2 CASTING

Before casting, the formwork was oiled and the end and bottom joints were sealed with petroleum jelly to avoid grout leakage. The reinforcing bars were fixed with the help of plastic spacers to hold them in their positions and allow for a concrete cover. The formwork assembly was then tightened up and the required thickness was checked at the top. A close adjustment was made possible by M12 counter bolted tie bolts at the top together with several pieces of timber cut to the required thickness. The sand was then thoroughly mixed for uniformity and the instant moisture determined so that the mix proportions could be established. The concrete was mixed in a 2 cubic-foot pan mixer. The constituents were mixed dry for about 2 minutes after which the correct proportion of water was added and the whole was left mixing for a further 2 minutes. The superplasticiser was then added and the stiff mixture was left until it would become more fluid. Depending on the beam size, one or two batches were required. The concrete was subsequently placed in the formwork with continuous compaction, the control specimens were cast and vibrated and the whole (beam and control specimens ) was covered with a soaked hessian and polythene sheets.

### 6.6.3 CURING

Twenty four hours after casting, the beam and control specimens were demolded and covered again with a damp hessian and polythene sheets for a further six days (fig.6.10). The beam was kept in a vertical position to minimise the warping effect. At the seventh day, the cover was taken off and the beam and control specimens were left to cure in air until the day of testing.

This curing method was compared with another method whereby the control specimens (cubes) were left constantly in water until testing. The control specimens, which consisted of (100x100x100) mm cubes, were tested at various ages. The results are plotted in fig.6.11 which shows that the two curing methods yield similar strengths up to 7 days. Afterwards, the method adopted, namely: moist curing for 7 days and subsequent air curing, resulted in higher strength.

## 6.7 TEST RIG

### 6.7.1 GENERAL ARRANGEMENT OF THE TEST RIG

The general arrangement of the test rig is shown in fig.6.12. It consists of two longitudinal heavy steel beams, top and bottom, connected to two pairs of vertical ties and two pairs of columns by cross beams. High strength friction grip bolts secured all the connections of the rigid testing frame which can accommodate tests up to 6000 kN. A metal

plate is bolted to the underneath of the top longitudinal beam to carry the jacks which themselves are bolted to tolleys. This enables them to move to any desired position within the length of the plate. However, such movement is a limited one and constrained the author from using the same span in series CD and CE of continuous beams.

### 6.7.2 LOADING SYSTEM

A servo-hydraulic jacking system, supplied by Dartec limited, was used for loading. It consisted of two single acting hydraulic jacks, a hydraulic power pack and a control unit as shown in fig.6.13. The two jacks have a capacity of 600 kN each and are mounted vertically (plate 3.1) as explained in section 6.7.1. They are connected at the top by small hydraulic hoses to a common manifold and, thus, exert both the same load. The oil which goes through the piston is returned through low pressure lines to the oil tank. In addition, any cross piston leakage escaping the low pressure return is collected by drain connections and returned to the oil tank. The hydraulic supply is controlled by a servo-valve and the pressure of the fluid is monitored by a pressure transducer.

The control unit (plate 6.2) provides the necessary controls such as the on-off switches, increase-decrease of pressure, operating the oil pump etc... . The pressure is converted automatically into load and displayed as load per each jack. From an LVDT transducer placed on the test specimen and connected<sup>to</sup> the control unit, the vertical deflection is

given by a displacement indicator. In addition, the control unit provides safety shut-down facilities; each time a preset load or displacement was exceeded, the hydraulic pressure was cut off immediately. This facility proved very useful in limiting the damage after failure of the specimen.

The jacks were calibrated every year by Dartec limited as a part of a contract between the university of Newcastle upon Tyne and them as suppliers. In addition, they were occasionally calibrated by the author to check their performance. A typical calibration graph is shown in fig.6.14

### 6.7.3 LOAD AND SUPPORT BEARINGS

In practice, reinforced concrete deep beams could have complex boundary conditions [53]. In laboratory tests, it is common practice to adopt ideally simple conditions such as the ones used by the author (shown in fig.6.15).

The top bearings (fig.6.15a) allowed for vertical displacement and out-of-plane rotation. The upper section (labelled D in fig.6.15a) of each bearing was mounted directly onto the body of the jacks. The lower part of each bearing (labelled E in fig.6.15a) consisted of a plate and a cylindrical segment bolted together through slotted holes to allow for any desirable load-eccentricity. The plate was bonded to the top of the beam at the desired loading position with a quick setting polyester

paste. It was then clamped to the beam sides with steel angles through slotted holes which allowed for different beam thicknesses. The clamping action eliminated the risk of any relative movement between the test specimen and the bearing. The bonding material, which would become very rigid, ensured an evenly loaded bearing area and protected the concrete from direct contact with the steel plates. The friction between the two cylindrical surfaces in fig.6.15a was reduced by the use of polytetrafluoroethylene (PTFE) sheet bearings placed between them and thus, allowed for the out-of-plane rotation.

At the supports, out-of-plane rotation, in-plane rotation and longitudinal translation were allowed for by the bottom bearings, the details of which are shown in fig.6.15b. The bottom bearing assembly consisted of a bearing plate (labelled A in fig.6.15b) bonded to the soffit of the beam with a rigid polyester filler and clamped to the beam sides with steel angles, a rocker bearing (labelled B in fig.6.15b) which allowed for the in-plane rotation, a steel block (labelled D in fig.6.15b) which transferred the load from the rocker bearing onto needle rollers (total of 18 type FF3525) placed in a raceway of hardened steel plates (C and E in fig.6.15b). These needle rollers allowed for the longitudinal translation. Such movement was prevented by clamping bolts during the setting-up of the beam. PTFE sheet bearings provided frictionless contact between the cylindrical surfaces of the bearing plate and the rocker bearing (labelled A and B in fig.6.15b respectively). The bottom bearing assembly rested on concrete blocks, put on the bottom longitudinal steel beam of the test rig (fig.6.12).

For the internal support of the continuous deep beams, a load cell was placed between the bearing assembly and a smaller size concrete block (fig.6.17a) to measure the reaction.

In the present tests, a great precaution was devoted to applying the load and reactions accurately at the desired line of action. A reference axis for the test rig with respect to the centres of the jacks was established, using a theodolite. The support bearing blocks were then aligned with the longitudinal axis of the jacks. This procedure, which was repeated every time the concrete blocks or the jacks were moved, eliminated any misalignment during the testing.

## 6.8 INSTRUMENTATION

### 6.8.1 DISPLACEMENT MEASUREMENTS

In the single span deep beam tests as well as in the continuous deep beams, 15 linear variable displacement transducers (LVDT) were used to measure any lateral deflection. The LVDT's were fixed through aluminium clamps to a purposely erected steel frame alongside the test rig (plate 3.2). They were arranged in three columns on the back of the test beams and could be removed shortly before failure. Fig.6.16 shows their locations in continuous deep beams. The transducers were calibrated individually by the manufacturer and had working range of  $\pm 50$  mm. They were energized by a constant input d.c of 6 volts and their output voltages were recorded by data logger. The vertical displacement was

measured by a similar LVDT placed in the middle of a span and connected to the control unit applying the load.

Mechanical dial gauges of 25 mm travel and 0.01 mm sensitivity were used to record the support settlement (fig.6.17a). For the simple span beams, a pair of similar dial gauges was used to monitor the out of plane movement of each support.

### 6.8.2 STRAIN MEASUREMENTS

On the back faces of the test beams, electrical demountable strain transducers were used to measure the surface concrete strains. For the continuous deep beams, strain transducers were arranged in sets of 45 degrees rosettes to monitor the strains in the inclined load paths defined by the line joining the support and load bearings. In addition, in series CD beams individual strain transducers were used to measure the longitudinal strain distribution at mid-span. The arrangement and location of the strain transducers in continuous deep beams is shown in fig.6.16.

These demountable strain transducers were originally developed by Cook [35] at the Cement and Concrete Association. Those used by the author were manufactured in the Civil Engineering Department at the university of Newcastle upon Tyne. The general arrangement and dimensions of the strain transducers used in the present tests are shown in fig.6.18a. Each transducer has a gauge length of 100 mm and consists of an aluminium

strip, 6 blocks and two conical pins glued together by a super-glue (cyanoacrylate). Four electrical resistance strain gauges type N11-FA-5-120-23 with 5 mm gauge length, supplied by Showa Measuring Instrument co. limited, were bonded in pairs on either side of the flexible strip using cyanoacrylate glue. The four gauges were wired up in full bridge circuit which is thought to be sensitive to the bending strain induced in the strip and insensitive to any axial strain. The bridge circuit was energized by a constant input of 6 volts d.c. supply connected to a data logger. Demec studs were glued on the concrete surface in 100 mm gauge length and the transducer was held against them through the conical pins by means of restraining springs bonded to the concrete (fig.6.18b). Any change in the gauge length will cause the aluminium strip to bend. Such bending will cause a change in electrical resistance and thus, the voltage of the strain gauge which is scanned by the data logger.

The transducers were individually calibrated using an extensometer as seen in fig.6.18c. They were attached to demec studs in the same manner as they would be fixed to the test beam and a micrometer was used to vary the gauge length and hence apply direct strains. The output voltages from the data logger and the corresponding strains from the micrometer were used to plot calibration graphs. A typical one is shown in fig.6.18d. The calibration procedure was repeated after each series of tests.

The advantage of using this type of strain measuring device was that after a brutal failure of the test beams, the transducer, if broken, would be reduced to its components which could be reassembled with the cyanoacrylate glue.

On the front faces of all the test beams, 4 inches mechanical strain gauge (demec gauge) with a gauge factor of  $2 \times 10^{-5}$  was used to measure the strains at various locations, particularly at the level of main tension reinforcement and along the depth at mid span. Fig.6.16 shows the location of the demec gauge readings in continuous deep beams. The mechanical gauge-based strain measurements were preferred on the front mainly to allow for clear marking of the cracks pattern and crack width measurement.

### 6.8.3 CRACK WIDTH MEASUREMENTS

Throughout the tests, particular attention was devoted to measuring crack widths, using a hand microscope, specification Ultra Lomara 250b. The microscope has a magnification of 40 times and an accuracy of 0.01 mm.

#### 6.8.4 REACTION MEASUREMENTS

In an aim to measure the reaction distribution in continuous deep beams, 100 ton capacity load cell was used at the interior support, between the concrete block and the bearing assembly (fig.6.17a). The load cell was calibrated before the tests, using the Avery compression machine, and was found very reliable (fig.6.17b). One of the purposes of the calibration was to have an idea about the settlement of the load cell. Previous elastic work [85] predicted that differential settlement could be critical for multiple supports deep beams. It was found from the calibration that up to a load of 350 kN, which is the range of the maximum reaction recorded in the test, the load cell settlement was below 0.3 mm.

From geometric and loading symmetry (see fig.6.1), the reactions of the two exterior supports were assumed equal and were not measured.

#### 6.8.5 DATA LOGGING EQUIPMENT

A Solartron Merlyn system, consisting of an adjustable d.c. voltage supply, an integrated measurement unit and an apple II micro-computer (plates 6.2), was used to record the data. The integrated measurement unit has a capacity of 64 channels, of which, 15 were used for the displacement transducers and 36 for strain transducers. The software controlling the data recording system was supplied with the equipment by Solartron Instrumentation Group. The software was fed to the computer

through a diskette to select the channels used and to set up the required measurement conditions. Instructions typed into the computer were then transmitted to the integrated measurement unit which scans the selected channels at high speed and send back the information to the computer which outputs the data as voltage in a printer, a Video Display Unit and a diskette. Displacements and strains were determined afterwards using the appropriate calibration factors.

#### 6.9 PREPARATION AND TESTING OF THE BEAMS

A few days before testing, the locations of strain measurements were marked on the beam. Demec studs were bonded with rapid-hardening araldite at the required locations on the concrete surface and the beam was whitewashed with an emulsion paint to facilitate cracks observation. A grid of 100x100 mm was then drawn on each face so that the cracks could be accurately located during the testing. Next, the restraining springs for the demountable strain transducers were glued to the concrete with araldite and the exact loading and support positions were established. In the single span deep beams, these positions were identified by recesses (local thickening of concrete) permanently incorporated in the formwork (fig.6.8) to prevent bearing failure. Due to the different geometric dimensions, these recesses could not be used in continuous deep beams. Lines were marked on the loading and support locations as references for either concentric or eccentric (series CB) loads and reactions. After that the top bearings were bonded to their positions with a quick setting polyester paste and clamped with steel angles. At

this stage, for single span beams, the specimen could be lifted to the test rig, secured with safety ropes and a clamp, then the bottom bearings would be bonded to the beam. For continuous beams, the rather difficult procedure of fixing the bottom bearing would be started with the interior one before the beam is in the test rig. Once the bonding material is hard enough, the beam is lifted to the rig and the two end bearings were accurately placed with the help of a hand operated Enerpac jack which lifts the relevant beam end.

Probably one of the most difficult tasks in testing multiple supports beams is to ensure that all the supports are at the same level. For this purpose, a theodolite was used to check the level of the three supports after the bearings were placed. 1 and 2 mm aluminium plates were used between the bearing assembly and the concrete blocks to adjust the level.

A final adjustment to ensure the alignment of the centre line of the bearing assembly with that of the longitudinal axis of the jacks (reference axis) was then made. After this, the dial gauges, the LVDT's and the strain transducers were secured in their positions. The testing would then begin after switching the load control unit and the data recording equipment on to warm up for few minutes. Operating the load control unit is itself a complicated process and took the author one full month to learn; particularly that the instructions manual supplied with the equipment was found misleading and not of straightforward application. After the jacks come down into contact with the beam, the bolts restraining the movement of the bearings were released, the clamp

securing the beam was removed and the initial readings were taken, the load was then applied in 50 kN increments. After each increment, the following measurements were taken

- load applied by each jack, read from the indicator on the control unit.
- Vertical deflection at mid-span read from the displacement indicator on the control unit.
- LVDT's and strain transducers were scanned and the voltage outputs recorded
- The internal support reaction was read from a load cell indicator
- dial gauge readings were taken for support settlement and for support movement in the case of single span beams
- Demec gauge readings were taken for the strain measurements on the front face
- The cracks were marked on the beam and graphically recorded on paper
- the crack widths were measured with the hand microscope.

In addition, photographs illustrating the cracks development were taken at each load increment.

The time required for the testing procedure varied between 3 and 5 hours. After the test, photographic records were taken, the tested beam was then lifted away from the testing frame, and the bearing plates and restraining springs were removed to be cleaned for future reuse.

The concrete control specimens for strengths were tested on the same day as the beam.

## CHAPTER SEVEN

### CONTINUOUS DEEP BEAMS - BEHAVIOUR UNDER LOAD AND TEST RESULTS -

#### 7.1 INTRODUCTION

The experimental program<sup>me</sup> is described in chapter 6. In this chapter, the behaviour of the 12 continuous deep beams is described and their test results are presented and discussed. Based on the test results and observations, design recommendations for continuous concrete deep beams are given in chapter 8.

#### 7.2 FORMATION OF CRACKS AND CAUSES OF FAILURE

The cracks patterns at failure of the 12 beams are shown in Fig.7.1. The load at which each crack was first observed is indicated together with the extent of the crack at that load.

Despite differences in web reinforcement, layout and quantity, the cracks patterns of series CD beams are similar. Those of series CE are similar between them but differ to a certain extent from those of series CD, particularly in orientation. This suggests that both the geometry and the loading characteristics have an influence on the behaviour of the beams. Such factors are usually taken into account by the parameters  $L/h$  and  $a/h$ , span/depth ratio and shear-span/depth ratio respectively. In the present tests, it was not attempted to isolate the effects of the two

parameters. It is, however, reported in the literature [66] that the latter parameter is more important in that it is a good indicator of the direction of the diagonal cracks.

Before describing the cracking behaviour, it is worth defining some terms which are repeatedly used in this work.

**Flexural cracks:** vertical cracks which form as a result of tensile stresses caused by bending action. They usually form at the maximum bending moment regions and are short at formation.

**Inclined cracks:** Cracks which form as a result of combined actions of shear and bending within the shear-span. They usually form at or very near the soffit of the beam in the vicinity of the support and are inclined towards the loading points.

**Diagonal cracks:** Cracks which form within the shear-span as a result of inclined tensile stresses caused by the direct transfer of load from the loading point to the support. These cracks are characterised by a loud cracking noise and are long at formation. They are parallel to the direction of load - support and initiate at about  $0.3h$  to  $0.4h$  from the soffit. A diagonal crack is harmful if not restrained by effective web reinforcement.

It is also important to distinguish between two modes of failure common in deep beams but which are often considered as the same by many researchers who identify them simply as bearing failure. In the present

continuous deep beam tests, observation on the cracks development during the testing procedure and crack width measurements revealed that a beam could fail by crushing at the bearing in two ways:

- After a relatively wide diagonal crack extends deeper into the compression zone at a bearing point. This often occurred when no or less effective web reinforcement was present. Such failure is defined here as shear-bearing failure.
- When the diagonal cracks are effectively restrained by web reinforcement, they hardly reach the compression zone and, even when they do so, they may not precipitate the crushing of concrete there. Following this, if bearing failure occurs, it is because the concrete is exhausted and has reached its ultimate strain in this area. Such failure is termed proper bearing failure in this work and is characterised by a relatively higher load.

These two types of failure occurred repeatedly in the present tests as discussed later.

According to Kong et al [66] [67] [69] who used cine-camera to record support crushing failure, these two failure modes are quite different from each other. They pointed out that a proper crushing at a load bearing block occurs only in the presence of highly effective web reinforcement and that most of the so-called crushing failures in deep beams fit into the first definition, namely shear-bearing, identified as mode 3 by the authors (see chapter 4).

In general, flexural cracks appeared first in the span in the region of maximum bending moment and away from it, at locations where the latter is supposed to be very small or hogging. This can be clearly seen from the cracks patterns in fig.7.1, where the spread of the flexural cracks over the spans revealed that the regions which in theory should have been under compression were in reality under tension. The next cracks to form were the inclined ones, usually near the inside edge of the supports. At higher loads, diagonal cracks would form, often accompanied by a loud noise. These were the widest and the longest of the three types at formation. At subsequent loading, more diagonal cracks appeared and the crack width increased. Finally, depending on the effectiveness of web reinforcement arrangement, the specimens collapsed in one of the two failure modes described above.

Because few tests have been carried out on continuous deep beams, it was thought useful to describe the cracking behaviour of each beam up to failure before making a summary of the principal characteristics.

#### Series CD beams

##### CD-0.5/V

The load was applied in 50 kN increments. At 150 kN, the first flexural cracks appeared in the spans despite that according to the shallow beam bending moment distribution, the flexural cracks should appear first above the internal support where the hogging moment would be higher. As can be seen from Fig.7.1, these cracks were small and very narrow at formation. They did not form only at the location where the

span moment was maximum but also at locations where the bending moment was expected to be close to null or hogging. While the load was maintained at 150 kN, a very loud diagonal crack formed at the left interior shear-span. It appeared very long,  $0.95h$ , and relatively wide, 0.4 mm. At 200 kN, more flexural cracks formed at the soffit and new types of cracks appeared near the supports and tended to incline towards the loading points. One flexural crack formed within the right interior shear-span and extended to just below the right support in a similar way as a diagonal crack. At 300 kN, a long diagonal crack formed within the left shear-span, extending from the support to about 100 mm below the loading point. The crack width reached 0.55 mm at about 400 mm up from the soffit at the left interior shear-span. The flexural cracks reached 0.1 mm in width and tended to close up as diagonal cracks developed on both sides of a span. Up to this level of loading only two tiny cracks formed at the top. Subsequent loading resulted only in the widening of the diagonal cracks, the maximum width of which reached 1.0 mm at 650 kN. Concrete spalling started at this load along the left interior diagonal crack. At 800 kN, a very long and wide (2.0 mm) diagonal crack formed at the right end shear-span, extending from support to loading point. As this load was maintained for measurements to be taken, the beam crushed at the right loading point. It was thought that such bearing failure was precipitated by the extension of the wide crack deep into the bearing area. Prior to failure the concrete was spalling severely along the crack at the left interior shear-span which reached 1.1 mm in width at 700 kN. The cracks pattern of the beam (Fig.7.1) reveals clearly a 'truss frame' with major cracks running diagonally from load point to the

nearest supports and small flexural and inclined cracks at the bottom from one end of the beam to the other. The concrete at the top central region was not cracked and contrary to the theory, no or very small tensile stresses seemed to be acting there. At the bottom, a value of 1197 micro-strain was recorded along the tensile steel.

#### CD-0.5/H

At 50 kN, a vertical crack developed above the interior support, running from soffit to top with a maximum width of 0.1 mm at 300 mm up from the bottom. This was believed to be the result of 0.05 mm differential settlement at that load. At 100 kN, flexural cracks formed at the spans in a similar way as CD-0.5/V. They were narrow at formation, 0.02mm, and relatively short. At the same load, a flexural crack within the left interior shear-span developed into a diagonal one, extending upward towards the loading point. Its maximum width reached 0.15 mm. At subsequent loadings, more flexural and inclined cracks formed at the spans with one of them develop~~ing~~ into a diagonal crack on the right interior shear-span at 150 kN. The serviceability limit state of cracking, preset at 0.3 mm by BS 8110 [16], was reached at 250 kN. At 800 kN, a diagonal crack developed loudly on the left end shear-span extending deep into the load bearing zone, with a maximum width of 0.7 mm. At this load level the cracks were finely distributed at the bottom spans, with inclined cracks at the faces of supports bending towards the loading points and small narrow flexural cracks (0.12 mm maximum crack width) in between. In addition to the long crack which crossed the whole depth, two small cracks formed at the top at the early

stages of loading but did not expand nor widen as the load was increased. The cracks distribution suggests that the beam was in tension from one end support to the other at the bottom while above the interior support at the top, such expected tension was negligible, even at ultimate. At 850 kN the beam crushed at the left loading point and split along a diagonal crack. The tensile strain at the bottom reached 1283 micro-strain at ultimate. In this beam, horizontal web reinforcement helped to restrain the diagonal cracks which stayed relatively narrow (just above 0.7 mm at ultimate) compared to CD-0.5/V with the same amount of steel used vertically (2.0 mm at ultimate).

#### CD-0.5/I

In this beam, inclined web reinforcement was arranged so as to be perpendicular to the line joining the centres of the support and bearing points since from observation on single span beam (chapter 3), the diagonal cracks are most likely to be parallel to that line. The same amount of web steel (0.5% in volume) as the two previous beams, namely CD-0.5/V and CD-0.5/H, was used. The reinforcement arrangement is shown in Fig 6.2.

At 150 kN, flexural cracks appeared at the bottom in the spans with a maximum width of 0.08 mm. At the same load, a vertical crack formed above the interior support and almost reached mid-depth. At 250 kN, more flexural cracks spread along the spans, giving sign that the shallow beam bending moment distribution may not be valid for this kind of beams. In the shear spans inclined cracks started to develop at the top of flexural cracks. Subsequent loadings resulted in more flexural and inclined

cracks, both of which stayed very narrow. At 700 kN, the maximum crack width was 0.28 mm compared to 1.1 mm in the beam with the same amount of web steel used vertically, CD-0.5/V, and 0.6 mm in that having the same amount horizontally, CD-0.5/H. The diagonal cracks, the first of which occurred at 750 kN at the right end shear-span, were very much delayed by the use of inclined bars. At 800 kN another diagonal crack formed loudly on the left. These diagonal cracks did not go deeper into the loading zone and were very much restrained. Their maximum width reached 0.38 mm at 900 kN at about 0.4h from the soffit. At 1000 kN, the cracks pattern was that of two-fan shapes from the spans towards the corresponding loading points. At the top, above the internal support, the concrete was still not cracked, a sign of non-existence of any hogging moment or if it existed it was negligible. The major cracks were still effectively restrained (0.4 mm maximum crack width). At this load the concrete in the bearing area at the left loading point reached its ultimate and crushed.

#### CD-1.0/V

In this beam, the quantity of web steel was increased to 1.0% in the form of vertical bars. This caused some shrinkage cracks to form, one of which crossed the whole depth along the position of a vertical bar at the left interior shear-span. With no horizontal bars present, this crack was fairly wide, particularly at mid-depth. Located in the path of a direct load transfer from loading point to support, it started to open soon after the application of the load. At 200 kN, the existing crack developed into a diagonal one, inclining towards the loading point at the

top and the support at the bottom and reached 0.55 mm in width. Flexural cracks had formed at 100 kN in the middle of the left span and spread over both spans as the load reached 250 kN. A vertical crack formed above the internal support at 200 kN, initiating at about 120 mm up and reaching just below mid-depth at 250 kN. At the same load, a flexural crack within the right interior shear-span developed into a diagonal one, bending towards the right support. At 350 kN, a long diagonal crack formed on the left end shear-span with a big noise. Concrete spalling started along the diagonal crack on the left interior shear-span which was 0.7 mm wide. At 550 kN, the diagonal crack width reached a maximum of 1.1 mm. Final failure occurred as a result of the opening of this diagonal crack at the left interior shear-span, almost splitting the beam, and its extension deeper into the load bearing area at a comparatively smaller load of 600 kN. The concrete at the hogging moment region was undisturbed by the loading and was uncracked at failure.

#### CD-1.0/H

The concrete web of this beam was reinforced with 1.0% of horizontal bars. Flexural cracks formed at 100 kN in both spans, even at regions where the theoretical bending moment was close to null or hogging. A flexural crack within the left interior shear span developed into a diagonal crack and extended upwards bending towards the left support; it appeared very narrow (0.05 mm). The flexural crack width was 0.02 mm when first formed. Earlier, a vertical crack had formed above the internal support. Subsequent loading resulted in the formation of inclined cracks near the faces of supports and more flexural cracks in

both spans. At 400 kN, a diagonal crack formed loudly on the left, extending from just above the support to just below the loading point (0.9h) and forming an angle of 70 degrees with the horizontal. This diagonal crack appeared relatively narrow (0.10 mm) compared to those in beams with vertical bars where their width often exceeded 0.3 mm at formation. At 450 kN, a similar diagonal crack appeared on the right. The horizontal bars used in this beam, though did not delay the formation of diagonal cracks, seemed to restrain effectively their width which was 0.16 mm at this load level compared to 0.95 mm in the corresponding beam with vertical bars, CD-1.0/V, and was comparable to that in beam having half the amount of web steel in the form of inclined bars (0.18 mm in CD-0.5/I). The serviceability limit state of cracking was reached at a high load of 800 kN compared to CD-1.0/V where such limit was exceeded at the early stages of loading. At this load level, the two fan-shapes were clearly defined above both spans and no cracking occurred at the top. Failure occurred at 850 kN by concrete crushing at the loading area on the left. It is to be noted that, despite a diagonal crack reaching the loading area, it was very narrow at the top to precipitate the crushing. At failure, the concrete burst beneath the loading plates, spalling sideways and leaving a wedge shape in the middle.

#### CD-1.0/I

In this beam, 1.0% of inclined steel placed in a similar way as in CD-0.5/I (Fig.6.2) was used to reinforce the concrete web against potential cracks. As a result, not only they were effectively restrained, 0.38 mm at 950 kN, but also the shortest in length. At

failure the diagonal cracks reached  $2/3$  of the depth up from the soffit. Their formation was delayed compared to the beams with other types of web reinforcement. Flexural cracks spread throughout the two-spans and, as in all the beams tested, a vertical crack formed above the interior support, reaching just below mid-depth. The flexural cracks did not follow the theoretical bending moment distribution, and no cracks formed at the hogging region whatsoever. At 1020 kN, the concrete failed at the left loading point, spalling sideways and leaving a form of wedge in the middle in a similar manner to beams CD-0.5/I and CD-1.0/H. The two fan shapes above both spans were clearly defined by the cracks, though not reaching the loading points as in other beams. This type of reinforcement proved very efficient in restraining the diagonal cracks which in most other beams, and indeed in deep beams in general, seem to be the main cause of failure.

#### CD-0.0

The concrete web of this beam did not have any reinforcement. It has always been a subject of argument by many researchers as to whether or not web reinforcement does contribute to the strength of a deep beam and what is the most effective way of reinforcing it. This point has already been dealt with in chapter 4 with single span beams and is further looked at in this continuous deep beam programme.

Flexural cracks formed as in other beams at a load of 150 kN with a maximum width of 0.04 mm. At the same load, a vertical crack appeared above the interior support and developed soon into a very brittle diagonal crack, bending towards the right support. Its width

reached 0.3 mm, the serviceability limit state of cracking. This was the same load level at which this crack width limit was reached in beams with vertical bars (CD-0.5/V, CD-1.0/V). In contrast, such limit was reached at 800 kN in beams CD-1.0/H and CD-1.0/I. At subsequent loadings, more diagonal cracks were formed in the shear spans, extending the full length from supports to loading points and opening wider. At 600 kN, the maximum crack width was 1.0 mm and spalling of concrete started along the widest crack. At 800 kN the diagonal cracks were wide open and danger was felt. The beam failed at the top of the crack on the right interior shear-span after it had extended to the loading area. Just prior to failure, three small cracks appeared at the top hogging moment region.

#### Series CE beams

In this series, the loading points were closer to the end supports, resulting in an end shear-span of 0.24 and a clear-shear-span of 0.). The interior shear-span was kept the same as in series CD beams (Fig.6.1). The specimens were reduced in spans due to the limitation of the test rig.

Because of the smaller shear span, the diagonal cracks were expected to be almost vertical and, consequently, no inclined web reinforcement was used since horizontal bars would be nearly normal to those cracks.

#### CE-0.5/V

Since the shear arm was smaller in this series, the flexural cracks were expected to be delayed. Indeed, in this beam, flexural cracks formed after inclined cracks at 300 kN compared to 150 kN in CD beams

(table 7.1). Earlier, a vertical crack appeared above the internal support in a similar way as in CD beams and extended across the full depth at subsequent load increment. The first diagonal crack developed on the left end shear-span with a loud noise at 400 kN with a maximum width of 0.3mm at formation. At 500 kN, another diagonal crack formed loudly on the right interior shear-span, running from support to loading point. At this load level, two small cracks formed at the top part of the beam. At the spans, the cracks were finely distributed from one end of the beam to the other, in complete disagreement with the shallow beam bending moment distribution. The beam finally failed at 650 kN after the right interior diagonal crack opened wider and extended deep into the loading area, resulting in the crushing of concrete there.

#### CE-0.5/H

Flexural cracks appeared very narrow (0.02 mm) at the soffit, directly below the loading point, at 200 kN and spread at subsequent loadings throughout both spans. They reached a maximum of 0.1 mm in width and tended to close up after diagonal cracking. At 300 kN, a vertical crack developed with a maximum width of 0.08 mm above the interior support. The first diagonal crack formed at the left end shear-span, from support to about 100 mm below the loading point at 350 kN. At 500 kN a similar diagonal crack appeared on the right end shear-span. The serviceability limit state of cracking of 0.3 mm was reached at 600 kN; at 800 kN, the maximum crack width was 0.4 mm. The beam failed while the load was maintained at 800 kN at the load bearing area on the right. It was thought that the diagonal crack, though exceeded the serviceability limit

state of cracking, did not precipitate failure. No flexural cracks formed at the top central part of the beam.

#### CE-1.0/V

Short and narrow flexural cracks formed in both spans at 200 kN together with a vertical crack, 0.1 mm wide, above the interior support which crossed the whole depth. More flexural cracks formed at subsequent loadings at the soffit. The first diagonal crack opened suddenly on the left at 400 kN with a maximum width of 0.6 mm between 0.35h and 0.65h up from the bottom and extended into the bearing areas at both ends. This diagonal crack widened as the load was further increased, reaching 1.0 mm at 700 kN. Final failure occurred at the top of this crack by concrete spalling and crushing. In this beam, more flexural cracks formed at the top above the interior support, spreading almost all the way between the loading points at higher loads.

#### CE-1.0/H

In this beam, the cracks pattern resembles that of a single span beam, with no major cracks at the interior shear-spans and no cracks at the top central part of the beam. Diagonal cracks formed at both ends before failure but were restrained in width by the horizontal web bars. Failure occurred by proper concrete crushing at the right loading area at 924 kN.

#### CE-0.0

No web reinforcement was used in this beam, and consequently the vertical crack which formed above the interior support crossed the whole

depth and widened, reaching a maximum of 0.3 mm at 350 kN. Flexural cracks formed at 300 kN in both spans and at the top above the interior support. A diagonal crack developed wider (0.4 mm) on the right, running from support to loading point. At 500 kN, a flexural crack on the left end shear-span developed into a diagonal one, extending deep into the left loading area. It opened wider at subsequent loadings, reaching 1.0 mm at 800 kN and brought about concrete failure at the loading zone on the right.

The cracks patterns of series CE beams reveal that the bulk of the load was transmitted to the supports through the end shear-spans. Indeed, in almost all the CE-beams, diagonal cracks occurred in the end shear-spans only. According to the theory of shallow beams, the loading of series CE should have resulted in an even transfer of load through both, end and interior, shear spans (see table 7.3)

The general behaviour can be summarized as follows:

1. Flexural cracks were in general the first to appear. However, their formation was not in accordance with the shallow beam bending moment distribution which predicts cracking at the top part of the beam above the interior support. Instead these flexural cracks formed only at the soffit and spread over the whole span. According to the shallow beam bending moment distribution, the span regions next to the interior support should be under compression, with a hogging moment at the top (fig.7.6). All the beams tested had flexural cracks up to the faces of supports and uncracked concrete at the top.

Earlier, Leonhardt and Walther [80] argued that the bending moment distribution in continuous deep beams is completely different from that of shallow beams. A close examination of the cracks patterns of their two specimens tested reveals a similar distribution of flexural cracks at the spans and practically none at the top. In the moderately deep beams tested by Rogowsky et al [96] [97], the flexural behaviour was in a "transition" between that of shallow beams and deeper beams. Indeed, with span/depth ratios ranging from 2.0 to 5.0 (as compared to 0.9 and 0.69 in the present tests and 0.9 in Leonhardt and Walther's), flexural cracks formed at the spans and at the hogging regions above the interior support. It was reported, however, that the bending moments were different from those of shallow beams and were higher in the spans than at the support.

2. One factor which has contributed to the change in bending moment distribution was the differential settlement between supports. Indeed, the present beams together with those of Leonhardt and Walther were allowed to settle. The average values of differential settlement were 0.29 mm and 0.21 mm in series CD and CE respectively. In Rogowsky et al tests [96] "Care was taken" to reduce differential settlement. In addition, the stiffnesses of their beams were small compared to those of the author's beams and, consequently, the settlement effect would be less critical in Rogowsky et al's beams. This explains the slight difference in flexural behaviour in the two tests.
3. Flexural cracks formed at tensile stresses ranging from  $2.0 \text{ N/mm}^2$  to  $3.4 \text{ N/mm}^2$  and were small at formation. Typically, their width

was 0.02 mm when first formed and reached a maximum of 0.1 mm before decreasing after formation of diagonal cracks on both shear spans. Occasionally (with vertical web bars and with no web reinforcement), they exceeded 0.1 mm but were never wide enough to cause failure. This suggests that for beams in the deeper range, flexural failure may not be a problem. Tensile strains very rarely reached 2000 micro-strain at the bottom.

4. Inclined cracks are another harmless type of cracks which form near the faces of supports and bend towards the loading points. They usually appeared after flexural cracks. However, with the smaller shear arms of series CE beams, they were the first to manifest, suggesting that they are more closely related to the shear force than bending moment, though the rather complex interaction of the effects which result in their formation is still not fully understood.
5. Most of the beams cracked vertically above the interior support at the early stages of loading. In beams without or with vertical web reinforcement, these cracks often crossed the full depth and reached up to 0.3 mm in width before closing up after full development of diagonal cracks. Such cracking was also reported by Leonhardt and Walther [80] but did not form in Rogowsky et al beams [96] [97]. Differential settlement is believed to be the cause of this type of vertical cracks.
6. The behaviour of continuous deep beams and, indeed in deep beams in general, depends more on the diagonal cracks which form as a result of the direct transfer of load from loading points to supports. It is argued [52] that, when the strut between the loading and support

points reaches its capacity, the concrete reaches its tensile splitting strength resulting in the formation of a diagonal crack which develops in a 'splitting fashion'. In the present tests, with equal end and interior shear-spans (series CD), diagonal cracks formed earlier at the interior shear-spans than at the end ones. This was probably due to differential settlement, resulting in more tensile stresses being added to those created by the diagonal compression. Plate 7.1 shows the progressive development of the three types of cracks with the loadings.

7. Typically, the maximum width of a diagonal crack when first formed varied between 0.1 mm and 0.2 mm where inclined or horizontal web bars were used and rarely exceeded 0.4 mm at failure. Where vertical web bars or no web reinforcement were used, it was always above 0.3 mm in width and exceeded 1.1 mm at failure.
8. When not effectively restrained, these diagonal cracks opened wider and extended deep into the compression zones at both ends, resulting in concrete crushing at the highly stressed areas of the loading points. Plate 7.2a shows a typical case of such failure.
9. In the presence of horizontal web reinforcement (1.0%) and particularly with inclined web reinforcement, the diagonal cracks were very much restrained and did not cause collapse. The ultimate loads of the corresponding beams (CD-0.5/I, CD-1.0/H, CD-1.0/I, CE-1.0/H) were relatively higher and final failure occurred by proper crushing of the concrete at a load bearing area. This was characterised by the formation of a concrete wedge, as reported by Wong [115], clearly noticeable after failure. A typical example of

such proper crushing is shown in plate 7.2b

### 7.3 CONTROL OF CRACKS

Cracks are commonly regarded as a source of concern among designers not only because of the possibility of corrosive action on the reinforcement but also because they reduce the stiffness of a concrete member. Beeby [11] pointed out, however, that cracks simply initiate the corrosion process, and that limiting the crack width is not necessarily a protective measure against corrosion. He argues that appearance and water tightness would be the two possible reasons for limiting crack width. The present tests showed that cracks may suddenly open wider and extend into critical areas, leading to catastrophic failures. Thus, safety appears to be the primary reason for controlling cracks.

In the test beams, cracks of 0.02 mm width were easily detected and the widest cracks were always the diagonal ones. Fig.7.2 shows the maximum crack widths for the two series of beams. Considering series CD beams, it can be clearly seen from fig.7.2a that inclined web reinforcement is the most effective arrangement that controls cracks in the concrete web of a deep beam. Horizontal bars are the next most effective. Vertical bars are not effective and, when used in greater number, may have an adverse effect on the serviceability and strength of the beams (CD-1.0/V in fig.7.2). The negative effects of vertical bars were also discussed in chapter 4 for the single span beams (CC-1.93/V).

Table 7.1 gives the loads at which both the 0.1 mm crack width limit, often required for liquid retaining structures, and the 0.3 mm crack width limit, required for all concrete structures under normal environment conditions, were reached in the tested beams. It can be seen from table 7.1 that in beams with no web reinforcement and in those with vertical web bars the 0.3 mm crack width loads were comparable and the smallest. In these beams, the diagonal cracks were often very brittle. Beams with both 0.5% and 1.0% of inclined bars and those with 1.0% of horizontal bars had the highest service loads. This is in line with the recommendations of the CIRIA Guide [85] and ACI (318-83) (revised 1986) [1] both of which emphasize on the use of horizontal bars and recognize the deficiency of vertical ones at lower shear-span/depth ratios. In contrast, Rogowsky et al [96] [97] think that strength improvement can only be achieved with vertical bars and recommend their use for beams even at the deeper range.

#### 7.4 MEASURED LOADS

##### 7.4.1 DIAGONAL CRACKING LOADS

A diagonal cracking load is defined here as the load at which the first major crack forms within a shear span. The diagonal cracking loads of both, end shear-span and interior shear-span for all the continuous beams tested are given in table 7.1. It can be seen from that table that, with equal end and interior shear-span (series CD beams), the diagonal cracking loads of the interior shear spans are lower than those

of the end ones. This was thought to be due to the effect of differential settlement at the interior support which will be discussed later. The diagonal cracks and their formation were similar to those in the single span beams described in chapter 3.

#### 7.4.2 ULTIMATE LOADS

The important strength reserve, commonly associated with single span deep beams, was also exhibited by the 12 continuous deep beams tested. Table 7.1 shows that the ultimate loads were in general more than twice the cracking loads of the end shear-spans and more than three times those at the interior shear spans even in beams without web reinforcement. This is in sharp contrast with the revised edition of the ACI code [1] which does not allow for such strength reserve.

It is argued that web reinforcement may not increase the ultimate strength of a deep beam [23] [32] [76] and can only limit the crack width and provide some ductility. The present tests showed that restraining the crack width is in itself a contribution towards an improvement of the ultimate strength. An increase of 25% in strength was achieved when inclined web reinforcement was used (CD-0.5/I and CD-1.0/I compared to CD-0.0). With horizontal bars, the strength increase was reduced to just over 6% (CD-0.5H, CD-1.0/H). In beam CE-1.0/H where horizontal bars were more nearly perpendicular to the major inclined cracks, the strength increase was 15.5%. From this, it can be concluded that using a suitable arrangement of web reinforcement does increase the ultimate strength of

deep beams. Kong et al [64] reported test results with a strength increase of more than 30% when inclined web reinforcement was used.

## 7.5 SETTLEMENT AT SUPPORTS

Deep beams are very sensitive to differential settlement because of their high stiffnesses. In real structures, differential settlement may be caused by foundation settlements or shortening at supports.

In the present tests, differential settlement was intentionally allowed to occur in order to study its effect on reactions, bending moment distribution and cracking. It was mainly due to the settlement of the load cell placed underneath the steel bearing assembly at the interior support and, to a lesser extent, the difference in size of the concrete support blocks which were identical at the ends and smaller at the interior (see fig.6.17a).

Fig.7.3 shows the total settlement at the interior support, the settlement of an exterior support and the difference between them presented in forms of histograms. It is to be noted that, within the sensitivity of the dial gauges ( $\pm 0.01$  mm), the settlement of the two end supports were identical. As expected, differential settlements were higher in series CD beams because of higher reactions at the interior support and hence their more pronounced effects (see section 7.6). Differential settlements were in general proportional to the load, with a maximum of 0.37 mm and a minimum of 0.10 mm in beams which had the

highest (CD-1.0/I) and the lowest (CD-1.0/V) ultimate loads respectively.

Fig.7.4 shows the variation of the settlement at both interior and exterior supports with the total load for most of the beams tested. The load-settlement curves at end supports are perfectly linear. The shape of those at interior support is attributed to the nature of the load cell which becomes stiffer at higher loads. The average values of differential settlement were 0.29 mm in series CD beams and 0.21 mm in series CE, representing  $0.00034 \times \text{span}$  and  $0.00032 \times \text{span}$  for the two series respectively.

## 7.6 REACTIONS AT SUPPORTS AND BENDING MOMENTS

### 7.6.1 REACTIONS AT SUPPORTS

Fig.7.5 shows the measured reactions at both interior and end supports as functions of the total load. In addition the theoretical reactions, calculated as in a shallow beam, have been plotted. It can be seen from fig.7.5 that the measured interior reaction curves, though linear as expected, are far below the theoretical line. Those of the measured end reactions are above their theoretical line. For the increment at or close to failure, the measured reactions together with the calculated ones are presented in table 7.3. Fig.7.5 and table 7.3 show that calculating the reactions in continuous deep beams according to a shallow beam theory, as is commonly done by designers, is erroneous and unsafe. For two-span beams with a point load at each mid-span as is the case of

CD beams, the theoretical reaction at the interior support would be  $0.69 \times$  total load on both spans. In the present case, such reactions ranged from 0.42 to 0.46 of the total load. For a similar loading configuration, Rogowsky et al [98] reported a mean value of  $0.62 \times$  total load for their moderately deep beams where settlement was minimised as compared to the author's tests. The end reactions of series CD beams varied from 0.27 to 0.29 of the total load as compared to a theoretical value of 0.155.

Series CE beams which have one point load at each span applied closer to the end support, had interior reactions varying from 0.32 to 0.36 of the total load compared to a theoretical value of 0.50. Fig.7.5 shows that differences between interior and end reactions and their respective theoretical values were smaller in series CE beams than in those of series CD. This was attributed to the fact that in the former, differential settlements were smaller (see fig.7.3). However, in both series, while differential settlements were small enough to be unavoidable in real structures (see chapter 8), reactions were completely different from those recommended by the present design document [1] [33] [85]; this will be discussed further in chapter 8.

### 7.6.2 BENDING MOMENTS

From the measured support reactions and the loads applied, the span and support moments were calculated. For the load increment at or near failure, the moments are given in table 7.3 and their distributions shown in fig.7.6. The theoretical bending moment distribution, determined as in shallow beams, is plotted in the same figure. It can be seen that the bending moments as measured from the tests reflect the flexural cracking behaviour and are entirely different from the theoretical ones. The moment at spans is higher than expected and that at a support is lower, becoming even sagging as in the case of series CD beams. Leonhardt and Walther [80] reported that bending moments in deep beams may differ from those of shallow beams by up to 100%. Rogowsky et al [98] pointed out that the behaviour of the two-span specimens they tested was somewhat between that of a two span continuous shallow beam and two adjacent single span beams for which the interior reaction would be  $0.50 \times$  total load. In the present case, the behaviour of the beams was much closer to that of two adjacent single span beams (fig.7.6). In addition to the reactions and bending moment distribution, such behaviour, particularly that of series CD beams, was confirmed by the cracking patterns and measured strains (see section 7.7).

Differential settlements in the order of that recorded in the present tests would result in negligible bending moments in shallow beams. In deep beams, however, because of the high flexural stiffness, differential settlements as small as those in fig.7.3 result in high bending moments

that the designer can not afford to ignore. Such flexural stiffness is, however, still not clearly quantified in deep beams [85], particularly after cracking.

## 7.7 STRAINS AND STRESSES

### 7.7.1 STRAINS

Strains were measured on the concrete surface at discrete positions using electrical demountable strain transducers on the back and 4 inches mechanical demec gauges on the front as shown in fig.6.16. The strain transducers were arranged in rectangular rosettes so that the magnitude and direction of the principal strains could be determined. The rosettes were placed in the notional load paths, considered as the critical regions of a deep beam in general. It is to be noted, however, that these rosettes were soon crossed by cracks, rendering their results unreliable for the determination of the principal strain values. Nevertheless, the knowledge gained from the single span deep beam tests helped the author to predict the direction of the diagonal cracks in the continuous deep beams. Consequently, for every rosette one transducer was placed along the expected diagonal crack and another one perpendicular to it. The strains recorded by these two transducers were expected to be very close to the principal compressive and tensile strains respectively. Indeed, this was always the case before the rosettes were perturbed by cracks. A sample of strain values (in micro-strain) is given below:

Beam	Direct Compression	Direct Tension	Principal $\epsilon_1$	Principal $\epsilon_2$
CD-0.5/V	-166	8	12	-170
CD-0.5/H	-296	176	176	-297
CD-1.0/H	-408	61	64	-411
CD-0.0	-141	32	34	-142
CE-0.5/V	-246	36	50	-260
CE-0.5/H	-336	41	51	-346

The graphs shown in fig.7.7 indicate that the load is transmitted to the supports through a limited area of concrete defined by the bands joining the bearing at a loading point to that at a support. These concrete bands are referred to as 'notional load paths' or 'inclined concrete struts' in this work. The strains are highest at the centre of the load path which tends to reduce in width as the beam gradually reaches its ultimate. It can be argued that at higher loads, the cracks reduce the area of concrete through which the load is transferred. This in turn results in a sharp increase of the compressive strains in the load path. Outside the notional load path, the strains are very small indeed.

Fig.7.8 shows a typical distribution of compressive strains along the load path. The maximum compressive strains occurred below the loading points and above the supports. In the middle part of the inclined strut, they hardly reached 1000 micro-strains, revealing that one important assumption of the plastic truss model proposed by Rogowsky et al [97] [98] is far from being fulfilled. Indeed Rogowsky et al's model considers crushing of concrete within the inclined strut and flexural failure as the two main failure modes in deep beams. Fig.7.9 shows

further that the maximum concrete strains recorded within the concrete web of the present test beams never reached the ultimate concrete strain, commonly accepted in design as 3500 micro-strain. The highest recorded values were:

Beam	Recorded Strain	Proportion of $\epsilon_{cu}$
CD - 0.5/I	2240	0.64
CD - 1.0/I	3130	0.89
CD - 0.0	2301	0.66
CE - 0.5/V	2573	0.74
CE - 1.0/H	2133	0.61

It was stated earlier that the diagonal cracks formed instantaneously in a manner similar to the split action of a concrete cylinder; throughout the tests, it was attempted to monitor the tensile strains in the load paths. Fig.7.10 shows a typical strain distribution up to the formation of a diagonal crack. It can be seen that, in general, these cracks developed at tensile strains ranging between 300 to 400 micro-strain. They may, however, form at lower than 300 micro-strain (at 209 and 186 in CE-1.0/H and CE-0.0 respectively). Furthermore, fig.7.10 reveals that, while strains parallel to the load path are compressive, those perpendicular to it are tensile throughout, supporting further the analogy between a split action in a deep beam and that in a concrete cylinder.

Strains were also recorded on the concrete surface, along the bottom and top main steel. It can be seen from fig.7.11 that in contrast to the shallow beam bending moment distribution which predicts compression near the interior support, strains were tensile throughout the spans. An

examination of Rogowsky et al work [96] [97] reveals similar strain distribution for beams with span/depth ratio of 2.0. When this latter increased to 5.0, the strain distribution followed more closely the shallow beam bending moment. Leonhardt and Walther [80] reported tensile strains and stresses near the intermediate support more than 50% of the maximum values in the span. At the top, very small tensile or compressive strains were recorded (fig.7.11) in comparison to those at the spans, explaining the absence of flexural cracks in most of the test beams. Compressive strains were also recorded at the top in Leonhardt and Walther tests. In Rogowsky et al tests [96] [98], strains at the top were tensile but much lower than those at the spans, particularly in their deeper beams. In general, despite crack disturbances, strains were not high enough to cause yielding of the tensile steel. It is, however, certainly wrong to distribute the longitudinal reinforcement according to the theoretical bending moment curve.

Longitudinal strain distributions above the interior support and below the loading point are shown in figs.7.12 and 7.13. These profiles, though disturbed by early cracks, reveal that the concrete above the interior support is in tension, highest at about  $0.3h$  up. Such tension caused the vertical cracks which always formed above the interior support. A compressive region exists above mid-depth but strains are not high enough to cause concern. Below the loading point, which corresponds to mid-span in CD beams, tensile strains are highest at the soffit, though an area of high tension can occur above mid-depth (see fig.7.13). The mid-span strain profiles reveal the need for spreading the tensile

steel over a larger area.

Vertical strains, which are usually neglected in shallow beams, can be very high in deep beams, particularly over a support. A typical vertical strain distribution above the interior support is shown in fig.7.14. As expected, these strains are compressive and highest above the support up to a depth of  $0.3h$  up and then decrease gradually towards zero at the top.

### 7.7.2 STRESSES

Internal stresses can not be directly measured, they can only be estimated from strains. In an elastic homogeneous material, plane stresses are given by [30] :

$$\sigma_x = \frac{E (\epsilon_x + \nu\epsilon_y)}{(1 - \nu^2)} \quad 7.1$$

$$\sigma_y = \frac{E (\epsilon_y + \nu\epsilon_x)}{(1 - \nu^2)}$$

Where  $\sigma_x$  and  $\sigma_y$  are the stresses in x and y directions respectively

E is the Young's modulus of the material

$\nu$  is the Poisson's ratio

$\epsilon_x$  and  $\epsilon_y$  are the measured strains in x and x directions respectively.

Reinforced concrete is not a homogeneous material and after initial cracking, it is no longer elastic and, thus, the above formulae are not valid at the post-cracking stage. Nevertheless, elastic analysis in general has been a powerful tool in the hands of reinforced concrete researchers. It can predict the stresses and the locations of the early cracks. Following this, an attempt was made to calculate the tensile stresses at which the early flexural cracks formed. The tensile strains,  $\epsilon_x$ , were those measured during the tests on the concrete surface along the tensile reinforcement. The vertical strains,  $\epsilon_y$ , were found to be maximum above the support and null at the top. Similarly, those below the loading points would be maximum at the top and null at the bottom. The stresses at which flexural cracks formed are given by :

$$\sigma_x = \frac{E(\epsilon_x + \nu\epsilon_y)}{(1 - \nu^2)}$$

Since  $\epsilon_y = 0$ , such equation simplifies to:

$$\sigma_x = \frac{E \epsilon_x}{(1 - \nu^2)} \quad 7.2$$

The Young's modulus  $E$  and the Poisson's ratio  $\nu$  are those of the concrete, determined from tests as  $28 \text{ N/mm}^2$  and  $0.2$  respectively (see chapter 6, section 6.5.3). Using equation 7.2, flexural cracking stresses were determined and are given below:

Beam	Tensile Strains ( $\mu s$ )	Flexural Stress ( $N/mm^2$ )
CD-0.5/V	122	3.4
CD-0.5/H	87	2.4
CD-1.0/V	73	2.0
CD-1.0/H	67	1.9
CD-0.0	72	2.0
CE-0.5/H	100	2.8
CE-1.0/V	98	2.7
CE-1.0/H	117	3.3
CE-0.0	107	3.0

In the present tests, every load increment lasted for about 15 minutes and hence could be considered as a short term loading, where creep strains are small enough to be neglected. Moreover, strain measurement revealed that a small concrete element within the load path is subject to a uniaxial compression, with tensile strains acting in a perpendicular direction. This is a similar stress-state as that of a concrete cylinder or cube under a compressive test. Consequently, the stress-strain curve of the concrete (fig.6.7) could be used to estimate the compressive stresses using the measured strains within the load path. Plots of total load against maximum stress are given in fig.7.15. It can be seen that the compressive stresses at failure were always below the cube strength given in table 6.1. On average the stress at failure was  $39.0 N/mm^2$ , representing 68% of the average cube strength ( $57.0 N/mm^2$ ). This confirms further that one of the assumptions on which the plastic truss model proposed by Rogowsky et al [97] [98] is based is not justified and crushing of the concrete within the load paths is not the main problem in deep beams.

## 7.8 DEFLECTIONS

### 7.8.1 OUT-OF-PLANE DEFLECTIONS

It was revealed in the single span deep beam tests that excessive out-of-plane deflection leads to premature failure by lateral buckling (see Chapter 5). It was also revealed that lateral buckling depends on the slenderness ratio,  $h/b$ ; members with high  $h/b$  ratios are more prone to buckling collapse. The present BS 8110 [16] stipulates that the slenderness effect should be taken into account for  $h/b$  values higher than 15. The single span tests (chapters 3, 4, 5) showed that deep beams with  $h/b$  of 20 may not exhibit larger lateral deflections so as to precipitate buckling, provided the loads and reactions are concentrically applied. Indeed, this was also the case in the continuous deep beams which all had a slenderness ratio of 20. The maximum lateral deflections recorded just prior to failure ranged from 0.44 mm (CD-1.0/I) to 1.0 mm (CD-0.0) for series CD beams and from 0.39 mm (CD-0.5/V) to 1.57 mm (CE-0.0) for CE beams and were comparable to those of series F of the single span beams..

From the experience gained in the single span tests, lateral deflections higher than 4 mm are likely to cause buckling failure.

### 7.8.2 IN-PLANE DEFLECTIONS

Owing to the high flexural stiffness of deep beams in general, vertical deflection is unlikely to be high enough to deter their serviceability which is rather controlled by excessive cracking.

In the present continuous deep beams, the presence of the interior support has further reduced vertical deflection. It varied from 1.6 mm (CD-1.0/H) to 2.5 mm (CD-1.0/V) and from 1.3 mm (CE-0.5/H) to 2.0 mm (CE-0.5/V) in series CD and CE respectively as compared to those in the geometrically identical single span deep beams (series F in chapter 3) which ranged between 3.0 mm and 4.0 mm at relatively lower loads. Fig.7.16 shows the load-deflection curves for the 7 beams of series CD. Specimens with horizontal web reinforcement had the smallest deflections while those with vertical bars had deflections comparable to those without web reinforcement.

## CHAPTER EIGHT

### CONTINUOUS DEEP BEAMS - INTERPRETATION OF TEST RESULTS AND DESIGN RECOMMENDATIONS -

#### 8.1 INTRODUCTION

Although deep beams such as transfer girders are frequently continuous over several supports, very little published data exist on such beams. Their design is inadequately covered by the current codes and design manuals [1] [33] [85] if not at all [23].

The continuous deep beam tests conducted by the author were primarily aimed at providing an insight into their real behaviour. They help to demonstrate that the above mentioned design documents [1] [33] [85] could lead to severe cracking and might be unsafe for this type of structural members.

Indeed, in all these documents, the bending moment distribution considered when designing a continuous deep beam is that used for shallow beams and a mere 10% increase is recommended for end reactions. The test results presented in chapter 7 showed that the actual bending moment distribution is completely different, with moments at spans higher and those at supports lower or even becoming sagging, rendering present design methods inadequate for continuous deep beams.

Another important conclusion which emerged from the tests is that the CIRIA Guide [85], considered as the main design document on deep beams in the British practice, tends to be too tolerant towards the bearing capacity, particularly under point-loads. In effect, most of the proper bearing failures in the tests occurred at bearing stresses below those allowed for, despite the use of proper additional reinforcement.

## 8.2 SETTLEMENT EFFECT ON CONTINUOUS DEEP BEAMS

One of the factors influencing the reactions and bending moment distribution and thus the internal stresses in continuous deep beams is the difference in settlement between adjacent supports. In a two-span beam where the interior support settles more, differential settlement creates a sagging moment at the interior support which will relieve its reaction and increase that at the exterior one. The hogging effect, created by the static condition, and the sagging one, created by relative settlement, are opposite and combine to give reactions and bending moments such as those in figs.7.5 and 7.6 and tables 7.2 and 7.3.

Differential settlement is a common problem in buildings in general. Terraced houses where severe cracks form as a result in the cladding are just one example. In buildings with shallow beams and slabs, the adverse effects of differential settlement are usually controlled by limiting the relative settlement between adjacent supports to  $(0.002 \text{ to } 0.003) \times \text{span}$ . To limit these effects to the same level in deep beams, it is argued [85] that differential settlement between adjacent supports should be less

than  $0.0003 \times \text{span}$ . the CIRIA Guide [85] points out that such condition would not only be technically difficult to meet but might be often costly. The difference between the two limits is due to the fact that the resulting bending moment, being proportional to the flexural stiffness, would be more important in deep beams because of their high flexural stiffness.

Differential settlements such as those measured in the present tests would have negligible effects if the beams were shallow. The average values recorded were 0.29 mm and 0.21 mm in CD and CE series respectively, representing  $0.00034 \times \text{span}$  and  $0.00032 \times \text{span}$ . In deep beams, however, such order of magnitude of relative settlement would still have serious effects. In Rogowsky et al tests [98] differential settlement was limited to  $0.00012 \times \text{span}$ .

### 8.3 REACTIONS AND BENDING MOMENT DISTRIBUTION

In deep beams, it is believed [80] [98] that reactions at supports and bending moment distribution are also affected by shear deformation and the 'truss frame' action, particularly after diagonal cracking. These two phenomena reduce the hogging effect created by the static condition and increase the sagging moment at spans. Indeed, in the moderately deep beams of Rogowsky et al [96] where differential settlement was restricted, the two effects, namely shear deformation and truss action, were probably the main ones that caused the reactions and bending moments to differ from those of shallow beams.

Leonhardt and Walther [80] argued that the major oblique cracks cause a relief in the intermediate support reaction and increase that at the end one. They added that after the diagonal cracks develop, truss action begins resulting in a complete redistribution of internal stresses. Rogowsky et al [98] pointed out that shear deformation effect becomes even more important in deeper beams. Indeed, in the present tests even beams CD-1.0/V and CE-0.5/H, which had the smallest differential settlements (fig.7.3) of  $0.00012 \times \text{span}$  and  $0.00015 \times \text{span}$  respectively, had reactions at supports and bending moments completely different from those of shallow beams (figs.7.5 and 7.6).

In general, diagonal cracks, characterising shear deformation, were very wide particularly in beams without web reinforcement or with vertical one where they often exceeded 1.1 mm before failure. The cracks patterns of fig.7.1, particularly those of series CD beams, all reveal 'truss frames'. This was confirmed by strain measurement on <sup>the</sup> concrete surface in the load paths (fig.7.7) and along the tensile reinforcement (fig.7.11).

The moderately deep beams of Rogowsky et al, being two-span continuous and subject to two point-loads, can reasonably be idealized by the truss shown in fig.8.1. In this truss, inclined or diagonal members represent the concrete in compression and bottom and top horizontal members represent the tensile steel with forces acting in the tension chord at the bottom higher than those at the top. In the author's beams, the absence of cracks at the top suggests that the tension force at the top

chord was very small and could be neglected resulting in the truss shown in fig.8.2. Such difference was certainly due to the fact that the beams in this work were deeper and settlement was not restricted.

To sum up, the reactions and bending moment distribution of the two-span beams tested were closer to those of two adjacent single span beams than to those of a two-span continuous shallow beam (fig.7.6, tables 7.2 and 7.3). Thus, designing continuous deep beams according to a shallow beam moment distribution is not safe. The span moments would be greatly underestimated and those at supports greatly overestimated. The hogging moments would be compensated by the three effects discussed previously, namely differential settlement, shear deformation and truss action. The net result might be such that horizontal tensile stresses would exist at interior supports (fig.7.6, CD beams). Such situation is more likely to occur in beams at the deeper range.

In the next section, a contribution towards an effective flexural design of continuous deep beams is proposed.

#### 8.4 FLEXURAL DESIGN AND DETAILING OF MAIN STEEL

According to the current codes and design manuals [33] [85], the longitudinal steel, both at spans and above supports, should be calculated on the basis of the highest moment at span and above support, calculated from shallow beam bending moment distribution. The formula used is as follows:

$$A_s = \frac{M}{z \times f_y / \gamma_m} \quad 8.1$$

where  $z$  is the lever arm, determined from elastic analysis as

$$z = 0.2L + 0.3h.$$

$f_y$  is the yield stress of the steel and  $\gamma_m$  is the material safety factor, taken as 1.15 for steel

Although equation 8.1 may have led to safe design so far, it is certainly based on a wrong assumption, that is the moments in continuous deep beams are the same as those in corresponding shallow beams. The fact that such formula has led to safe design is because the lever arm expression used is that derived from elastic analysis [33] [85]; that is before the concrete cracks. In reality, after cracking, the lever arm increases, particularly as <sup>the</sup> support settles.

Following the close similarity between the bending moment of two adjacent single span beams and that of a two-span continuous deep beam (fig.7.6), it is prudent to calculate the longitudinal steel at spans of a continuous deep beam on the basis of the maximum moments of corresponding single span adjacent beams with similar geometric and

loading properties but without the continuity effect. The steel so calculated should be carried through the interior support to take any tensile stresses resulting from the possibility of a sagging moment which might exist there. This detailing is also required by the truss action which aggravates the tensile stresses near the supports.

In the beams tested, flexural cracks, though very narrow, were widest above the longitudinal reinforcement and extended  $0.2h$  to  $0.3h$  up. It is thus wise to distribute the area of steel so calculated over a band width of at least  $0.2h$  from the soffit. Such distribution of tensile reinforcement will also prevent any congestion of steel at bearing areas which might contribute towards premature crushing of concrete there.

For the longitudinal reinforcement above an internal support, the present tests showed that for deeper beams, this reinforcement could be safely omitted. For moderately deep beams, however, Rogowsky et al [97] suggested that the interior support moment calculated according to a shallow beam bending moment distribution should be reduced by 40%. This recommendation is based on ideal support conditions where relative settlement was minimised. In practical cases, the reduction would be greater, even for beams of such depth. From this, the author suggests that for the purpose of designing the tensile reinforcement above an internal support in a continuous deep beam, a corresponding shallow beam bending moment at support, reduced by 40%, should be used in equation 8.1. This will, no doubt, result in a conservative area of steel. However, an efficient detailing of this reinforcement so as to contribute effectively to the shear strength by restraining the diagonal cracks will

offset the conservatism aspect of the design. the reinforcement so calculated should be distributed as follows:

- For beams in the deeper range, that is beams with  $L/h < 1$ , the steel should be distributed over a depth extending from  $0.2h$  to the top. In the tested beams, tensile strains and crack widths over the interior support were highest at about  $0.3h$  from the soffit (fig.7.12). In beams without web reinforcement or with vertical bars, vertical cracks induced by settlement crossed the whole depth above the support (fig.7.1). Such detailing of the longitudinal steel will also restrain diagonal cracking which forms within the interior shear-spans and have a direct bearing on the ultimate strength. This view is shared by Leonhardt and Walther [80] who suggest the arrangement of main steel above the interior support within a depth extending from  $L/4$  to  $3L/4$  in the form of small diameter bars.
- For moderately deep beams such as those tested in Canada [96] ( $2 < L/h < 5$ ), flexural cracks at top were contained within a depth of about  $0.3h$  and occasionally extended further down, particularly in the deeper ones ( $L/h = 2$ ). It is tempting to suggest that  $2/3$  of the steel should be arranged within a depth of  $0.2h$  from the top. The remainder should be distributed over the rest of the section down to  $0.2h$  from the bottom.
- For beams in between, that is with  $1 < L/h < 2$ , no tests are available. However, the CIRIA Guide [85] recommends that a portion of steel equal  $0.5(L_{max}/h - 1)$  should be placed within  $0.2h$  from the top and the remainder distributed over a depth extending from  $0.2h$  at the top

to  $0.2h$  from the bottom.

It is wise, however, to suggest that more experimental work should be carried out on continuous deep beams, particularly in the range of  $1 < L/h < 2$ , so that more understanding of their behaviour will become available and lead to better design.

Rogowsky et al [97] [98] have put forward a design method based on a plastic truss model. However, one of the basic assumptions of this model was not fulfilled in the present tests. Such assumption stipulates that failure of deep beams is mainly concrete crushing at a load path or flexural failure characterised by yielding of tensile steel. None of these failures occurred in the author's tests and both compressive strains within the load paths and tensile strains along the longitudinal steel were well below their ultimate values. Instead, proper concrete crushing at the bearing and failure precipitated by diagonal cracking occurred repeatedly. Both of these types of failure are not recognized by their model. According to many researchers [12] [64] [67] [91] [93], bearing failure and failure related to diagonal cracking are commonly associated with deep beams in general. The design method proposed by Rogowsky et al can only be applied to particular cases of moderately deep beams where flexure might be the problem. The plastic truss model is certainly not applicable and will not be safe for the present beams.

## 8.5 SHEAR CONSIDERATIONS

In reinforced concrete, shear failures are not primarily caused by excessive shear stresses. They could be rather defined as those associated with the transfer of loads to the supports. Since the method of transfer in deep beams is very different to that in normal beams - it is an arching action rather than a bending one -, it is to be expected that the terms 'shear failure' and 'shear reinforcement' have somewhat different meanings in the two cases.

In deep beams, failures which are caused or influenced by diagonal cracks are commonly referred to as shear failures. Since a diagonal crack is the result of concrete weakness in tension, it appears that tensile stresses rather than shear stresses are the causes of such failure in deep beams. Leonhardt and Walther's argument [80] that this failure is initiated by excessive compressive stresses is not convincing. Due to the absence of a simple mathematical model to express the tensile stresses within the load paths, researchers and designers have been using shear strength as the main parameter to study and prevent this type of brittle failure.

In the present experimental programme, the continuous beams tested did not fail in proper shear (diagonal failure) compared to the identical single span beams. This is shown in figs.7.1 and 3.2 and in tables 8.1 and 8.2 where the shear strengths of the continuous span beams and those of the single span ones are respectively given. It can be seen from

these two tables that, at failure, the maximum design shear stress set by the CIRIA Guide [85] was exceeded in all the single span beams while, in the continuous ones, this was not always the case; some beams failed before this parameter was reached. Since failure in the two types of beams was different, a direct comparison of their strengths is inconclusive. Nevertheless, the addition of one support had increased the total ultimate load considerably; the ultimate loads of 4 continuous beams and their identical single span ones are given below:

Single Span Beams	Ultimate Load (kN)	Continuous Beams	Ultimate Load (kN)
F-0.21-0.5/V	500	CD-0.5/V	800
F-0.21-0.5/H	540	CD-0.5/H	850
F-0.0-0.5/V	396	CE-0.5/V	650
F-0.0-0.5/H	650	CE-0.5/H	800

The increased ultimate loads together with the type of failures which occurred in the continuous beams suggest that bearing stresses are likely to be more critical than their shear capacity as compared to single span beams; this will be discussed in the next section.

The CIRIA shear formula (equation 3.6), which gives the maximum shear force within a shear span that a beam should be designed to carry, is also intended for use in continuous deep beams. However, following the arguments and test observations presented in chapters 3 and 4, it is not surprising to find equation 3.6 inadequate for the design of continuous deep beams of slender type; the safety factors obtained are indeed very small (table 8.1). Equation 3.6 was modified by the author to be used for slender deep beams and resulted in equation 3.8, reprinted below:

$$V/bh = R \lambda_1 \left(1 - 0.35 \frac{a}{h}\right) \sqrt{f_{cu}} + \lambda_2 \Sigma \frac{100 A_y \sin^2 \alpha}{bh^2} \quad 8.2$$

where the meanings of symbols are as in equation 3.6. Improved safety factors were obtained (table 8.1) when this equation was used. It is to be noted that since proper shear failure (diagonal failure) did not occur in the continuous beams, the safety factors were smaller than those obtained for the single span beams (table 8.2 and 3.6) which all split diagonally.

Table 8.1 shows that the CIRIA equation modified according to the author's recommendations given in chapter 3 can be used in continuous deep beams of slender type for shear design purpose.

Regarding web reinforcement, the tests showed that the ideal way of reinforcing a concrete web so as to effectively restrain the growth of the diagonal cracks is to place the bars perpendicular to their expected direction. Indeed inclined bars were the most effective in controlling the cracks, both in length and in width, and in enhancing ultimate strengths. The next most effective were horizontal bars, particularly when <sup>a</sup>sufficient amount was used. Vertical bars were found inefficient and could have adverse effects on cracking and strength when used in higher quantity. When no web reinforcement was used, the concrete was very brittle and made the tests look dangerous to perform.

In conclusion the author recommends that for shear consideration of concrete continuous deep beams, the CIRIA equation (equation 3.6) can be used for stocky beams. For continuous deep beams of slender type, such equation may not be safe for shear design and equation 8.2 should be used instead.

Whenever possible, inclined bars should be used for a better control of cracks and resistance of tensile stresses within the load paths. This will in turn result in shear strength enhancement. From the view point of economy, it should be noted that under normal site conditions, this kind of reinforcement could be more expensive to bend and fix. However, according to the present tests, a lesser amount of inclined steel is required to produce similar or better results than a higher amount of horizontal bars, found to be the next most effective (CD-0.5/I and CD-1.0/H). Hence the cost involved in the handling and fixing of inclined bars might be offset by the quantity of steel required. Horizontal bars, particularly when used in higher quantity (around 1.0%) will also be effective. Vertical bars should only be used in moderately deep beams where the shear-span/depth ratio,  $a/h$ , is likely to exceed 1.0.

## 8.6 BEARING CAPACITY

Failure at the bearing is very common in deep beams [12], particularly with unstiffened supports. Often in practice, additional reinforcement is added to strengthen the bearing areas. However, the continuous beams tested in this work showed that such strength enhancement is limited.

In the British practice, the CIRIA Guide [85] limits the bearing stress to  $0.4f_{cu}$ . The Guide stipulates that at end supports and at internal supports for continuous beams, such bearing stress limit may be increased to  $0.6f_{cu}$  and  $0.8f_{cu}$  respectively, provided the stressed zone is adequately confined. Under concentrated loads, the bearing stress is allowed to rise up to  $0.8f_{cu}$  provided adequate confining reinforcement is present.

In this experimental programme, the concrete was adequately compacted and additional bars were used at the loading and support points (fig.6.2). Yet, most of the proper concrete crushing failures occurred at the bearings at stresses below the  $0.8f_{cu}$  limit allowed by the CIRIA Guide for similar conditions. The specimens that failed by proper concrete crushing at the bearing are given in table 8.3 together with the bearing stresses. In these beams, the crushing was very little or not at all affected by diagonal cracks. Where the concrete crushing was precipitated by cracks the bearing stresses were even lower as in table 8.4.

In the American practice, clause 10-15-1 of ACI (318-83) (revised 1986) [1] limits the bearing stress to :

$$\Phi \times 0.85 \times f'_c$$

where  $\Phi$  is the strength reduction factor, taken as 0.7 for concrete bearing and  $f'_c$  the compressive strength of a concrete cylinder, taken as  $0.8 f_{CU}$  in this thesis (see chapter 6, equation 6.2).

That is:

$$0.7 \times 0.85 \times 0.8 f_{CU} = 0.48 f_{CU} \qquad 8.3$$

Such bearing stress was largely exceeded at failure, even in beams where diagonal cracks caused premature concrete cracking (see tables 8.3, 8.4). The American code does not allow for bearing capacity improvement which could be achieved by proper confinement of concrete and additional reinforcement.

Following this, the author recommends that where concrete is not confined and no additional reinforcement is used at the bearing areas, the bearing stress should not be allowed to exceed the  $0.4f_{CU}$  limit set by the CIRIA Guide. Where adequate confinement of concrete is present and additional bars are used at the bearing regions, the bearing stress limit should be increased to  $0.6f_{CU}$  at both, supports and loading points. Tables 8.3 and 8.4 show that the  $0.6f_{CU}$  limit is reasonably safe. Ideal conditions such as in the present tests are hardly achievable in practice where concrete strength is likely to be affected by poor concrete compaction and steel congestion. The  $0.8f_{CU}$  limit

given in the CIRIA Guide [85] may be too high and unsafe as, indeed, was in the author's continuous deep beams.

## CHAPTER NINE

### GENERAL CONCLUSIONS AND SUGGESTIONS FOR FURTHER RESEARCH

#### 9.1 GENERAL CONCLUSIONS

##### 9.1.1 SINGLE SPAN DEEP BEAMS

Tests conducted on simply supported slender concrete deep beams revealed the following major experimental observations:

- (1) The beams developed distinctive diagonal cracks running from support to loading point. These cracks, which formed well below the failure load (30% to 60%), were sudden, complete and accompanied by a loud cracking noise. Their formation was akin to a splitting action of a concrete cylinder and could not be prevented by web reinforcement.
- (2) By comparison to stocky deep beams reported in the literature, the diagonal cracks of slender deep beams make a smaller angle with the horizontal and could be more accurately represented by the line joining the middle of the support to that of the loading point (full line in fig.3.6). In addition, they form relatively earlier. The two experimental observations are explained using Mohr circle analysis.
- (3) The diagonal cracks form as a result of the concrete within the load path reaching its ultimate tensile strength, initiating not at the soffit but at about  $0.4h$  up. Their width was always a maximum in the interval  $(0.3h - 0.6h)$  up.

- (4) Equation 3.3, which was proposed earlier by Kong et al [68] for predicting the diagonal cracking load of stocky deep beams, was found not suitable for slender deep beams. Such equation was modified by the author as explained in section 3.3.4 to take account of the two distinct features listed previously, namely :
- (i) the clear-shear-span,  $x$ , was replaced by the total shear-span,  $a$ .
  - (ii) a reduction factor  $R$  was used, established as 0.75 from test data.
- The modified formula (equation 3.4) resulted in a better estimation of the diagonal cracking loads (table 3.5)
- (5) The nature of diagonal cracking in slender deep beams has important implications in deep beam design and in the application of the shear-strength equation in cl.3.4.2 of the CIRIA Deep Beam Guide (equation 3.6 in this thesis). Such equation would give reduced safety factors and could even be unsafe for slender deep beams. Instead, equation 3.8 which is a modified form of equation 3.6 encompassing all the test observations (see section 3.4) should be used for the design of slender deep beams of height/thickness ratios of 20 and more.
- (6) For the same reasons, Kong et al formula (equation 4.2) was found to overestimate the ultimate loads of slender deep beams. Adopting the same modifications as in equation 3.8, the ultimate loads of the slender deep beams tested were better predicted by equation 4.3. Equation 4.11 proposed by the author on the basis of test results and observations also gave a satisfactory estimation of the ultimate shear capacities (table 4.1) and could be used for design purposes as

specified at the end of chapter 4, section 4.4.3.

- (7) After diagonal cracking, the specimens behaved more like trusses or tied-arches. Concrete compression struts were often defined by cracks running from loading points to supports. Concrete strain measurements confirmed the existence of these struts even if not specifically outlined by cracks. Strain measurements along the tensile reinforcement revealed strains at the faces of supports as high as those at the maximum moment region rather than the variation of strains expected from the bending moment diagram. This indicates the existence of a uniformly strained tension member caused by truss action.
- (8) The diagonal cracks, which in all the single span beams tested caused failure, were widest in beams without web reinforcement or with vertical bars. In these beams the serviceability limit state of cracking was often reached at formation of the first diagonal crack, though their ultimate loads were still more than twice the cracking load. This suggests that despite the important strength reserve associated with deep beams, the serviceability limit state of excessive cracking is likely to be reached at service loads in beams where web reinforcement is non-existent or ineffective. Indeed, the present tests indicated that for deep beams the serviceability limit state of cracking could be a more important design criterion than the ultimate limit state.
- (9) Vertical web bars were found not to be effective in restraining diagonal cracks nor were they effective in improving the ultimate shear strength of deep beams. When used in higher quantity, this

type of reinforcement could have adverse effects on both serviceability and ultimate limit states particularly at lower shear-span/depth ratios. In contrast, horizontal bars are more effective in restraining the cracks. Strength enhancement can also be achieved with this type of reinforcement. However, increasing the steel quantity beyond a certain limit does not guarantee a strength improvement. There seems to be an optimum web steel ratio beyond which no gain in strength can be achieved.

- (10) The conclusion on the relative effectiveness of vertical and horizontal bars to control potential diagonal cracks is in line with both the CIRIA Guide and the American code ACI(318-83) (revised 1986). The author agrees with these two documents that vertical bars could be effective in moderately deep beams where often the shear-span/depth ratio is higher than 1.0.

An ideal web reinforcement is one that is placed directly perpendicular to a diagonal crack. The tests on continuous deep beams and data from other independent investigators confirm that inclined bars are the most effective type of reinforcement. They protect the concrete web effectively and result in a marked shear strength enhancement. Such layout of web reinforcement is, however, not recognized by the American code.

- (11) Shear strength appears to be strongly dependent on concrete strength. Beams of series CC made of moderately high strength concrete ( $f_{cu}$  around  $60 \text{ N/mm}^2$ ) had smaller ultimate loads compared to that of a

geometrically identical beam made of high strength concrete ( $f_{cu} = 97 \text{ N/mm}^2$ ) despite the use of more web steel in the former.

- (12) Slender deep beams present the additional problem of excessive lateral deflection which could result in a premature buckling collapse.

Buckling failure becomes more dominant as the slenderness ratio  $h/b$  increases. In other words, beams with higher  $h/b$  ratios are more likely to buckle particularly if the loads are slightly eccentric.

- (13) In the present tests when the loads were perfectly concentrically applied, failure was by shear even for  $h/b$  ratios as high as 50. When the loads were applied eccentrically, beams of  $h/b$  ratios higher than 25 buckled at loads below their ultimate shear capacities. The transition from shear failure to buckling is often accompanied by a significant reduction in the ultimate load. In addition to  $h/b$  ratio, the eccentricity/thickness ratio is another important parameter in out-of-plane buckling.

- (14) Buckling failures were sudden, catastrophic and without warning. They were always difficult to predict; thus, any design method should yield a high safety factor.

- (15) The CIRIA Guide gives three methods for the buckling design of deep beams : the supplementary rules, the single panel method and the two panel method. All the three methods were found to be safe and

generally too conservative, particularly the supplementary rules and the single panel method; these two methods need more refinement. The designer is advised to by-pass them and move directly to the two panel method. For those beams of  $h/b$  ratios of 25 to 40, this method gave an average safety factor of 5.0 which, for buckling failure, should not be considered too high. In general, the three methods of the CIRIA Guide are difficult to follow and apply to a practical design problem particularly for engineers with little or no experience in the design of deep beams.

- (16) The Portland Cement Association method for predicting buckling strength of tilt-up panels is simple to apply to deep beams. Such a method was found safe and more realistic than all of the three methods in the CIRIA Guide. However, the simplicity and the realism of this method are offset by its restrictions on concrete and steel strengths, dimensions and boundary conditions. Where applicable, the author recommends its use for the buckling check of slender concrete deep beams and panels.

### 9.1.2 CONTINUOUS DEEP BEAMS

The important conclusions emerging from the continuous deep beams tested are as follows :

- (1) The potential diagonal cracks, having the greatest impact on the behaviour of the beams, are similar in all respects to those in the simply supported beams. The selection of the different type of web

reinforcement and their ability to restrain the major cracks and increase the ultimate shear capacity is also valid for continuous deep beams. In addition, the tests showed further that with ineffective web reinforcement, diagonal cracks can extend into a compression zone and cause premature concrete crushing.

- (2) Proper bearing failure by concrete crushing at a loading point occurred with more effective web reinforcement at relatively higher loads. Nevertheless, the bearing stresses at failure were below those allowed for by the CIRIA Guide. Based on the test results, recommendations are given in chapter 8 whereby in no circumstances should the bearing stress be allowed to exceed  $0.6f_{cu}$ . In current practice, with the presence of confining reinforcement, the bearing stress is permitted to rise up to  $0.8f_{cu}$ .
- (3) Differential settlement is an important factor influencing the reactions and bending moment distribution in continuous deep beams. In the beams tested, the reactions and bending moment diagrams were completely different from those of shallow beams. Thus, it is certainly wrong and may be unsafe to design continuous beams in the deeper range according to shallow beam support reactions and bending moment distribution. The moments at span would be greatly underestimated and those at interior supports overestimated. Equally, the reactions at end supports would be underestimated while those at interior ones would be overestimated. Using reactions and bending moment diagram of single span adjacent beams would be safer and more accurate. Based on the results and observations from the present tests and from others reported in the literature,

recommendations for the design and detailing of the main flexural steel at spans and above a support are given in chapter 8.

- (4) Shear deformation and truss action are two other factors which influence the reactions and bending moments in continuous deep beams. Truss shapes were defined in most of the beams by cracks and confirmed by strain measurements.
- (5) In general, the addition of one support has increased the ultimate load considerably and changed the failure mode from shear proper to shear-bearing or proper bearing failures. For shear consideration, the CIRIA equation modified as recommended by the author (equation 3.8) can be used for continuous deep beams of slender type. Recommendations are given in chapter 8 for the selection of a more effective arrangement of web reinforcement to control cracks and protect the concrete web and to increase the shear capacity.

## 9.2 SUGGESTIONS FOR FURTHER RESEARCH

A major aim of this thesis was to investigate the effects of web reinforcement in deep beams; different arrangement and quantities have been used. However, the range over which the shear-span/depth ratio varied was not wide enough. It is suggested that more tests should be carried out in this direction with shear-span/depth ratios covering the whole range over which deep beam action is believed to occur ( $a/d < 2.5$ ). The web reinforcement to be considered should be : no web reinforcement, minimum and maximum vertical reinforcement, minimum and maximum horizontal reinforcement and minimum and maximum inclined web

reinforcement. Consideration should be given to using high yield deformed bars rather than plain bars since the former are more likely to be used in practice.

In the present work it was revealed that increasing the web steel ratio beyond a certain limit does not guarantee an increase in the ultimate shear strength. There seem to be an optimum limit beyond which no strength increase is achieved; this view is also shared by Kong et al [65] [66]. Varying the amount of the different types of web reinforcement will help in defining this optimum value of web steel ratio. Preference should be given to larger specimens to minimise the scale effect.

The beam-panels tested for investigating the stability problem in this experimental programme (series CB beams) had unrestrained vertical edges. Consequently, they buckled in a uniaxial curvature similar to that of a slender column. In practice, however, the vertical edges are always restrained by cross-walls and, hence, buckling might be in a biaxial curvature similar to that of a plate under compression; the collapse loads will be relatively higher. Experimental tests on deep beams with restrained vertical edges are, thus, required to provide more information on the stability problem and to present a further assessment on the CIRIA buckling recommendations. Panels with restrained vertical edges are not covered by the PCA Design Aid [88].

To this date, very little work exists on continuous deep beams. In the range of span/depth ratios between 1.0 and 2.0, no data is available in the literature. More experimental work is required on continuous deep beams to provide a further understanding on their behaviour and, particularly, to assess the actual reactions and bending moment distribution. It would also be interesting to investigate the effects of shear deformation and truss action by reducing differential settlement.

Deep beams are very stiff. Because of this high stiffness, smaller values of differential settlement are likely to have great effects on bending moments and cracks. Thus, the stiffness in deep beams in general, and in continuous ones in particular, needs to be fully investigated and defined.

## REFERENCES

1. ACI COMMITTEE 318. Building Code Requirements for Reinforced Concrete (ACI 318-83) (Revised 1986). American Concrete Institute, Detroit, November 1983.
2. ACI COMMITTEE 318. Commentary on Building Code Requirements for Reinforced Concrete (ACI 318-83). American Concrete Institute, Detroit, November 1983.
3. ACI COMMITTEE 363. State-of-the-art Report on the High-strength Concrete. ACI journal, Proceedings, Vol.81, No.4, July-August 1984, pp.364-411.
4. ACI-ASCE COMMITTEE 426. The Shear Strength of Reinforced Concrete Members. Proceedings ASCE, Vol.99, ST6, June 1973, pp.1091-1187.
5. ALBRITON, G. E. Review of Literature Pertaining to the Analysis of Deep Beams. Technical Report No.1-701, U.S. Army Engineer Waterways Experiment Station, Vicksburg, Miss., November 1965, 80pp.
6. ALLEN, H. G. and BULSON, P. S. Background to Buckling. McGraw-Hill Book Company (UK) Limited, 1980, 582pp.
7. AL-NADJIM, A. G. Post-cracking Behaviour of Reinforced Concrete Deep Beams, Ph.D Thesis, Central Polytechnic of London, 1981.
8. Amine, H. Shear Strength of Slender Concrete Deep Beams. M.Sc Dissertation, University of Newcastle upon Tyne, 1987.
9. ARCHER, F. E. and KITCHEN, E. M. Stress in Deep Beams. Australian Journal of Applied Science, Vol.7, No.4, December 1956, pp.314-326.
10. ARCHER, F. E. and KITCHEN, E. M. Stress Distribution in Deep Beams. Civil Engineering and Public Works Review, Vol.55, No.643, February 1960, pp.230-234.
11. BEEBY, A. W. Cracking: what are Crack Width Limits for ?. Concrete, the Journal of the Concrete Society, Vol.12, No.7, July 1978, pp.31-33.
12. BESSER, I. I. and CUSENS, A. R. Reinforced Concrete Deep Beam Panels with High Depth/Span Ratios. Proc. Instn. Civil Engrs., Part2, Vol.77, No.6, June 1984, pp.265-278.
13. BHATT, P. Deep Beams on Statically Indetermined Supports. Journal of the Engineering Mechanics Division, ASCE, Vol.99, No.EM4, August 1973, pp.793-802.
14. BOOTH, E. Discussion on CUSENS, R. A. and BESSER, I. I. (1985). The Structural Engineer, Vol. 64B, No.2, June 1986, pp.48.

15. BROOKS, J. J. and WAINWRIGHT, P. J. Properties of Ultra-high Strength Concrete Containing a Superplasticiser. Magazine of Concrete Research, Vol.35, No.125, December 1983, pp.205-212.
16. BS 8110 (1985). The Structural Use of Concrete, Part 1. British Standards Institutions, London, 1985, 121pp.
17. BS 1881 : Part 116. Method for Determination of Compression Strength of Concrete Cubes. British Standards Institutions, London, 1983.
18. BS 1881 : Part 117. Method for Determination of Tensile Splitting Strength. British Standards Institution, London, 1983.
19. BS 1881 : Part 110. Methods for Making Test Cylinders from Fresh Concrete. British Standards Institutions, London, 1983.
20. BS 12. Specification of Ordinary and Rapid-hardening Portland Cement. British Standards Institutions, London, 1978 (amended 1983).
21. BS 882. Specification for Aggregates from Natural Sources for Concrete. British Standards Institutions, London, 1983 (amended 1986).
22. BS 18 : Part 2. Method for Tensile Testing of Metals. British Standards Institutions, London, 1971.
23. CAN-A23.3-M84. Design of Concrete Structures for Buildings. Canadian Standards Association, CSA Committee A23.3, Rexdale, December 1984, 281pp.
24. CHANA, P. S. Mechanism of Shear Failure. Proceedings of the Research Seminar on the Behaviour of Concrete Structures, Organised by Cement and Concrete Association, June-July 1986, pp.222-226.
25. CHANA, P. S. Some Aspects of Modelling the Behaviour of Reinforced Concrete Under Shear Loadings. Cement and Concrete Association, Technical Report No.543, July 1981.
26. CHOW, L., CONWAY, H. D. and WINTER, G. Stresses in Deep Beams. Proceedings ASCE, Vol.78, Separate No.127, May 1952, pp.686-708.
27. CEMENT ADMIXTURES ASSOCIATION and CEMENT and CONCRETE ASSOCIATION. Superplasticizing Admixtures in Concrete. Report of a Joint Working Party. Wexham Springs, Cement and Concrete Association, 1976 (reprinted with amendments 1978), 30pp. Publication 45.030.
28. CEMENT and CONCRETE ASSOCIATION. Bibliography on Deep Beams. Library Bibliography No.ch.71(3/69), Cement and Concrete Association, London, 1969.
29. CHENG, D. H. and PEY, M. L. Continuous Deep Beams. Proceedings, ASCE, Structural Division, Vol.80, No.450, June 1954, pp.1-17.

30. COATES, R. C., COUTIE, M. G. and KONG, F. K. Structural Analysis. Van Nostrand Reinhold (UK) Co.limited, Third Edition, 1987, 605pp.
31. COLLINS, M. P. and MITCHELL, D. A Rational Approach to Shear Design - The 1984 Canadian Code Provisions. ACI Journal, Vol.83, No.6, November-December 1986, pp.925-933.
32. COLLINS, M. P. and MITCHELL, D. Shear and Torsion. Chapter 4 of CPCA Concrete Design Handbook, Canadian Portland Cement Association, Ottawa, 1985, pp.4-1 - 4-51.
33. COMITE EURO-INTERNATIONAL du BETON and FEDERATION INTERNATIONALE de la PRECONTRAINTTE. CEB-FIP Model Code for Concrete Structures, 3rd Edition, 1978, 348pp.
34. COMITE EUROPEEN du BETON - FEDERATION INTERNATIONALE de la PRECONTRAINTTE. International Recommendations for the Design and Construction of Concrete Structures. English edition, Cement and Concrete Association, London, 1970.
35. COOK, C. F. An Electrical Demountable Strain Transducer. Journal of the British Society of Strain Measurements, Vol.16, No.3, July 1980, pp.113-119.
36. CP 110. The Structural Use of Concrete. British Standards Institutions, London, Part 1, 121pp.
37. CRANSTON, W. B. Analysis and Design of Reinforced Concrete Columns. Research Report No.20, Cement and Concrete Association, London, 1972, 54pp.
38. CRIST, R. A. Static and Dynamic Shear Behaviour of Uniformly Reinforced Concrete Deep Beams. Ph.D Thesis, University of New-Mexico, 1971.
39. CUSENS, A. R. and BESSER, I. I. Shear Strength of Reinforced Concrete Wall-beams under Combined Top and Bottom Loads. The Structural Engineer, Vol.63B, No.3, September 1985, pp.50-56
40. DE PAIVA, H. A. R. and SIESS, C. P. Strength and Behaviour of Deep Beams in Shear. Proceedings, ASCE, Vol.91, ST5, October 1965, pp.19-41.
41. DESAYI, P. A Method for Determining the Shear Strength of Reinforced Concrete Beams with Smaller ( $a_v/d$ ) ratios. Magazine of Concrete Research, Vol.26, March 1974, pp.29-38
42. DISHINGER, F. Contribution to the Theory of Wall-like Girders. International Association for Bridge and Structural Engineers Publications, Zurich, Vol.1, 1932, pp.69-93.
43. ERNST, G. C., HRMADIK, J. J. and RIVELAND, A. R. Inelastic

Buckling of Plain and Reinforced Concrete Columns, Plates, and Shells. University of Nebraska Engineering Experiment Station, Bulletin No.3, August 1953, 65pp.

44. ETTOUNEY, M. M. and SCHMIDT, W. Finite Element Solutions of Deep Beams. Proceedings, ASCE, SE Journal, Vol.109, No.7, July 1983, pp.1569-1584.
45. EUROCODE No.2 (draft version). Common Unified Rules for Concrete Structures. Commission of the European Communities, Luxembourg, 1984.
46. FENWICK, R. C. and PAULAY, T. Mechanism of Shear Resistance of Concrete Beams. Journal of the Structures Division, ASCE, Vol.94, No.ST10, Proceedings, Paper 6167, October 1968, pp.2325-2350.
47. GARCIA, R. C. Strength and Stability of Concrete Deep Beams. Ph.D Thesis, University of Cambridge, 1981.
48. GEER, E. Stresses in Deep Beams. Proceedings, ACI, Vol.56, January 1960, pp.651-661.
49. JOHNSTON, B. G. Column Buckling Theory : Historic Highlights. Journal of the Structural Division, ASCE, Vol.109, No.ST9, September 1983, pp.2086-2096.
50. KANI, G. N. J. The Riddle of Shear Failure and its Solution. ACI Journal, Proceedings, Vol.61, No.4, April 1964, pp.441-467.
51. KANI, G. N. J. Kani on Shear in Reinforced Concrete. Edited by KANI, W., Huggins, W. and WITTKOPP, R., Department of Civil Engineering, University of Toronto, University of Toronto Press, 1979, 225pp.
52. KONG, F. K. Reinforced Concrete Deep Beams. Chapter 6 of 'Concrete Framed Structures - Stability and Strength'. (Edited by NARAYANAN, R.), Elsevier Applied Science Publishers, London, 1986, pp.169-191.
53. KONG, F. K. Deep Beams : Recent Research at Newcastle University. Lecture Delivered at Ove Arup & Partners, London, on 3 October 1986.
54. KONG, F. K. Structural Principles - their Use and Misuse. Lecture Delivered at the Institution of Structural Engineers, Northern County Branch, Tyneside, 13 October 1987.
55. KONG, F. K. and CHALTON, T. M. The Fundamental Theorems of the Plastic Theory of Structures. In Proceedings, M. R. HORNE Conference on Instability and Plastic Collapse of Steel Structures, Manchester (Editor J. R. MORRIS), Granada Publishing, London, 1983, pp.9-15.
56. KONG, F. K. and CHEMROUK, M. Design of Reinforced Concrete Deep Beams - State-of-the-art. Chapter 1 of 'Reinforced Concrete Deep Beams', a book being edited by KONG, F. K., scheduled for publication

by The Blackie Publishing Group, Glasgow, in 1989.

57. KONG, F. K. and EVANS, R. H. Reinforced and Prestressed Concrete. Van Nostrand (UK) Co.limited, 3rd Edition (BS 8110), 1987, 508pp.
58. KONG, F. K., GARCIA, R. C., PAINE, J. M., WONG, H. H. A., TANG, C. W. J. and CHEMROUK, M. Strength and Stability of Slender Concrete Deep Beams. The Structural Engineer, Vol.64B, No.3, September 1986, PP.49-56.
59. KONG, F. K., WONG, H. H. A., TANG, C. W. J. and CHEMROUK, M. Worked Examples on the Used of CIRIA Guide No.2 to Calculate the Buckling Strengths of Slender Deep Beams. Technical Report STRUCT 7/3A, Department of Civil Engineering, university of Newcastle upon Tyne, 1987, 17pp. + 2 tables + 2 figures.
60. KONG, F. K., PAINE, J. M., CHEMROUK, M., TANG, C. W. J. and WONG, H. H. A. Worked Examples on the Use of CIRIA Guide No.2 ( in Conjunction with CP 110 : 1972) to Calculate the Buckling Strengths of Slender Deep Beams. Technical Report STRUCT 5/9A, Department of Civil Engineering, university of Newcastle upon Tyne, 1985, 15pp. + 2 figures + 2 tables.
61. KONG, F. K., TANG, C. W. J., WONG, H. H. A. and CHEMROUK, M. Diagonal Cracking of Slender Reinforced Concrete Deep Beams. Proceedings of the Research Seminar on the Behaviour of Concrete Structures. Organised by Cement and Concrete Association, June-July 1986, pp.213-217.
62. KONG, F. K., PAINE, J. M., CHEMROUK, M., WONG, H. H. A. and TANG, C. W. J. Worked Examples on the Buckling Design of Slender Concrete Deep Beams. Technical Report STRUCT 6/4A, Department of Civil Engineering, university of Newcastle upon Tyne, 1986, 22pp. + 1 fig.
63. KONG, F. K., ROBINS, P. J. and COLE, D. F. Web Reinforcement Effects on Deep Beams. ACI Journal, Proceedings, Vol.67, No.12, December 1970, pp.1010-1017.
64. KONG, F. K. and ROBINS, P. J. Web Reinforcement Effects on Lightweight Concrete Deep Beams. ACI Journal, Proceedings, Vol.68, No.7, July 1971, pp.514-520.
65. KONG, F. K., ROBINS, P. J., KIRBY, D. F. and SHORT, D. R. Deep Beams with Inclined Web Reinforcement. ACI Journal, Proceedings, Vol.69, No.3, March 1972, pp.172-176.
66. KONG, F. K. and SINGH, A. Diagonal Cracking and Ultimate Loads of Lightweight Concrete Deep Beams. ACI Journal, Proceedings, Vol.69, No.8, August 1972, pp.513-527.
67. KONG, F. K. and SINGH, A. Discussion on KONG, F. K. and SINGH, A. (1972) by SELVAM, V. K. M., ALDRIDGE, W. W. and authors; ACI

- journal, Vol.70, No.2, february 1973, pp.167-170.
68. KONG, F. K., ROBINS, P. J., SINGH, A. and SHARP, G. R. Shear Analysis and Design of Reinforced Concrete Deep Beams. The Structural Engineer, Vol.50, No.10, October 1972, pp.405-409.
  69. KONG, F. K. and SINGH, A. Shear Strength of Lightweight Concrete Deep Beams Subjected to Repeated Loads. ACI-ASCE Special Publication SP-42, American Concrete Institute, Shear in Reinforced Concrete, Vol.2, 1974, pp.461-476.
  70. KONG, F. K., ROBINS, P. J. and SHARP, G. R. The Design of Reinforced Concrete Deep Beams in Current Practice. The Structural Engineer, Vol.53, No.4, April 1975, pp.173-180.
  71. KONG, F. K. and SHARP, G. R. Shear Strength of Lightweight Reinforced Concrete Deep Beams with Web Openings. The Structural Engineer, Vol.51, No.8, August 1973, pp.267-275.
  72. KONG, F. K. and SHARP, G. R. Structural Idealization for Deep Beams with Web Openings. Magazine of Concrete Research, Vol.29, No.99, June 1977, pp.81-91.
  73. KONG, F. K., SHARP, G. R., APPLETON, S. C., BEAUMONT, C. J. and KUBICK, L. A. Structural Idealization for Deep Beams with Web Openings : Futher Evidence. Magazine of Concrete Research, Vol.30, No.103, June 1978, pp.89-95.
  74. KOTSOVOS, M. D. Mechanism of 'Shear' Failure. Magazine of Concrete Research, Vol.35, No.123, June 1983, pp.99-106.
  75. KOTSOVOS, M. D. Behaviour of Reinforced Concrete Beams with Shear-span-to-depth Ratio Between 1.0 and 2.5. Proceedings, ACI, Vol.81, No.3, May-June 1984, pp.279-298.
  76. KOTSOVOS, M. D. Design of Reinforced Concrete Deep Beams. The Structural Engineer, Vlo.66A, No.2, January 1988, pp.28-32.
  77. KUBICK, L. A. Strength and Serviceability of Reinforced Concrete Deep Beams. Ph.D Thesis, University of Cambridge, 1978.
  78. KUMAR, P. Collapse Load of Deep Reinforced Concrete Beams. Magazine of Concrete Research, Vol.28, No.94, March 1976, pp.30-36.
  79. KUMAR, P. Discussion on KUMAR (1976). Magazine of Concrete Research, Vol.29, No.98, March 1977, pp.42-44.
  80. LEONHARDT, F. and WALTHER, R. Wandrtige Trager (Deep Beams). Deutscher Ausschuss fur Stahlbeton, Berlin 1966, (CIRIA Translation, January 1970).
  81. MACGREGOR, J. G. and HAWKINS, N. M. Suggested Revisions to ACI

Building Code Clauses Dealing with Shear Friction and Shear in Deep Beams and Corbels. ACI Journal, Vol.74, No.11, November 1977, pp.537-545.

82. **MANUAL, R. F.** Failure of Deep Beams. ACI-ASCE Special Publication SP-42, American Concrete Institute, Shear in Reinforced Concrete, Vol.2, 1974, pp.425-440.
83. **NAWI, E. G.** Shear, Diagonal Tension and Torsional Strength. In Handbook of Structural Concrete, Edited by KONG, F. K., EVANS, R. H., COHEN, E. and ROLL, F., Pitman, London, and MacGraw-hill, New york, 1983, Chapter 12.
84. **NEWMARK, N. M.** Numerical Procedure for Computing Deflections, Moments and Buckling Loads. Transaction, ASCE, Vol.108, Paper No.2202, 1943, pp.1161-1188.
85. **OVE ARUP & PARTNERS.** The Design of Deep Beams in Reinforced Concrete. Constructional Industry Research and Information Association, CIRIA Guide 2, London, 1977, 131pp.
86. **PFANG, E. D. and SIESS, C. P.** Behaviour of Reinforced Concrete Columns. Journal of the Structural Division, ASCE, Vol.90, No.ST5. October 1964, pp.113-136.
87. **PFANG, E. D. and SIESS, C. P.** Predicting the Structural Behaviour Analytically, Journal of the Structural Division, ASCE, Vol.90, No.ST5, October 1964, pp.99-111.
88. **PORTLAND CEMENT ASSOCIATION.** Tilt-up Load-bearing Walls - A Design Aid. Publication No.EB074.02D, Illinois, 1979, 27pp.
89. **PORTLAND CEMENT ASSOCIATION.** Design of Deep Girders. Concrete Information, No.ST66, 1946, 10pp.
90. **PORTLAND CEMENT ASSOCIATION.** Notes on ACI 318-83 : Building Code Requirements for Reinforced Concrete with Design Applications. 4th Edition, Revised 1984, Illinois, pp.18-1 to 18-14.
91. **RAMAKRISHNAN, V. and ANANTANARAYANA, Y.** Ultimate Strength of Deep Beams in Shear. ACI Journal, Proceedings, Vol.65, No.2, February 1968, pp.87-98.
92. **RAY, S. P.** Shear Strength of Reinforced Concrete Deep Beams without Web Openings : Further Evidence. Journal of Bridge Structural Engineers, Vol.14, No.2, 1984, pp.37-65.
93. **RAY, S. P. and REDDY, C. S.** Strength of Reinforced Concrete Deep Beams with and without Openings in the Web. Indian Concrete Journal, September 1979, pp.242-246.
94. **ROBINS, P. J.** Reinforced Concrete Deep Beams Studied Experimentally

and by the Finite Element Method. Ph.D Thesis, University of Nottingham, 1971.

95. ROBINS, P. J. and KONG, F. K. Modified Finite Element Method Applied to Reinforced Concrete Deep Beams. Civil Engineering and Public Works Review, Vol.68, November 1973, pp.963-966.
96. ROGOWSKY, D. M., MACGREGOR, J. G. and ONG, S. Y. Tests on Reinforced Concrete Deep Beams. ACI Journal, Proceedings, Vol.83, No.4, July-August 1986, pp.614-623.
97. ROGOWSKY, D. M. and MACGREGOR, J. G. Design of Reinforced Concrete Deep Beams. Concrete International, August 1986, pp.49-58.
98. ROGOWSKY, D. M. and MACGREGOR, J. G. Shear Strength of Deep Reinforced Concrete Continuous Beams. Structural Engineering, Report 110, Department of Civil Engineering, University of Alberta, Edmonton, November 1983.
99. SCHUMAN, L. and BACK, G. Strength of Rectangular Flat Plates Under Edge Compression. National Advisory Committee for Aeronautics, Technical Report No.356, 1930.
100. SMITH, K. N. and VANTSIOTIS, A. S. Shear Strength of Deep Beams. ACI Journal, Proceedings, Vol.79, No.3, May-June 1982, pp.201-213.
101. SMITH, K. N. and VANTSIOTIS, A. S. Deep Beam Test Results Compared with Present Building Code Models. ACI Journal, Proceedings, Vol.79, No.4, July-August 1982, pp.280-286.
102. SUBEDI, N. K. The Behaviour of Reinforced Concrete Flanged Beams with Stiffeners. Magazine of Concrete Research, Vol.35, No.122, March 1983, pp.40-54.
103. SUBEDI, N. K. Reinforced Concrete Deep Beams : a method of analysis. Proc. Instn. Civil Engrs., part2, vol.85, March 1988, pp.1-30.
104. SUBEDI, N. K., VARDY, A. E. and KUBOTA, N. Reinforced Concrete Deep Beams - Some Test Results. Magazine of Concrete Research, Vol.38, No.137, December 1986, pp206-219.
105. SWARTZ, S. E., ROSEBRAUGH, V. H. and BERMAN, M. Y. Buckling Tests on Rectangular Concrete Panels. ACI Journal, Proceedings, Vol.71, No.1, January 1974, pp.33-39.

106. SWARTZ, S. E. and ROSEBRAUGH, V. H. Buckling of Reinforced Concrete Plates. Journal of the Structural Division, ASCE, Vol.100, No.ST1, January 1974, pp.195-208.
107. TANER, N., FAZIO, P. P. and ZIELINSKI, Z. A. Strength and Behaviour of Beam-Panels - Tests and Analysis. ACI Journal, Vol.74, No.10, October 1977, pp.511-520.
108. TANG, C. W. J. Reinforced Concrete Deep Beams : Behaviour, Analysis and Design. Ph.D Thesis, University of Newcastle upon Tyne, October 1987.
109. TAYLOR, H. P. J. The Fundamental Behaviour of Reinforced Concrete Beams in Bending and Shear. ACI Publication SP-42, Shear in Reinforced Concrete, 1974, Vol.1, pp.43-77.
110. TAYLOR, H. P. J. Shear Strength of Large Beams. Proceedings, ASCE, Journal of the Structural Division, Vol.98, No.ST11, November 1972, pp.2473-2490.
111. TIMOSHENKO, S. and GERE, J. Theory of Elastic Stability. MacGraw-Hill International Book Company, International Student Edition, 2nd Edition, 15th Printing, 1982, 541pp.
112. UHLMANN, H. L. B. The Theory of Girder Walls with Special Reference to Reinforced Concrete Design. The Structural Engineer, Vol.30, August 1952, pp.172-181.
113. VON KARMAN, T., SECHLER, E. E. and DONNEL, L. H. The Strength of Thin Plates in Compression. Transaction ASME, Vol.54, No.2, January 1932, pp.195-208.
114. WONG, H. H. A. Buckling and Stability of Slender Reinforced Concrete Deep Beams. Ph.D Thesis, University of Newcastle upon Tyne, August 1987.
115. WONG, K. K. Shear Strength and Bearing Capacity of Reinforced Concrete Deep Beams. Ph.D Thesis, University of Leeds, August 1986.

## APPENDIX A

### PREDICTION OF BUCKLING STRENGTHS

#### A.1 USE OF CIRIA GUIDE

First time users of the CIRIA provisions for buckling [85] tend to find them difficult to follow. Strictly speaking, these provisions are intended for design and do not have a straightforward application for predicting ultimate buckling strengths. The author jointly with others [59] [60] have adapted the CIRIA's procedure to predict the ultimate buckling strengths of slender deep beams. This appendix gives an illustration on how such procedure can be adapted to calculate the buckling strengths of the beam-panels described in chapter 5 (series C3 beams); beam CB-40-0.182 of table 5.1 is taken as an example.

##### A.1.1 Supplementary Rules

Step 1 : Determine maximum compressive stress

The maximum applied compressive stress (see comment (a)) is at supports or under loads. Hence,

$$N_v = \frac{\text{Support Reaction (= P/2)}}{\text{Length of Support Bearing (= 0.23 m)}} \\ = 2.17P \quad (\text{kN/m})$$

where P is the buckling load in kN.

Step 2 : Calculate effective height  $h_e$

From CIRIA Guide cl.3.2.2,  $h_e = 1.5h = 1.5 \times 1400 = 2100 \text{ mm}$

Step 3 : Calculate additional and total moments

From BS 8110 cl.3.8.3.1,

$$M_t = M_i + M_{add} = \frac{N_v b}{2000} \left[ \frac{h_e}{b} \right]^2 + M_i$$

where  $M_t$ ,  $M_i$ ,  $M_{add}$  are the total, initial and additional moments per unit width respectively

$N_v$  is the load per unit width

From BS 8110 cl.3.8.3.2,

$$M_i = 0.4 N_v e_1 + 0.6 N_v e_2$$

$$M_{add} = N_v e_{add} = N_v \frac{b}{2000} \left[ \frac{h_e}{b} \right]^2$$

hence

$$M_t = 0.4 N_v e_1 + 0.6 N_v e_2 + N_v e_{add}$$

$$M_t = N_v (0.4 e_1 + 0.6 e_2 + e_{add})$$

with further transformations, this equation becomes :

$$\frac{M_t}{f_{cu} b_1 b^2} = \frac{N_v}{f_{cu} b_1 b} \left( \frac{0.4e_1}{b} + \frac{0.6e_2}{b} + \frac{e_{add}}{b} \right)$$

or

$$\frac{N_v}{f_{cu} b_1 b} = [b/(0.4e_1 + 0.6e_2 + e_{add})] \frac{M_t}{f_{cu} b_1 b^2}$$

where  $b_1$  is a unit width,  $f_{cu}$  the cube strength and  $b$  the beam thickness.

Substituting

$$e_1 = 0 \text{ (eccentricity at bottom, see fig.5.1);}$$

$$e_2 = 0.182b = 0.182 \times 35 = 6.37 \text{ mm (eccentricity at top, fig.5.1)}$$

$$e_{\text{add}} = \frac{35}{2000} \left[ \frac{2100}{35} \right]^2 = 63 \text{ mm}$$

$$\frac{N_V}{f_{\text{cu}} b_1 b} = 0.52 \frac{M_t}{f_{\text{cu}} b_1 b^2}$$

Step 4 : Buckling load

This equation is drawn as a straight line OA which intersects the interaction diagram of beam CB-40-0.182 shown in fig.A.1, giving

$$\frac{N_V}{f_{\text{cu}} b_1 b} = 0.015$$

$$N_V = 0.015 \times 42.2 \times 35 = 22.16 \text{ kN/m}$$

$N_V$  is the load per metre width at which the vertical strip of the panel will collapse; it is therefore the maximum vertical applied stress as stated on p.25 of CIRIA Guide.

From step 1,

$$N_V = 2.17P, \text{ where } P \text{ is the CIRIA buckling load (kN)}$$

$$P = N_V / 2.17 = 10.2 \text{ kN}$$

The experimental buckling load (table 5.1) is 280 kN

The factor of safety is :  $R_{\text{SR}} = 280 / 10.2 = 27.4$  (table 5.1)

#### A.1.2 The Single Panel Method

Step 1 : The equivalent panel

The notional safe equivalent panel (fig.123 of CIRIA Guide) is in this case simply a rectangle of length and height equal to the actual values (fig.5.1 : length = 1700 mm, height = 1400 mm).

Step 2 : The equivalent applied stresses

From p.106 of CIRIA Guide, the equivalent applied vertical

stress (see comment (a) below) is :

$$N_v = \frac{\text{Support Reaction (= P/2)}}{\text{Length of Support Bearing (= 0.23 m)}} \\ = 2.17P \text{ (kN/m)}$$

The equivalent applied horizontal stress is taken from fig.57 of the CIRIA Guide at mid-height (see comment (b) below) :

$$N_h = \frac{0.33 P}{\text{span length (= 1.4 m)}} = 0.24 P$$

The shear stress applied at the ends of the equivalent panel may be taken as zero (see comment (c) below). That is  $\tau = 0$

Step 3 : The critical stresses

From fig.127 of CIRIA Guide,

$$\text{vertical critical stress } N'_{vcr} = \frac{k\pi^2 EI'}{(1.4)^2} = 4.83 EI'$$

From fig.126 of CIRIA Guide,

$$\text{horizontal critical stress } N'_{hcr} = \frac{k\pi^2 EI'}{(1.4)^2} = 4.83 EI'$$

where k is a buckling coefficient given in a graphical form on p.111 of CIRIA Guide; k = 0.96 in this case.

Step 4 : The stress ratios  $R'_v$ ,  $R'_h$ ,  $R'_s$

$$R'_v = \frac{N_v \text{ (step 2)}}{N'_{vcr} \text{ (step 3)}} = \frac{2.17 P}{4.83 EI'} = 0.45 \frac{P}{EI'}$$

$$R'_h = \frac{N_h \text{ (step 2)}}{N'_{hcr} \text{ (step 3)}} = \frac{0.24 P}{4.83 EI'} = 0.05 \frac{P}{EI'}$$

$$R'_s = 0 \text{ since } \tau = 0 \text{ (step2)}$$

step 5 : The stress ratios  $R'_1$ ,  $R'_2$ ,  $R''_2$

In this case, the shorter edges of the equivalent panel are the vertical ones; the CIRIA Guide introduces new stress ratios as follows :

$$R'_1 = R'_h \text{ of step 4 } (= 0.05 P/EI')$$

$$R'_2 = R'_v \text{ of step 4 } (= 0.45 P/EI')$$

$$R''_2 = R'_2/M'_2 \text{ (see comment (d) below)}$$

From fig.129 of CIRIA Guide, for  $R'_s = 0$ ,  $M'_2 = 1.0$

Therefore

$$R''_2 = R'_2/1.0 = R'_2 = 0.45 P/EI'$$

Step 6 : The modification factors  $M_1$  and  $M_2$

$$R''_2/R'_1 = R'_2/R'_1 = (0.45 P/EI')/(0.05 P/EI') = 9.0$$

referring to fig.130 of CIRIA Guide, with  $\Phi = 1700/1400 = 1.2$ ,

the modification factors are :

$$M_1 = 0.10 \quad \text{and} \quad M_2 = 0.91$$

The modified critical stresses are then :

$$\begin{aligned} N_{vcr} &= M_2 \times N'_{vcr} \text{ (of step 3)} \\ &= 0.91 \times 4.83 EI' = 4.40 EI' \end{aligned}$$

$$\begin{aligned} N_{hcr} &= M_1 \times N'_{hcr} \text{ (of step 3)} \\ &= 0.10 \times 4.83 EI' = 0.48 EI' \end{aligned}$$

Step 7 : The effective height  $h_e$

$$\begin{aligned} h_e &= \sqrt{\pi^2 EI' / N_{vcr}} \quad \text{where } N_{vcr} = 4.40 EI' \text{ from step 6} \\ &= 1.50 \text{ m} = 1500 \text{ mm} \end{aligned}$$

Step 8 : The additional and total moments

From BS 8110 cl.3.3.3.1

$$M_t = N_V (0.4e_1 + 0.6e_2 + e_{add})$$

with  $M_i = 0.4 N_V e_1 + 0.6 N_V e_2$

$$M_{add} = N_V e_{add}$$

with similar transformations as in the Supplementary Rules,  
the total moment equation becomes :

$$\frac{M_t}{f_{cu} b_1 b^2} = \frac{N_V}{f_{cu} b_1 b} \left( \frac{0.4e_1}{b} + \frac{0.6e_2}{b} + \frac{e_{add}}{b} \right)$$

or

$$\frac{N_V}{f_{cu} b_1 b} = [b / (0.4e_1 + 0.6e_2 + e_{add})] \frac{M_t}{f_{cu} b_1 b^2}$$

Substituting

$$e_1 = 0 \text{ (eccentricity at bottom, see fig.5.1)}$$

$$e_2 = 0.182b \text{ (eccentricity at top, see fig.5.1)}$$

$$e_{add} = \frac{b}{2000} \left[ \frac{h_e}{b} \right]^2 = \frac{35}{2000} \left[ \frac{1500}{35} \right]^2 = 32.1 \text{ mm}$$

$$\frac{N_V}{f_{cu} b_1 b} = 0.97 \frac{M_t}{f_{cu} b_1 b^2}$$

Step 9 : Buckling load

This equation is drawn as a straight line OB which intersects the interaction diagram of beam CB-40-0.182 shown in fig.A.1, giving

$$\frac{N_V}{f_{cu} b_1 b} = 0.030$$

$$N_V = 0.030 \times 42.2 \times 35 = 44.3 \text{ kN/m}$$

$N_V$  is the load per metre width at which the notional column

strip of the equivalent panel will collapse;  $N_v$  is therefore the 'equivalent applied compressive stress' as defined on p.106 of the CIRIA Guide.

From Step 2,

$$N_v = 2.17P, \text{ where } P \text{ is the buckling load in kN}$$

$$P = N_v / 2.17 = 20.4 \text{ kN}$$

The experimental buckling load (table 5.1) is 280 kN

The safety factor is  $R_{sp} = 280 / 20.4 = 13.7$  as in table 5.1

#### Comments

- (a) Appendix C of the CIRIA Guide defines stresses as force per unit width (kN/m)
- (b) The use of an upper-bound horizontal stress is to ensure a suitably low restraint of the conceptual 'vertical strip' by the conceptual 'horizontal strip'. In the beam considered here, the stiffness of the 'horizontal strip' at mid-height is the most relevant. Hence in step 2, the upper-bound horizontal stress at mid-height has been taken. In practical design, the engineer could either use his judgement in choosing where to take the upper-bound stress or he could take the absolute maximum value from the relevant stress distribution figure in the CIRIA Guide as was done in a design example in reference [62]. Choosing the absolute maximum value will err on the safe side.
- (c) According to p.89 of the CIRIA Guide, the boundary shear stress may be taken as :

$$\tau = \frac{\text{Support reaction (= P/2)}}{\text{Panel height ( 1.4 m)}} = 0.34 P \text{ kN.m}$$

$$\text{From fig.125 of the Guide, } \tau'_{cr} = \frac{4.7 \pi^2 EI'}{1.4^2} = 23.67 EI'$$

$$\text{The applied shear stress ratio } R'_s = \frac{\tau}{\tau'_{cr}} = 0.014 P/EI'$$

To eliminate the effect of the shear stress, the modification factor  $M'_2$  and the modified stress ratio  $R''_2$  are determined as follows:

$$\frac{R'_2 \text{ (see step 5)}}{R'_s \text{ (above)}} = (0.45 P/EI') / (0.014 P/EI') = 32.1$$

From fig.129 of the Guide and with  $\Phi = 1.2$ ,  $M'_2 = 0.99$

Therefore,  $N''_{vcr} = M'_2 \times N'_{vcr}$  of step 3

$$= 0.99 \times 4.83 EI' = 4.78 EI'$$

$$\text{Hence } R''_2 = \frac{N_v \text{ (step 1)}}{N''_{vcr} \text{ (above)}} = \frac{2.17 P}{4.78 EI'} = 0.45 \frac{P}{EI'} = R''_2 \text{ of step 5}$$

Hence, the influence of shear on the critical stresses is negligible.

(d) The relation in step 5, namely

$$R''_2 = R'_2 / M'_2$$

is misprinted in the CIRIA Guide as

$$R'_2 = R'_2 = R'_2 / M'_s$$

### A.1.3 Two panel method

Step 1 : The equivalent panel

As in the single panel method; length = 1700 mm, height = 1400 mm

step 2 : The equivalent applied stresses

### PANEL No.1

For Panel No.1, the effective height is calculated using an upper-bound horizontal stress and a lower-bound vertical stress. From p.109 of CIRIA Guide, the lower-bound vertical stress is taken at mid-height of the panel. From fig.57 of the CIRIA Guide

$$N_v = \frac{0.55 P}{1.4} = 0.39 P \text{ kN/m}$$

where P is the buckling load in kN and 1.4 is the span L in m. The upper-bound horizontal stress is also taken a mid-height of the panel (see comment (b) of Single Panel method).

From fig.57 of CIRIA Guide,

$$N_h = \frac{0.33 P}{1.4} = 0.24 P \text{ kN}$$

### PANEL No.2

for Panel No.2, the effective height is calculated using an upper-bound vertical stress and a lower-bound horizontal stress. From p.108 of CIRIA Guide, the upper-bound vertical stress may be taken at one quarter of the panel height above the support level. From fig.57 of the Guide

$$N_v = \frac{2.48 P}{1.4} = 1.77 P \text{ kN}$$

Page 109 of the CIRIA Guide states that the lower-bound horizontal stress may be taken as two-third of the maximum value. The maximum value was taken at mid-height of fig.57 of the Guide as 0.33

$$N_h = \frac{2/3 \times 0.33 P}{1.4} = 0.16 P$$

Step 3 : The critical stresses

As in step 3 of the Single Panel method :

$$N'_{vcr} = N'_{hcr} = 4.83 EI'$$

Step 4 : The stress ratios  $R'_v$ ,  $R'_h$ ,  $R'_s$

PANEL No.1

$$R'_v = \frac{N_v \text{ (step 1) } 0.39 P}{N'_{vcr} \text{ (step 3) } 4.83 EI'} = 0.0807 P/EI'$$

$$R'_h = \frac{N_h \text{ (step 3) } 0.24 P}{N'_{hcr} \text{ (step 3) } 4.83 EI'} = 0.05 P/EI'$$

$$R'_s = 0 \text{ (as in step 4 of the Single Panel method)}$$

PANEL No.2

$$R'_v = \frac{N_v \text{ (step 1) } 1.77 P}{N'_{vcr} \text{ (step 3) } 4.83 EI'} = 0.366 P/EI'$$

$$R'_h = \frac{N_h \text{ (step 1) } 0.16 P}{N'_{hcr} \text{ (step 3) } 4.83 EI'} = 0.0331 P/EI'$$

$$R'_s = 0$$

Step 5 : The stress ratios  $R'_1$ ,  $R'_2$ ,  $R''_2$

As in step 5 of the Single Panel method, for both panels :

$$R'_1 = R'_h$$

$$R''_2 = R'_2 = R'_v$$

PANEL No.1

$$\frac{R''_2}{R'_1} = \frac{R'_v}{R'_h} = (0.0807 P/EI') / (0.05 P/EI') = 1.6$$

PANEL NO.2

$$\frac{R''_2}{R'_1} = \frac{R'_v}{R'_h} = (0.366 P/EI') / (0.0331 P/EI') = 11.06$$

Step 6 : The modification factors  $M_1$  and  $M_2$

PANEL No.1

$$R''_2 / R'_1 = 1.6$$

With reference to fig.130 of CIRIA Guide and with  $\Phi = 1.2$ ,

$$M_1 = 0.39 \text{ and } M_2 = 0.636$$

Therefore the modified critical stresses are :

$$N_{vcr} = 0.636 \times 4.83 EI' = 3.07 EI'$$

$$N_{hcr} = 0.39 \times 4.83 EI' = 1.88 EI'$$

PANEL No.2

$$R''_2 / R'_1 = 11.06$$

From fig.130 of the Guide :  $M_1 = 0.089$  and  $M_2 = 0.93$

The modified critical stresses are :

$$N_{vcr} = 0.93 \times 4.83 EI' = 4.49 EI'$$

$$N_{hcr} = 0.089 \times 4.83 EI' = 0.43 EI'$$

Step 7 : The effective height  $h_e$

PANEL No.1

$$h_e = \sqrt{\pi^2 EI' / N_{vcr}} \quad \text{where } N_{vcr} = 3.07 EI'$$
$$= 1.79 \text{ m} = 1790 \text{ mm}$$

PANEL No.2

$$h_e = \sqrt{\pi^2 EI' / N_{vcr}} \quad \text{where } N_{vcr} = 4.49 EI'$$
$$= 1.48 \text{ m} = 1480 \text{ mm}$$

The effective height to be used is the larger of the two values,

that is  $h_e = 1.79 \text{ m} = 1790 \text{ mm}$

step 8 : The total moment

$$M_t = M_i + M_{add}$$

$$M_t = N_v (0.4e_1 + 0.6e_2 + e_{add})$$

After a similar transformation as in the Supplementary Rules,  
this equation becomes :

$$\frac{N_v}{f_{cu} b_1 b} = [b/(0.4e_1 + 0.6e_2 + e_{add})] \frac{M_t}{f_{cu} b_1 b^2}$$

where  $b_1$  is a unit width,  $b$  the thickness and  $f_{cu}$  the cube strength.

Substituting

$$e_1 = 0 ; \quad e_2 = 0.182b = 0.182 \times 35 = 6.37 \text{ mm}$$

$$e_{add} = \frac{b}{2000} \left[ \frac{h_e}{b} \right]^2 = \frac{35}{2000} \left[ \frac{1790}{35} \right]^2 = 45.77 \text{ mm}$$

The above equation becomes :

$$\frac{N_v}{f_{cu} b_1 b} = 0.71 \frac{M_t}{f_{cu} b_1 b^2}$$

Step 9 : Buckling load

This equation is drawn as a straight line OC which intersects the interaction diagram of beam CB-40-0.182 shown in fig.A.1, giving

$$\frac{N_v}{f_{cu} b_1 b} = 0.02$$

$$N_v = 0.02 \times 42.2 \times 35 = 29.54 \text{ kN/m}$$

$N_v$  is the vertical load per unit length of the beam at which

buckling failure is considered to occur. Hence, for overall length L of 1.7 m, the CIRIA buckling load is

$$P = N_v \times 1.7 = 50.2 \text{ kN}$$

From table 5.1 the experimental buckling load is 280 kN

The safety factor  $R_{tp} = 280 / 50.2 = 5.57$  as in table 5.1

## A.2 USE OF PCA DESIGN AID

The Portland Cement Association Design Aid [88] is used in conjunction with the American ACI code [1].

Step 1 : The load capacity coefficient

The capacity of a slender beam-panel is given by equation 5.12, namely :

$$P = \phi b_1 b f'_c$$

where  $\phi$  is the load capacity coefficient given in the PCA [88] design tables.

$b_1$  is a unit width

$b$  is the panel thickness

$f'_c$  is the cylinder compressive strength of concrete

Following the arguments in chapter 5, section 5.6.2, table A1 of the PCA Design Aid is represented here in a graphical form in fig.5.7 and was used to read the capacity coefficient,  $\phi$ , of the deep beams of series CB. For beam CB-40-0.182 with an eccentricity/thickness ratio  $e/b$  of 0.182, a vertical steel ratio of 0.5% and a height/thickness ratio  $h/b$  of 40, the load capacity coefficient  $\phi$  is 0.203.

The cylinder compressive strength of concrete is :

$$f'_c = 0.8 f_{cu} = 33.76 \text{ N/mm}^2 \quad (\text{see equation 6.2})$$

Step 2 : Effective width

Each concentrated load is assumed distributed over an effective width of the panel as in section 14.2.4 of ACI(318-83) code, that is :

(a) centre-to-centre distance between loads (= 600 mm, fig.5.1)

(b) width of bearing plus four times the panel wall

$$(C + 4xb = 230 + 4 \times 35) = 370 \text{ mm}$$

For the two point loads, the effective width is (2 x 370) mm

Step 3 : The reduction factor  $\eta$  for isolated footings

From fig.7 of the PCA Design Aid, for  $h/L = 1400/1700 = 0.82$ ,

and  $C/L = 230/1700 = 0.14$ , the reduction factor  $\eta$  is 0.73.

Step 4 : Buckling load

Taking account of the isolated footings, the load capacity becomes:

$$P_{pca} = \phi \eta^2 (230 + 4b) b f'_c$$

$$P_{pca} = 0.203 \times 0.73 \times 740 \times 35 \times 33.76$$

$$= 129.6 \text{ kN}$$

The experimental buckling load is 280 kN

The safety factor  $R_{pca} = 280 / 129.6 = 2.16$  (as in table 5.1)

Table 3.1 : Properties of Simply Supported Deep Beams Tested.

Beam #	Thickness b (mm)	Span/ depth L/h	Total Shear- Span/height a/h	Clear-Shear- Span/depth x/h	Cube Strength $f_{cu}$ (N/mm <sup>2</sup> )	Splitting Strength $f_t$ (N/mm <sup>2</sup> )	Main Steel		Web Steel		Steel *	
							Size (mm)	%	Horizontal Size (mm)	%	Vertical Size (mm)	%
CA-50-0.0	20	1.4	0.40	0.17	96.4	5.25	12	1.70	5	0.49	5	0.49
CA-40-0.0	25	1.4	0.40	0.17	96.0	5.02	12	1.36	5	0.39	5	0.39
CA-33-0.0	30	1.4	0.40	0.17	97.7	5.20	12	1.13	5	0.33	5	0.33
CA-29-0.0	35	1.4	0.40	0.17	95.3	4.75	16	1.72	5	0.28	5	0.28
CA-25-0.0	40	1.4	0.40	0.17	92.8	4.78	16	1.51	5	0.24	5	0.24
CB-70-.182	20	1.0	0.29	0.12	41.2	3.34	10	0.84	6	0.50	6	0.50
CB-50-.182	28	1.0	0.29	0.12	41.0	2.96	10	0.60	6	0.50	6	0.50
CB-40-.182	35	1.0	0.29	0.12	42.2	2.92	12	0.69	6	0.50	6	0.50
CB-35-.182	40	1.0	0.29	0.12	36.9	2.70	10	0.84	6	0.50	6	0.50
CB-30-.182	47	1.0	0.29	0.12	41.7	2.97	10	0.72	6	0.50	6	0.50
CB-25-.182	56	1.0	0.29	0.12	40.4	2.98	12	0.87	6	0.50	6	0.50
CB-20-.182	70	1.0	0.29	0.12	44.4	3.69	12	0.69	6	0.50	6	0.50
CC-0.79/V	30	1.4	0.40	0.17	59.3	3.36	12	1.13	/	0.0	8	0.79
CC-1.93/V	30	1.4	0.40	0.17	62.2	3.56	12	1.13	/	0.0	8	1.93
CC-0.82/H	30	1.4	0.40	0.17	63.5	3.29	12	1.13	8	0.82	/	0.0
CC-1.98/H	30	1.4	0.40	0.17	61.1	3.53	12	1.13	8	1.98	/	0.0
CC-1.96/O	30	1.4	0.40	0.17	61.0	3.43	12	1.13	8	0.99	8	0.97
CC-0.0	30	1.4	0.40	0.17	62.1	4.19	12	1.13	/	0.0	/	0.0
F-0.21-.5/V	47	1.79	0.45	0.21	56.2	3.60	12	0.75	/	0.0	6	0.5
F-0.21-.5/H	47	1.79	0.45	0.21	58.7	3.72	12	0.75	6	0.5	/	0.0
F-0.0-.5/V	47	1.38	0.24	0.0	54.6	3.17	12	0.75	/	0.0	6	0.5
F-0.0-.5/H	47	1.38	0.24	0.0	51.2	3.39	12	0.75	6	0.5	/	0.0

\* For series CC and F : web steel ratio = volume of web steel / volume of concrete

# BEAM NOTATION : The first letter C refers to the author's initial and then the notation changes according to the series main parameter. In series CA, A is the series letter; after the first hyphen the h/b ratio is given and the e/b ratio is given after the second hyphen. In series CB, B refers to the series letter, followed by h/b ratio and then e/b ratio. In series CC, after the series letter C comes the web steel percentage and then the type of reinforcement. In series F, x/h is given after the series letter and the quantity and type of web steel are given after the second hyphen.

Table 3.2 : Failure Modes, Total Ultimate Loads, Flexural Cracking Loads, Inclined Cracking Loads, Diagonal Cracking Loads and 0.3 mm Crack Width Loads - Single Span Deep Beams -

#Beam	Failure modes	Total Ultim. Load (kN)	Flexural Cracking Load (kN)	Inclined Cracking Load (kN)	Diagonal Cracking Load (kN)	0.3 mm Load (kN)
CA-50-0.0	shear	422	50 (0.12)	50 (0.12)	250 (0.59)	100
CA-40-0.0	shear	550	50 (0.07)	100 (0.18)	200 (0.36)	/
CA-33-0.0	shear	630	50 (0.08)	100 (0.16)	300 (0.48)	200
CA-29-0.0	shear	880	50 (0.06)	150 (0.17)	250 (0.28)	225
CA-25-0.0	shear	980	60 (0.06)	180 (0.18)	300 (0.31)	300
CB-25-0.182	shear	750	100 (0.13)	350 (0.47)	500 (0.67)	
CC-0.79/V	shear	450	100 (0.22)	200 (0.44)	250 (0.56)	165
CC-0.93/V	shear	350	50 (0.14)	100 (0.29)	300 (0.86)	165
CC-0.82/H	shear	480	100 (0.21)	150 (0.31)	300 (0.63)	250
CC-1.98/H	shear	500	100 (0.20)	150 (0.30)	250 (0.50)	400
CC-1.96/O	buckling	250	50 (0.20)	100 (0.40)	250 (1.0)	/
CC-0.0	shear	450	100 (0.22)	150 (0.33)	250 (0.56)	175
F-0.21-0.5/V	shear	500	100 (0.20)	150 (0.30)	300 (0.60)	170
F-0.21-0.5/H	shear	540	100 (0.19)	150 (0.28)	300 (0.56)	250
F-0.0 -0.5/V	shear	396	150 (0.38)	200 (0.51)	200 (0.51)	200
F-0.0 -0.5/H	shear	650	100 (0.15)	200 (0.31)	300 (0.46)	250

# Beam notation as in table 3.1.

- Numbers in brackets are proportions of the total ultimate load.

Table 3.3 : Position of Initiation of Diagonal Cracks.

Beam	Shear-span	Formation of Diagonal Cracks : interval of initiation as first observed	
		Along the depth	Along the shear-span
CA-50-0.0	left	$(0.35 - 0.5)h$	$(3/4x - x)$
CA-40-0.0	left	$(0.25 - 0.45)h$	$(x/2 - x)$
CA-33-0.0	right	$(0.35 - 0.5)h$	$(3/4x - x)$
CA-29-0.0	left	$(0.25 - 0.45)h$	$(x/4 - x)$
CA-25-0.0	left	$(0.25 - 0.45)h$	$(x/4 - x)$
CB-25-0.182	left & right	/	/
CC-0.79/V	right	$(0.35 - 0.55)h$	$(x/2 - x)$
CC-1.93/V	left	$(0.35 - 0.5)h$	Close to face of support
CC-0.82/H	right	$(0.30 - 0.5)h$	
CC-1.98/H	left	$(0.30 - 0.45)h$	$(x/4 - x)$
CC-1.96/0	left	$(0.35 - 0.5)h$	$(x/2 - x)$
CC-0.0	left	$(0.25 - 0.45)h$	$(x/4 - 3/4x)$
F-.21-0.5/V	left	$(0.30 - 0.45)h$	$(x/2 - x)$
F-.21-0.5/H	left	$(0.30 - 0.45)h$	$(x/2 - x)$
F-0.0-0.5/V	left	along vertical bar	
F-0.0-0.5/H	right	$(0.30 - 0.5)h$	Close to face of support
Common Interval for all the beams		$(0.35 - 0.45)h$	$(x/2 - \text{face of support})$
Most likely Position		0.4h	$3x/4$

\*  $x$  = Clear shear span, starting from the outside face of the loading.

\*\* The diagonal crack considered in this table is not necessarily the first diagonal crack but the best observed in terms of location.

Table 3.4 : Length and Inclination of Diagonal Cracks

Beam	Shear-span	Length	Measured Angle $\theta_m$ (degrees)	CIRIA Angle $\theta_1$ (degrees)	Proposed Angle $\theta_2$ (degrees)	Angle $\theta_3$ (degrees)
CA-50-0.0	L	0.8 h	66	80	68	58
CA-40-0.0	L	0.9 h	74	~	~	~
CA-33-0.0	L	0.65h	64	~	~	~
CA-29-0.0	L	0.6 h	65	~	~	~
CA-25-0.0	R	0.9 h	61	~	~	~
CC-0.79/V	R	0.95h	65	80	68	58
CC-1.93/V	L	0.75h	68	~	~	~
CC-0.82/H	R	0.8h	62	~	~	~
CC-1.98/H	L	0.85h	67	~	~	~
CC-1.96/O	L	0.7 h	64	~	~	~
CC-0.0	L	0.7 h	66	~	~	~
F-0.21-0.5/V	L	0.75h	67	78	66	55.5
F-0.21-0.5/H	L	0.9 h	62	78	66	55.5
F-0.0-0.5/V	L	0.8 h	90	90	76.5	64.5
F-0.0-0.5/H	R	0.8 h	74	90	76.5	64.5

Table 3.5 : Diagonal Cracking Loads of Single Span Deep beams  
- Measured and Predicted -

Beam	Measured $P_m$ (kN)	Kong et al Equa. 3.3 $P_{cr1}$ (kN)	Modified Kong et al Equa. 3.4		ACI Code Equa. 3.5 $P_{cr3}$ (kN)	$P_{crm}$ $P_{cr3}$	
			$P_{crm}$ $P_{cr1}$	$P_{cr2}$ (kN)			
CA-50-0.0	250	268.8	0.93	184.4	1.35	92.4	2.71
CA-40-0.0	200	335.2	0.60	229.8	0.87	105.2	1.90
CA-33-0.0	300	406.0	0.74	278.5	1.08	118.8	2.53
CA-29-0.0	250	467.8	0.53	320.8	0.78	161.8	1.55
CA-25-0.0	300	527.6	0.57	361.9	0.83	173.7	1.73
CC-0.79/V	250	316.4	0.79	216.9	1.15	101.4	2.47
CC-1.93/V	300	323.9	0.93	222.1	1.35	102.8	2.92
CC-0.82/H	300	327.2	0.92	224.4	1.33	103.5	2.90
CC-1.98/H	250	321.0	0.78	220.2	1.13	102.4	2.44
CC-1.96/O	250	321.0	0.78	220.2	1.13	/	/
CC-0.0	250	323.8	0.77	222.0	1.12	102.8	2.43
F-.21-0.5/v	300	456.6	0.66	311.4	0.96	125.6	2.39
F-.21-0.5/H	300	466.7	0.64	318.4	0.94	127.6	2.35
F-0.0-0.5/V	200	485.4	0.40	332.3	0.60	145.2	1.38
F-0.0-0.5/H	300	496.8	0.64	322.5	0.93	142.6	2.10
CB-50-0.182	250	350.0	0.71	246.6	1.01	/	
CB-50-0.182	350	474.0	0.74	334.1	1.05	/	
CB-50-0.182	450	592.0	0.76	417.5	1.08	/	
CB-50-0.182	500	694.7	0.72	489.6	1.02	251.8	1.99
CB-50-0.182	700	910.0	0.77	641.3	1.09	/	
Mean			0.72		1.04		2.26
Standard Deviation			0.13		0.19		0.46

Note : For beams failing in buckling, the ACI cracking load could not be calculated since equation 3.5 is dependent on the ultimate shear  $V_u$ .

Table 3.6 : Shear Strength Values of Single Span Deep beams  
- Measured and Predicted -

Beam	Measured $V_m$ (kN)	CIRIA Equa. 3.6 $V_1$ (kN)	$V_m$ --- $V_1$	Modified CIRIA Equa. 3.8 $V_2$ (kN)	$V_m$ --- $V_2$	ACI Code $V_3$ (kN)	$V_m$ --- $V_3$	*
								$M_{ut}$ --- $M_{uf}$
CA-50-0.0	211	149.16	1.41	116.5	1.81	93.2	2.26	0.76
CA-40-0.0	275	169.2	1.63	130.2	2.11	116.2	2.37	0.99
CA-33-0.0	315	190.15	1.66	144.9	2.17	140.8	2.24	1.13
CA-29-0.0	440	256.1	1.72	199.3	2.20	159.6	2.76	0.89
CA-25-0.0	490	274.3	1.79	211.7	2.31	175.2	2.80	1.00
CB-25-0.182	375	347.8	1.08	276.4	1.36	241.0	1.56	0.54
CC-0.79/V	225	155.9	1.44	120.43	1.87	100.6	2.24	0.81
CC-1.93/V	175	158.2	1.10	124.11	1.41	112.3	1.56	0.63
CC-0.82/H	240	177.3	1.35	137.30	1.75	113.5	2.11	0.87
CC-1.98/H	250	206.7	1.21	163.82	1.53	111.3	2.25	0.90
CC-1.96/O	125	179.8		141.8		111.2	1.12	0.45
CC-0.0	225	158.1	1.42	180.60	1.87	84.2	2.67	0.81
F-0.21-0.5/V	250	197.3	1.27	146.6	1.71	136.2	1.83	0.91
F-0.21-0.5/H	270	206.95	1.30	154.0	1.75	163.7	1.65	0.98
F-0.0-0.5/V	198	208.7	0.95	159.32	1.24	131.7	1.50	0.43
F-0.0-0.5/H	325	210.9	1.54	162.6	2.00	152.8	2.13	0.71
Mean			1.39		1.81		2.13	
Standard Deviation			0.22		0.31		0.42	

$$* M_{ut}/M_{uf} = \frac{\text{Ultimate Moment at Failure}}{\text{Flexural Capacity Moment}}$$

Table 4.1 : Ultimate Loads of Single Span Deep beams  
- Measured and Predicted -

Beam	Measured	Kong et al Equa. 4.2	$P_m$ ----- $P_1$	Modified	$P_m$ ----- $P_2$	ACI	$P_m$ ----- $P_3$	Author's	$P_m$ ----- $P_4$
	Ultimate Load $P_m$ (kN)			Kong et al Equa. 4.3		Code Equa. 4.4		Method Equa. 4.11	
		$P_1$ (kN)		$P_2$ (kN)		$P_3$ (kN)		$P_4$ (kN)	
CA-50-0.0	422	477	0.88	371.3	1.13	219.4	1.92	360.0	1.17
CA-40-0.0	550	543.4	1.01	416.8	1.32	273.4	2.01	432.2	1.27
CA-33-0.0	630	614.2	1.03	465.4	1.35	331.2	1.90	512.2	1.23
CA-29-0.0	880	796.6	1.10	635.7	1.38	375.6	2.34	612.0	1.43
CA-25-0.0	980	856.4	1.14	676.8	1.45	412.2	2.38	677.8	1.44
CB-25-0.182	750	1120.6	0.67	885.4	0.85	566.9	1.32	877.4	0.85
CC-0.79/V	450	502	0.89	385.8	1.16	236.7	1.90	387.0	1.16
CC-1.93/V	350	509.5	0.69	397.5	0.88	264.2	1.32	402.3	0.87
CC-0.82/H	480	568.4	0.84	438.2	1.09	267.0	1.80	427.6	1.12
CC-1.98/H	500	658.7	0.76	519.6	0.96	261.9	1.91	457.3	1.09
CC-1.96/O	250			failed by buckling					
CC-0.0	450	509.4	0.88	386.5	1.16	198.2	2.27	392.0	1.15
F-0.21-0.5/V	500	639.2	0.78	472.9	1.06	320.3	1.56	538.7	0.93
F-0.21-0.5/H	540	669.4	0.81	495.2	1.09	385.2	1.40	570.3	0.95
F-0.0-0.5/V	396	676.2	0.59	513.6	0.77	310	1.28	565.3	0.70
F-0.0-0.5/H	650	681.7	0.95	522.7	1.24	359.6	1.81	571.4	1.14
Mean			0.87		1.12		1.81		1.10
stand. devia.			0.16		0.20		0.35		0.21

Table 5.1 : Buckling Loads - Measured and Predicted -

Beam	Measured Load (kN)	Equation 4.3 (kN)	Supp. Rules		Sing. Panel		Two Panel		PCA		
			Load (kN)	R <sub>sup</sub>	Load (kN)	R <sub>sp</sub>	Load (kN)	R <sub>tp</sub>	Load (kN)	R <sub>pca</sub>	
CB-20-0.182	800	1045.7	failed at the bearings								
CB-25-0.182	750	885.4	44.0	16.93	99.0	7.57	250.0	3.0	453.5	1.65	
CB-30-0.182	620	691.2	22.6	27.47	56.4	11.0	133.2	4.65	284.6	2.18	
CB-35-0.182	560	611.3	13.6	41.2	30.6	18.31	75.2	7.45	168.0	3.33	
CB-40-0.182	280	516.4	10.2	27.4	20.4	13.7	50.2	5.57	129.6	2.16	
CB-50-0.182	280	387.0	4.0	70.56	8.6	32.57	22.0	12.75	62.8	4.46	
CB-70-0.182	90	315.6	1.4	63.24	2.9	31.6	8.8	10.28	/	/	
Mean			41.13		19.12		7.28		2.76		

Table 6.1 : Properties of continuous deep beams tested.

Beam	Span/ depth L/h	Total Shear- Span/depth a/h	Clear- Shear- Span/depth x/h	Cube Strength $f_{cu2}$ (N/mm <sup>2</sup> )	Splitting Strength $f_t$ (N/mm <sup>2</sup> )	Main Steel				Web Steel *					
						Top		Bottom		Horizontal		Vertical		Inclind	
						Size (mm)	%	Size (mm)	%	Size (mm)	%	Size (mm)	%	Size (mm)	%
CD-0.5/V	0.90	0.45	0.21	50.5	2.96	12	0.75	12	0.75	/	0.0	6	0.5	/	0.0
CD-0.5/H	0.90	0.45	0.21	50.7	4.32	12	0.75	12	0.75	6	0.5	/	0.0	/	0.0
CD-0.5/I	0.90	0.45	0.21	56.4	3.06	12	0.75	-	-	/	0.0	/	0.0	6	0.5
CD-1.0/V	0.90	0.45	0.21	66.1	4.22	12	0.75	-	-	/	0.0	6	1.0	/	0.0
CD-1.0/H	0.90	0.45	0.21	52.7	4.49	12	0.75	-	-	6	1.0	/	0.0	/	0.0
CD-1.0/I	0.90	0.45	0.21	51.2	3.15	12	0.75	-	-	/	0.0	/	0.0	6	1.0
CD-0.0	0.90	0.45	0.21	63.0	5.35	12	0.75	-	-	/	0.0	/	0.0	/	0.0
CE-0.5/V	0.69	0.24	0.0	57.7	4.17	12	0.75	-	-	/	0.0	6	0.5	/	0.0
CE-0.5/H	0.69	0.24	0.0	53.7	3.80	12	0.75	-	-	6	0.5	/	0.0	/	0.0
CE-1.0/V	0.69	0.24	0.0	62.2	4.02	12	0.75	-	-	/	0.0	6	1.0	/	0.0
CE-1.0/H	0.69	0.24	0.0	57.1	4.46	12	0.75	-	-	6	1.0	/	0.0	/	0.0
CE-0.0	0.69	0.24	0.0	60.2	4.11	12	0.75	-	-	/	0.0	/	0.0	/	0.0

$$* \text{ web steel ratio} = \frac{\text{volume of web steel}}{\text{volume of concrete}}$$

Table 6.2 : Steel Properties

Type of Steel	Bar Diameter (mm)	Young's Modulus E (kN/mm <sup>2</sup> )	Yield Stress $f_y$ (N/mm <sup>2</sup> )	Ultimate Stress $f_u$ (N/mm <sup>2</sup> ).
Deformed bars	8	268	500	646
	10	183	518	668
	12	250	480	599
	16	/	480	607
Plain round bars	2	/	348	
	5	400	485	698
	6	241	410	526

**Table 7.1 : Failure Modes, Total Ultimate Loads, Flexural Cracking Loads, Diagonal Cracking Loads and the Serviceability Limit State of Cracking loads**  
 - Continuous Deep Beams -

Beam	Failure Mode	Total Ultimate Load (kN)	Flexural Cracking Load (kN)	Diagonal Cracking Load (kN)		0.3 mm Crack Width Load (kN)	0.1 mm Crack Width Load (kN)
				End Shear-span	Interior Shear-span		
CD-0.5/V	Shear+ Bearing	800	150 (0.19)	300 (0.38)	150 (0.19)	150 (0.19)	/
CD-0.5/H	Shear+ Bearing	850	100 (0.12)	800 (0.94)	100 (0.12)	350 (0.41)	50
CD-0.5/I	Bearing	1000	150 (0.15)	750 (0.75)	/	750 (0.75)	250
CD-1.0/V	Shear+ Bearing	600	100 (0.17)	350 (0.58)	200 (0.34)	150 (0.25)	/
CD-1.0/H	Bearing	850	100 (0.12)	400 (0.48)	/	800 (0.94)	200
CD-1.0/I	Bearing	1020	150 (0.15)	550 (0.54)	/	800 (0.79)	450
CD-0.0	Shear+ Bearing	800	150 (0.19)	500 (0.63)	150 (0.19)	150 (0.19)	/
CE-0.5/V	Shear+ Bearing	650	300 (0.46)	400 (0.62)	500 (0.77)	400 (0.61)	/
CE-0.5/h	Bearing	800	200 (0.25)	350 (0.44)	/	600 (0.75)	300
CE-1.0/V	Shear+ Bearing	700	200 (0.29)	400 (0.57)	/	360 (0.51)	200
CE-1.0/H	Bearing	924	200 (0.22)	300 (0.32)	/	600 (0.71)	300
CE-0.0	Shear+ Bearing	800	300 (0.38)	400 (0.50)	/	350 (0.44)	/

- Numbers in brackets are proportions of the total ultimate load.

**Table 7.2 : Reactions at Supports at or close to Ultimate**  
 - Measured ones Compared to those calculated According to Shallow Beam theory -

Beam	Total Applied Load 2P (kN)	Measured Reactions		Calculated Reactions as in Continuous Shallow beams		Reactions of Two Adjacent Single Span Beams	
		End (kN)	Interior (kN)	End (kN)	Interior (kN)	End (kN)	Interior (kN)
CD-0.5/V	800	217.5	365.0	124.0	552.0	200.0	400.0
CD-0.5/H	800	210.0	380.0	124.0	552.0	200.0	400.0
CD-0.5/I	900	243.0	414.0	139.5	621.0	225.0	450.0
CD-1.0/V	550	150.0	250.0	85.3	375.5	137.5	275.0
CD-1.0/H	800	225.0	350.0	124.0	552.0	200.0	400.0
CD-1.0/I	950	268.5	413.0	147.3	655.5	237.5	475.0
CD-0.0	800	237.0	326.0	124.0	552.0	200.0	400.0
CE-0.5/V	650	211.0	228.0	162.5	325.0	211.7	226.5
CE-0.5/h	700	244.5	211.0	175.0	350.0	228.0	243.9
CE-1.0/V	700	222.5	255.0	175.0	350.0	228.0	243.9
CE-1.0/H	924	/	/	/	/	/	/
CE-0.0	800	240.5	319.0	200.0	400.0	260.6	278.8

**Table 7.3 : Bending Moments at or close to Ultimate**  
 - Measured and Calculated -

Beam	Total Applied Load 2P (kN)	Measured Bending Moment (kN.m)		Calculated Bending Moment as in continuous Shallow beams (kN.m)		Bending Moment of a Single Span Beam (kN.m)
		Span	Support	Span	Support	
CD-0.5/V	800	93.5	15.1	53.3	-65.4	86.0
CD-0.5/H	800	90.3	8.6	53.3	-65.4	86.0
CD-0.5/I	950	104.5	15.5	60.0	-73.5	97.0
CD-1.0/V	550	64.5	10.8	36.7	-44.9	59.1
CD-1.0/H	800	96.8	21.5	53.3	-65.4	86.0
CD-1.0/I	475	115.5	26.7	63.3	-77.6	102.1
CD-0.0	800	101.9	31.8	53.3	-65.4	86.0
CE-0.5/V	650	48.5	-0.5	37.4	-32.5	48.7
CE-0.5/h	700	56.2	10.9	40.3	-35.0	52.4
CE-1.0/V	700	51.2	-3.7	40.3	-35.0	52.4
CE-1.0/H	924	/	/	/	/	/
CE-0.0	800	55.3	-13.3	46.0	-40.0	60.0

Table 8.1 : Shear Strengths at Ultimate - Continuous Deep Beams -

Beam	End Shear-span		Interior Shear-span		Max. Design Stress # (N/mm <sup>2</sup> )	Measured/Predicted shear	
	V <sub>U</sub> (kN)	v <sub>U</sub> (N/mm <sup>2</sup> )	V <sub>U</sub> (kN)	v <sub>U</sub> (N/mm <sup>2</sup> )		Equation 3.6	Equation 3.8
* CD-0.5/V	217.5	4.82	182.5	4.04	4.07	1.14	1.54
* CD-0.5/H	221.0	4.90	204.0	4.52	4.07	1.11	1.48
CD-0.5/I	270.0	5.98	230.0	5.10	4.29	1.30	1.74
CD-1.0/V	165.0	3.66	135.0	2.99	4.68	0.79	1.07
CD-1.0/H	238.0	5.27	187.0	4.14	4.38	1.08	1.44
CD-1.0/I	287.9	6.38	217.2	4.81	4.10	1.37	1.80
CD-0.0	250.8	5.56	174.3	3.86	4.54	1.21	1.64
* CE-0.5/V	211.0	4.68	114.0	2.53	4.34	0.92	1.29
* CE-0.5/H	280.0	6.21	120.0	2.66	4.20	1.28	1.65
CE-1.0/V	222.5	5.00	127.5	2.83	4.50	1.08	1.32
CE-1.0/H	/	/	/	/	/	/	/
CE-0.0	240.5	5.33	159.5	3.53	4.44	1.10	1.45

Note : In some beams the interior reaction could not be recorded at failure and the corresponding shear values were extrapolated from the ultimate loads according to the previous increments

\* These continuous beams are identical to the single span beams below.

# The maximum design stress given in the CIRIA Guide (85) is :  $1.3 \lambda_1 \sqrt{f_{cu}}$

Table 8.2 : Shear Strength at Ultimate - Single Span Deep Beams -

Beam	V <sub>U</sub> (kN)	v <sub>U</sub> (N/mm <sup>2</sup> )	Max. Design Stress (N/mm <sup>2</sup> )	Measured/Predicted Shear	
				Equation 3.6	Equation 3.8
F-0.21-0.5/V	250.0	5.54	4.30	1.27	1.71
F-0.21-0.5/H	270.0	5.98	4.38	1.30	1.75
F-0.0-0.5/V	198.0	4.39	4.23	0.95	1.24
F-0.0-0.5/H	325.0	7.20	4.10	1.54	2.00

Table 8.3 : Bearing Stresses at Loading Points

- Beams which failed in proper concrete crushing -

Beam	Bearing Stress N/mm <sup>2</sup>	CIRIA Guide Limit: $0.8f_{cu}$ N/mm <sup>2</sup>	ACI code Limit (equation 8.3) N/mm <sup>2</sup>	$0.6f_{cy}$ N/mm <sup>2</sup>
CD-0.5/I	46.3	45.1	27.1	33.8
CD-1.0/H	39.3	47.0	28.2	35.2
CD-1.0/I	47.2	41.0	24.6	30.7
CE-0.5/H	37.0	43.0	25.8	32.2
CE-1.0/H	42.7	45.7	27.4	34.3

Table 8.4 : Bearing stresses at Loading Points

- Beams where Concrete Crushing was Precipitated by Cracks -

Beam	Bearing Stress N/mm <sup>2</sup>	CIRIA Guide Limit: $0.8f_{cu}$ N/mm <sup>2</sup>	ACI code Limit (equation 8.3) N/mm <sup>2</sup>	$0.6f_{cy}$ N/mm <sup>2</sup>
CD-0.5/V	37.0	40.4	24.2	30.3
CD-0.5/H	39.3	40.1	24.3	30.4
CD-1.0/V	27.8	52.9	31.7	39.7
CD-0.0	37.0	50.4	30.2	37.8
CE-0.5/V	30.1	46.2	27.7	34.6
CE-1.0/V	32.4	49.8	29.9	37.3
CE-0.0	37.0	48.2	28.9	36.1

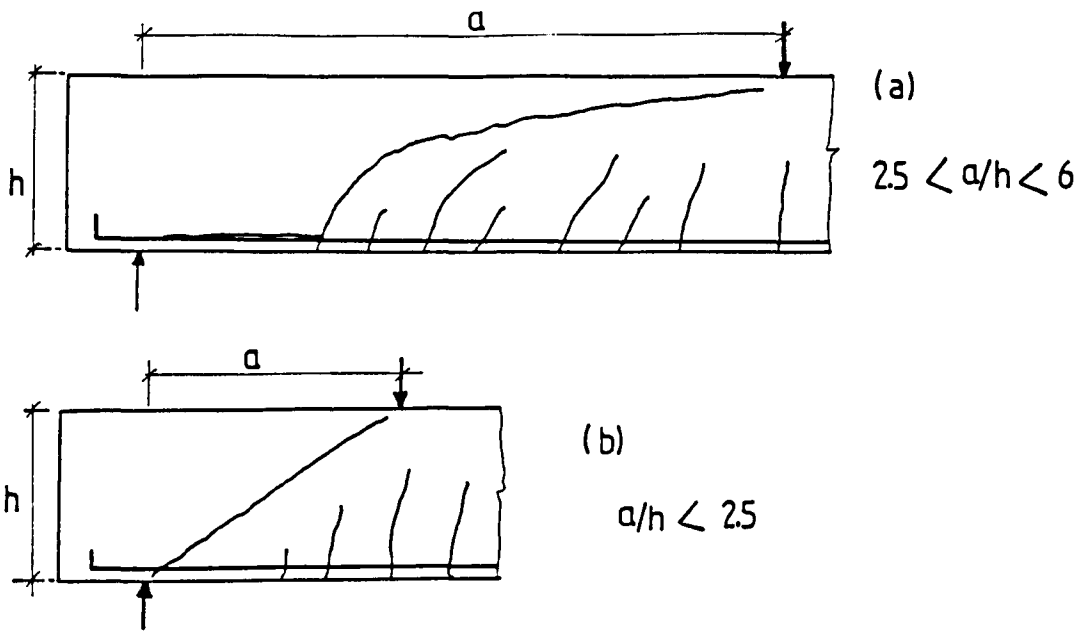


Fig.1.1: Cracks pattern of an ordinary beam

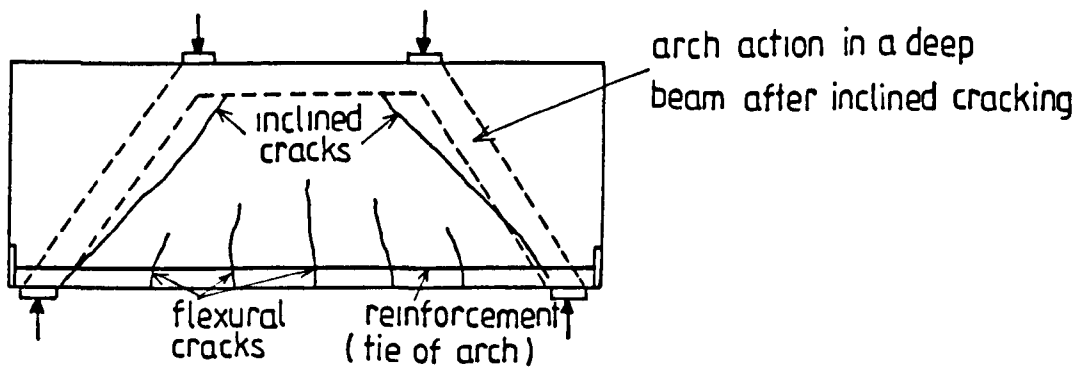


Fig.1.2: The tied-arch of De paiva and Siess [40]

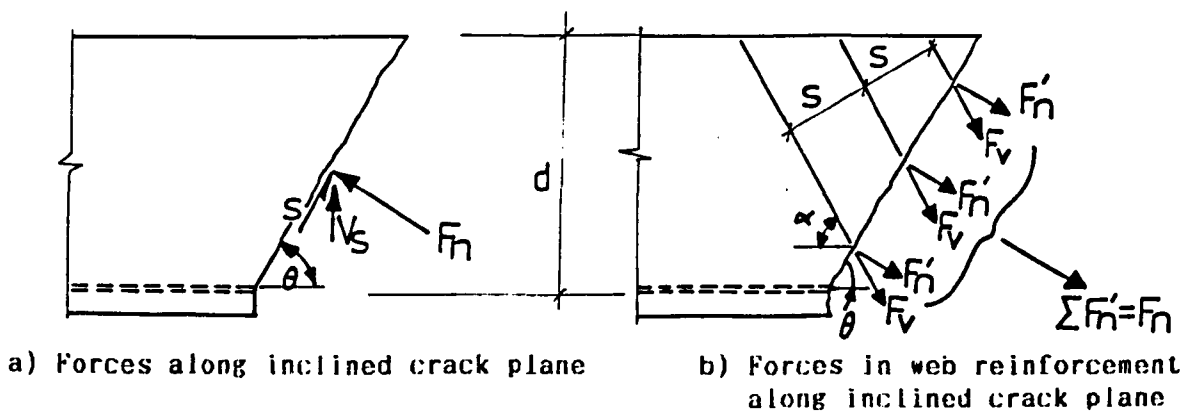


Fig.1.3: Shear capacity of web reinforcement. Crist [38]

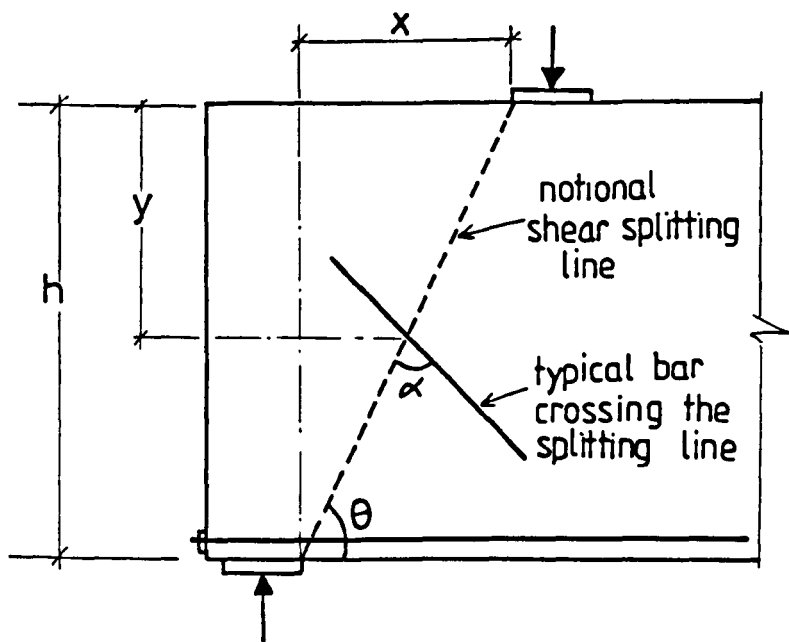


Fig.1.4: Meaning of symbols in equation 1.15

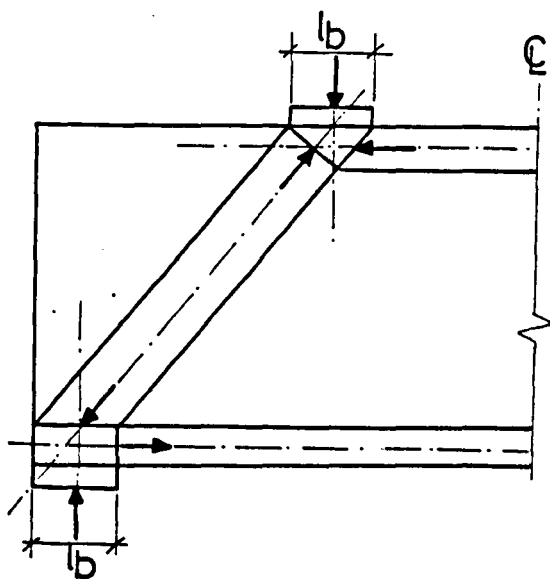


Fig.1.5: The lower-bound truss model of Kumar [78]  
 - equilibrium condition not satisfied -

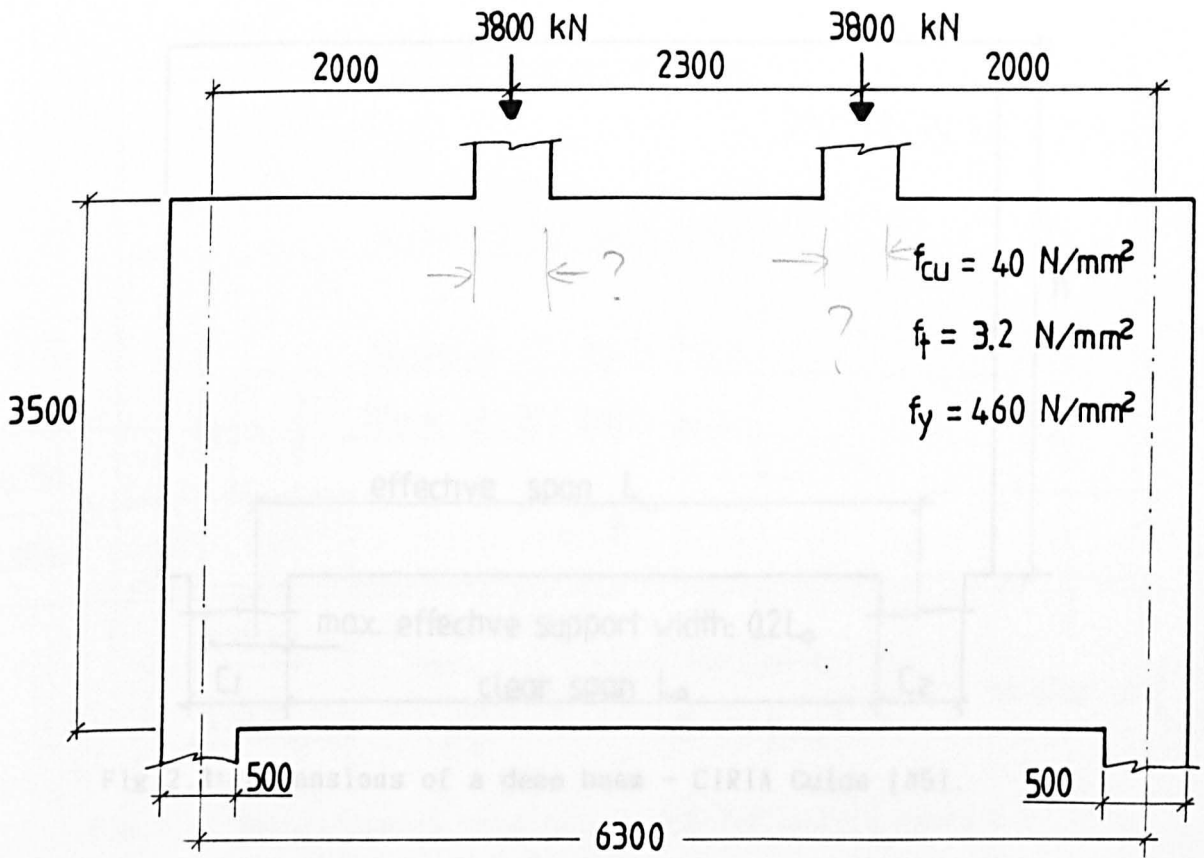


Fig.2.1: Design example - geometry and loading -

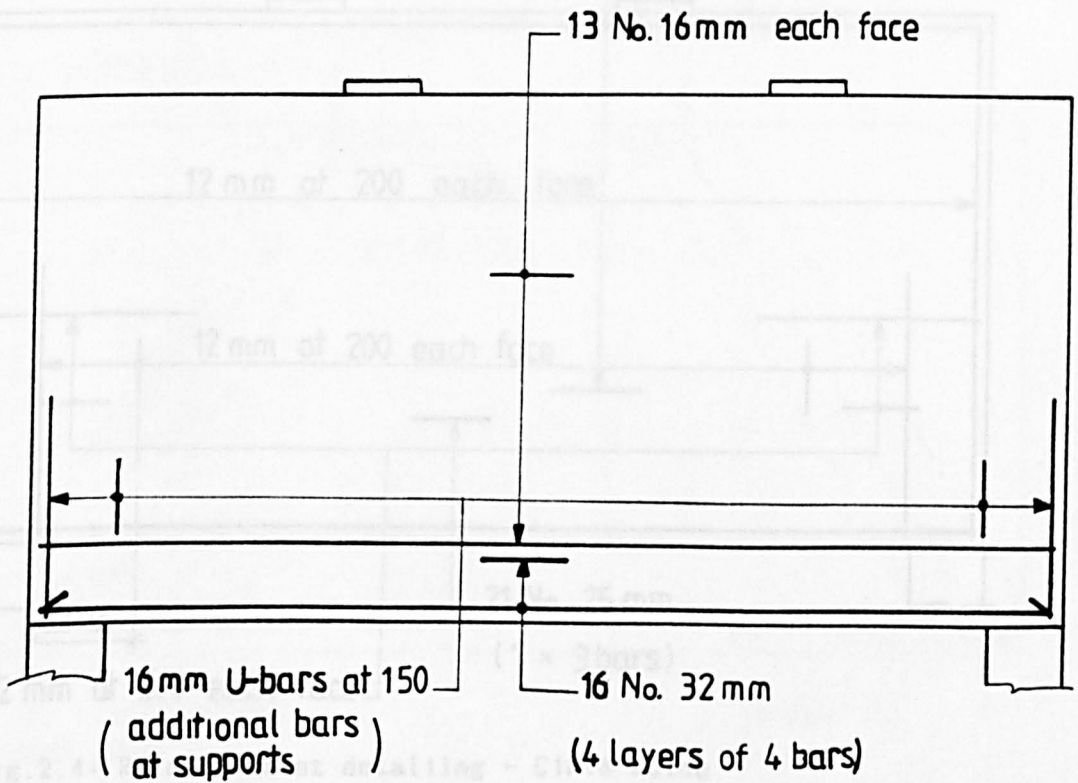


Fig.2.2: Reinforcement detailing - Kong et al recommendations design example

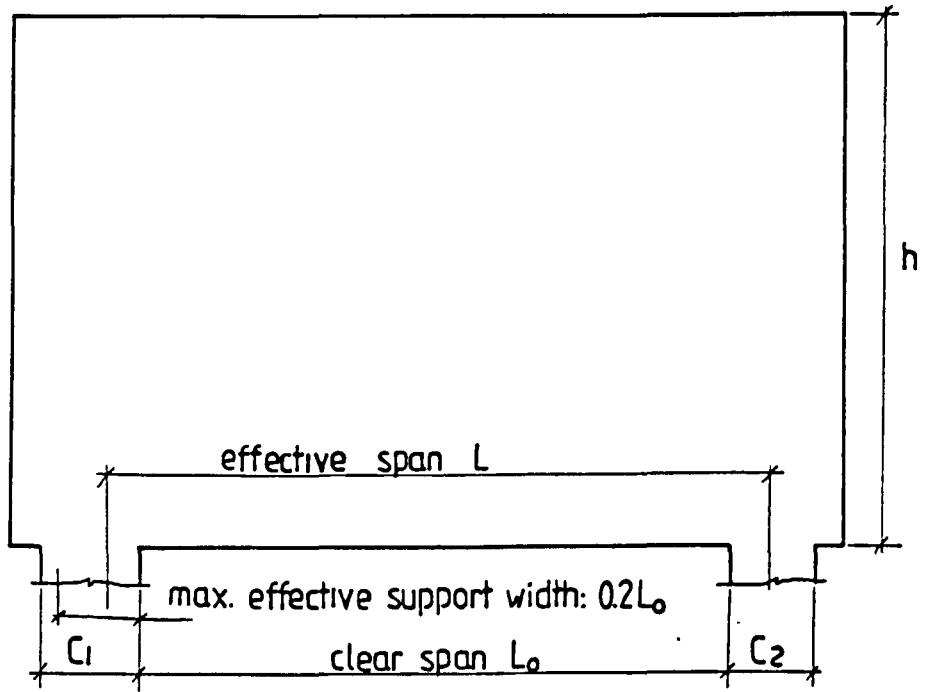


Fig.2.3: Dimensions of a deep beam - CIRIA Guide [85].

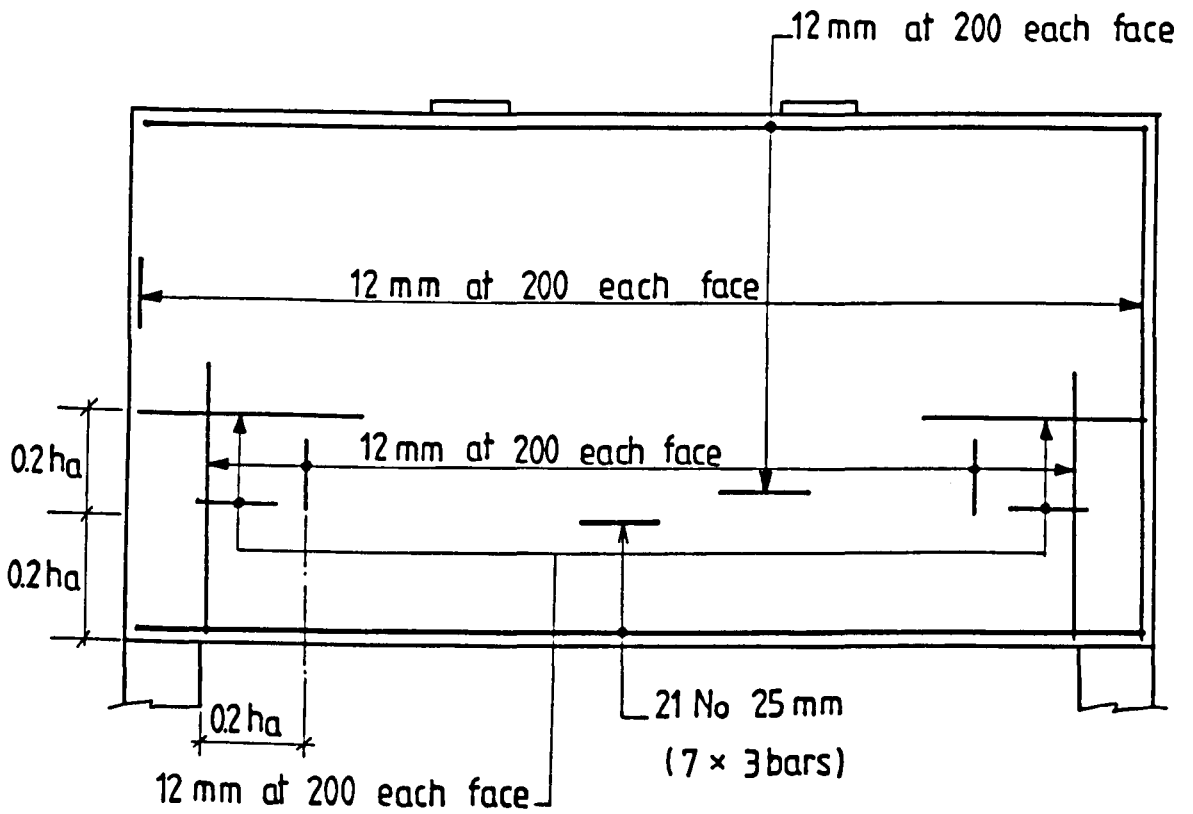


Fig.2.4: Reinforcement detailing - CIRIA Guide design example-

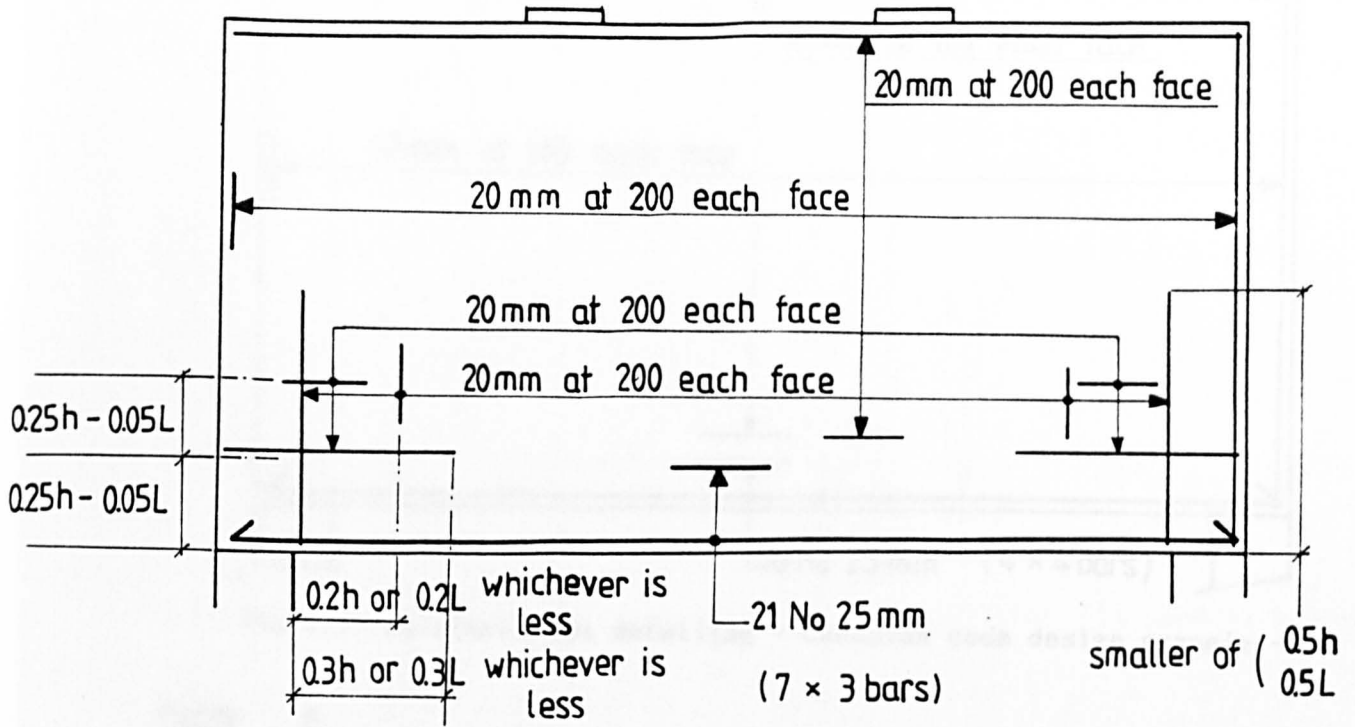


Fig.2.5: Reinforcement detailing - CEB-FIP design example -

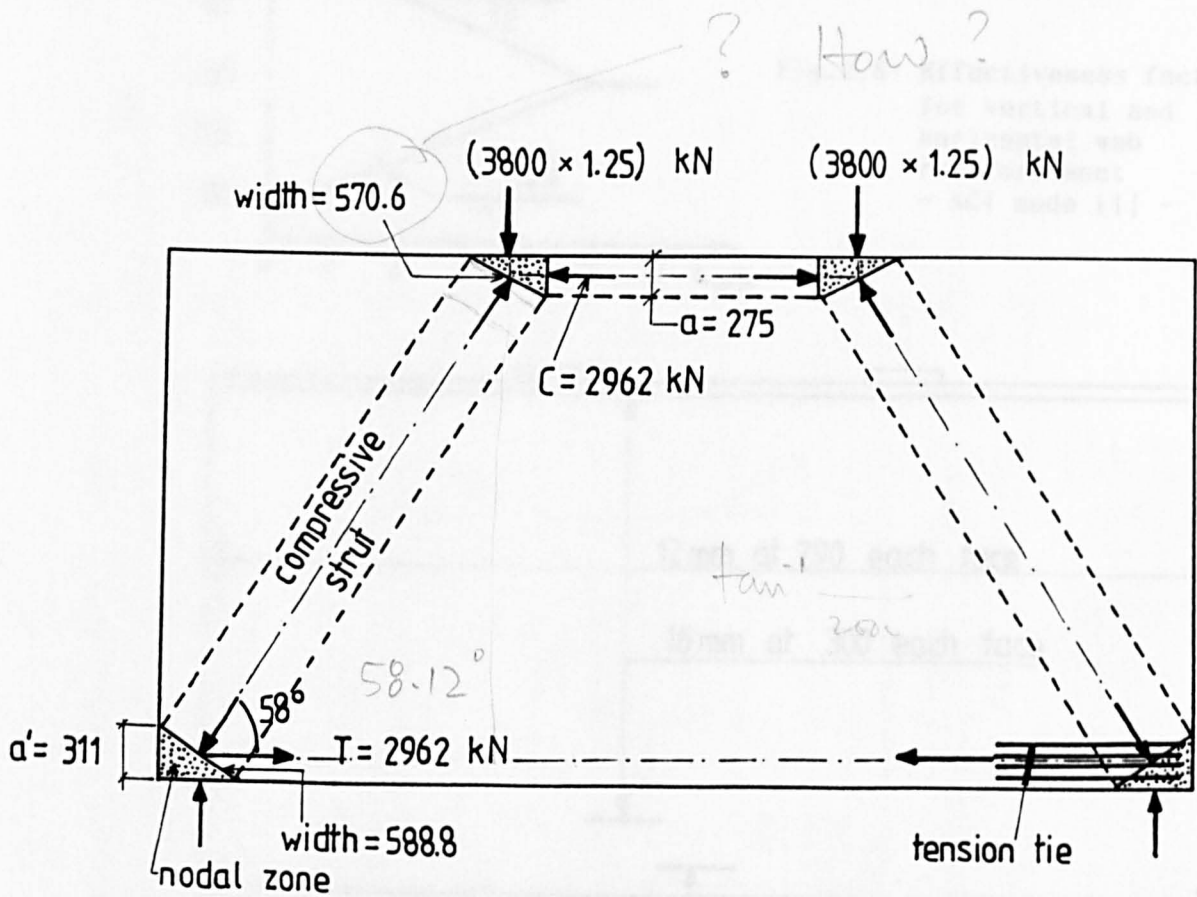


Fig.2.6: Deep beam truss model according to the Canadian code [23].

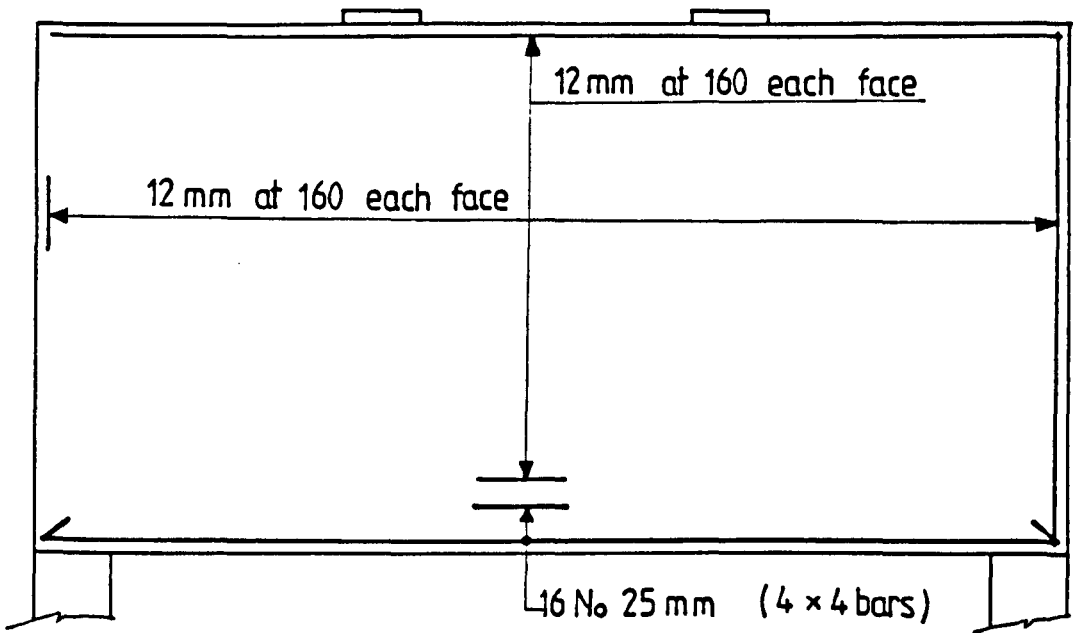


Fig.2.7: Reinforcement detailing - Canadian code design example -

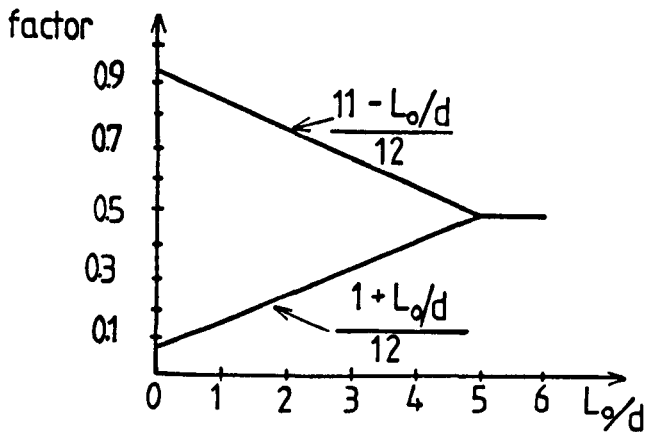


Fig.2.8: Effectiveness factors for vertical and horizontal web reinforcement - ACI code [1] -

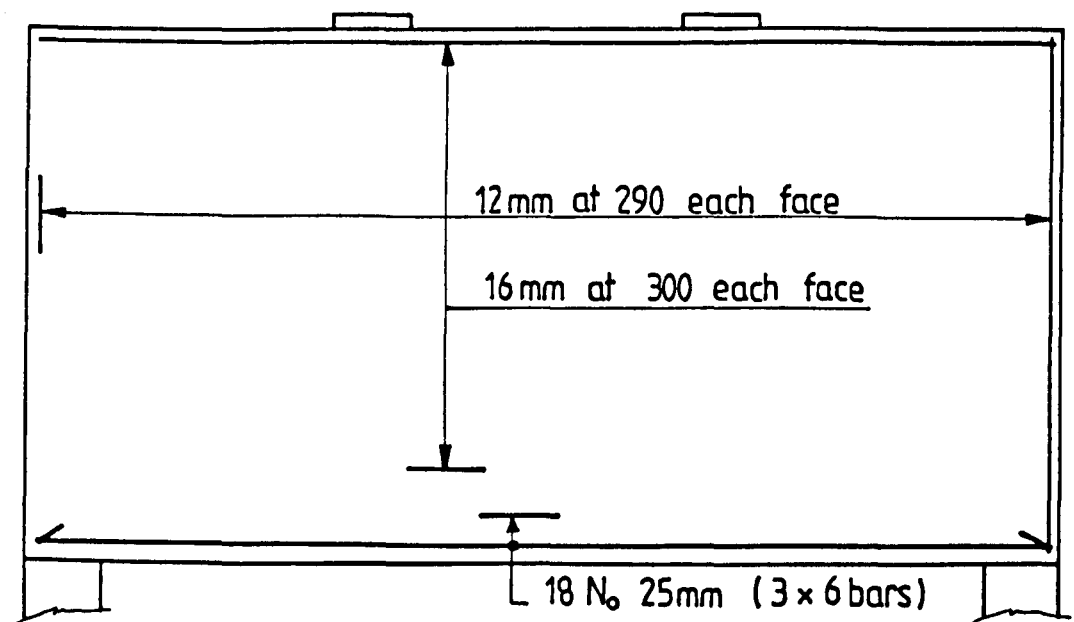
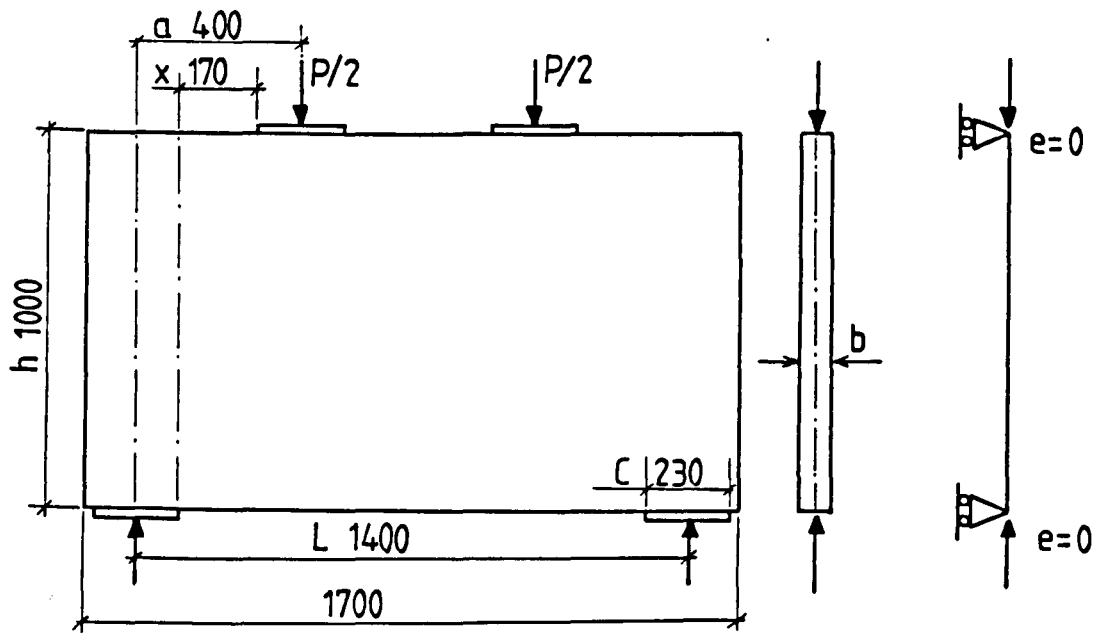
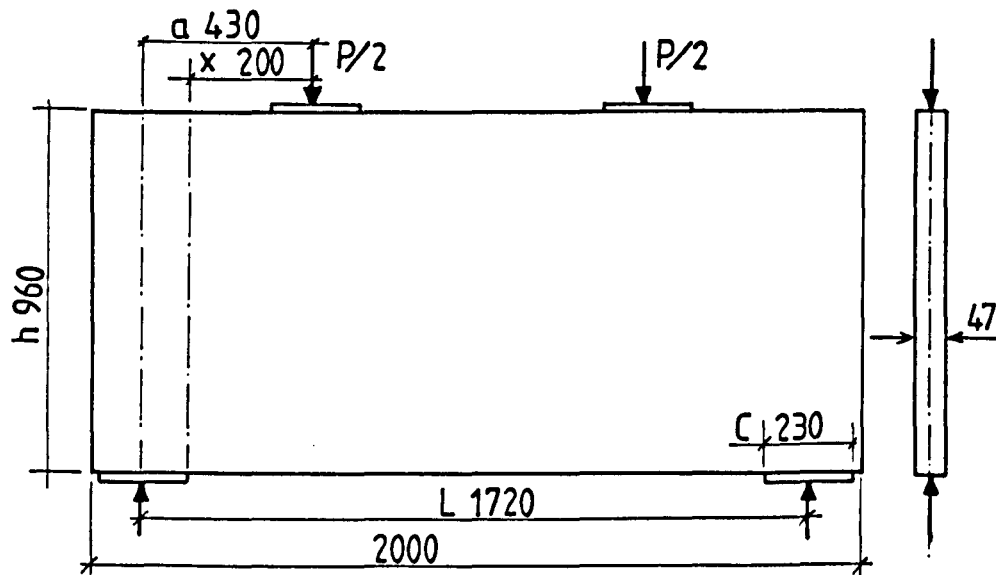


Fig.2.9: Reinforcement detailing - ACI code design example -



a) Dimensions of test beams - series CA, CC -

b) Loading scheme



c) series F beams

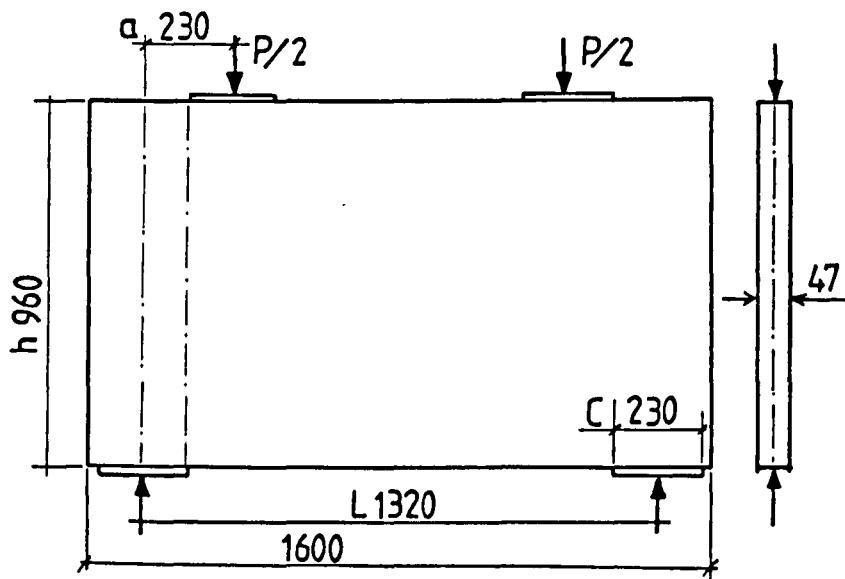


Fig.3.1: Details of test beams

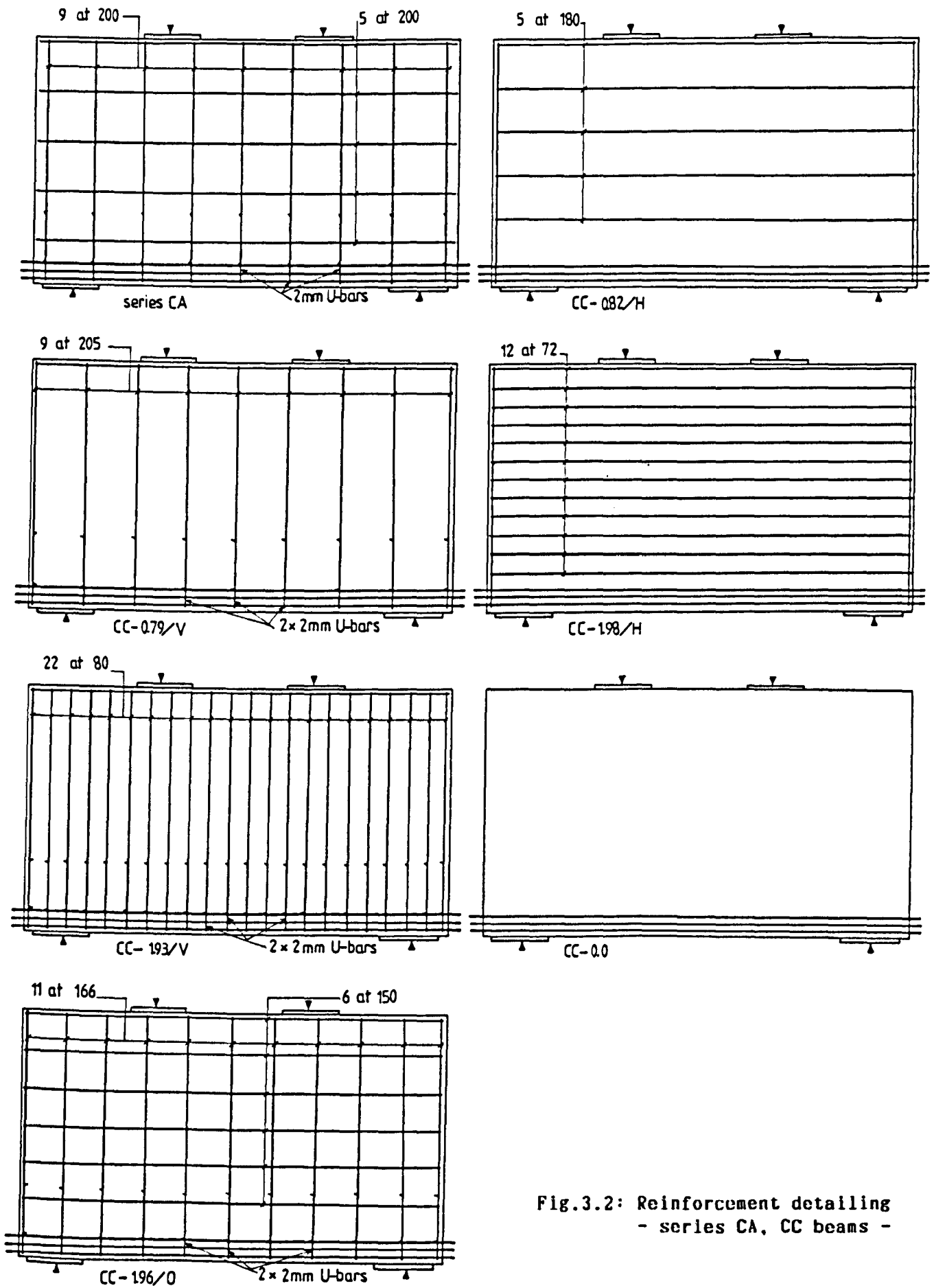


Fig.3.2: Reinforcement detailing  
- series CA, CC beams -

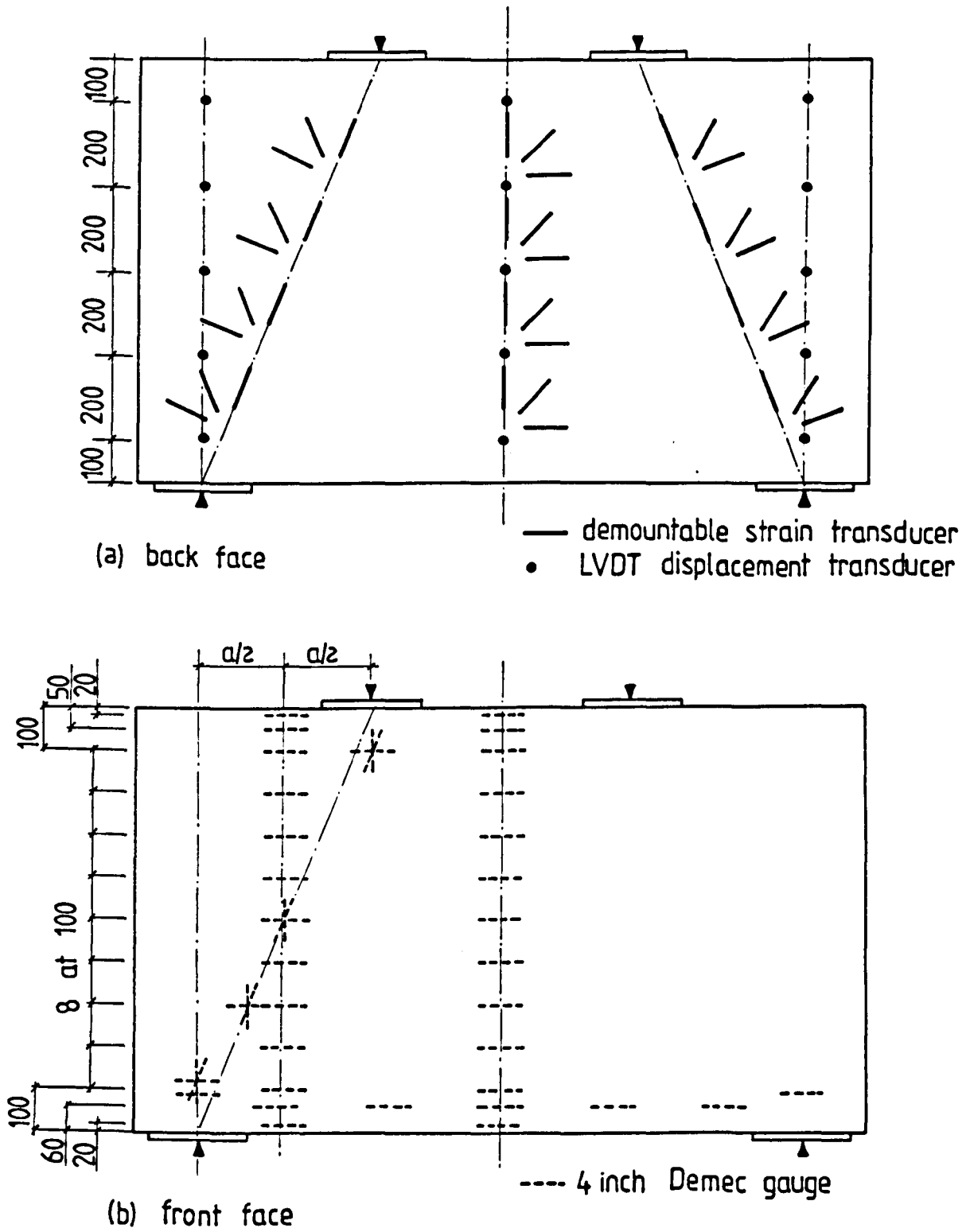


Fig.3.3: Arrangement of LVDT's and strain transducers  
- series CA and CC beams -



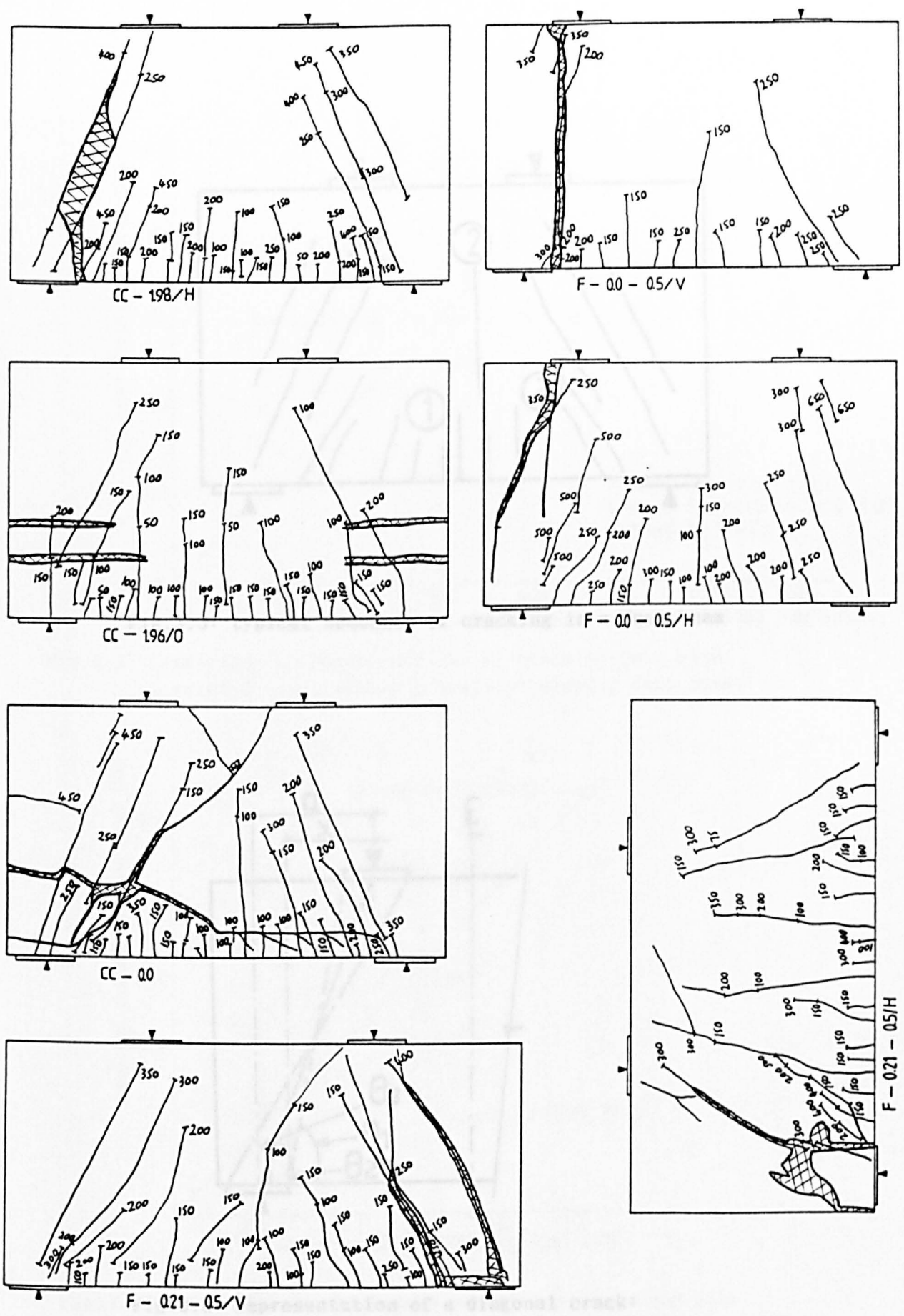


Fig.3.4: contd. Cracks patterns at failure - series CA, CC, F beams - the load at which each crack was first observed is indicated.

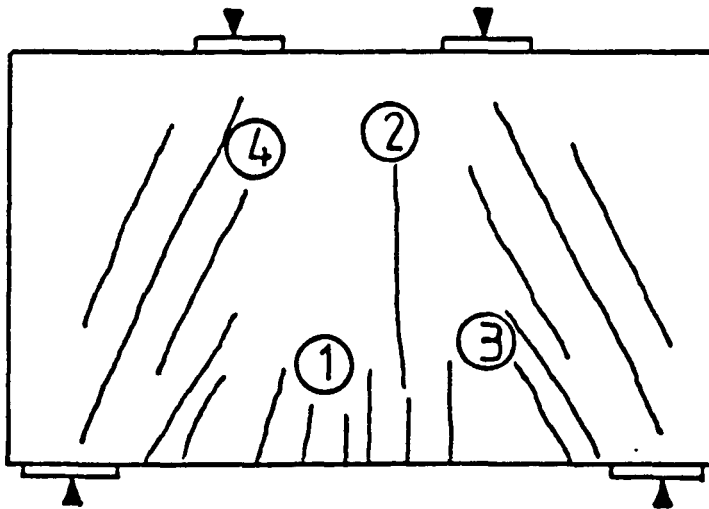


Fig.3.5: typical sequence of cracking in a deep beam

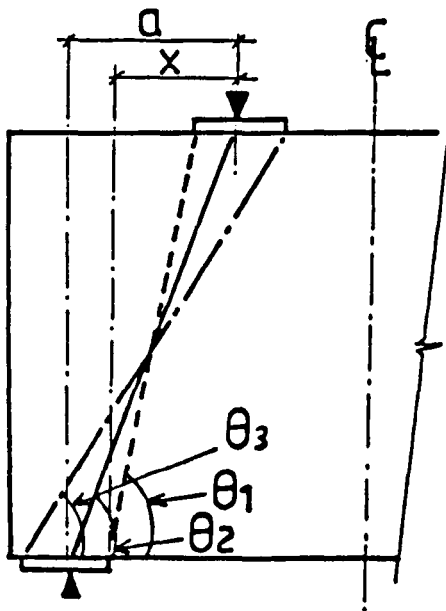


Fig.3.6: Representation of a diagonal crack:  
 - dotted line for stocky deep beams  
 - full line for slender deep beams

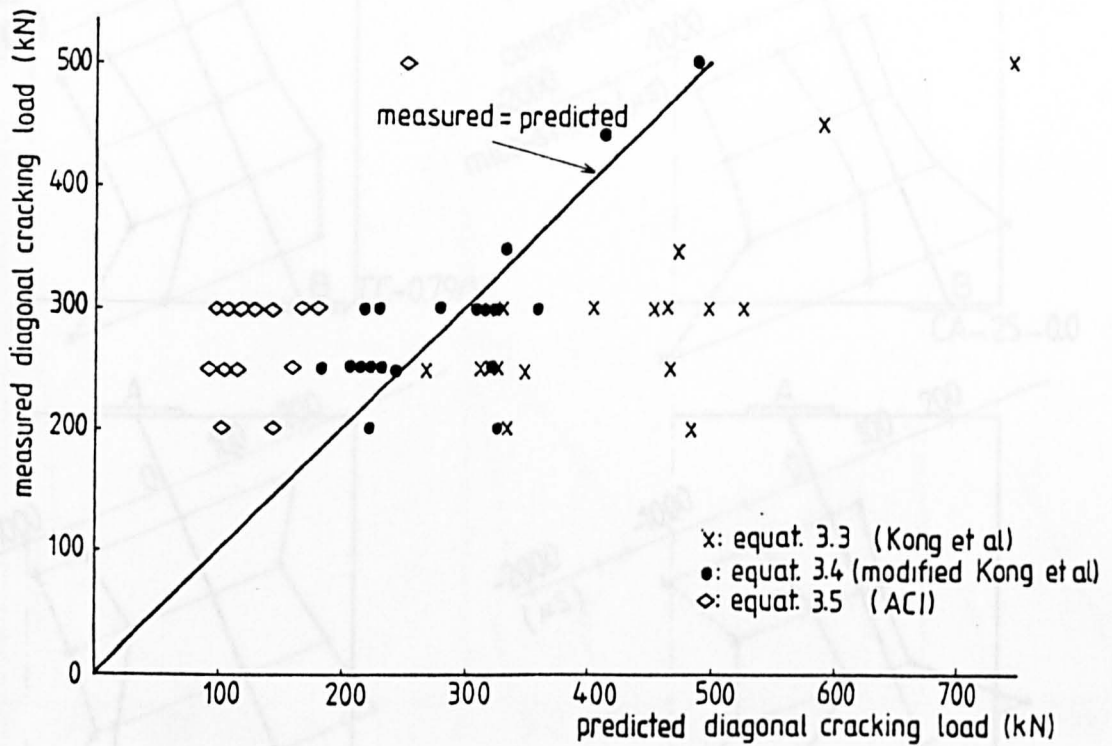


Fig.3.7: Comparison of measured diagonal cracking load with predicted one - author's tests on slender deep beams -

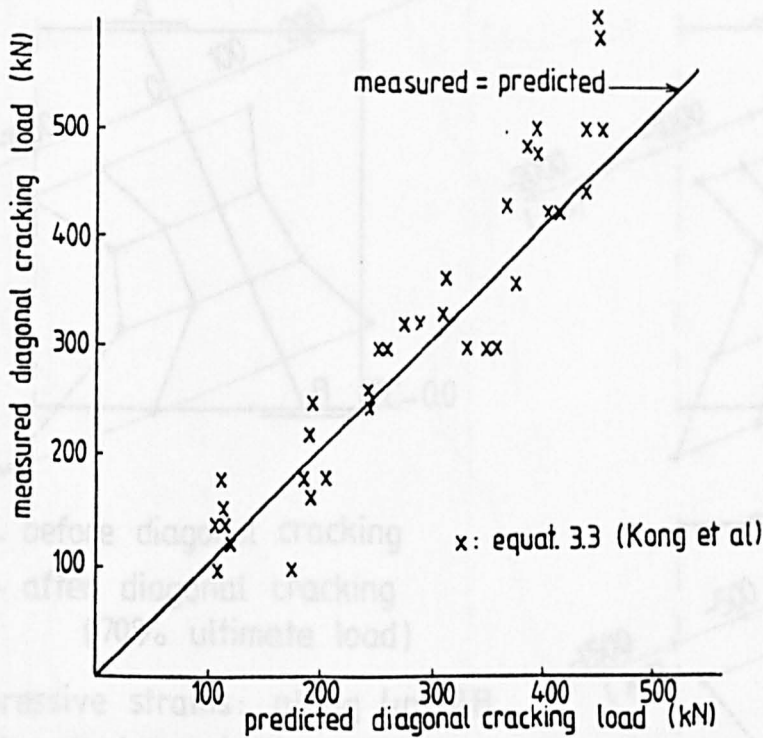
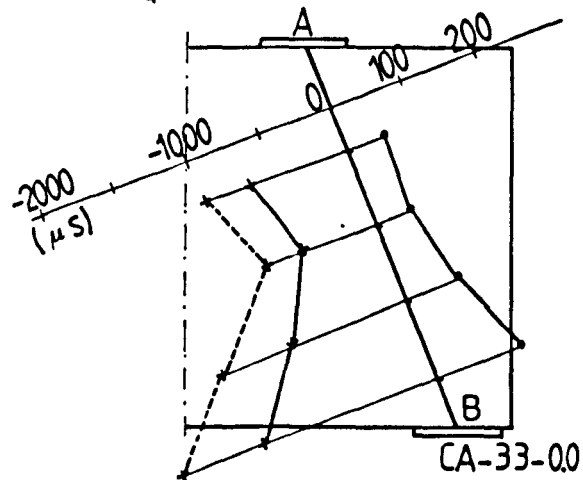
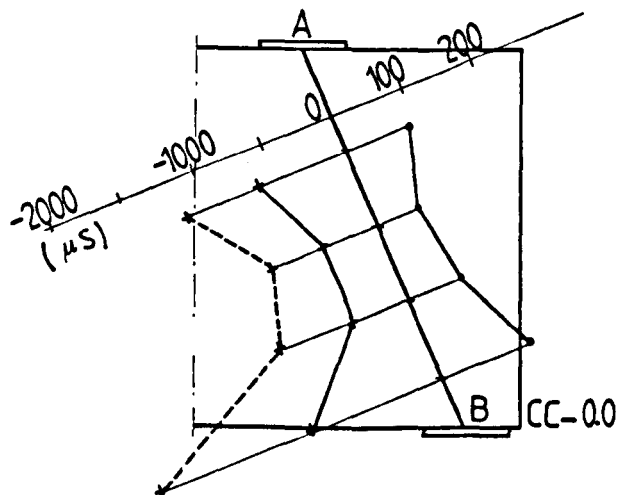
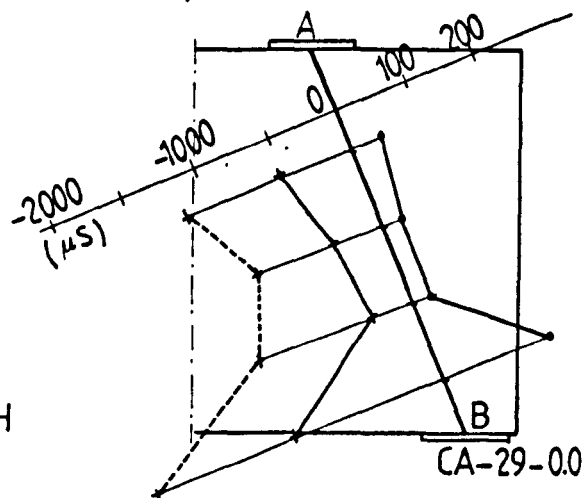
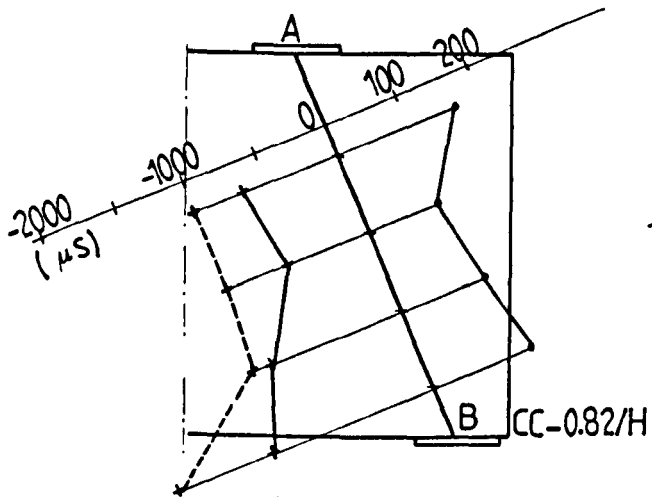
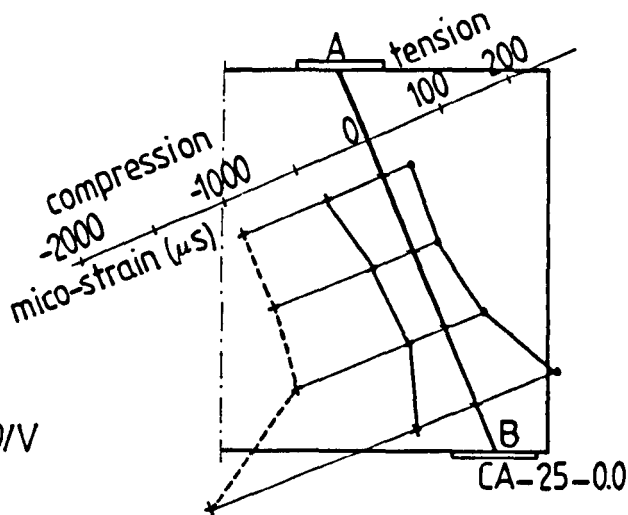
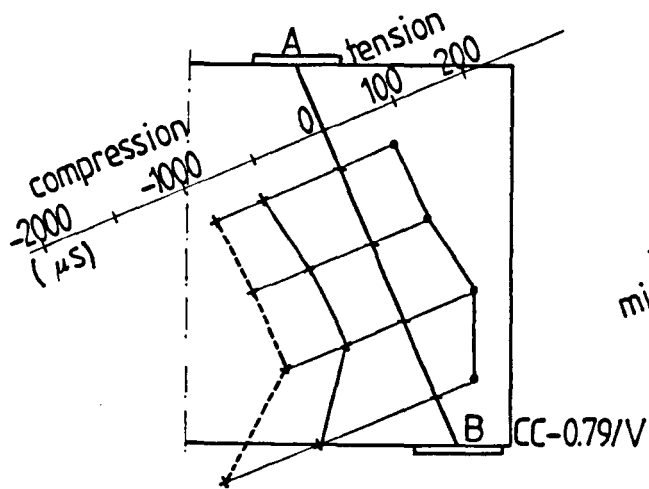


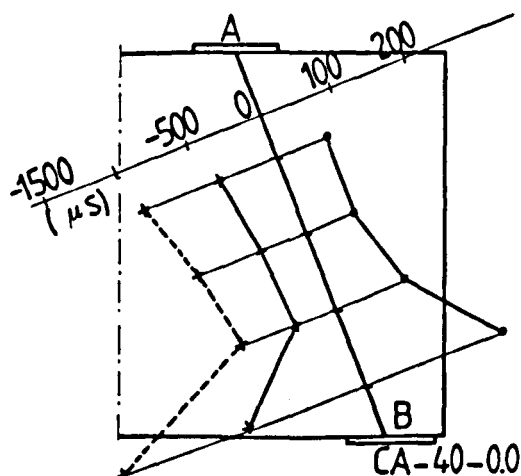
Fig.3.8: Comparison of measured diagonal cracking load with predicted one - Robins tests [94] on stocky deep beams -



— before diagonal cracking  
 - - - after diagonal cracking  
 (70% ultimate load)

compressive strains: along line AB  
 tensile strains:  $\perp$  line AB

Fig.3.9: Typical strains in the inclined "load paths"



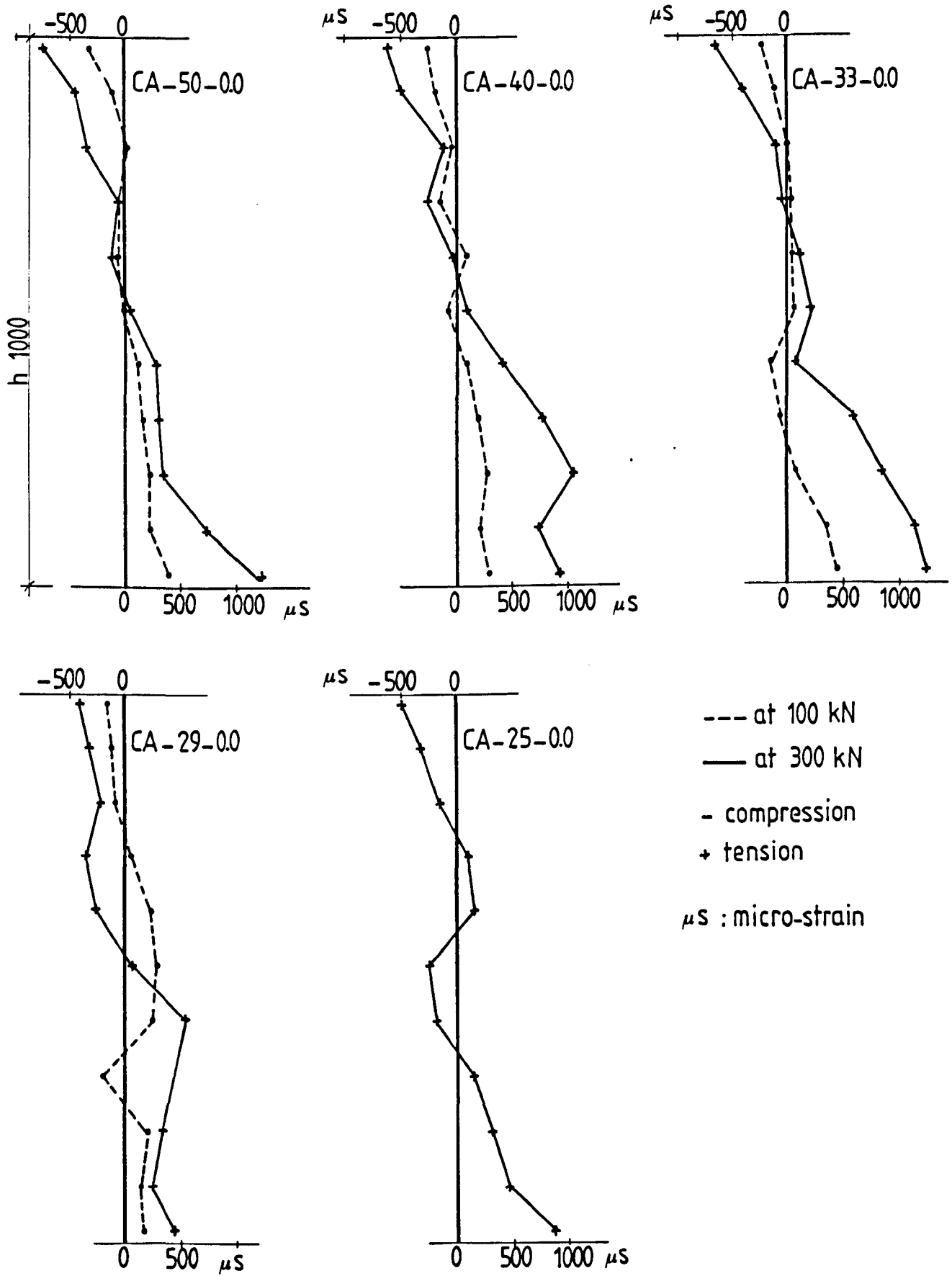


Fig.3.10: Longitudinal strain distribution at mid-span sections  
 - series CA beams : span/depth ratio = 1.4 -

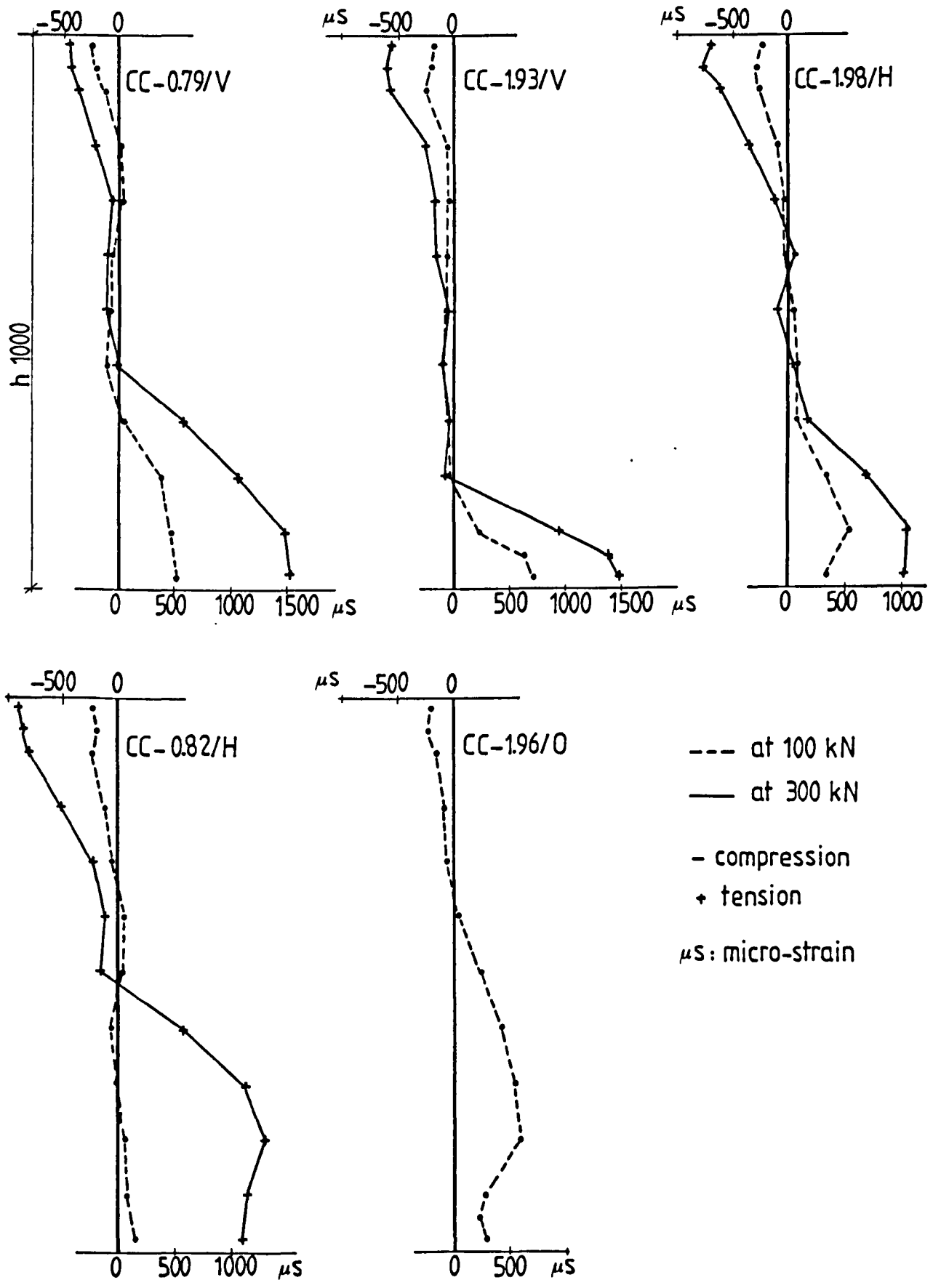


Fig.3.10: contd. Longitudinal strain distribution at mid-span sections  
 - series CC beams : span/depth ratio = 1.4 -

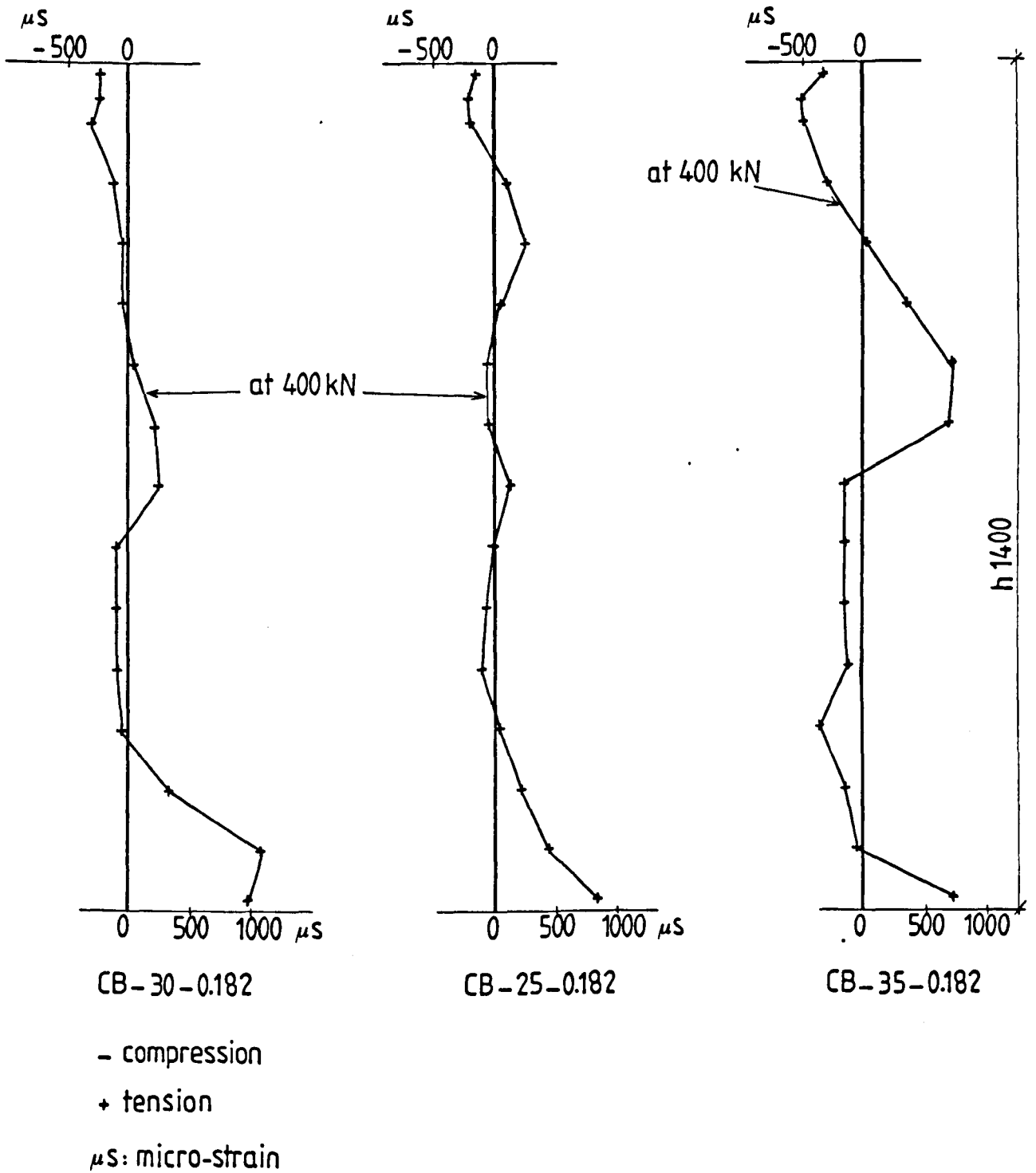


Fig.3.10: contd. Longitudinal strain distribution at mid-span sections  
 - series CB beams (chapter 5) : span/depth ratio = 1.0 -

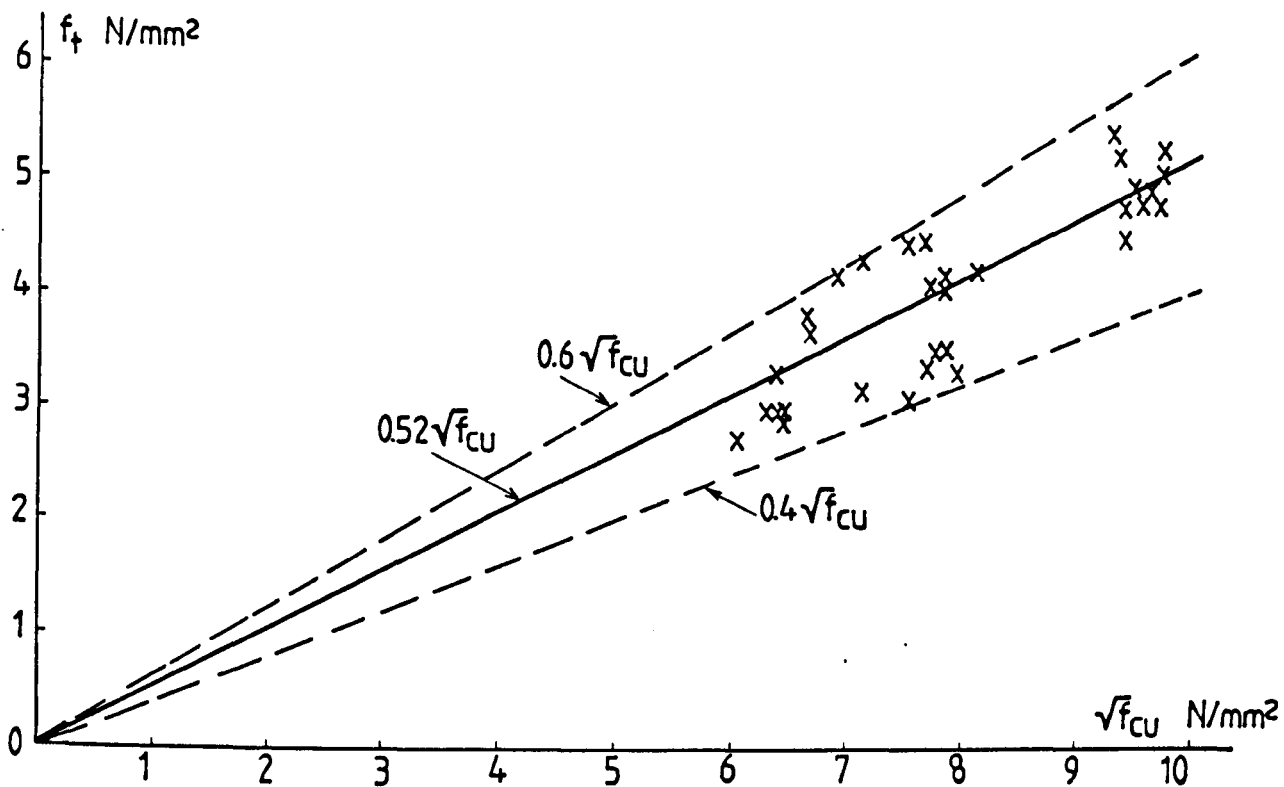


Fig.3.11: Relation between tensile splitting strength of concrete,  $f_t$ , and compressive strength,  $f_{cu}$

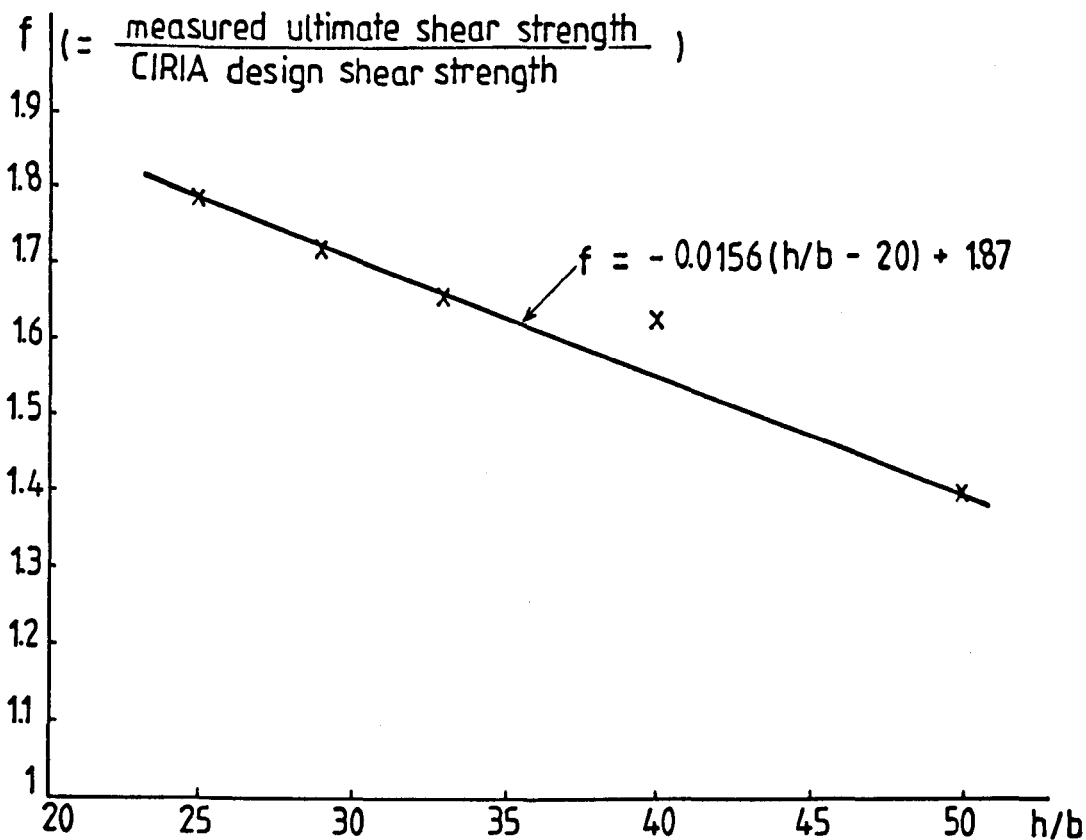
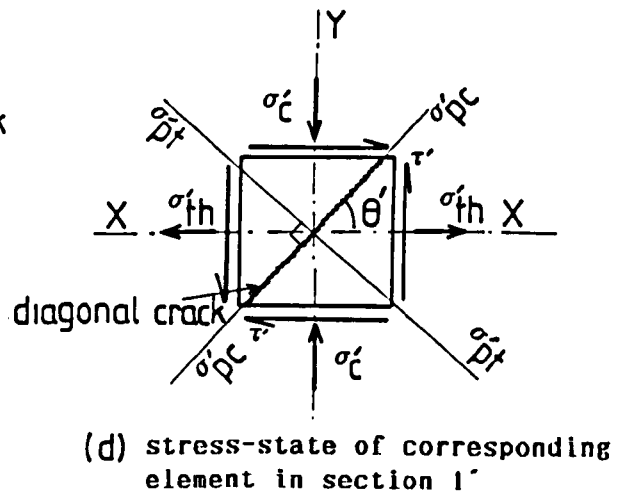
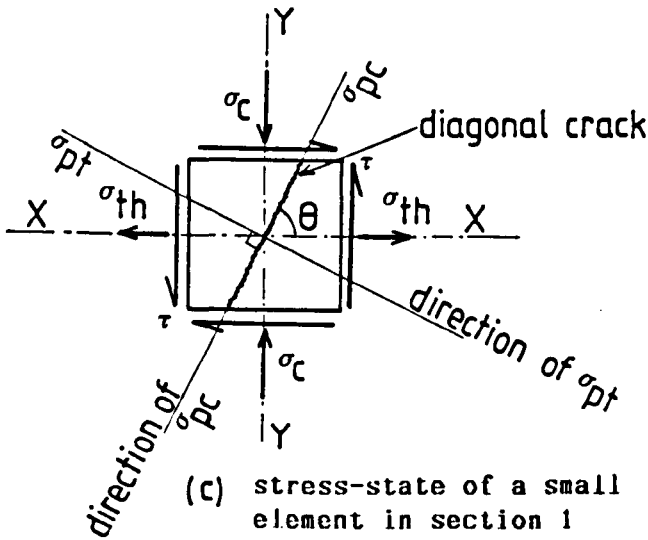
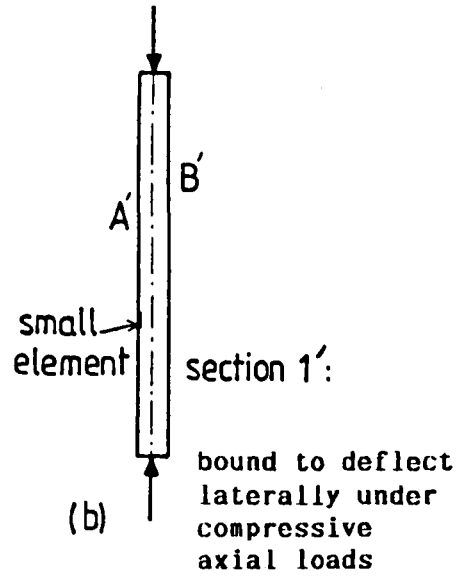
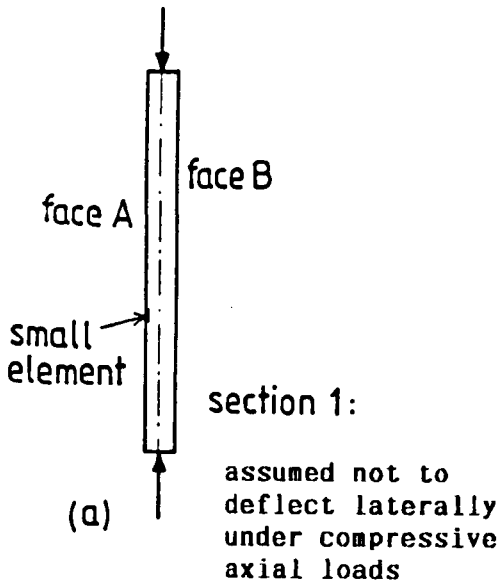


Fig.3.12: Variation of safety factor,  $f$ , with  $h/b$  ratio



(e) Mohr-circle representation

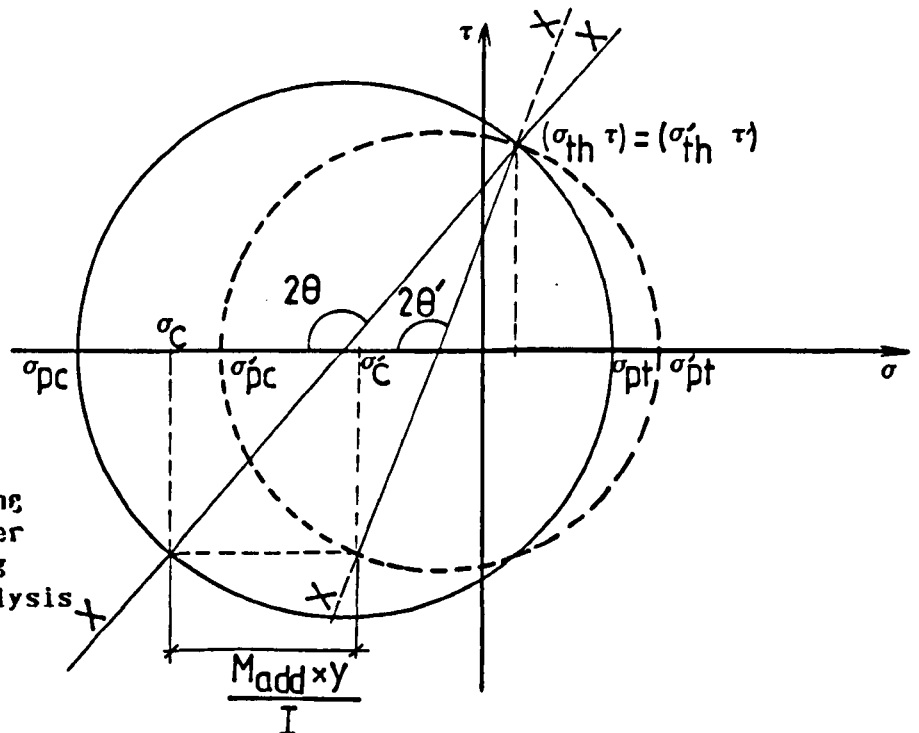


Fig3.13: Explanation of diagonal cracking nature in slender deep beams using Mohr-circle analysis

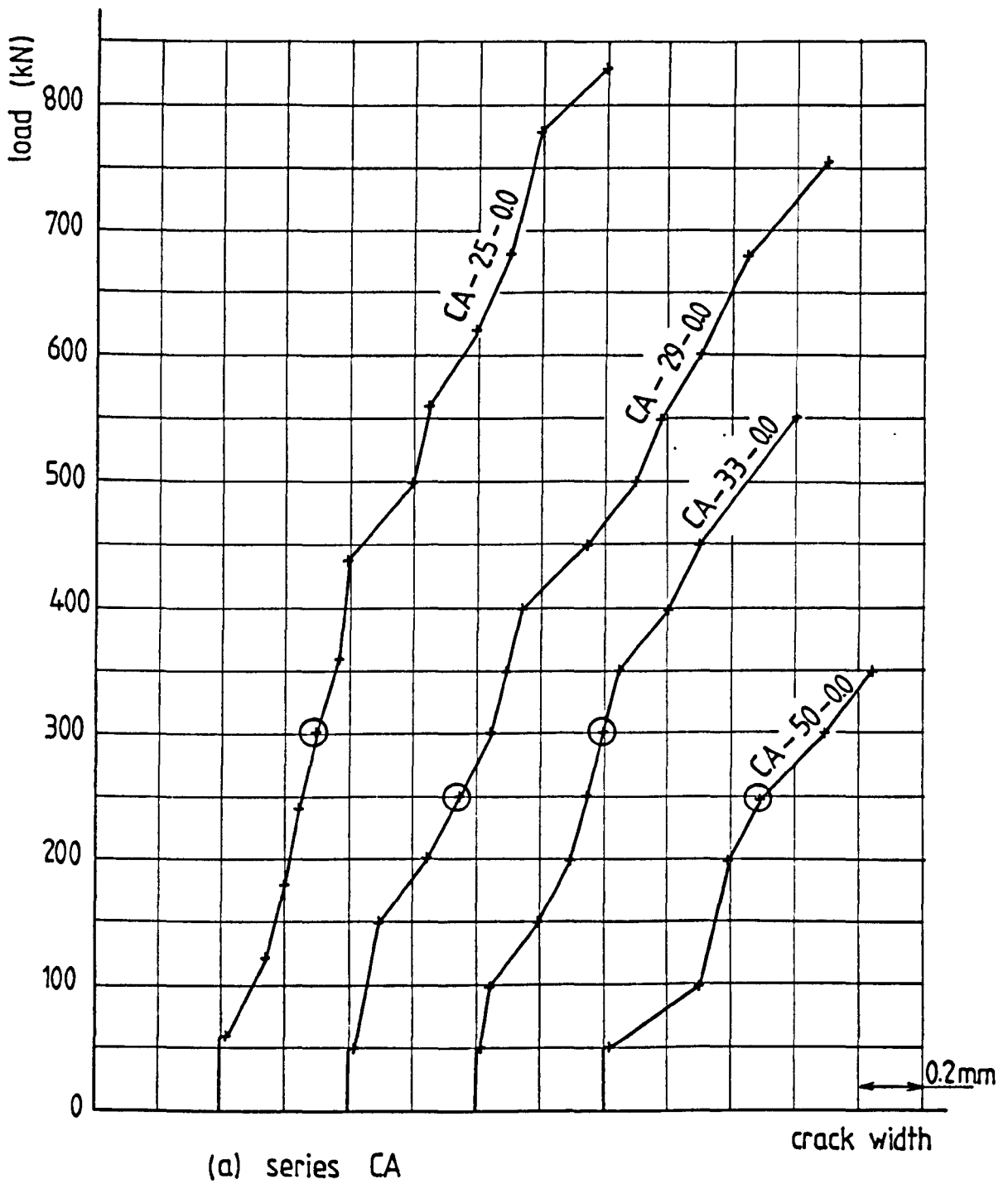


Fig.4.1: Load against maximum crack width

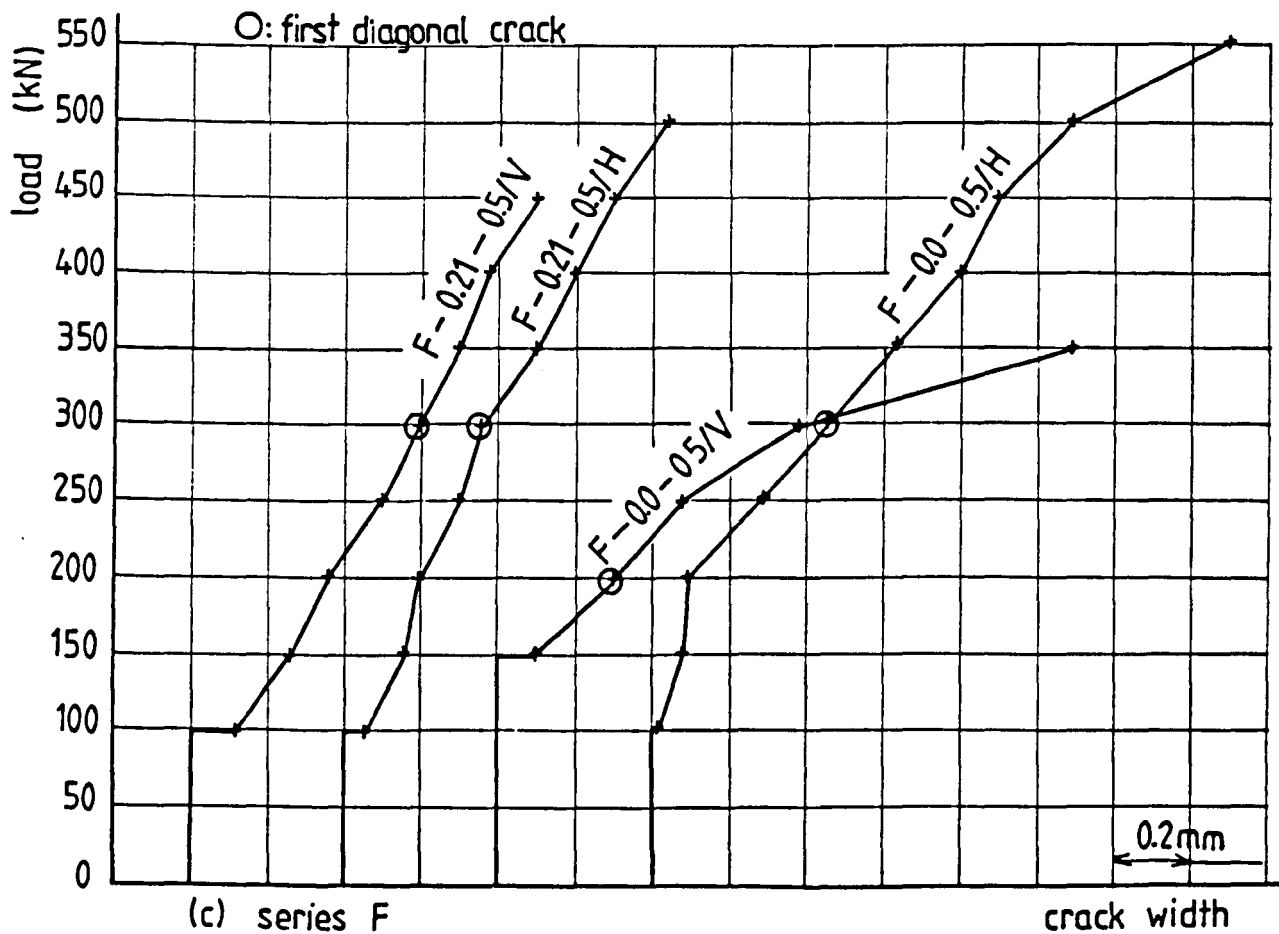
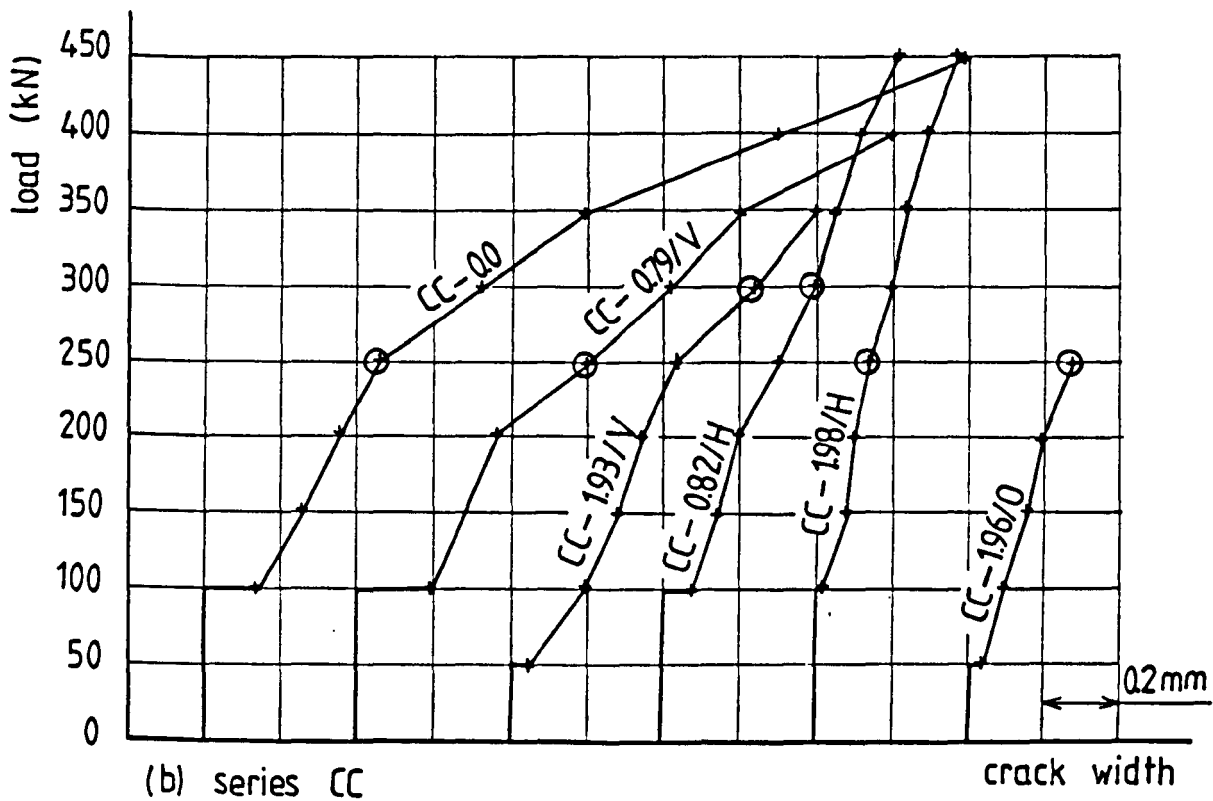


Fig.4.1: contd. Load against maximum crack width

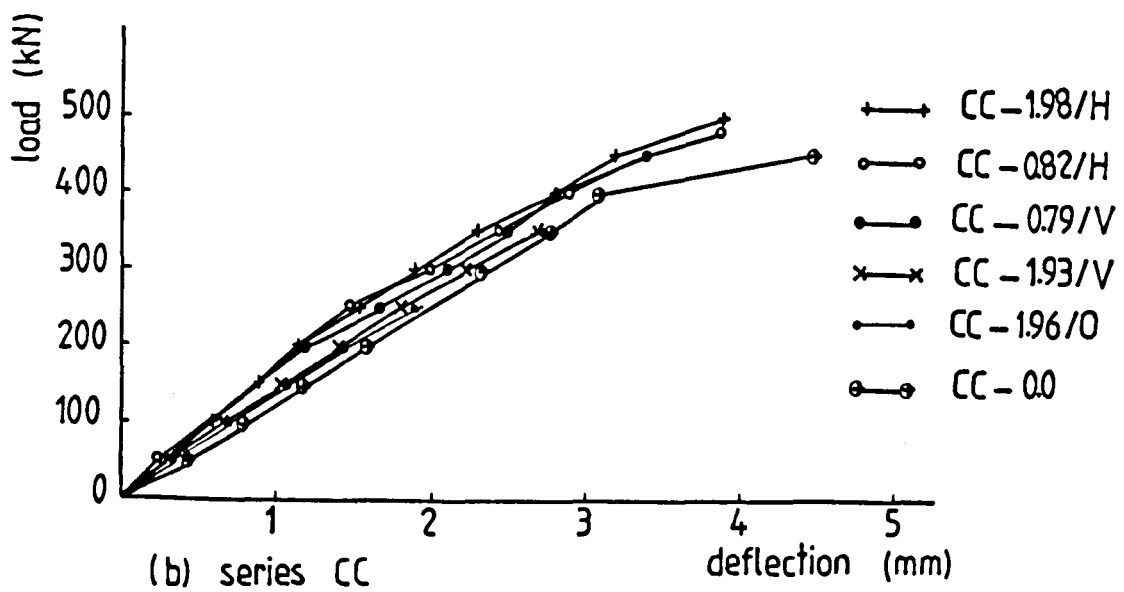
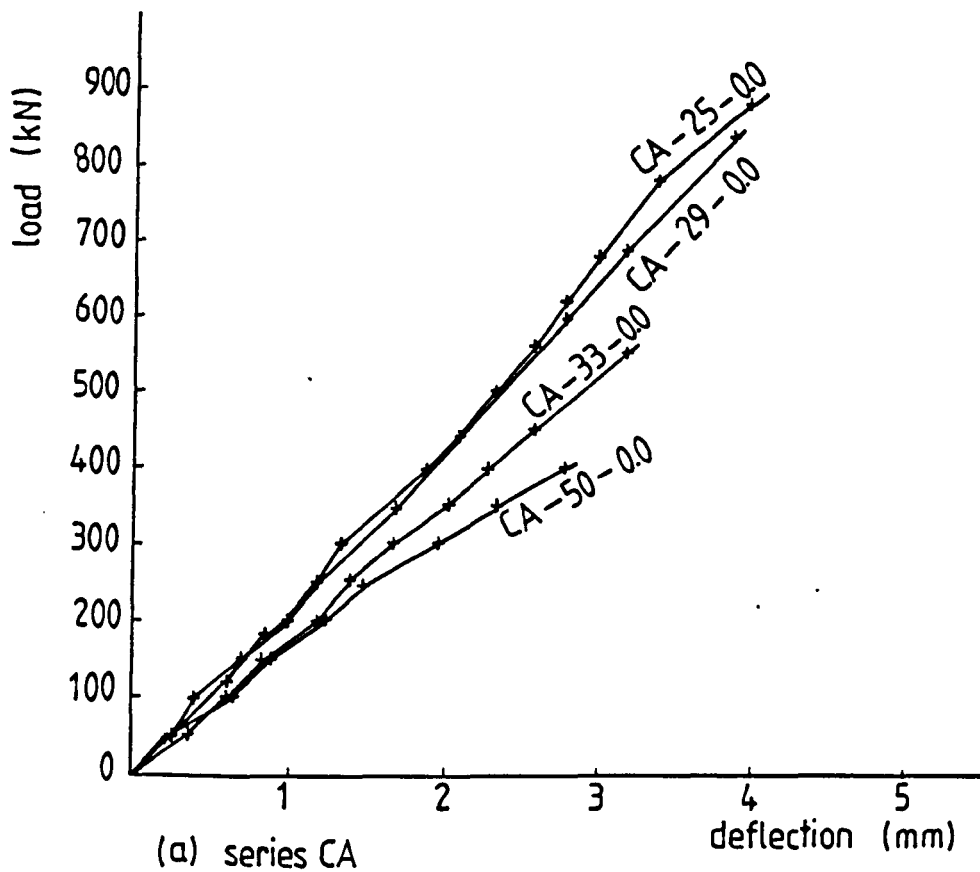


Fig.4.2: Load against vertical deflection

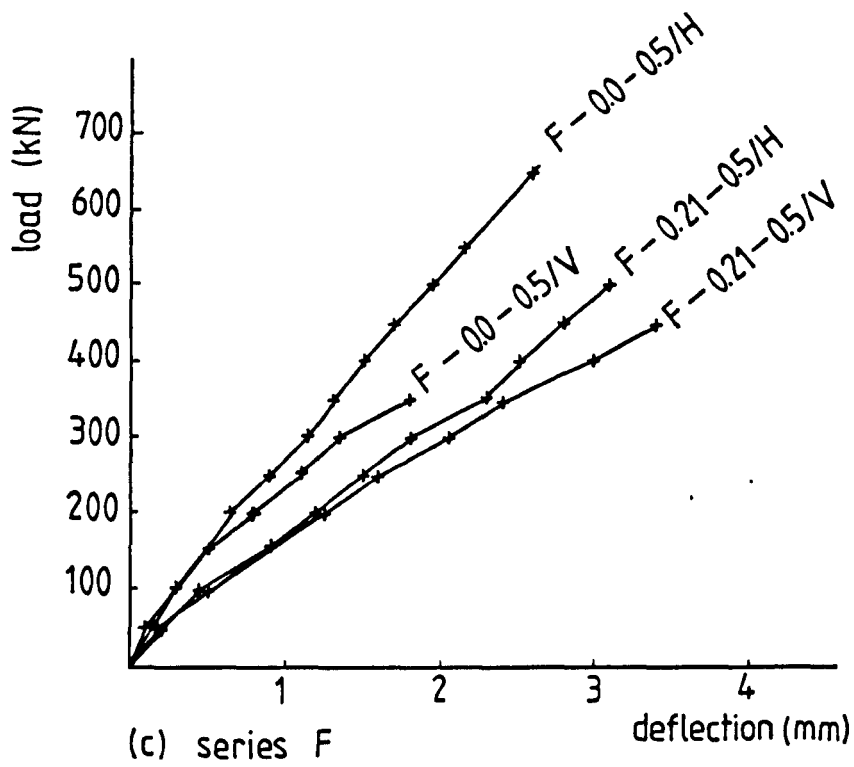
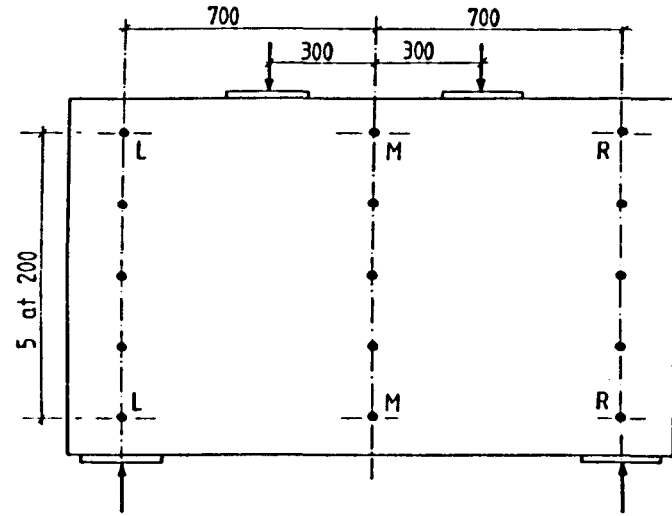
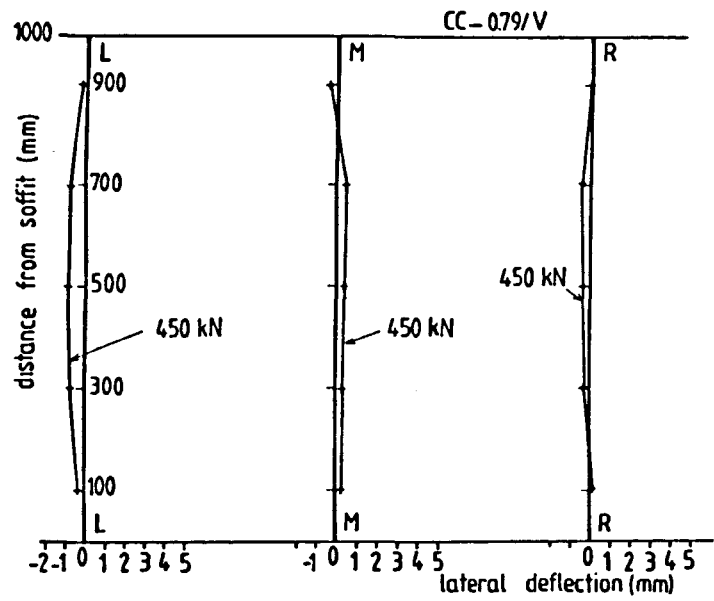


Fig.4.2: contd. Load against vertical deflection



Locations of measurements of lateral deflections

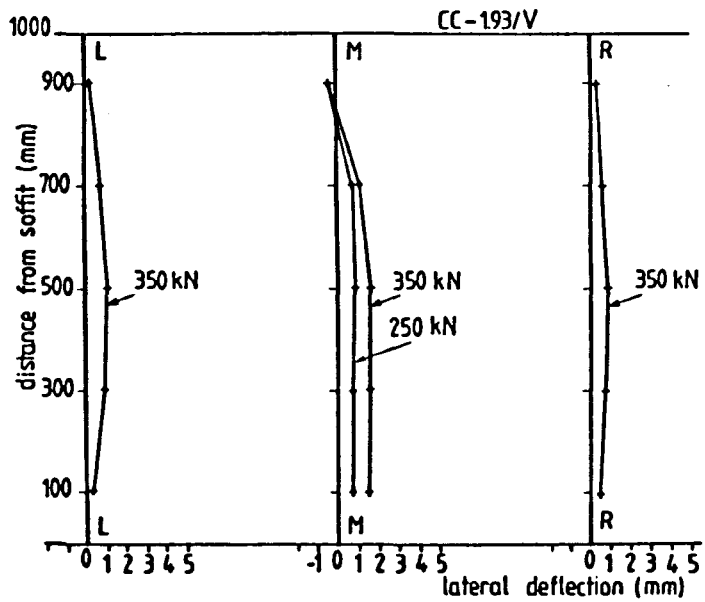


Fig.4.3: Lateral deflections - series CC beams -

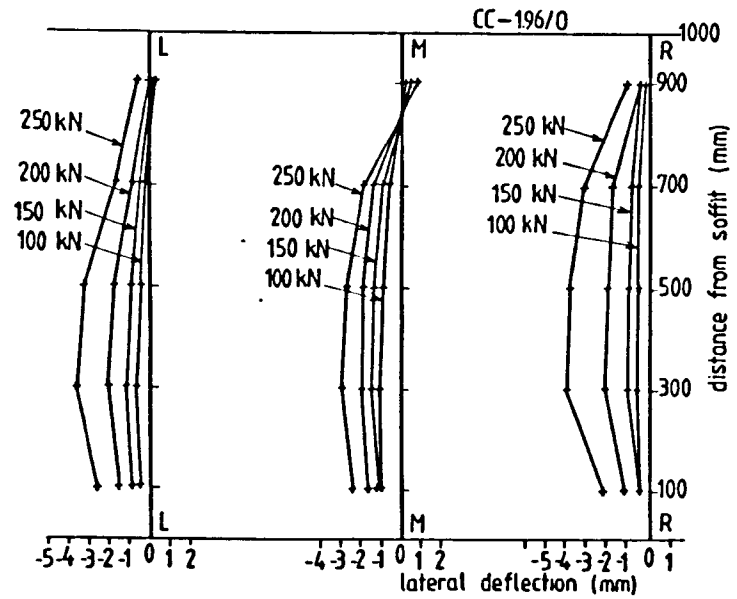
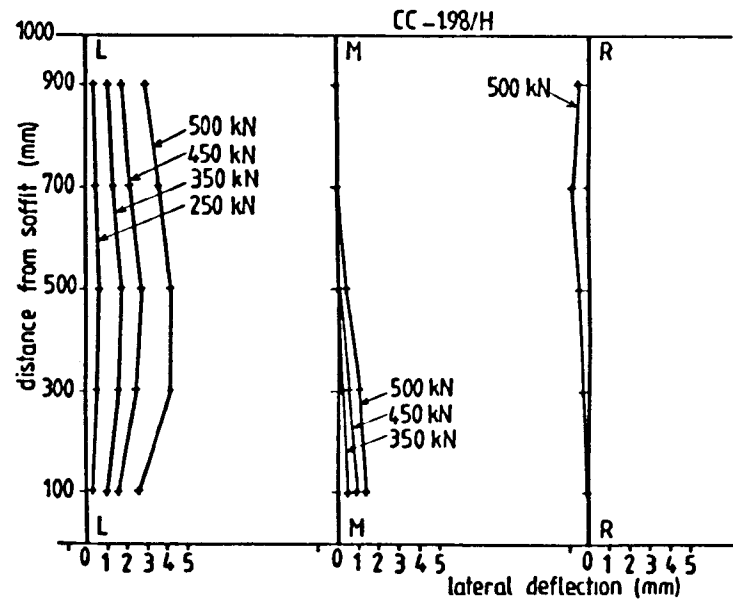
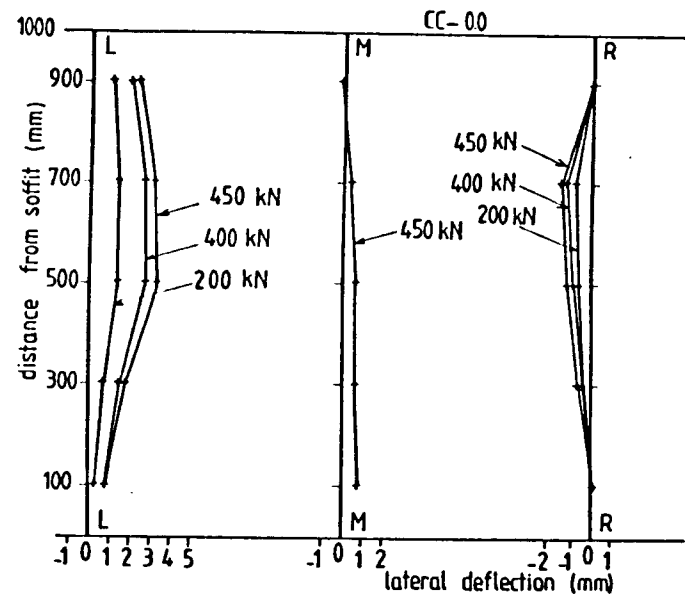
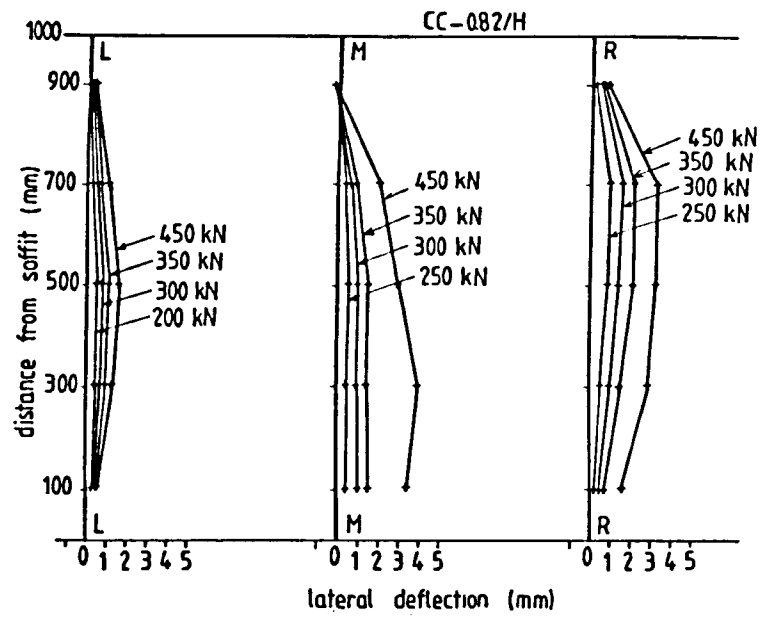
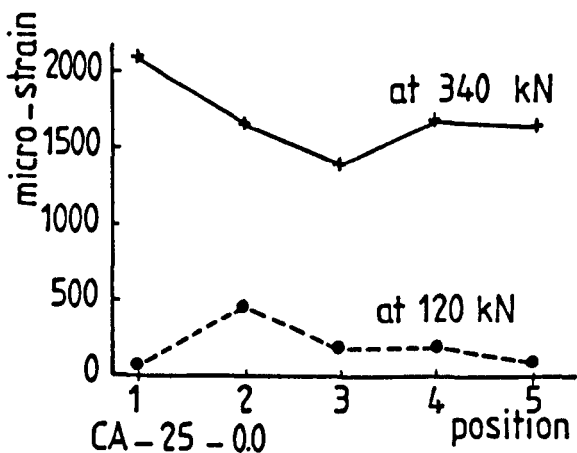
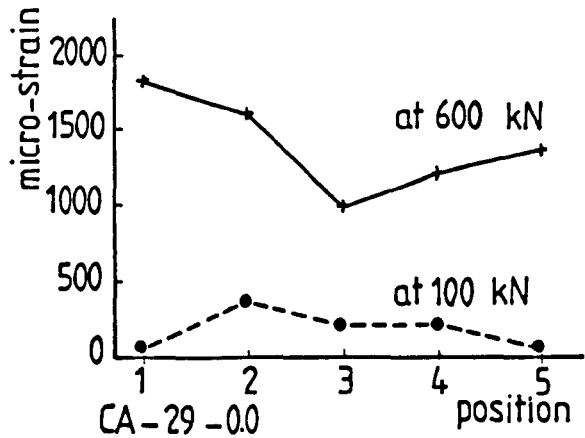
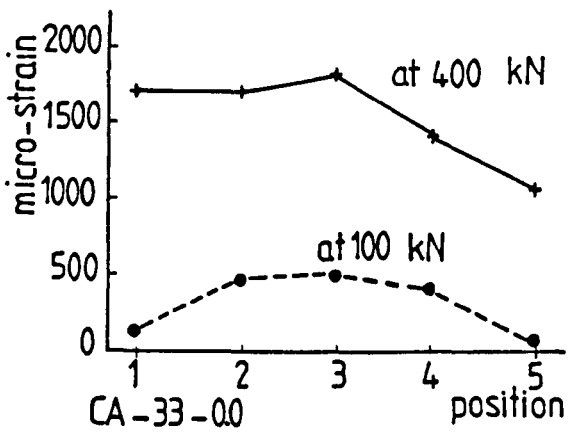
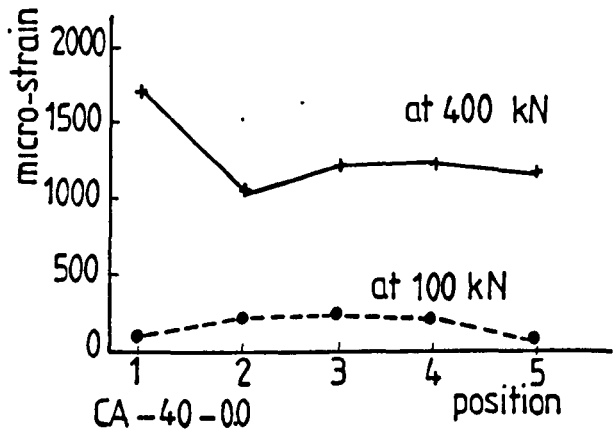
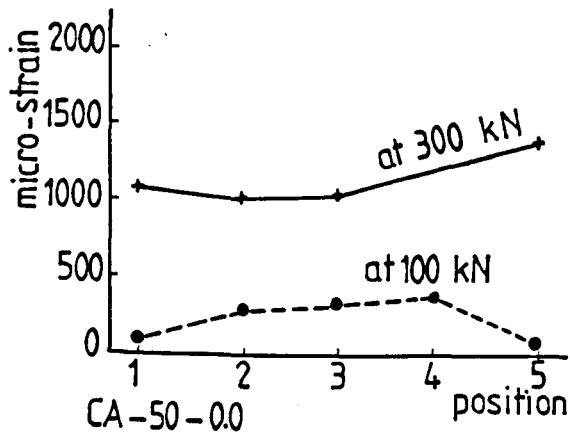
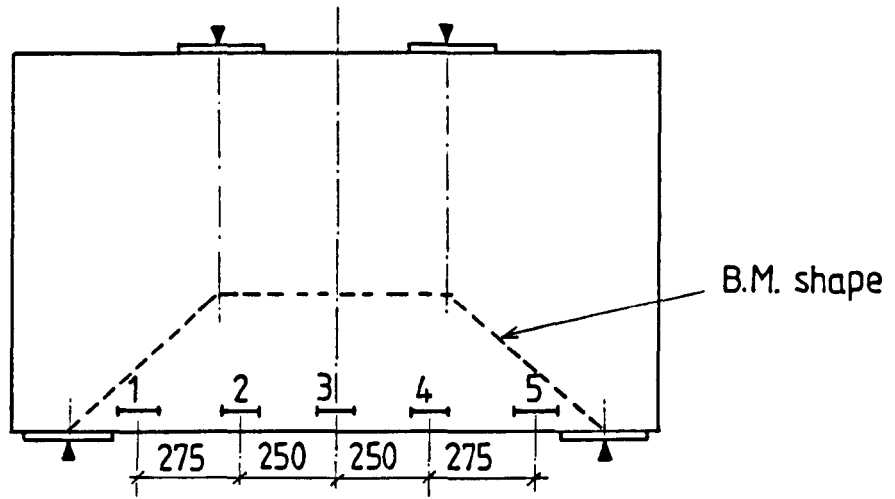
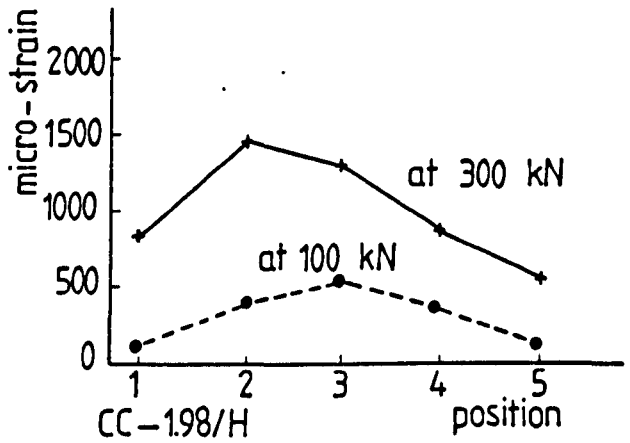
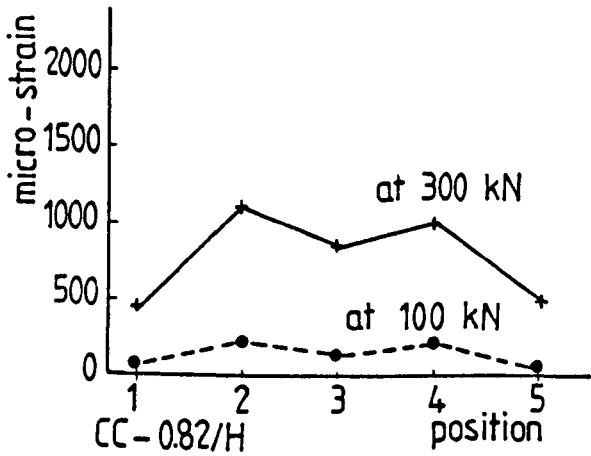
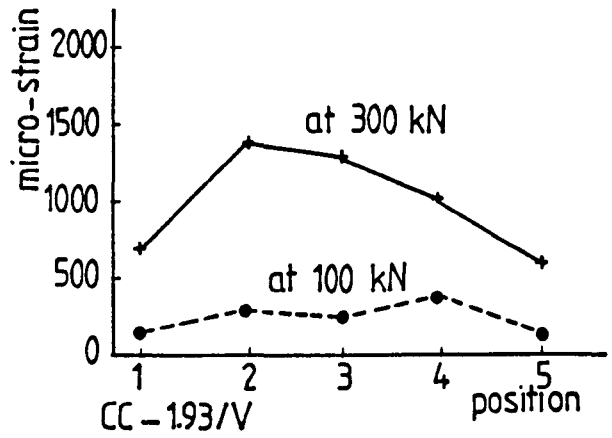
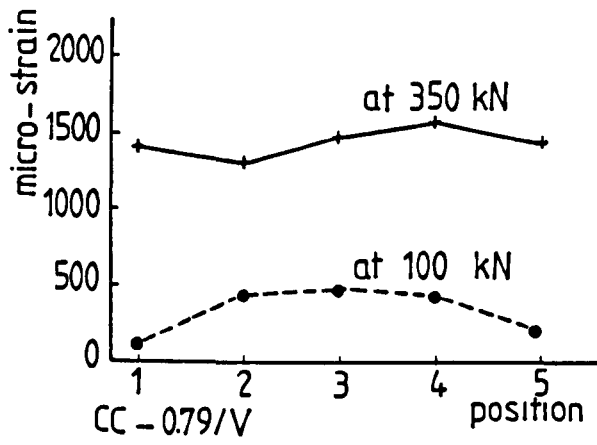


Fig.4.3: contd. Lateral deflections - series CC beams -



--- before diagonal cracking  
 — after diagonal cracking  
 (70% of ultimate load)

Fig.4.4: Typical strain measurements at level of main tensile steel

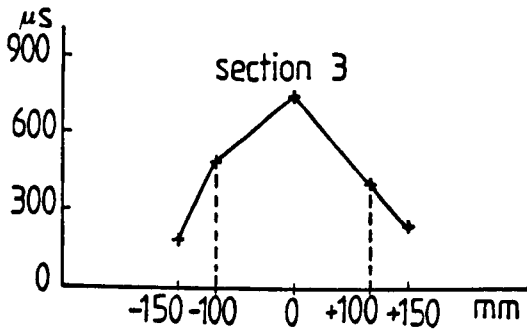
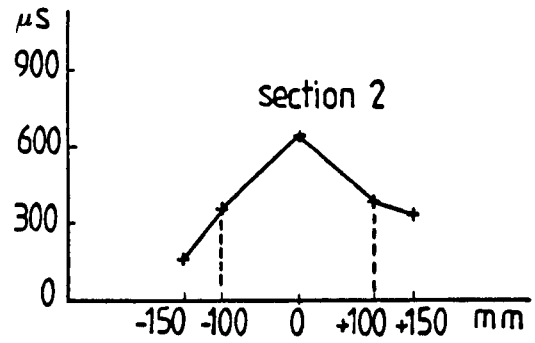
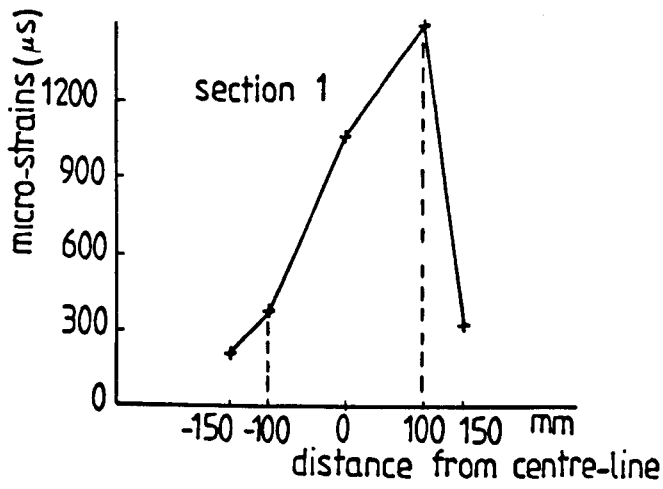


----- before diagonal cracking

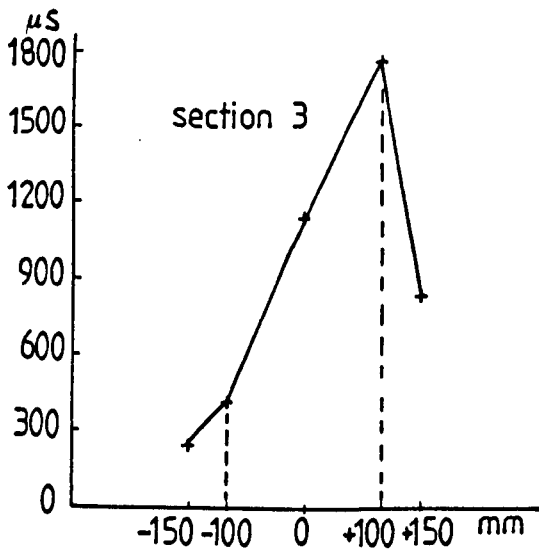
———— after diagonal cracking  
(70% of ultimate load)

Fig.4.4: contd. Typical strain measurements at level of main tensile steel





F-0.0-05/V — strains at 350 kN  
 — ultimate load 396 kN



F-0.0-05/H — strains at 400 kN  
 — ultimate load 650 kN

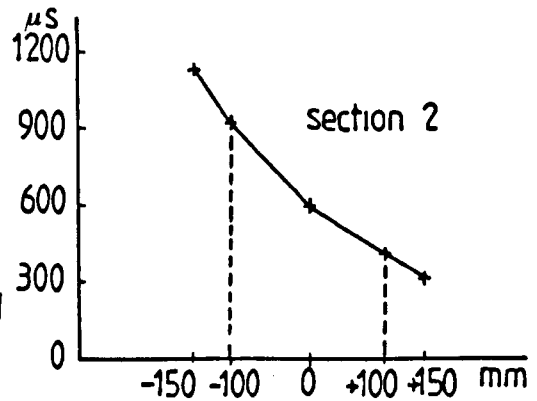
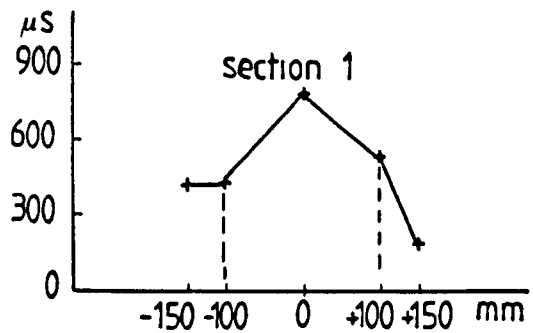


Fig.4.5: contd. Compressive strain distribution at sections perpendicular to the load path

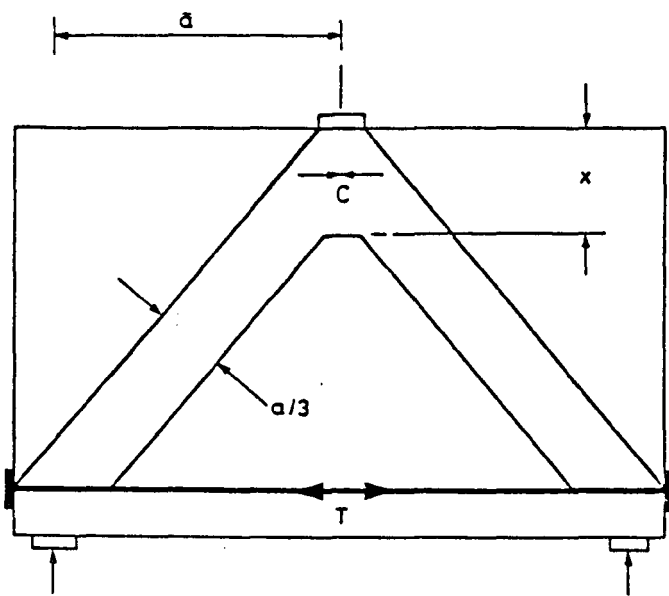
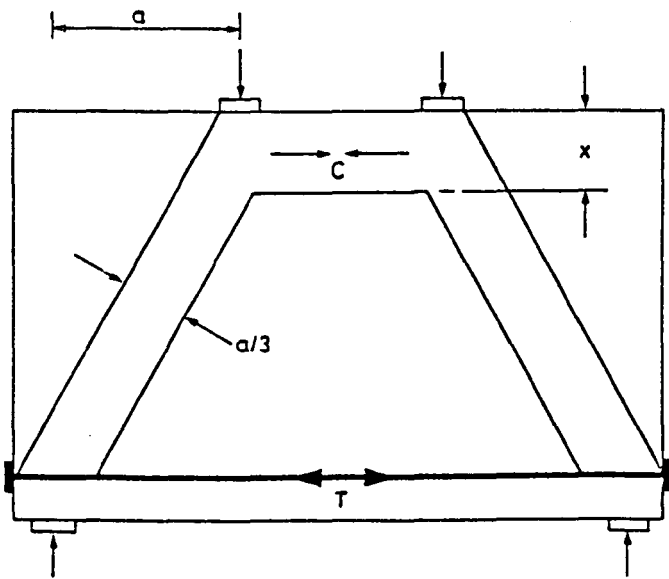


Fig.4.6: Truss model of a deep beam proposed by Kotsovos [76]

a) one point-load



b) two point-loads

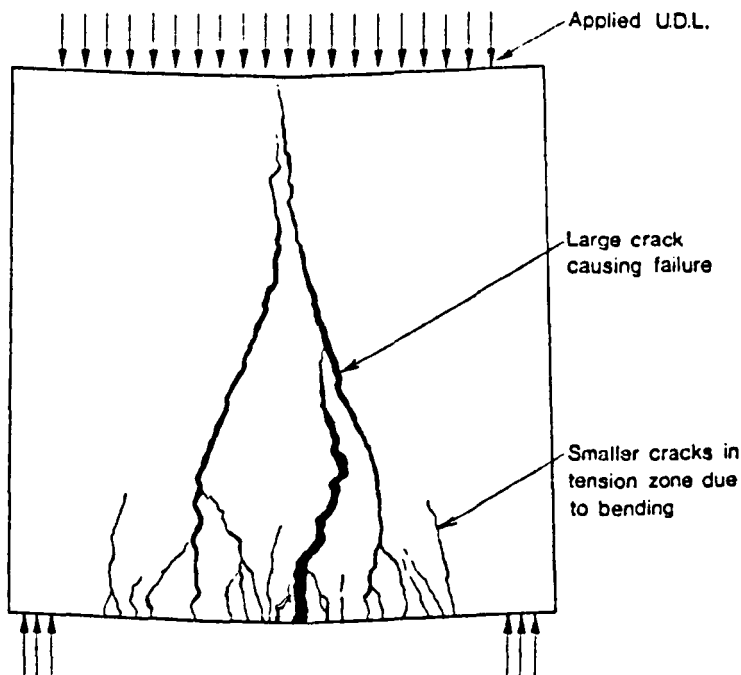
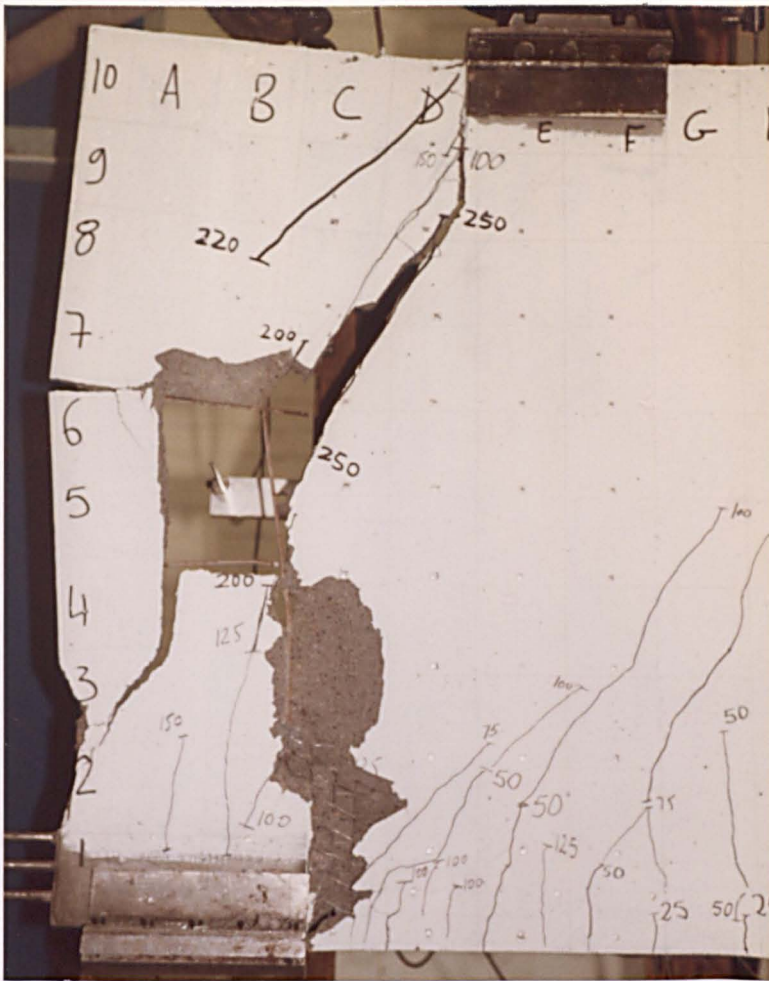
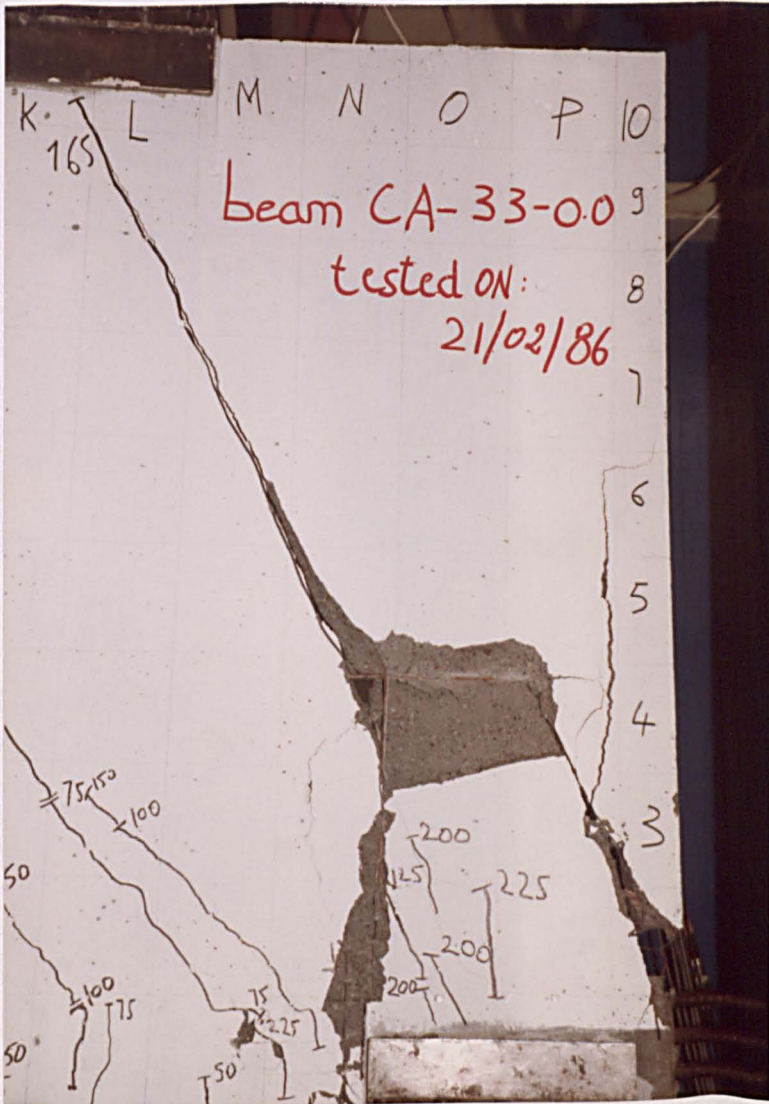


Fig.4.7: Typical flexural failure (CIRIA Guide) [85]



CA-40-0.0

Fig.4.8: Rotational motion of the end of the beam clearly visible at failure



CA-33-0.0

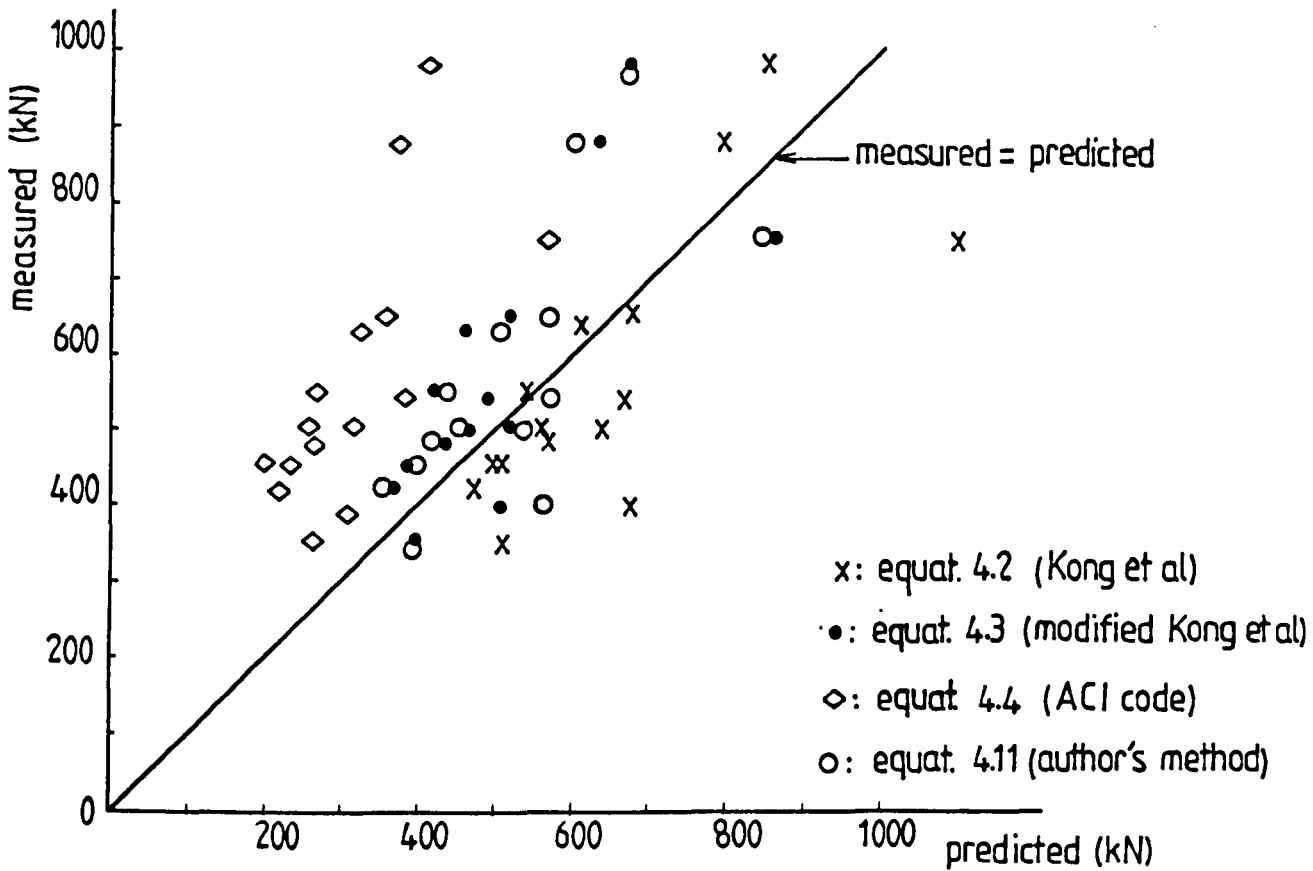


Fig.4.9: Ultimate loads - measured against predicted - series CA, CC, F beams

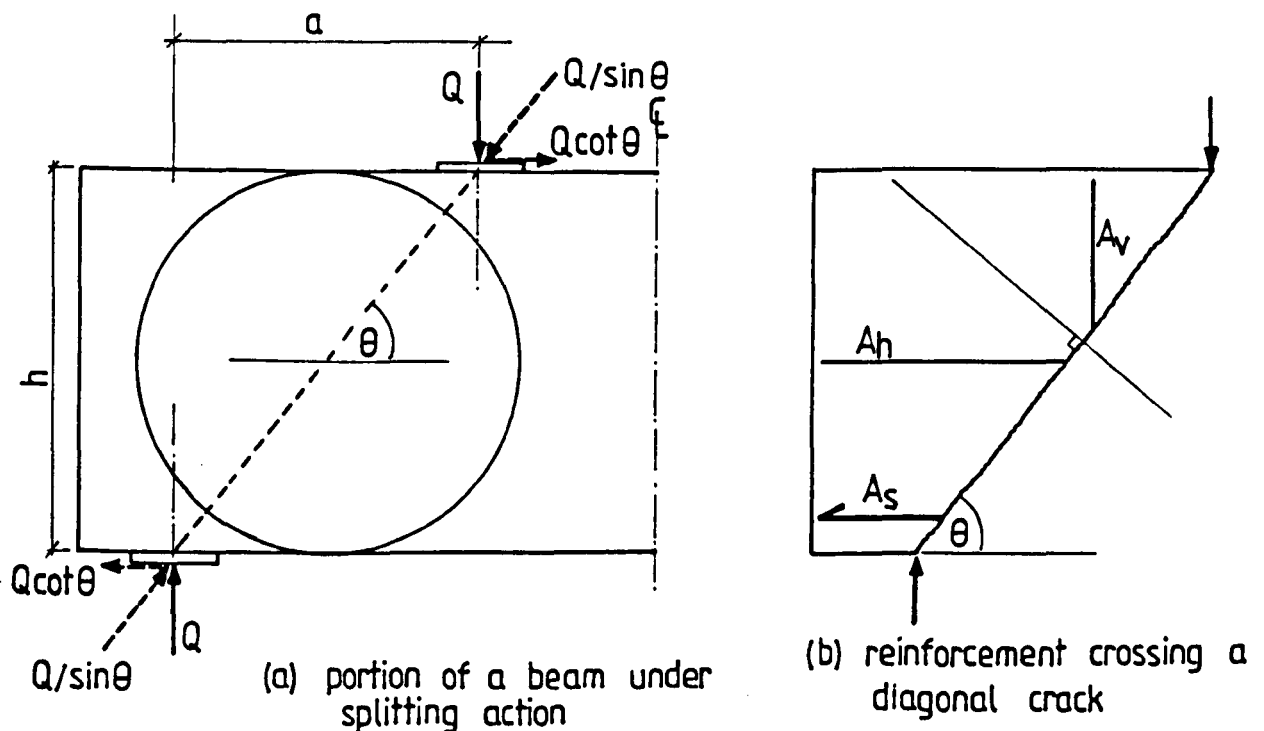


Fig.4.10: Derivation of equation 4.11

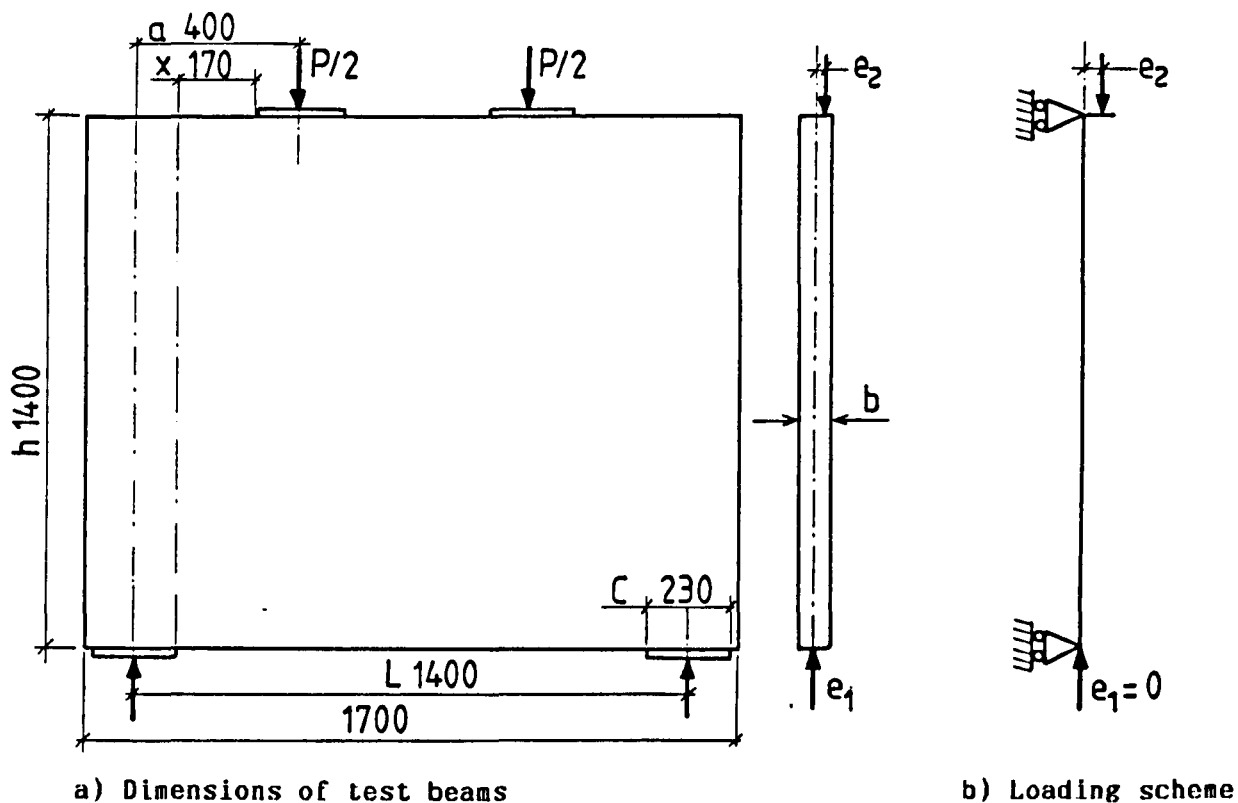
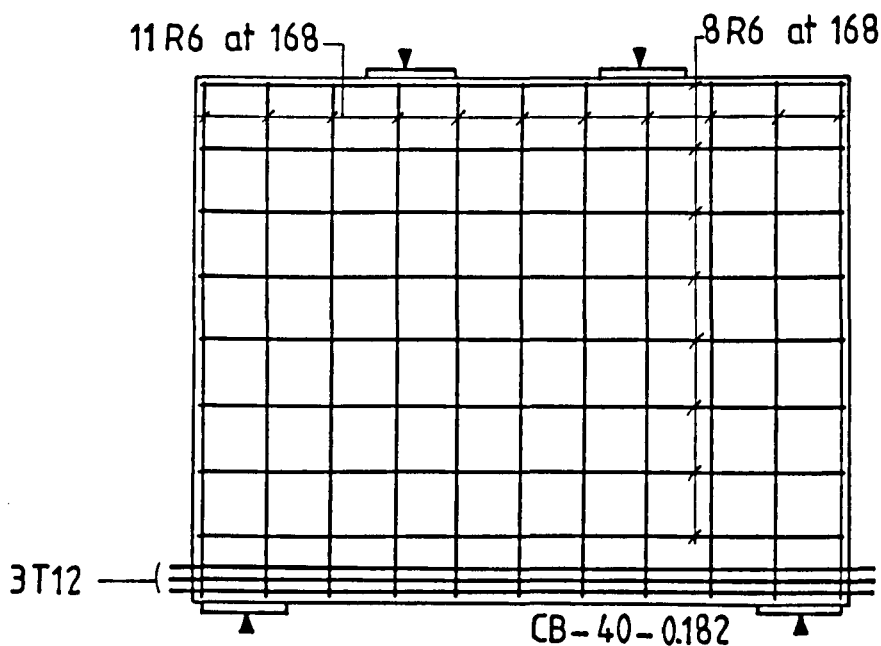


Fig.5.1: Details of test beams - series CB -



beam	CB-20-0.182	CB-25-0.182	CB-30-0.182	CB-35-0.182	CB-50-0.182	CB-70-0.182
web bars	vert.	21R6 at 84	17R6 at 105	13R6 at 140	12R6 at 151	9R6 at 210
	hori.	15R6 at 84	12R6 at 105	9R6 at 140	9R6 at 151	6R6 at 210
main bars	3 × 2T12	3 × 2T12	3 × 2T10	3 × 2T10	3T10	3T10

Fig.5.2: Reinforcement details - series CB beams -



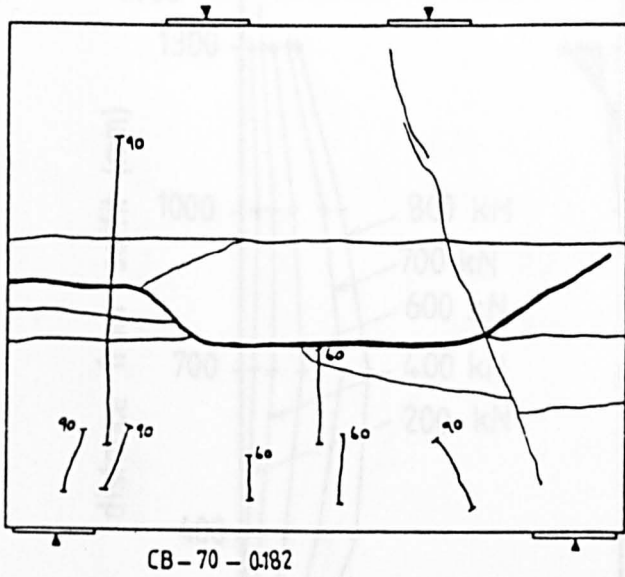


Fig.5.3: contd. Cracks patterns at failure  
- series CB beams -

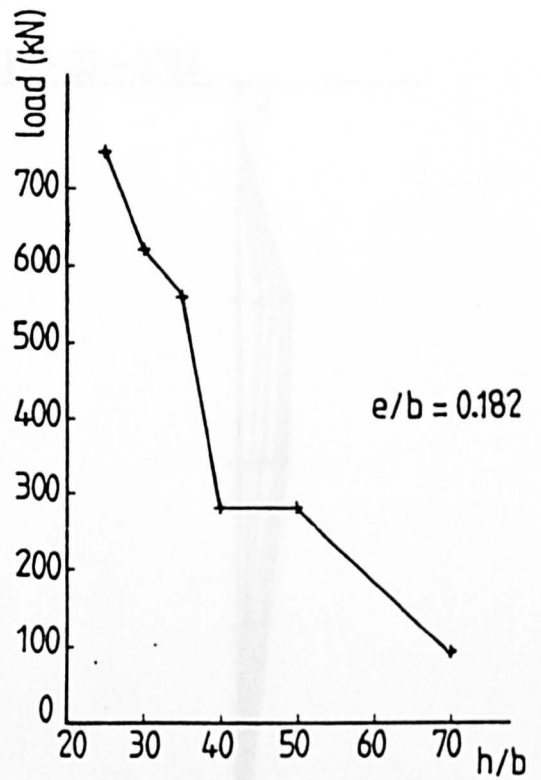


Fig.5.4: Buckling load  
against  $h/b$  ratio

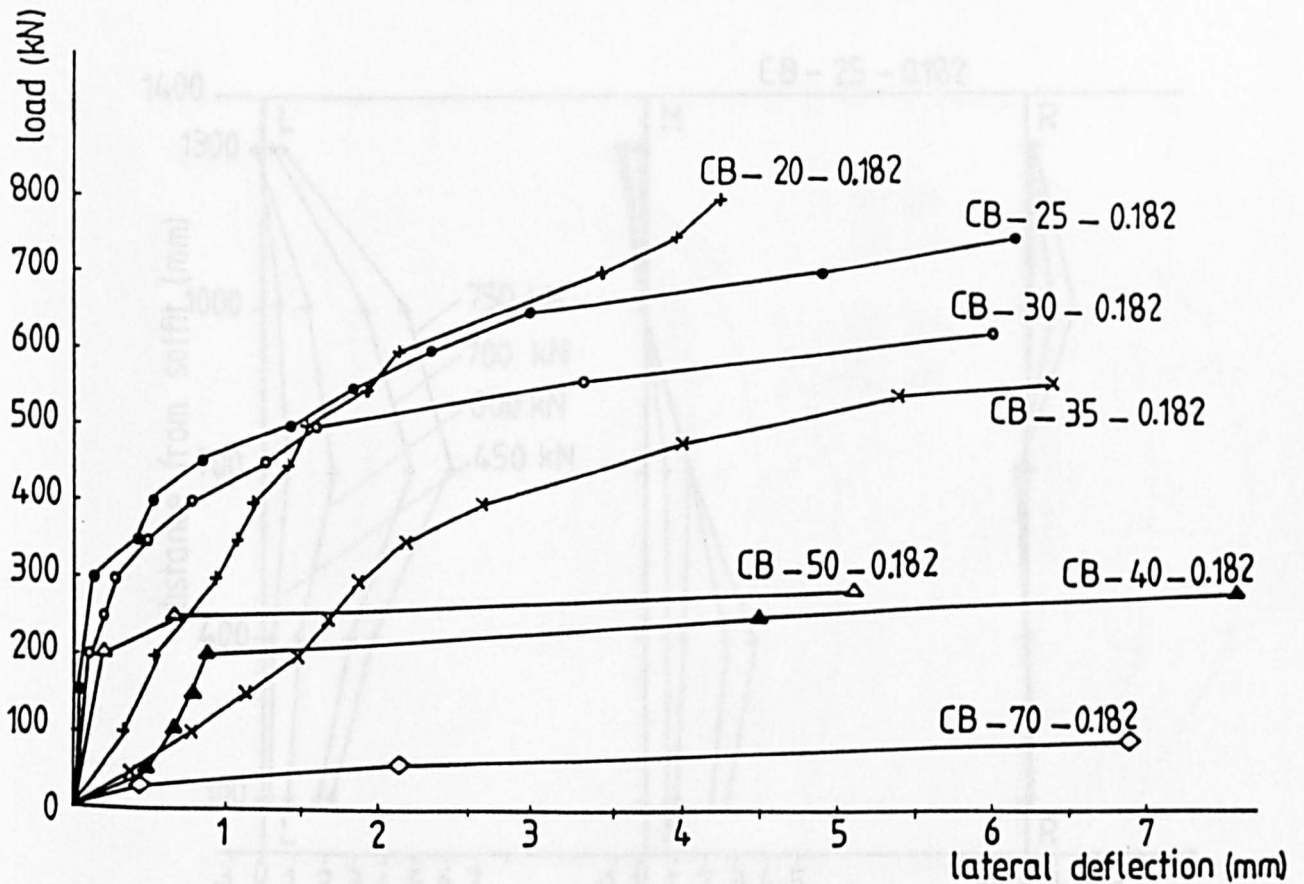


Fig.5.5: Buckling load against lateral deflection  
at mid-height - series CB beams -

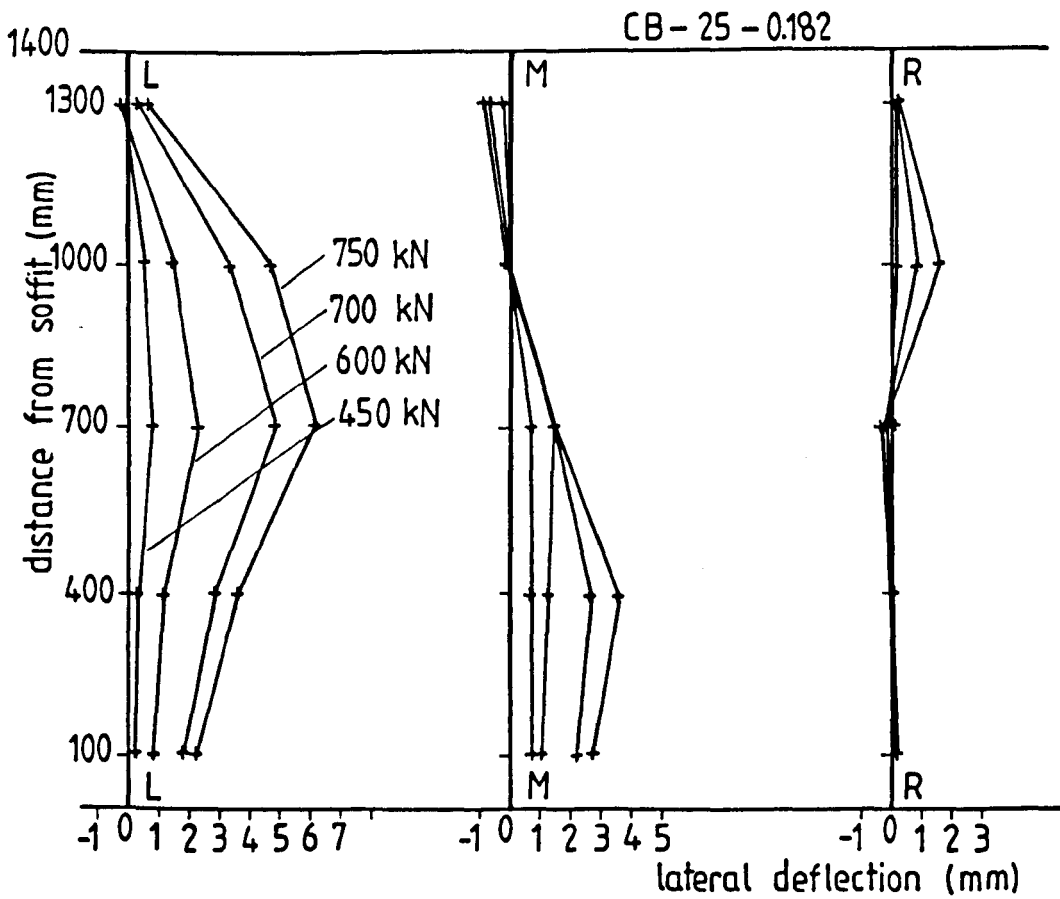
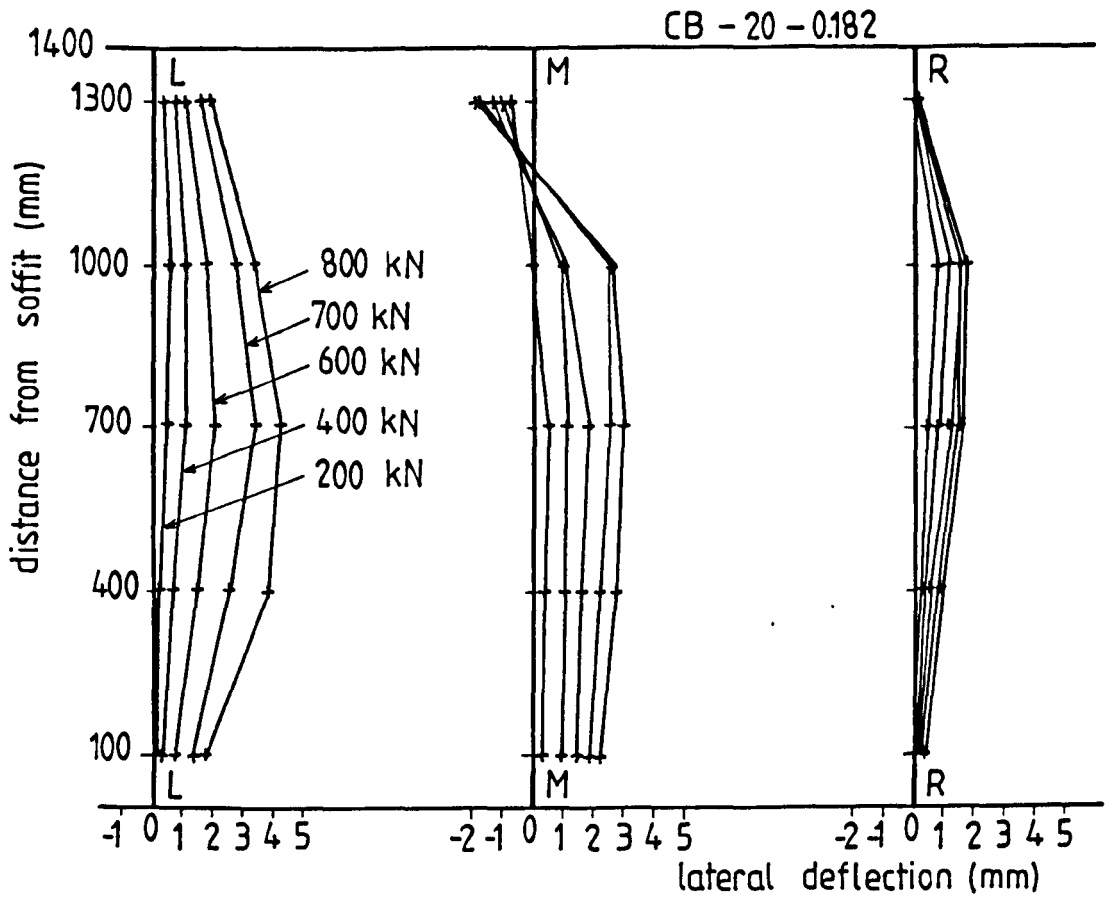


Fig.5.6: lateral deflection profiles - series CB beams -

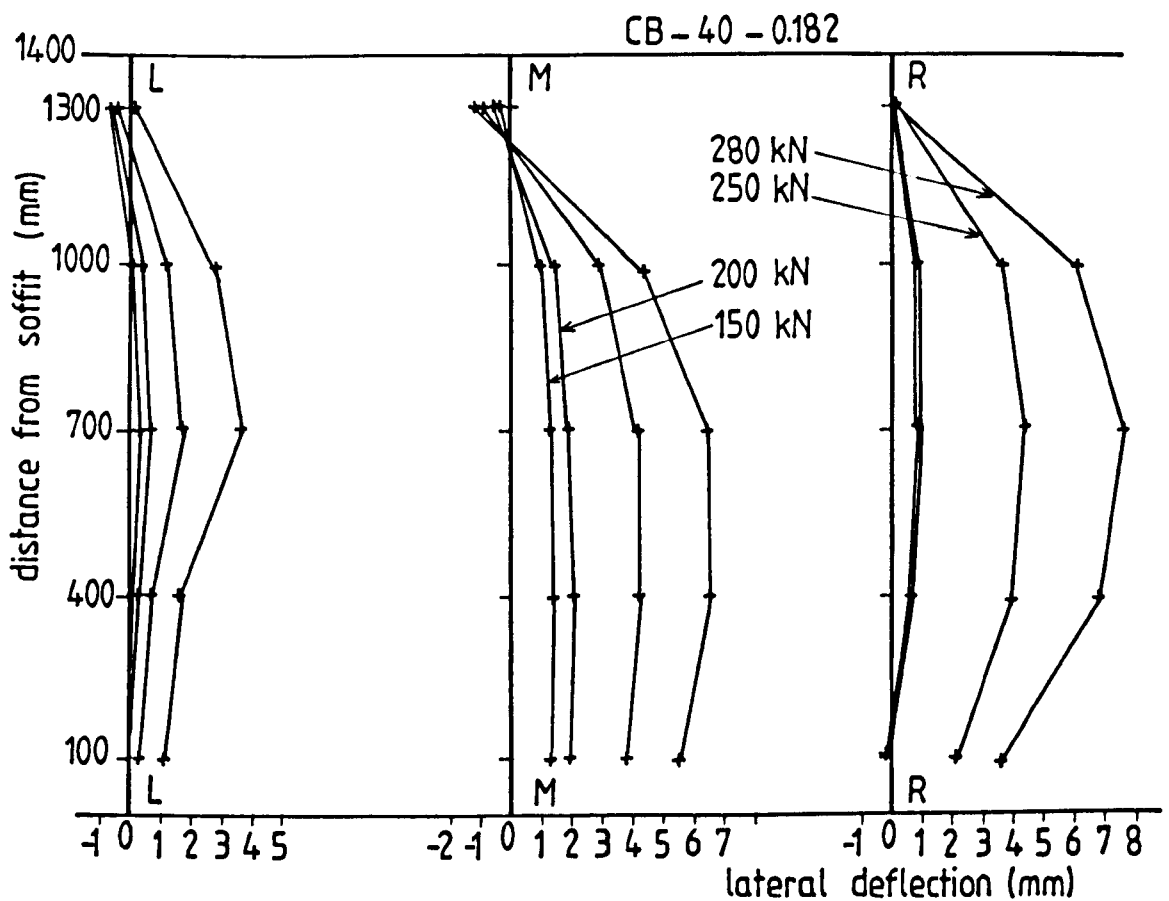
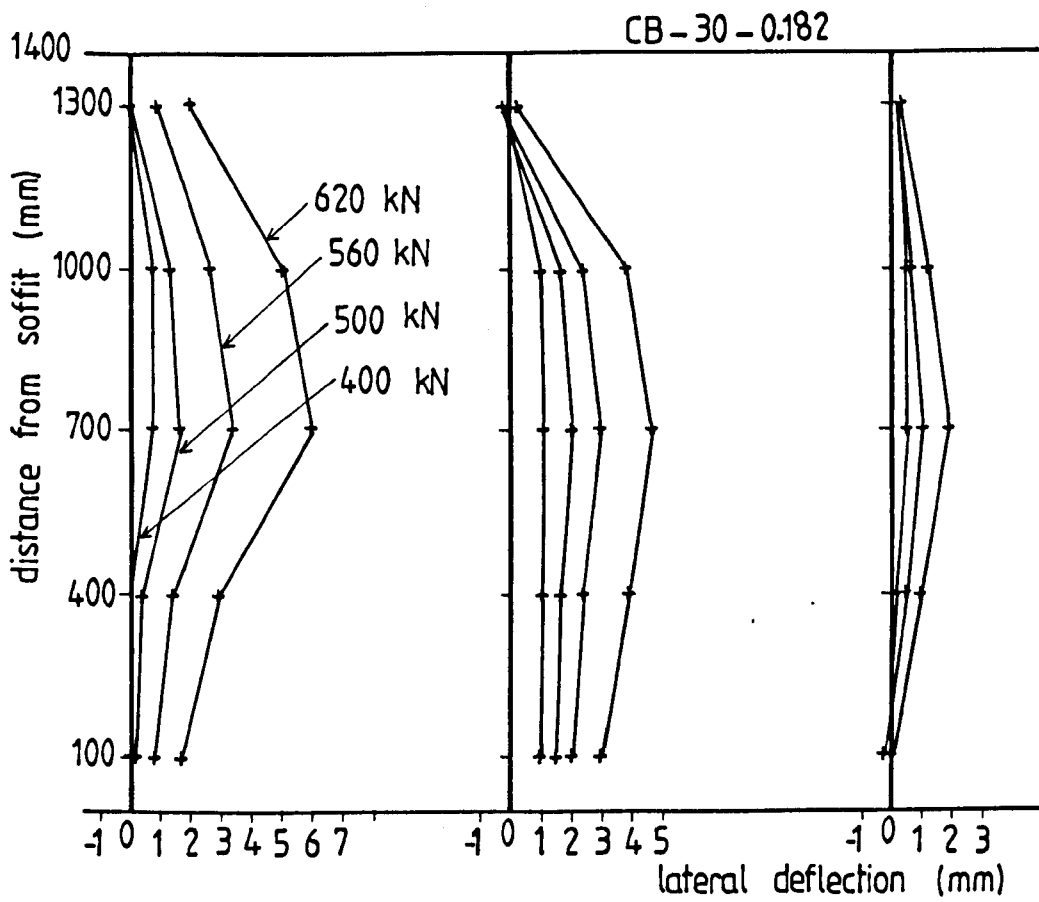


Fig.5.6: contd. Lateral deflection profiles - series CB beams -

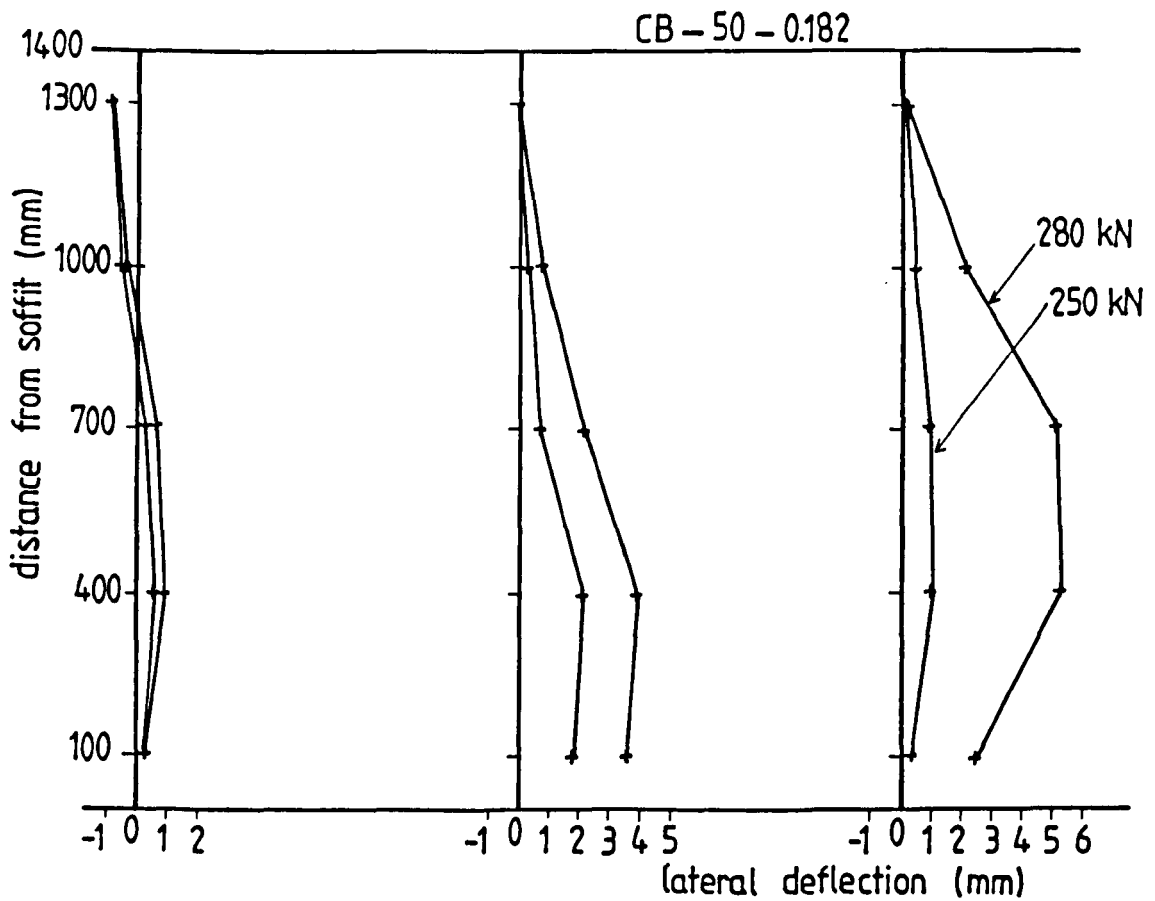
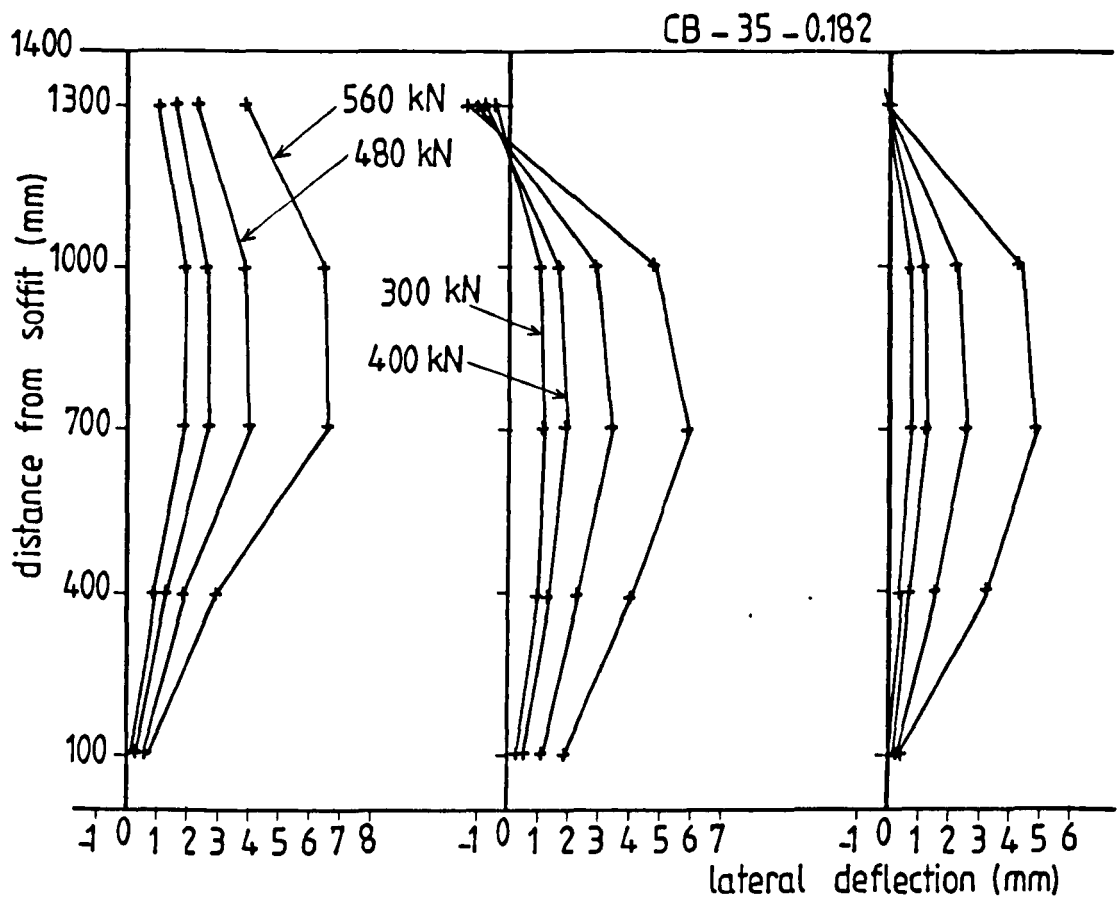


Fig.5.6: contd. Lateral deflection profiles - series CB beams -

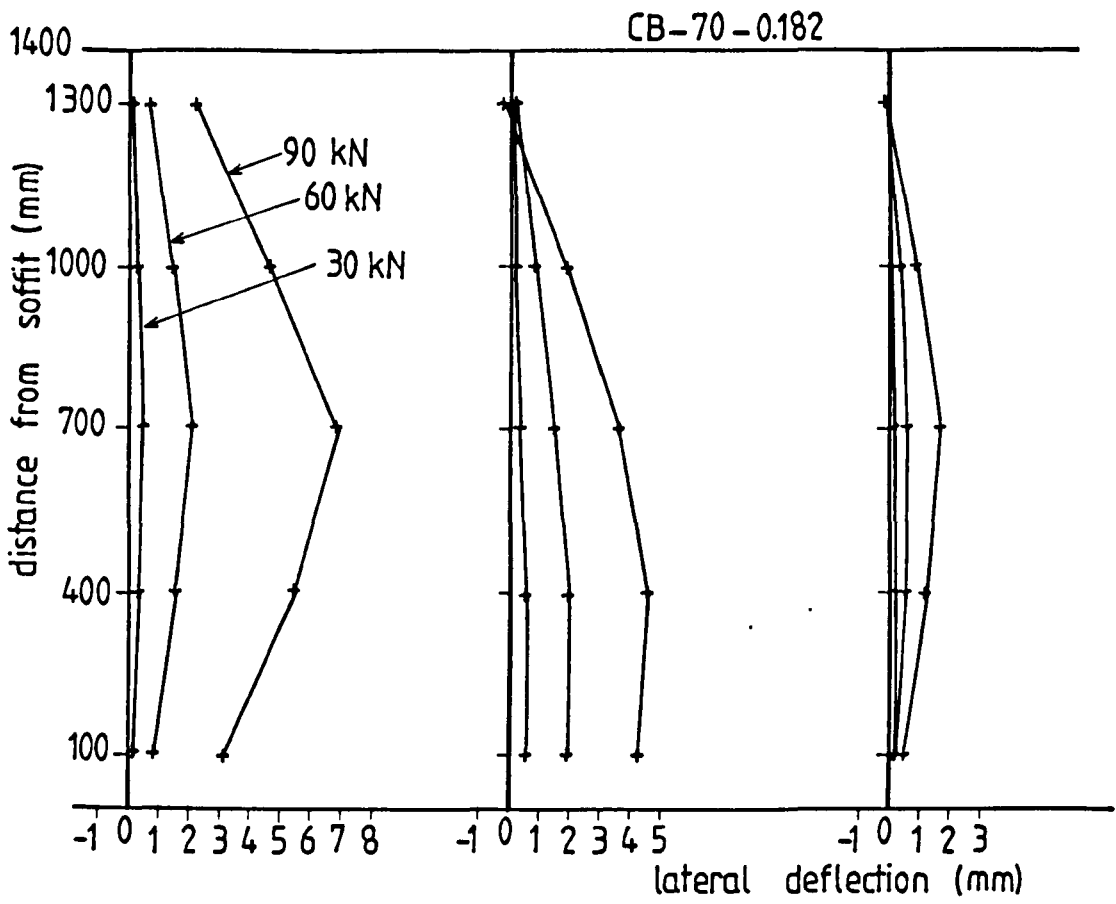


Fig.5.6: contd. Lateral deflection profiles- series CB beams -

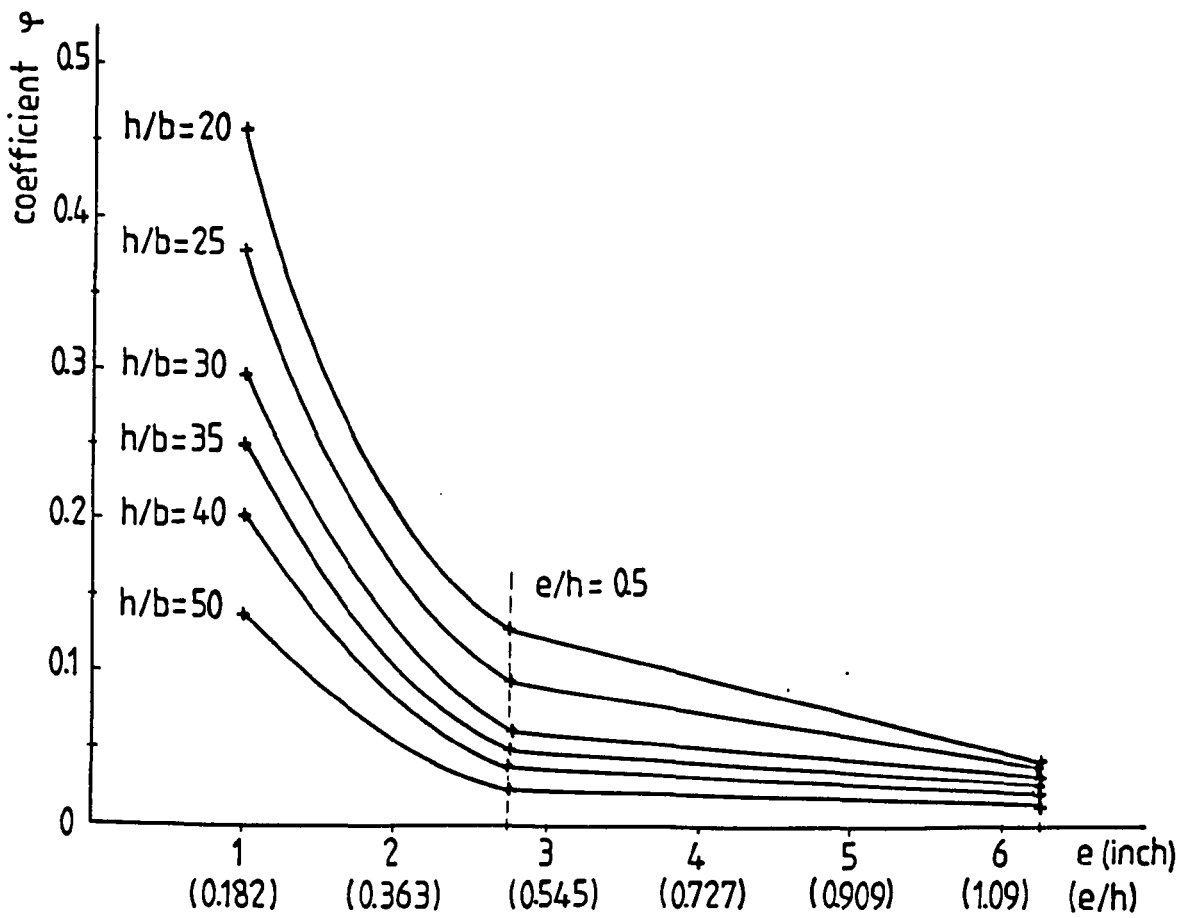


Fig.5.7: PCA design table A1 interpolated  
- load capacity coefficient against  $e/h$  -

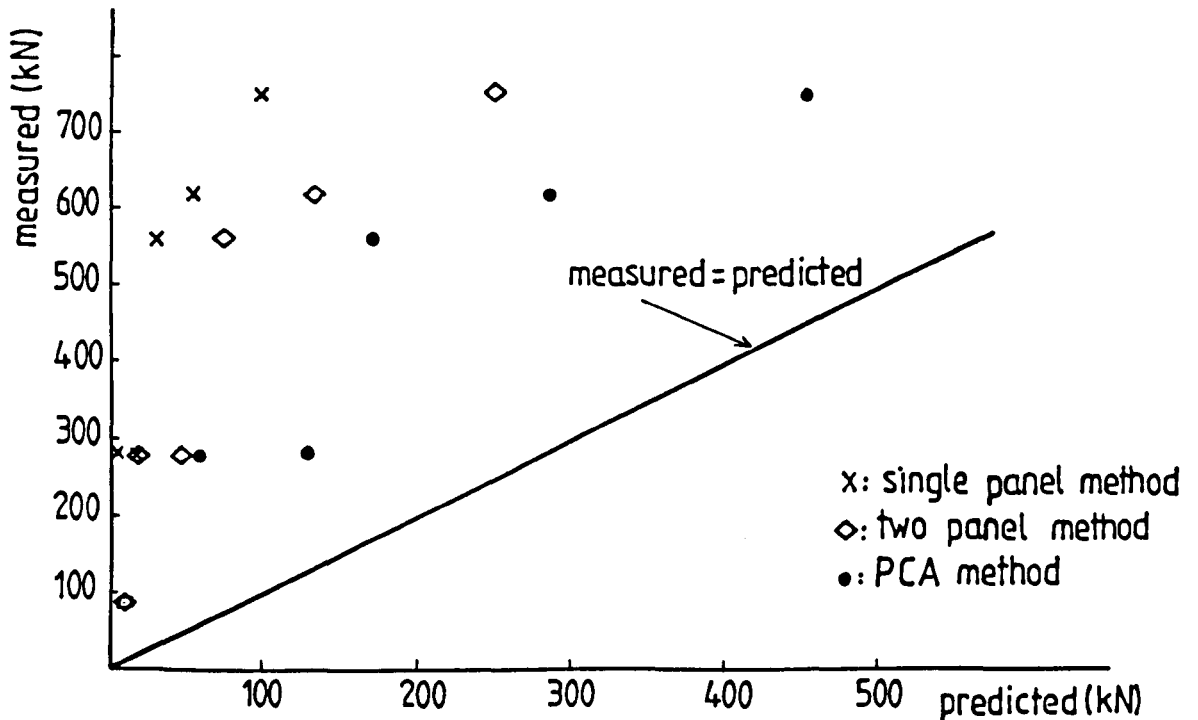


Fig.5.8: Buckling loads - measured against predicted -

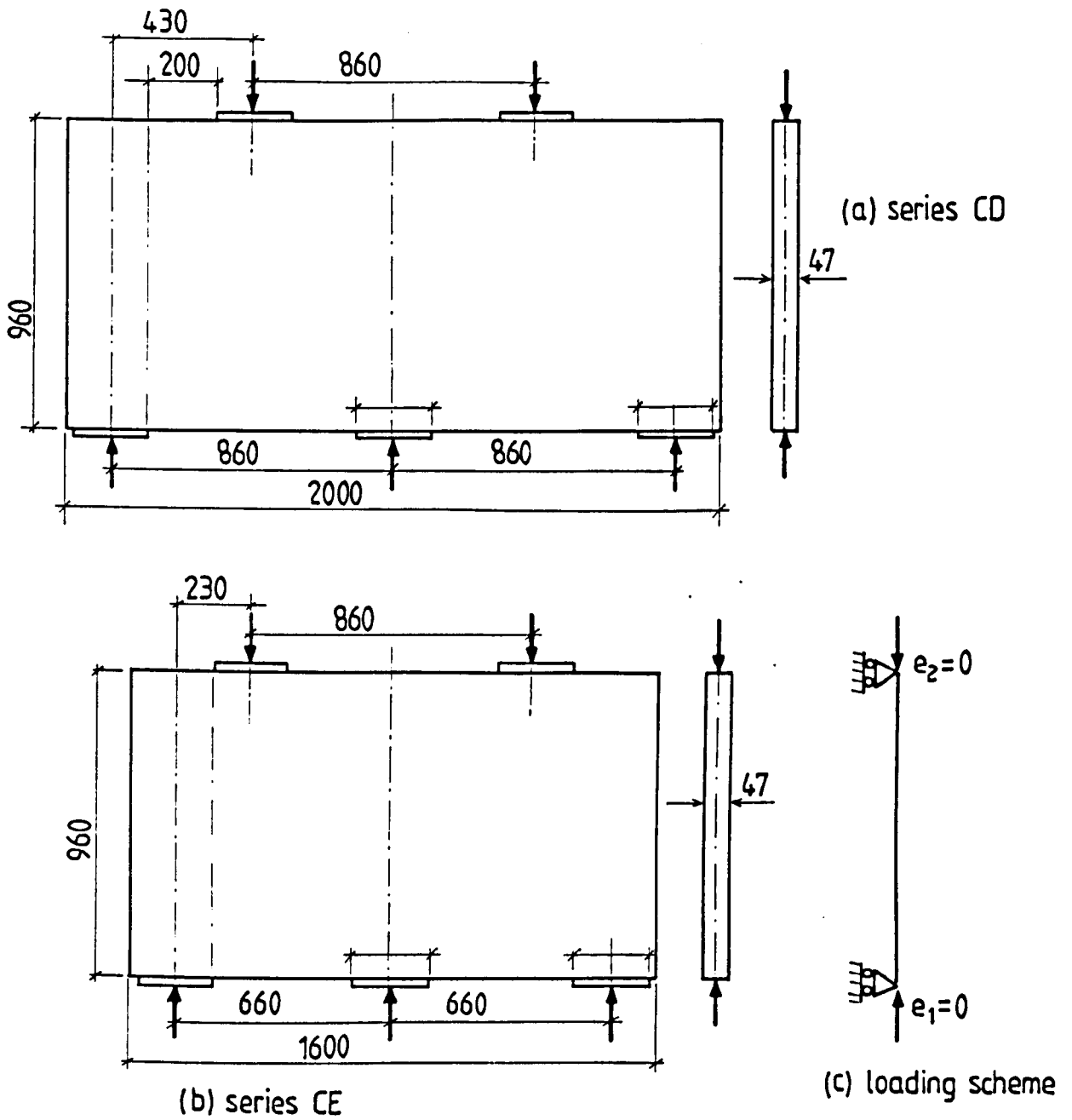


Fig.6.1: Details and loading scheme of continuous beams

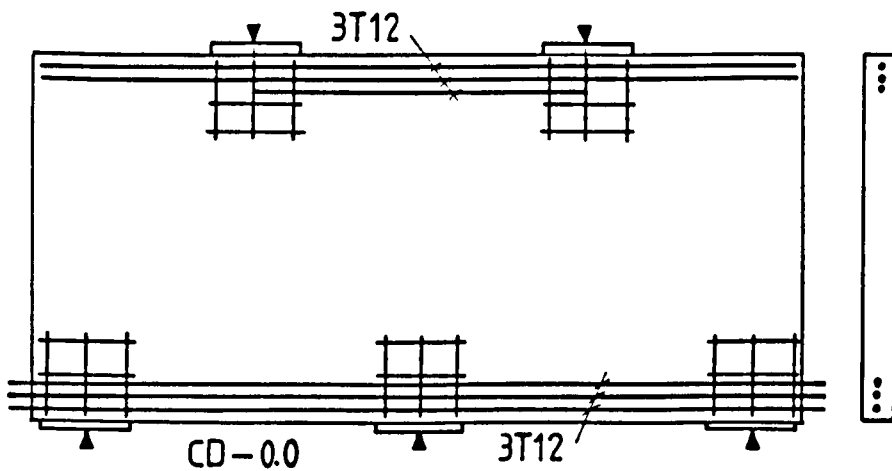


Fig.6.2: Reinforcement detailing for continuous beams

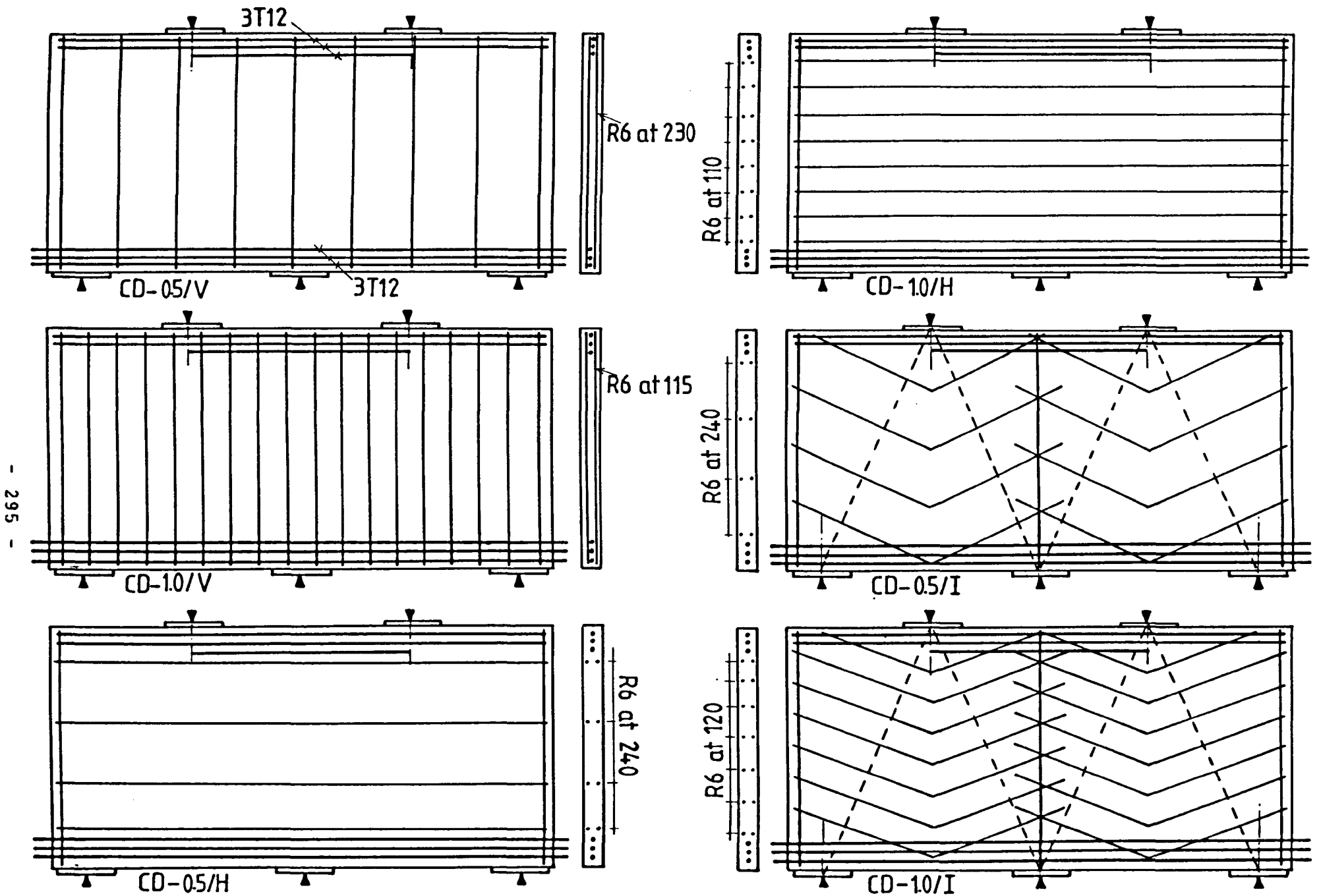


Fig.6.2: contd. Reinforcement detailing for continuous beams

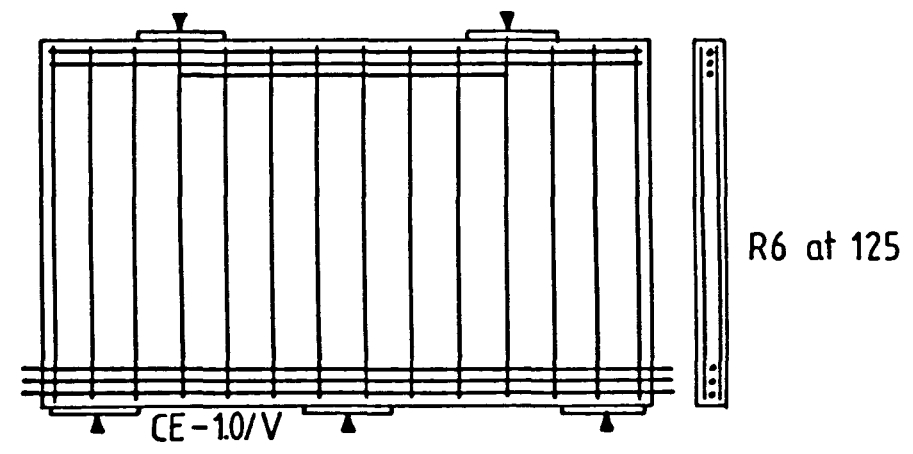
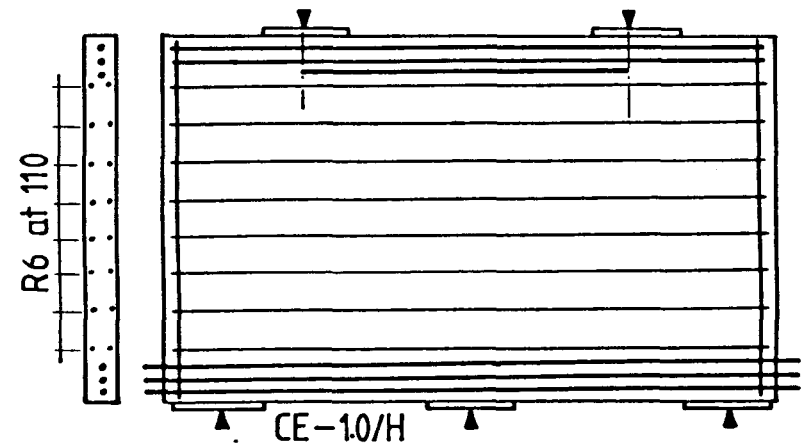
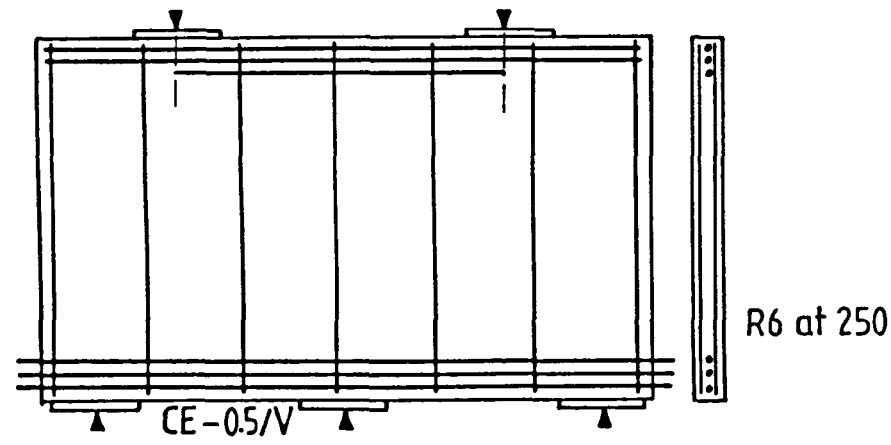
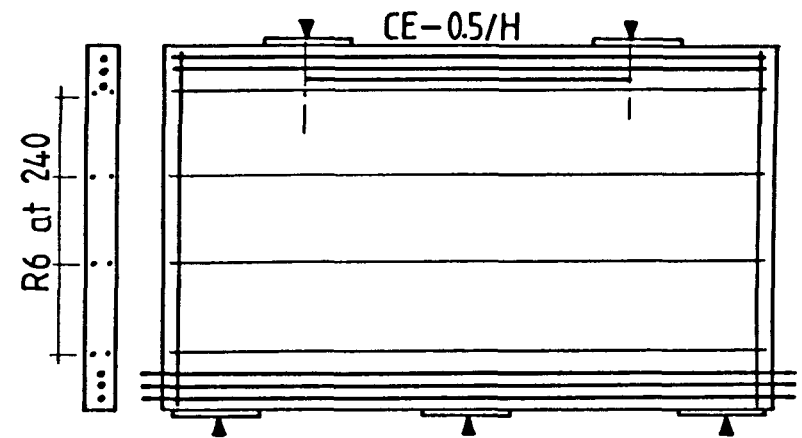
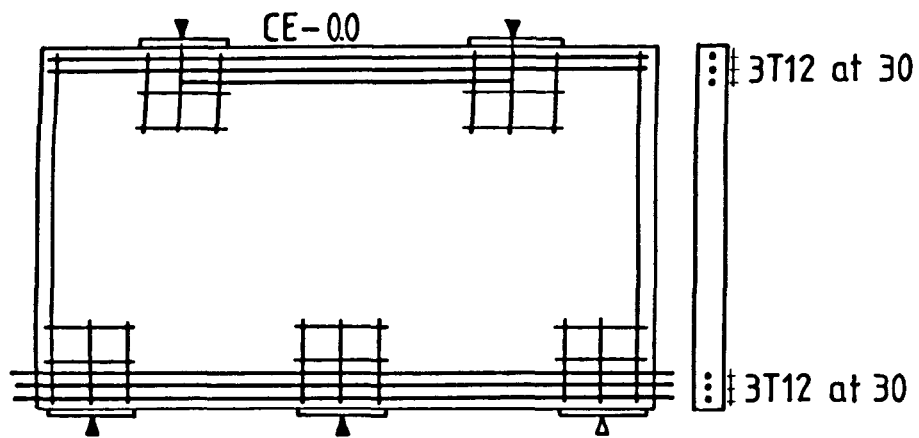


Fig.6.2: contd. Reinforcement detailing for continuous beams

- except in beams without web reinforcement, additional bars at supports and loading points were omitted for clarity
- tension bars at top and bottom are the same for all the beams

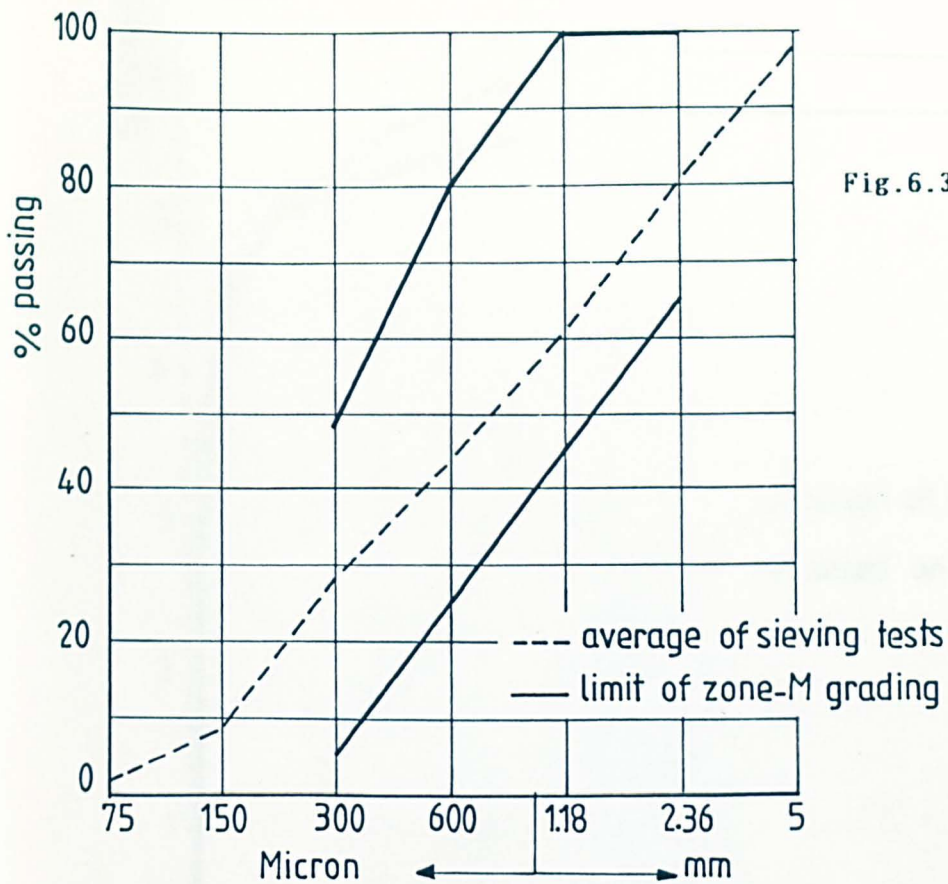


Fig.6.3: Grading curve of aggregates

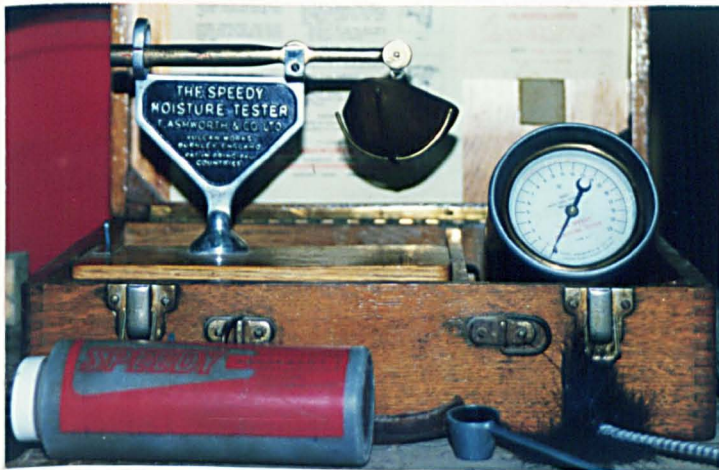


Fig.6.4a: Speedy moisture tester

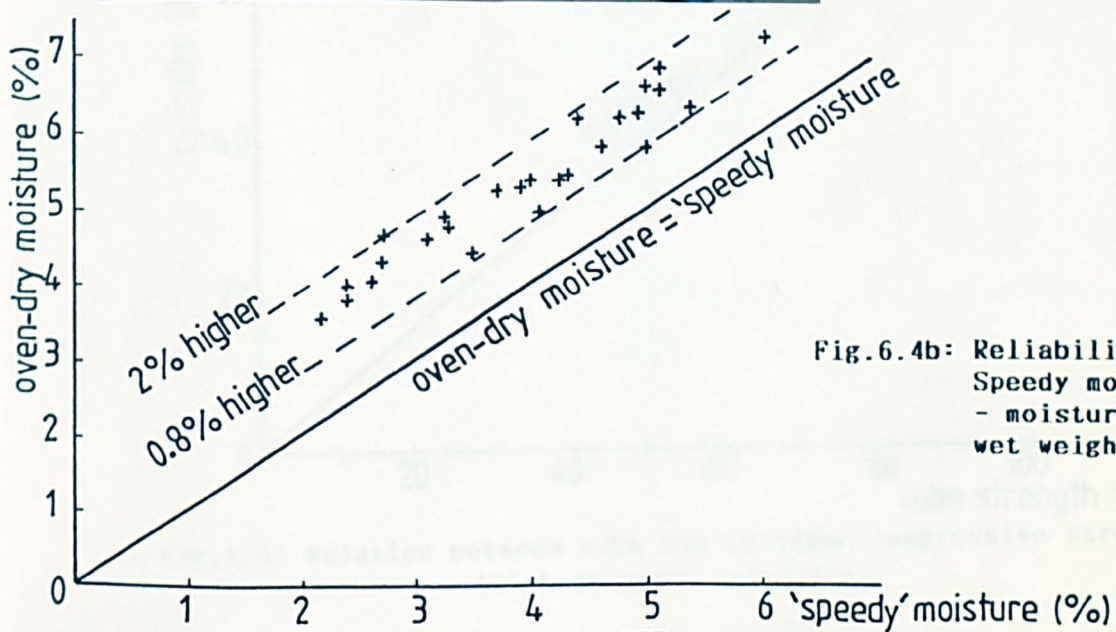


Fig.6.4b: Reliability of Speedy moisture tester - moisture in % of wet weight of aggregates

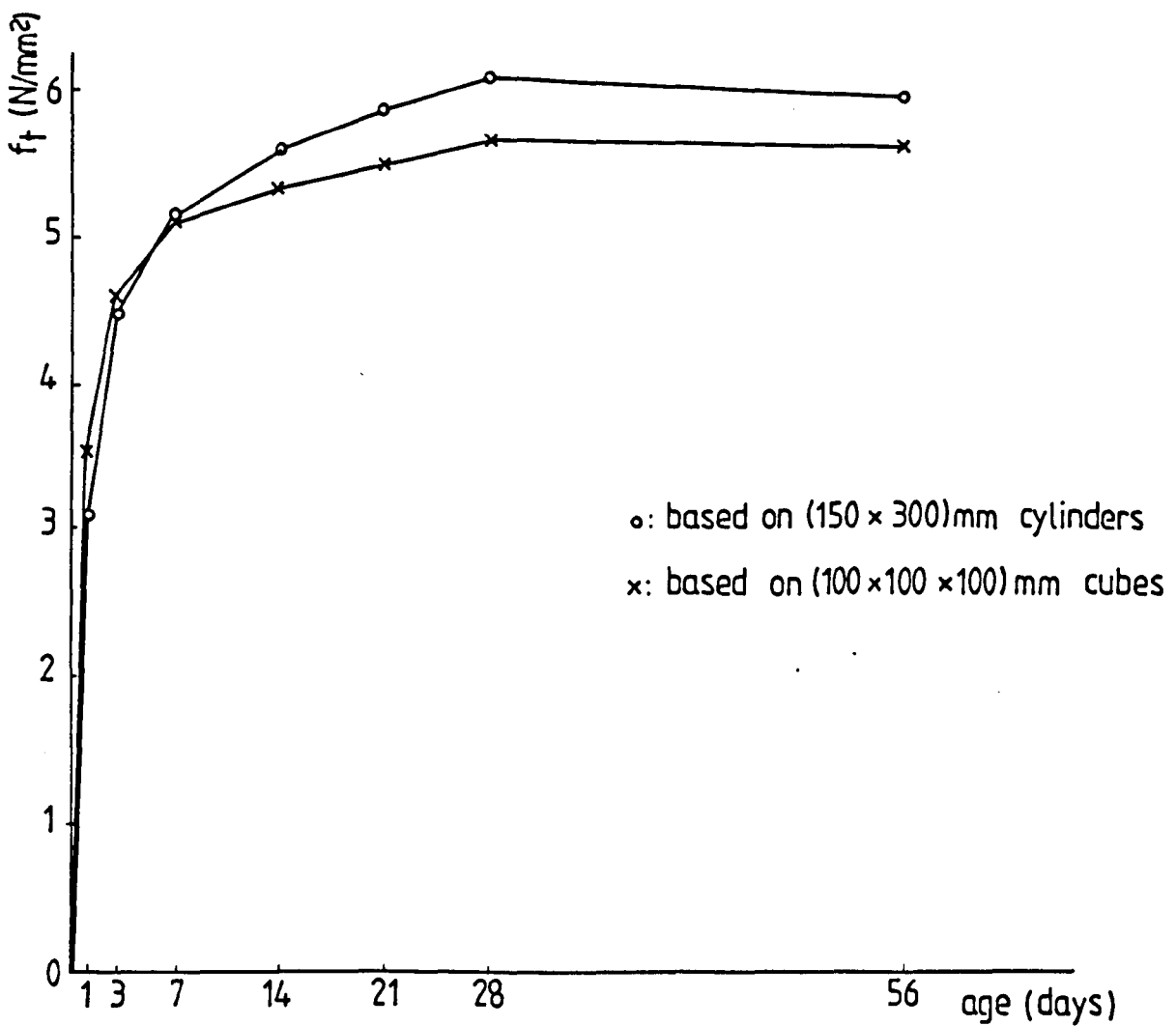


Fig.6.5: Development of tensile strength of concrete,  $f_t$ , with age (high-strength concrete)

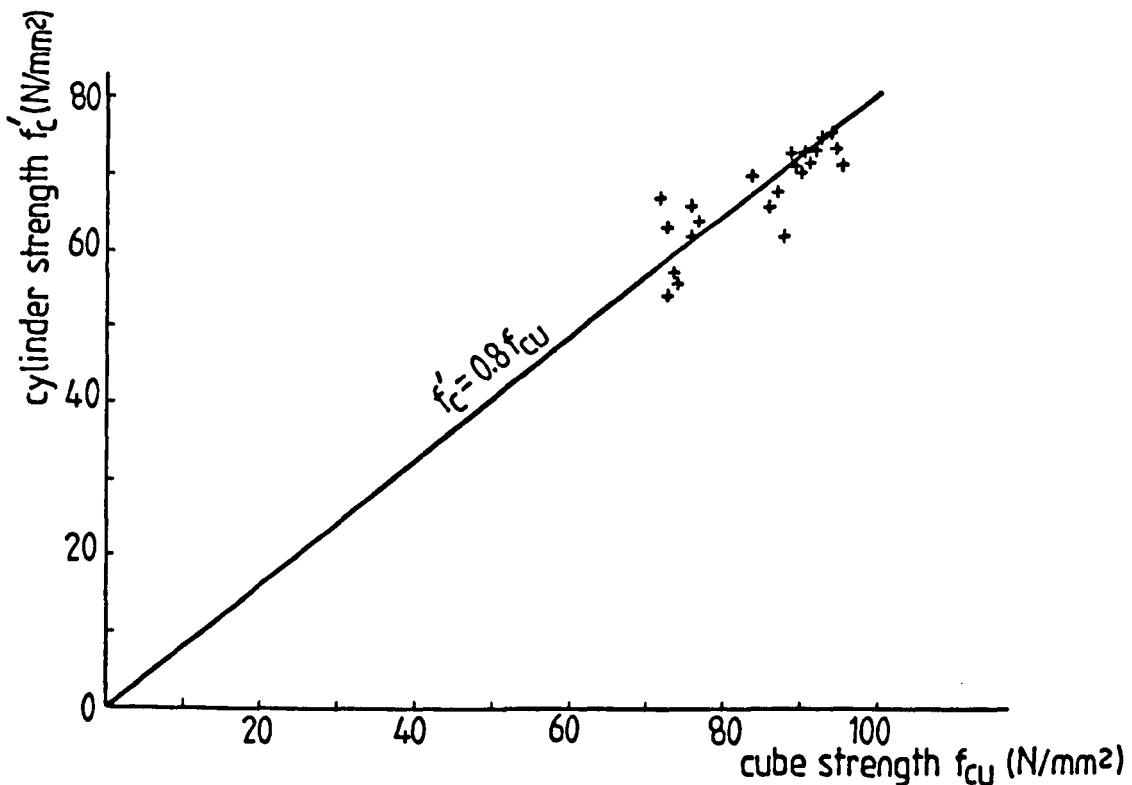


Fig.6.6: Relation between cube and cylinder compressive strengths of concrete (high-strength concrete)





Fig.6.9: A beam being demolded from the big formwork



Fig.6.10: A beam being cured with the control specimens

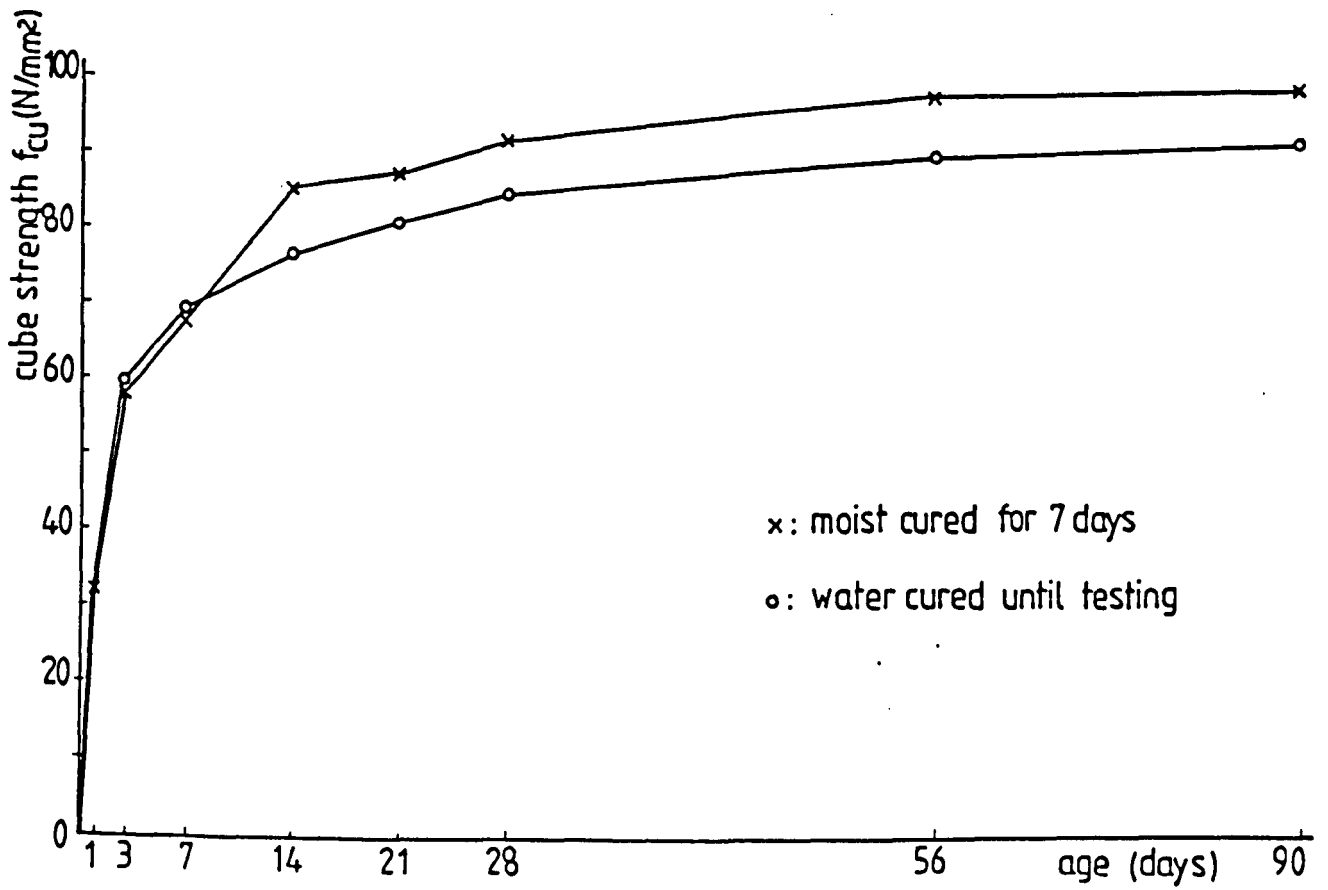


Fig.6.11: Comparison between two concrete curing methods

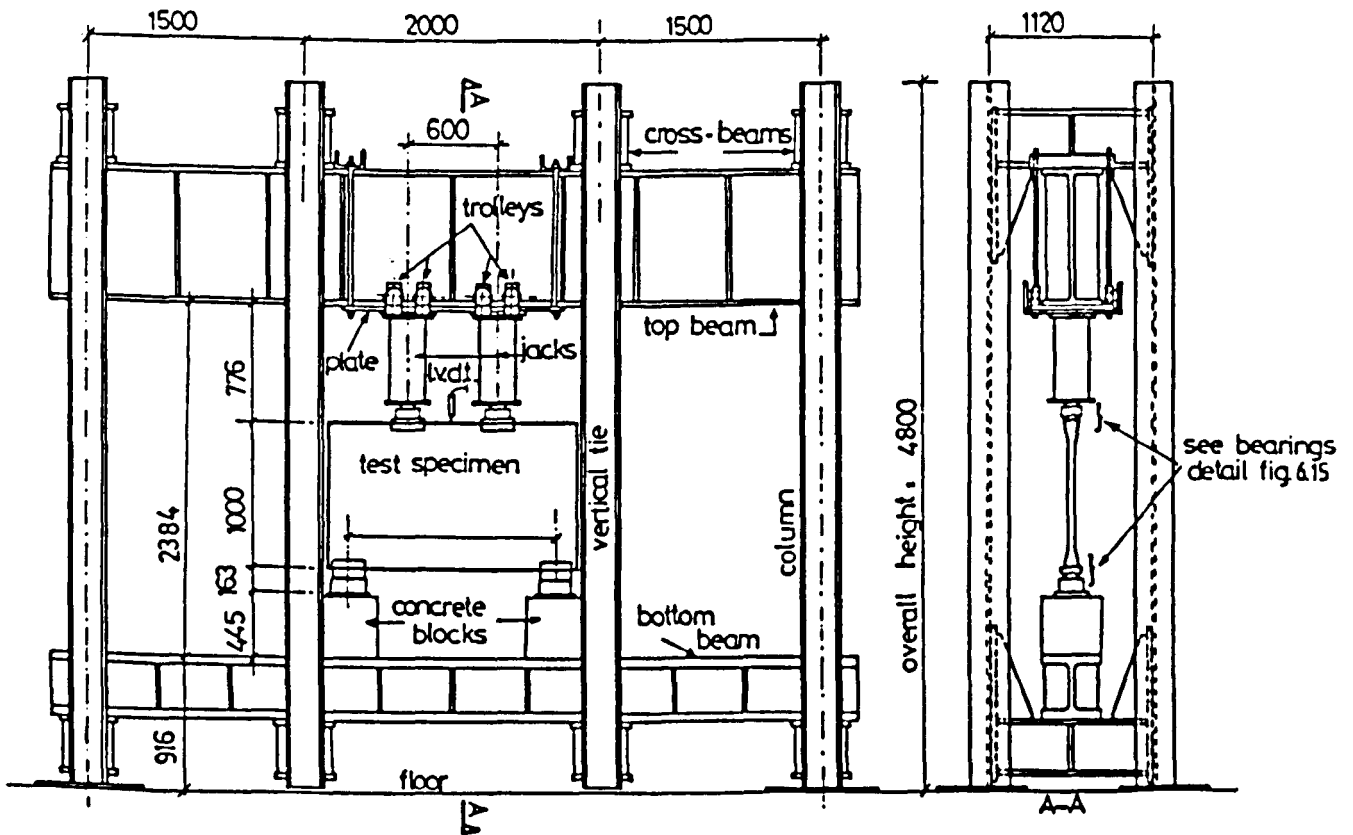


Fig.6.12: Testing rig arrangement

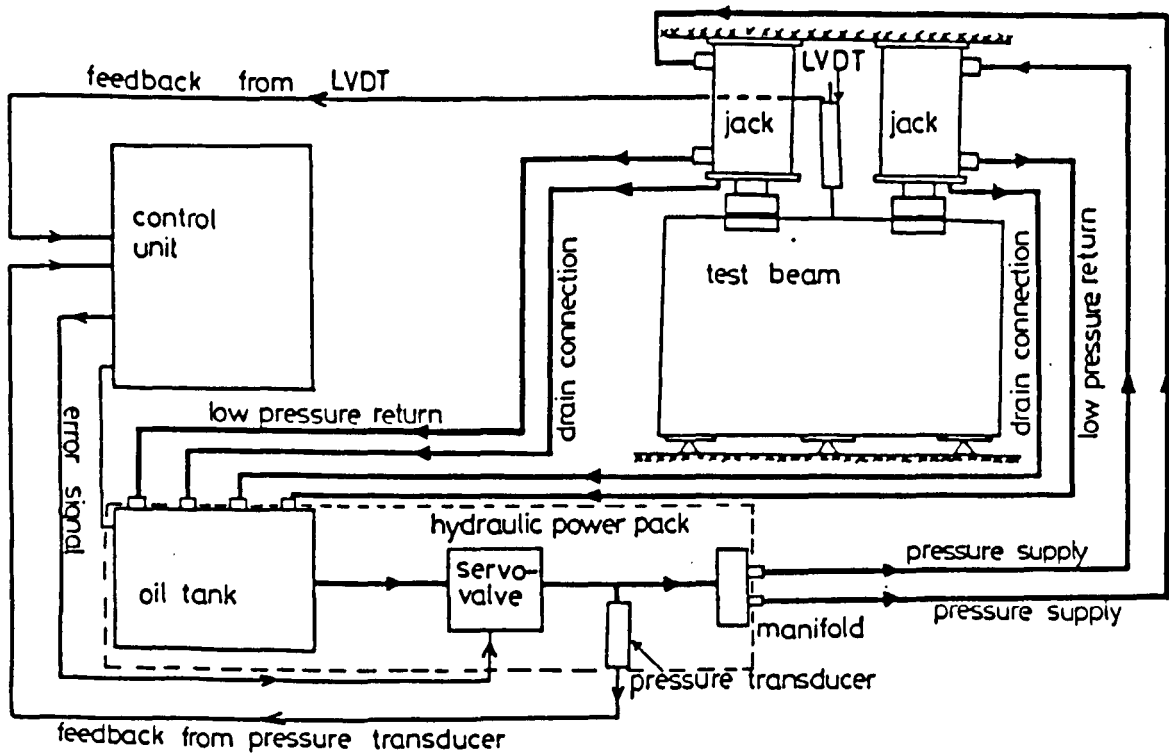


Fig.6.13: Schematic representation of the loading system

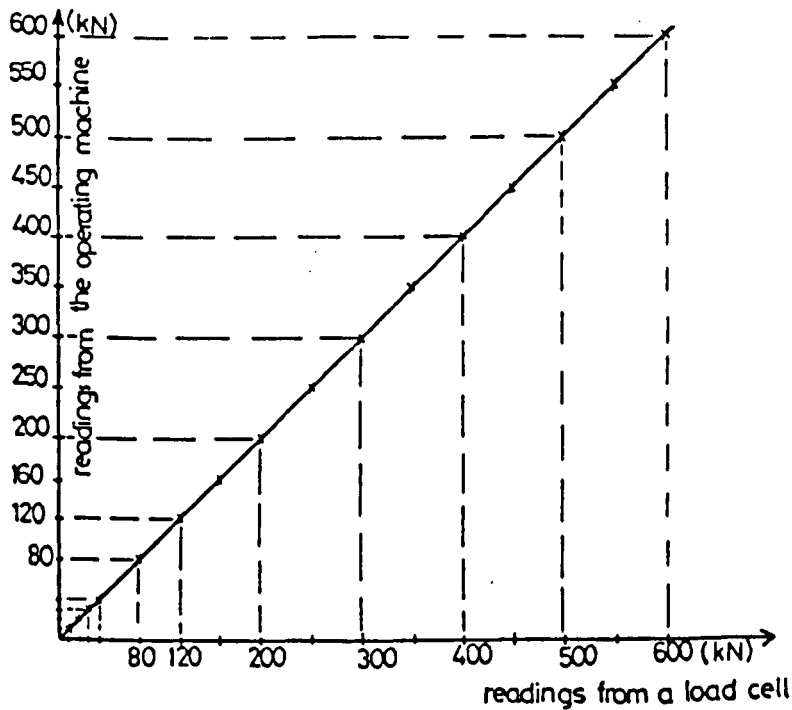
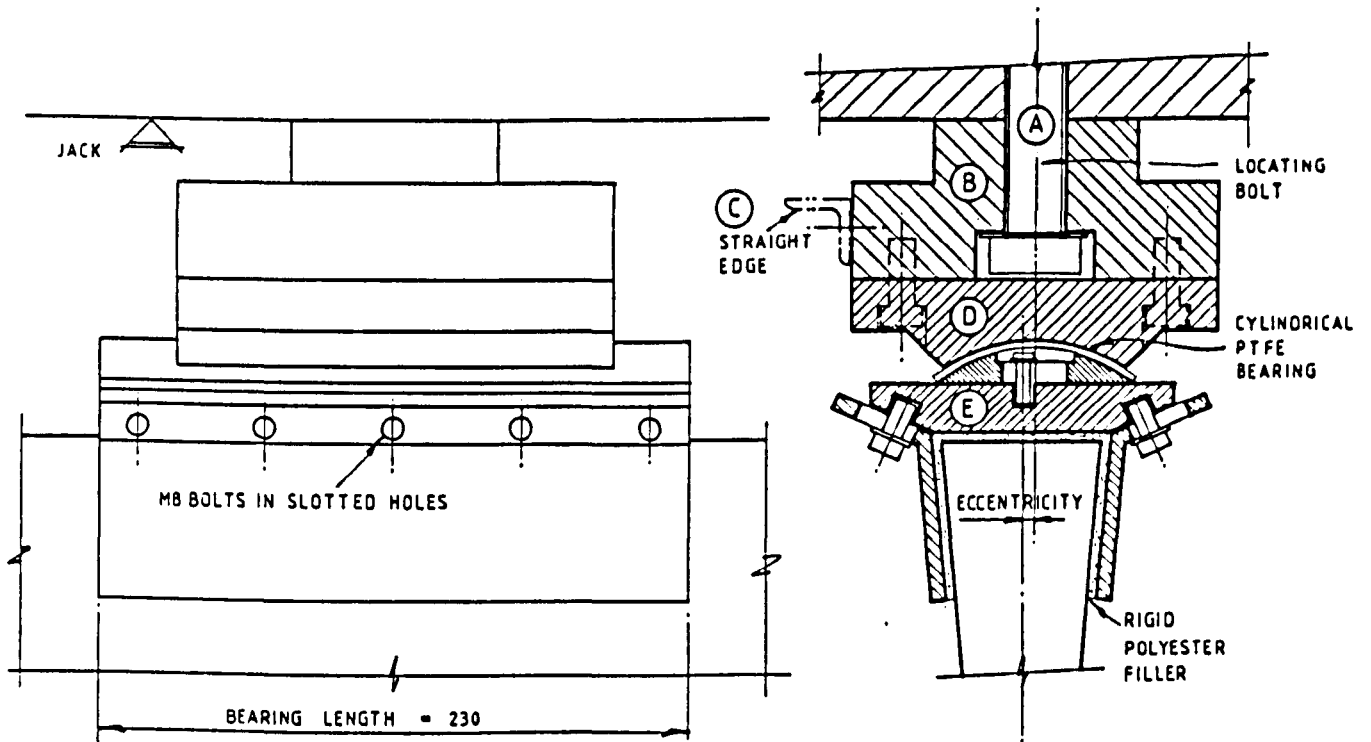
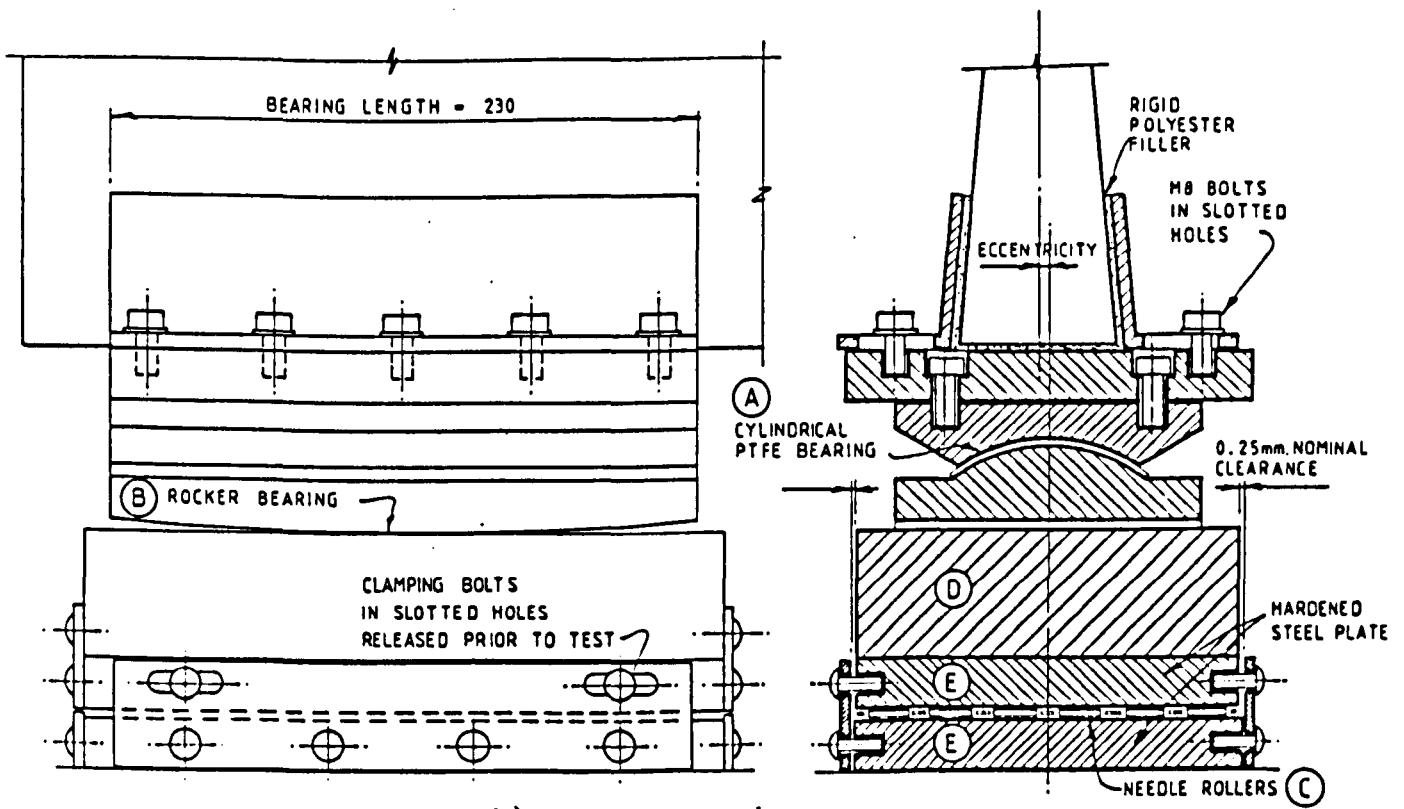


Fig.6.14: Typical calibration graph of the jacks



a) at loading points



b) at support points

Fig.6.15: Bearing details

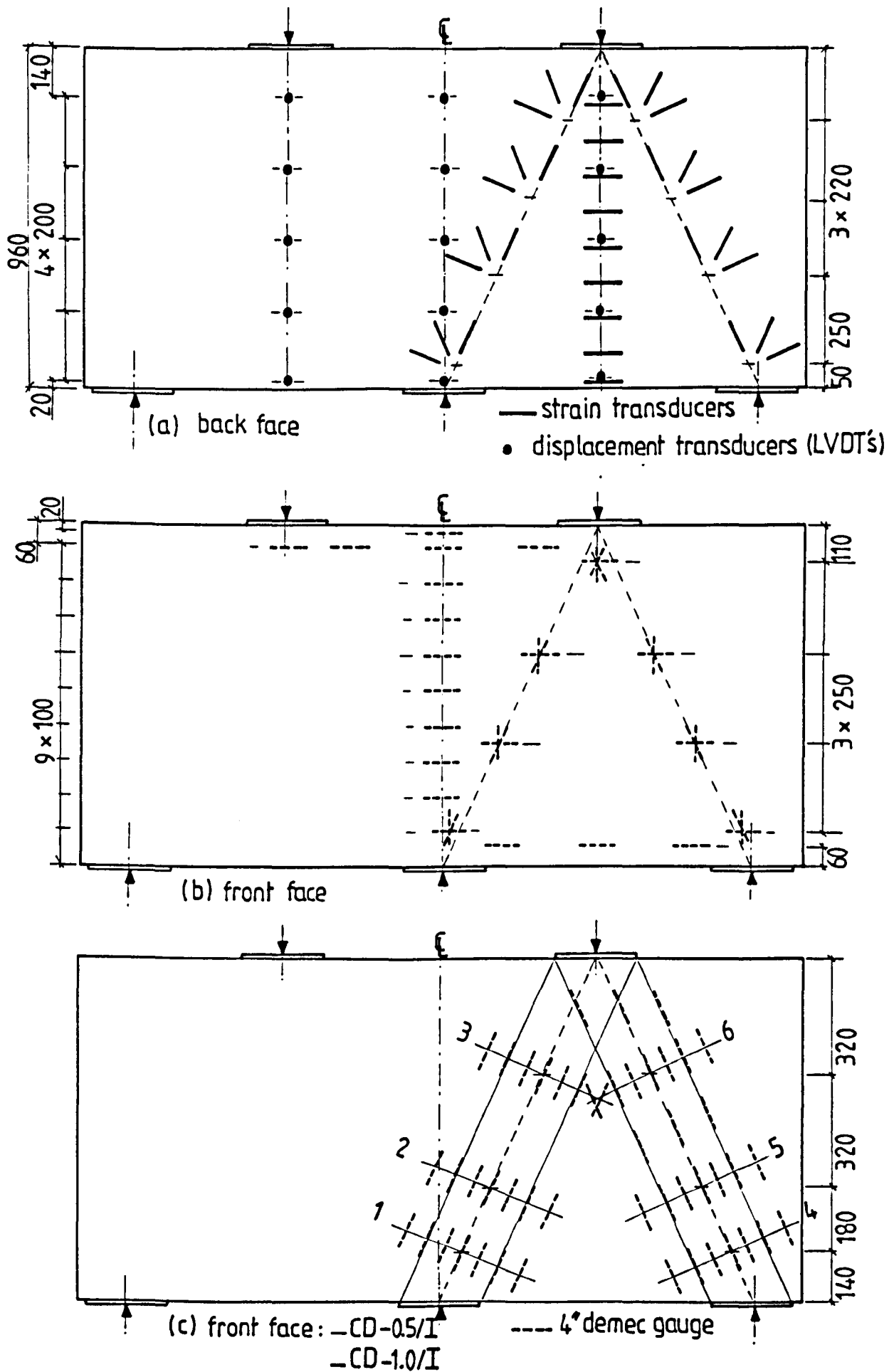
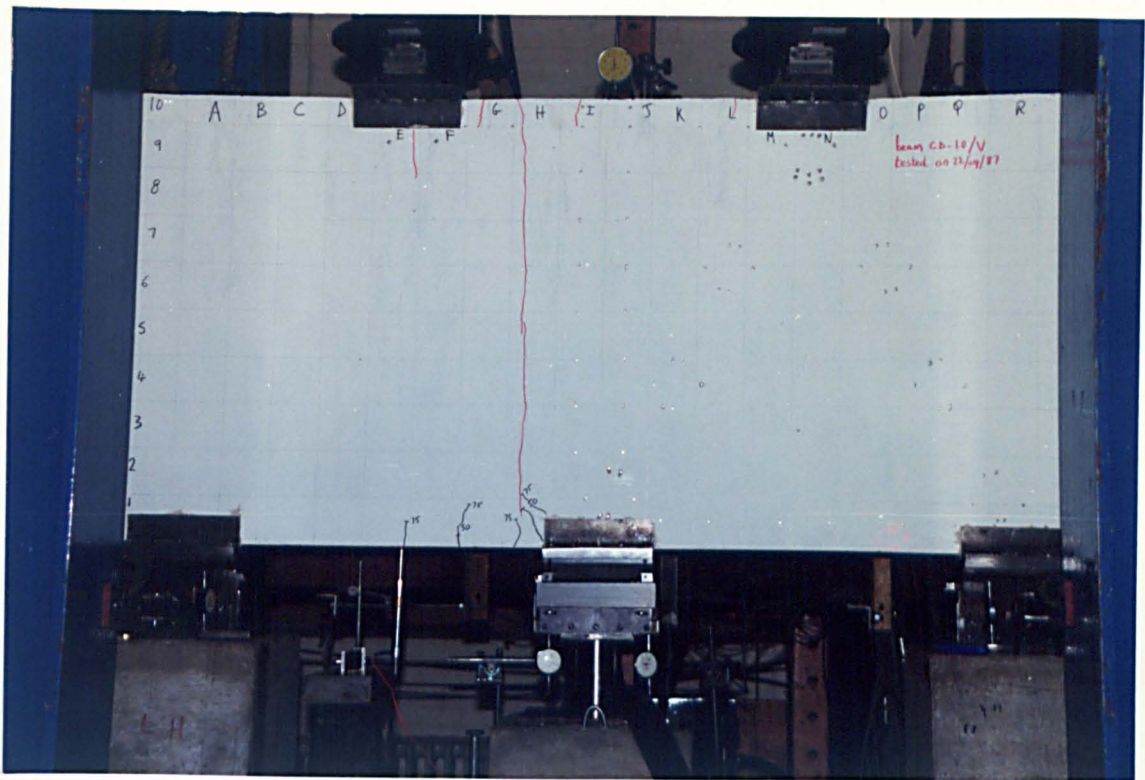


Fig.6.16: Locations of lateral displacement and strain measurements in continuous beam:



- a) - dial gauges monitoring settlement  
 - load cell monitoring reaction

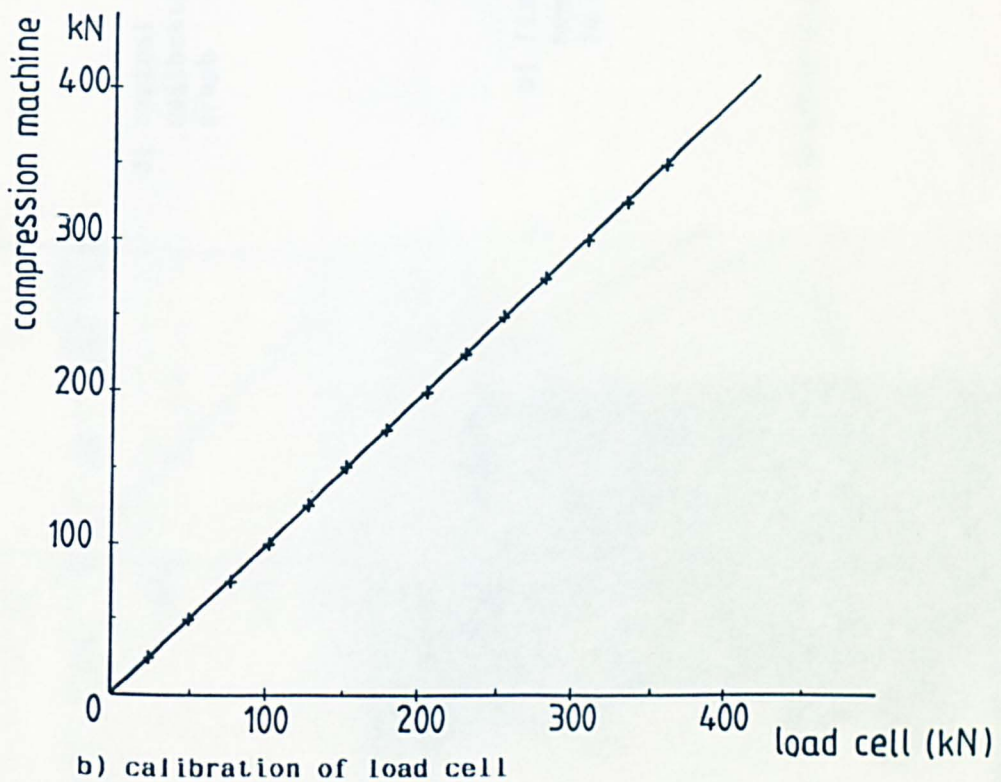
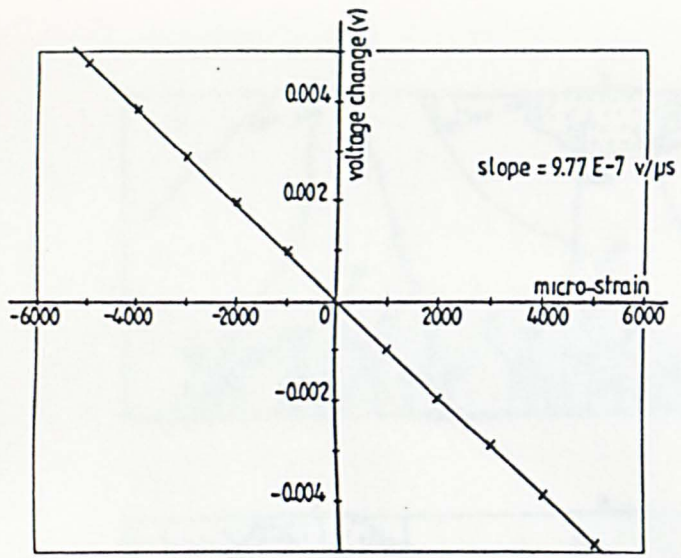
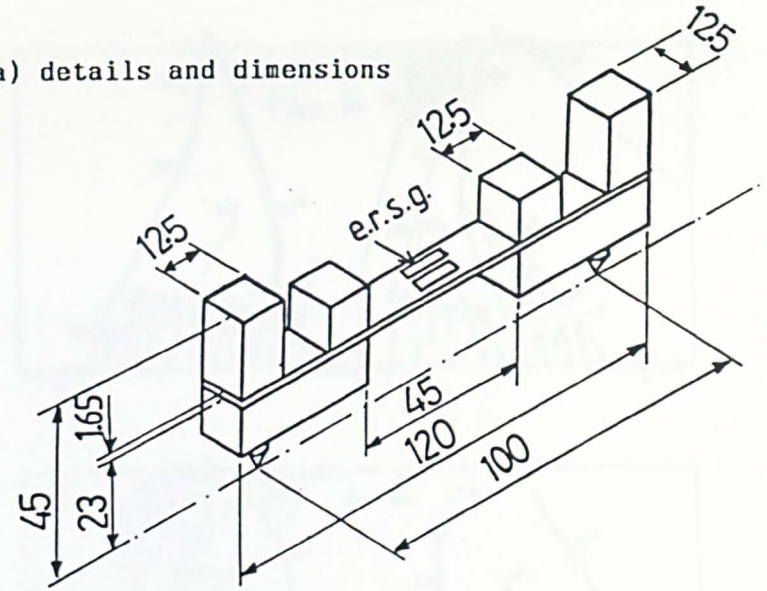


Fig.6.17: Interior support - reaction and settlement measurements -

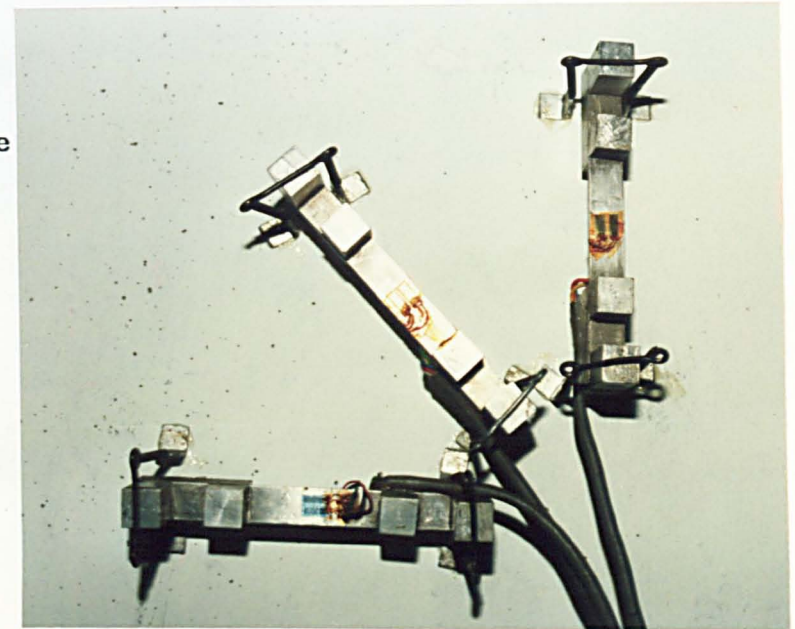


d) typical calibration graph

a) details and dimensions



b) fixed on the concrete surface in 45° rosette



c) calibration

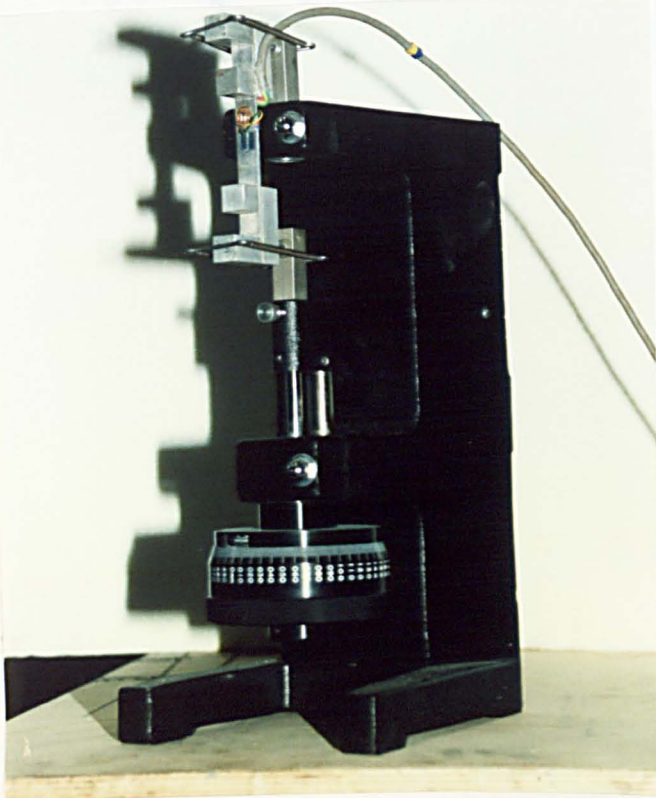
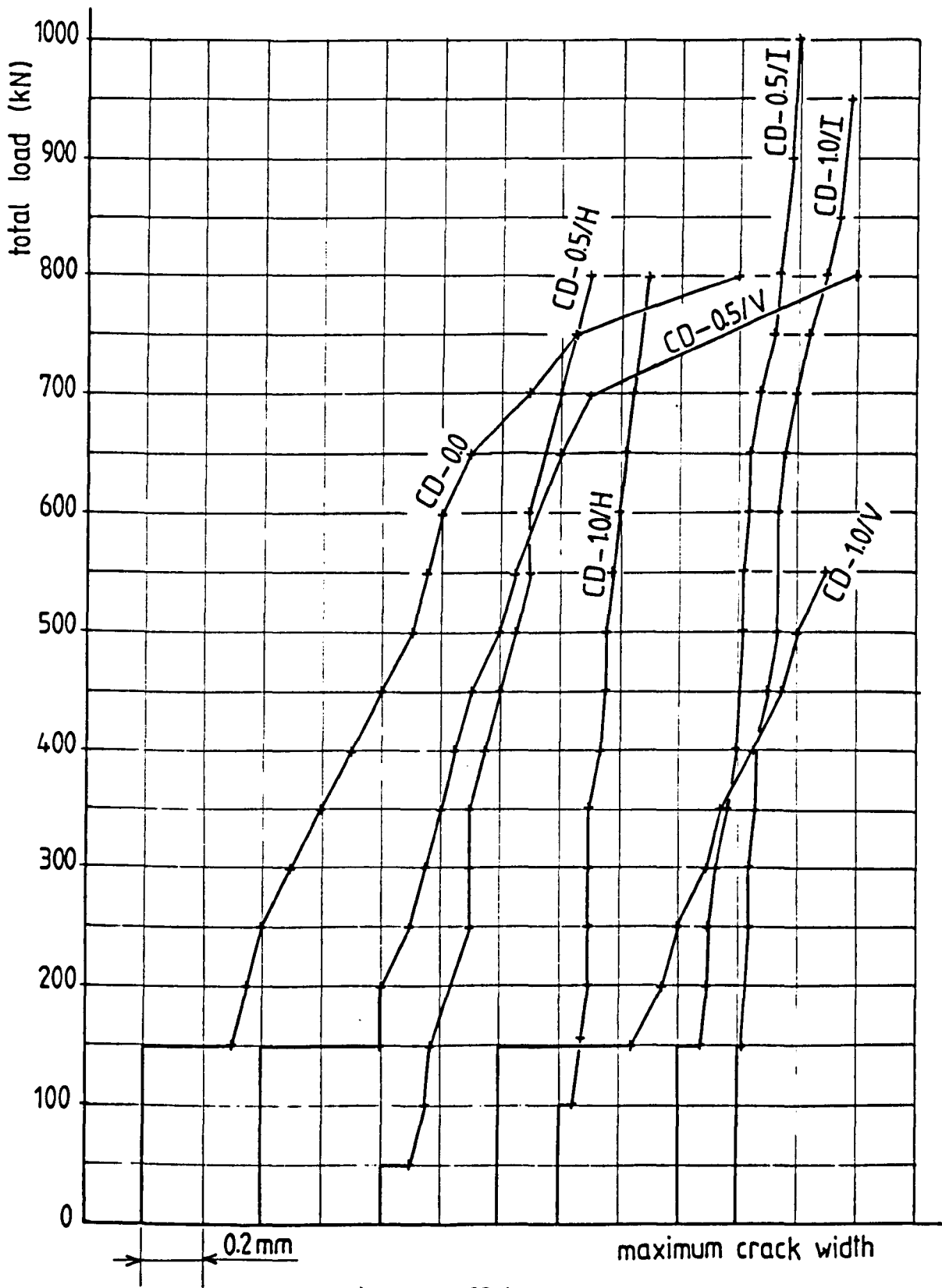


Fig.6.18: A demountable strain transducer







a) series CD beams

Fig.7.2: Load against maximum crack width

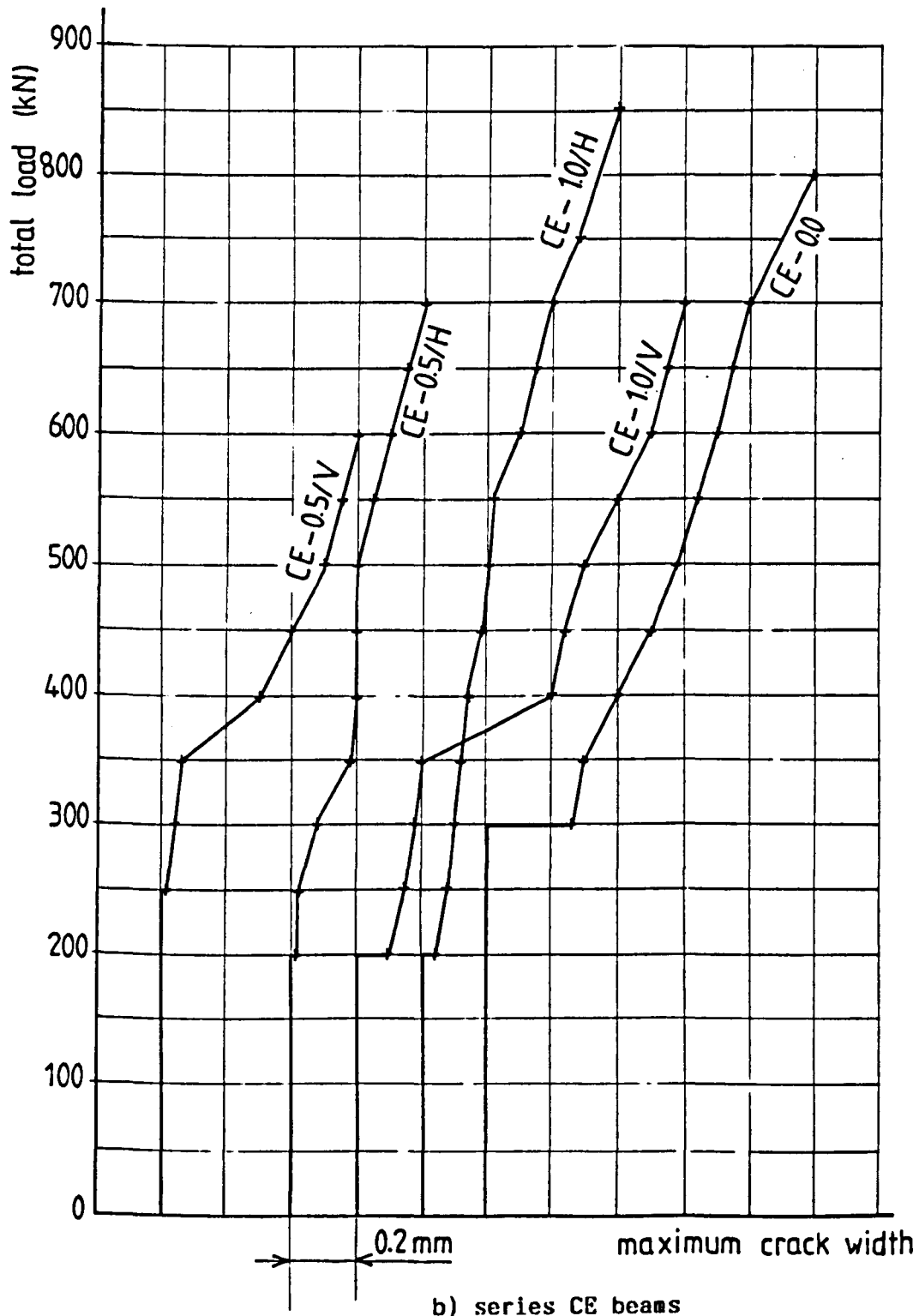


Fig.7.2: contd. Load against maximum crack width

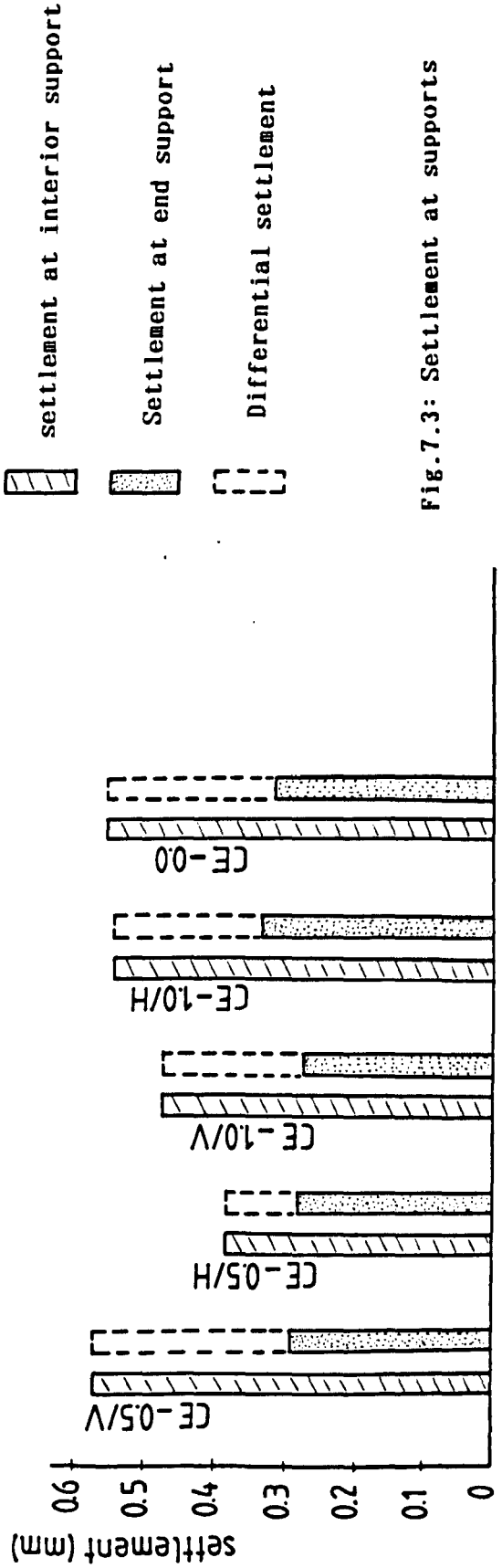
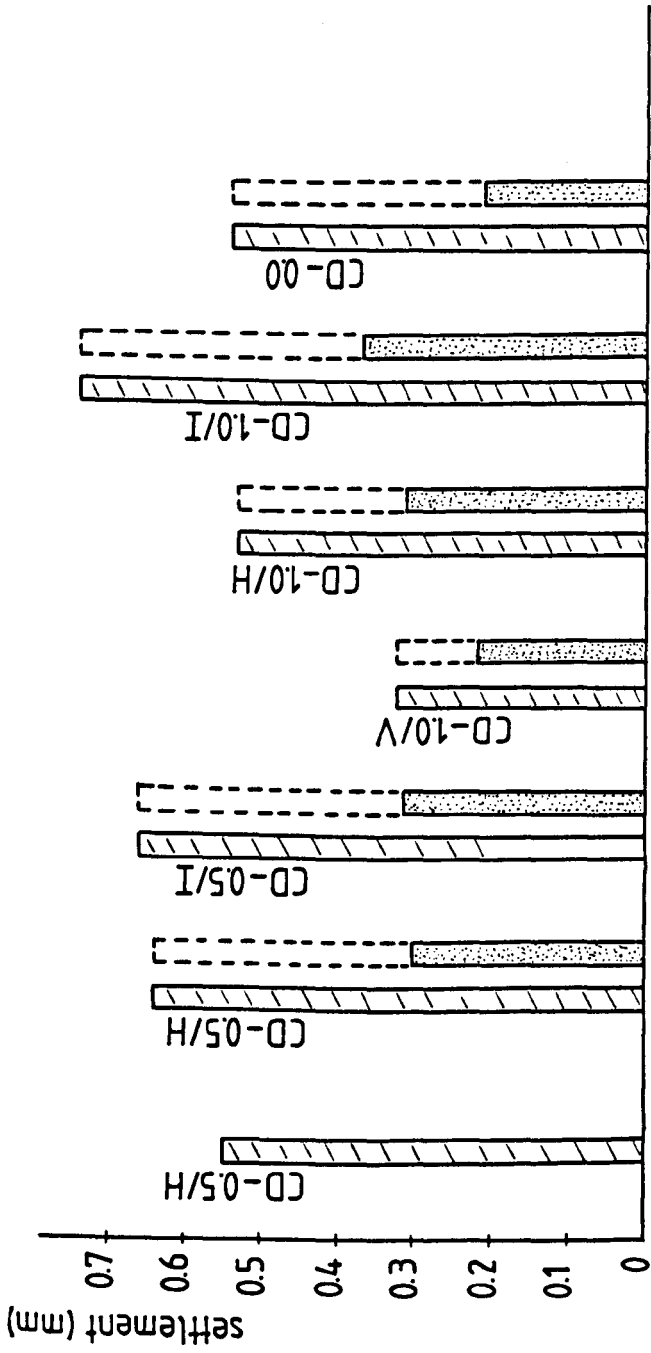


Fig. 7.3: Settlement at supports

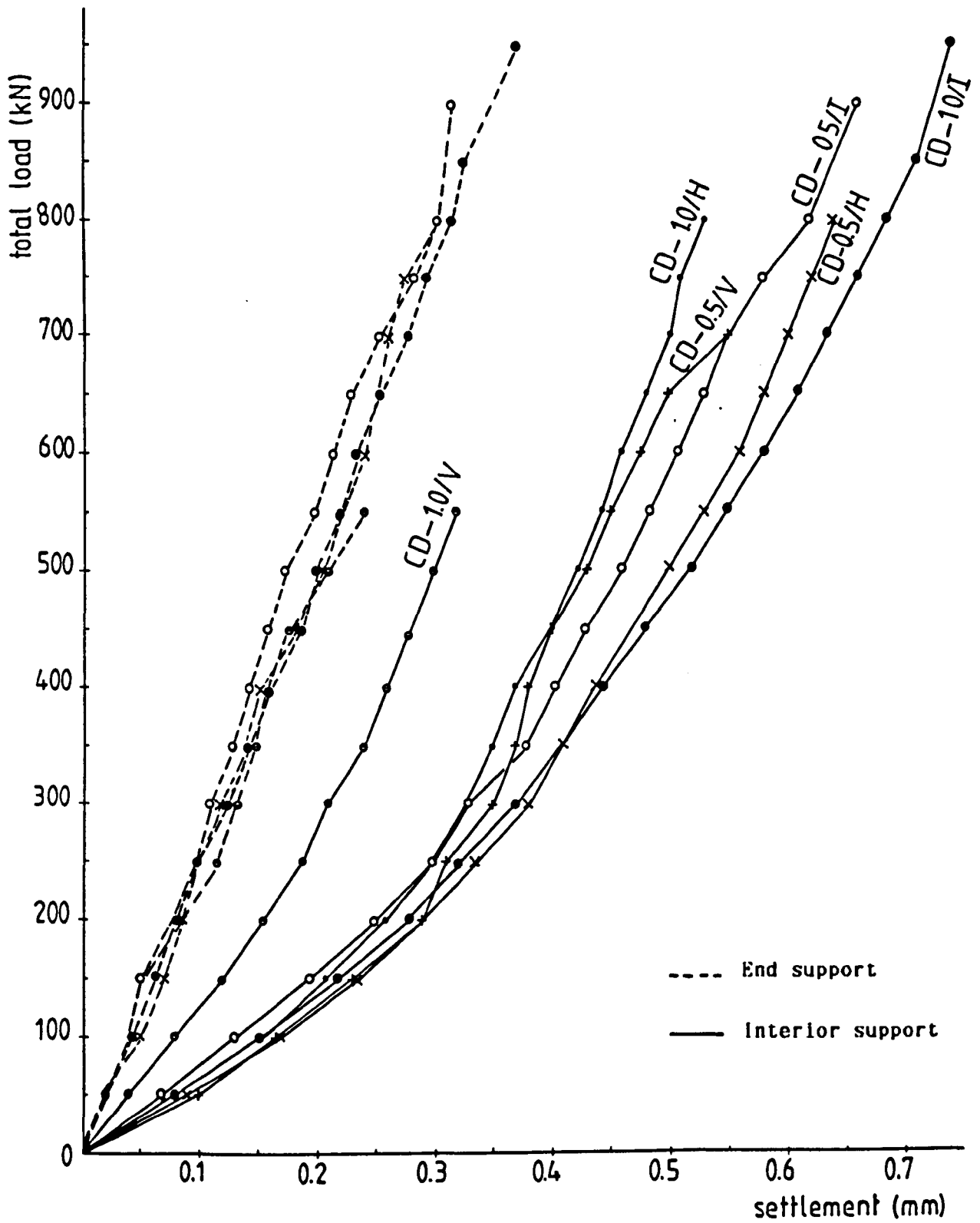


Fig.7.4: Load against settlement  
 - series CD beams -

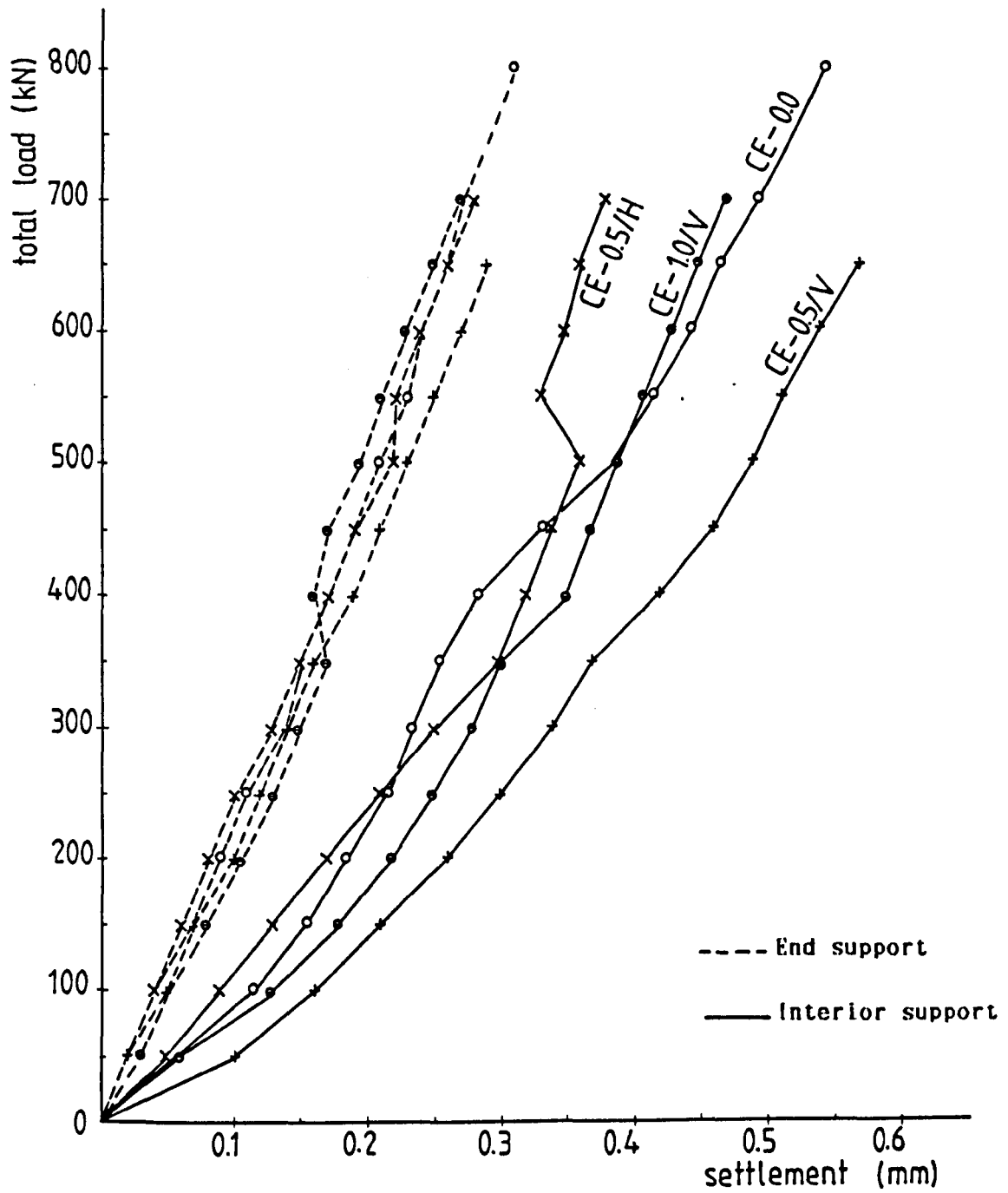


Fig.7.4: contd. Load against settlement  
 - series CE beams -

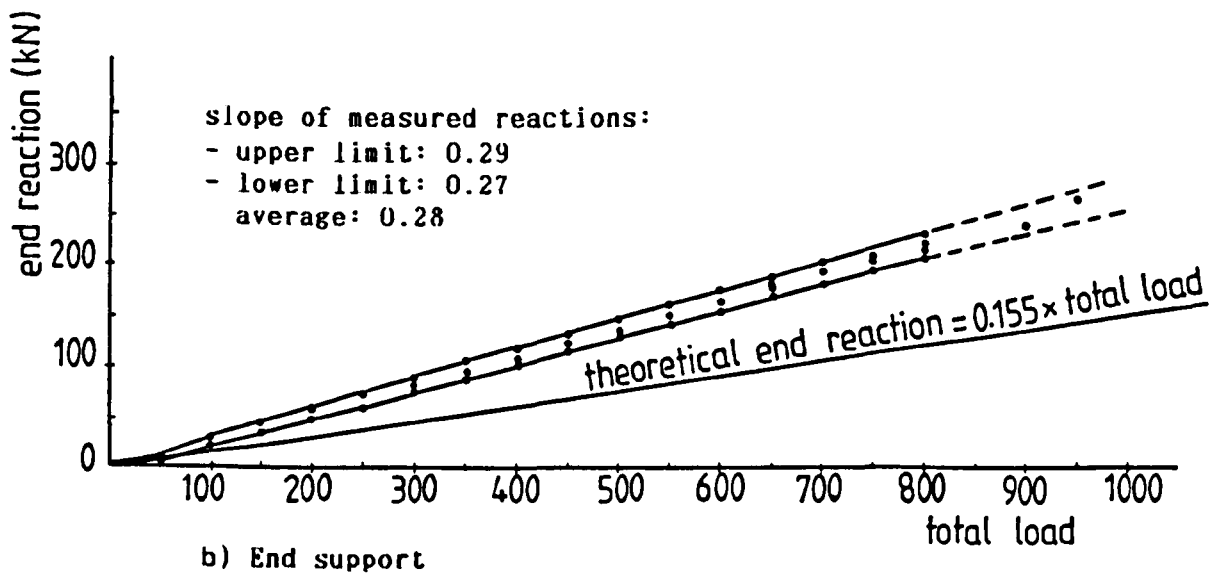
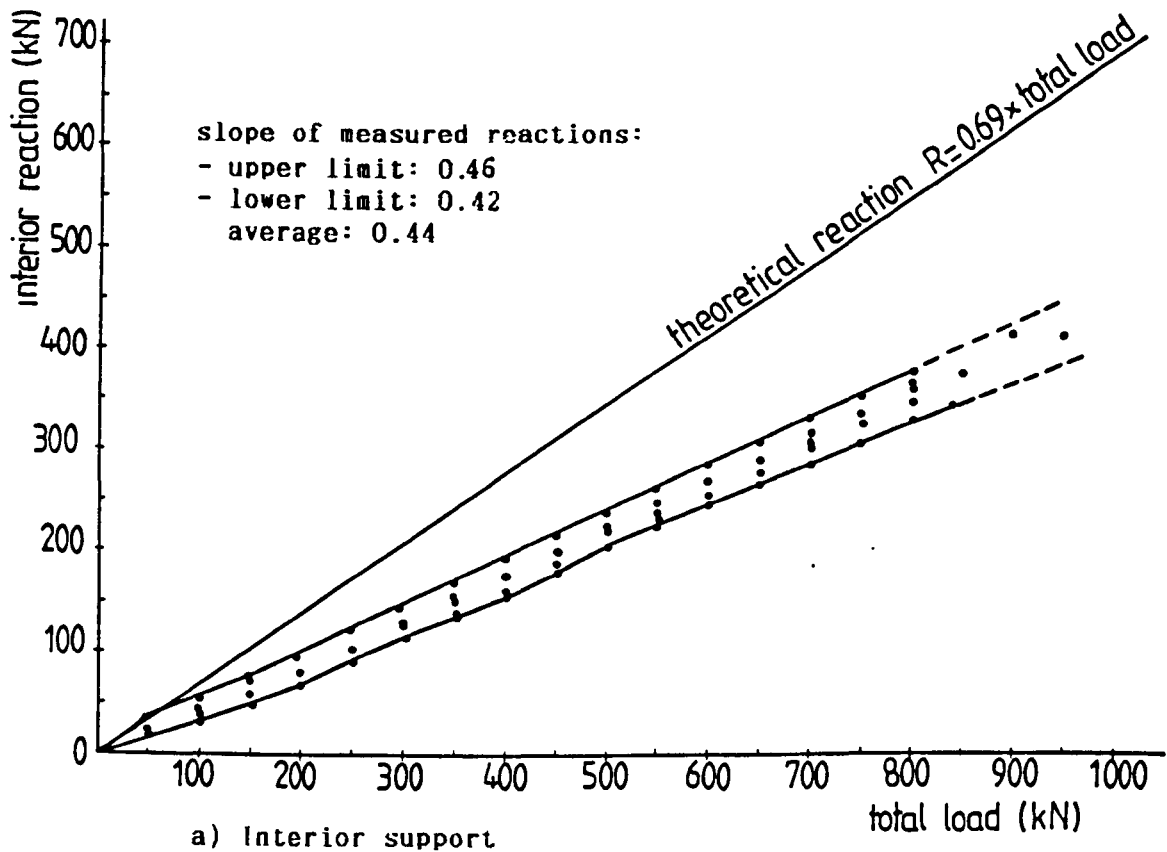


Fig.7.5: Reactions at supports - series CD beams -

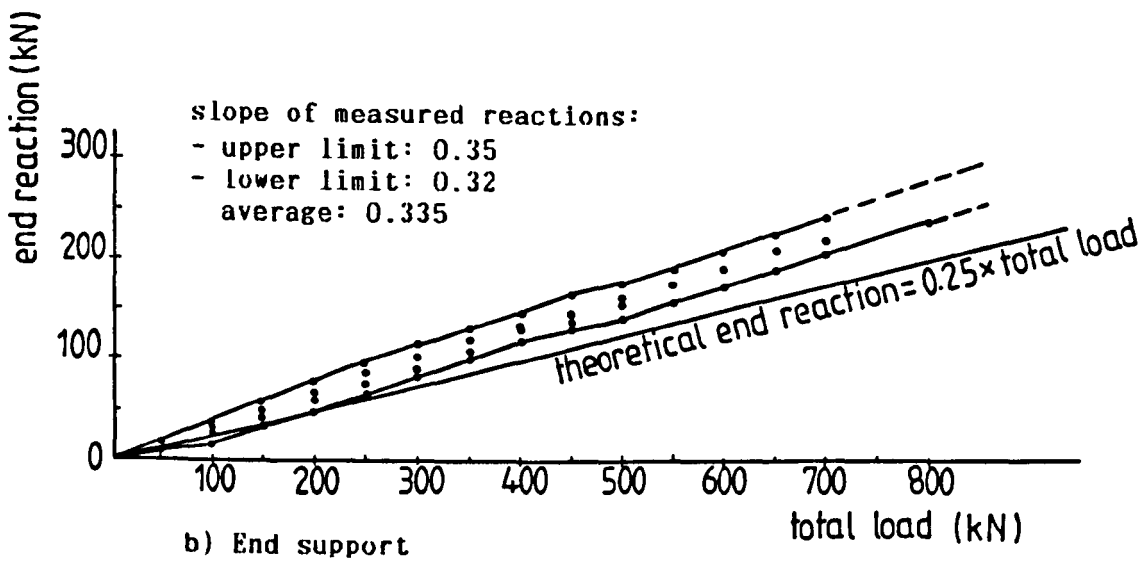
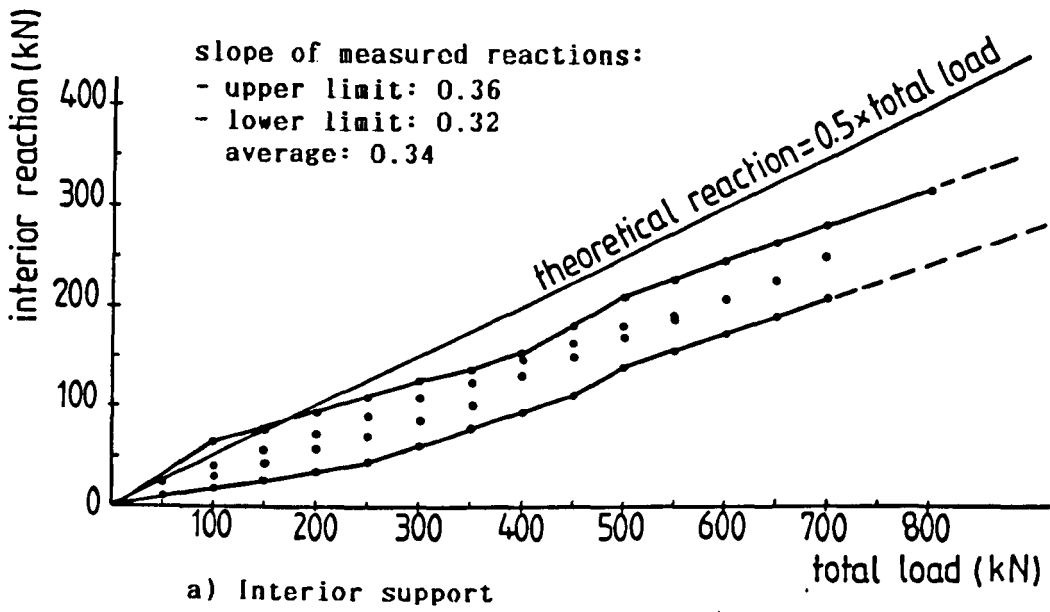
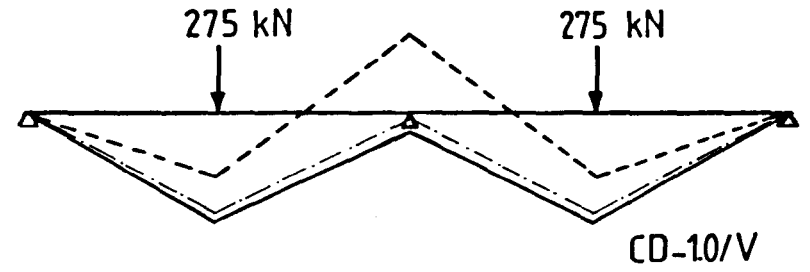
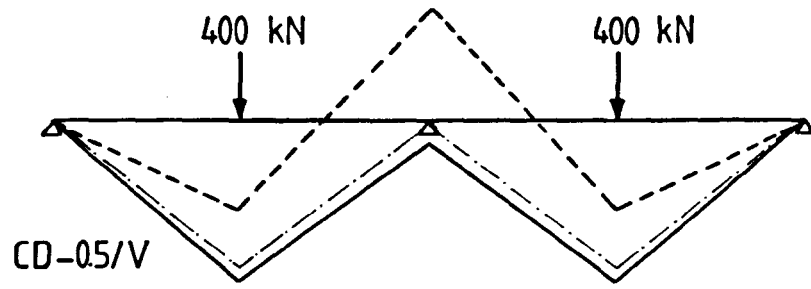
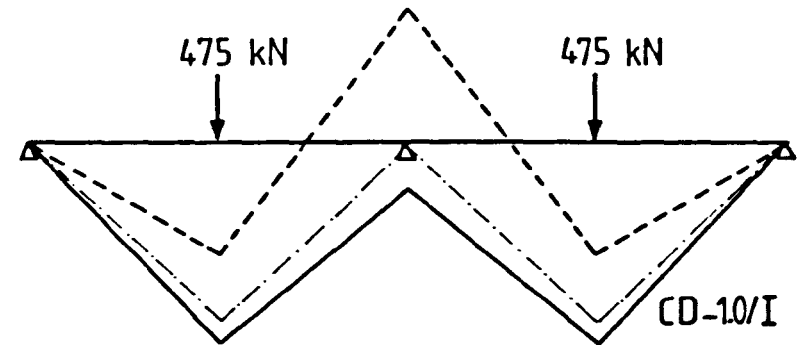
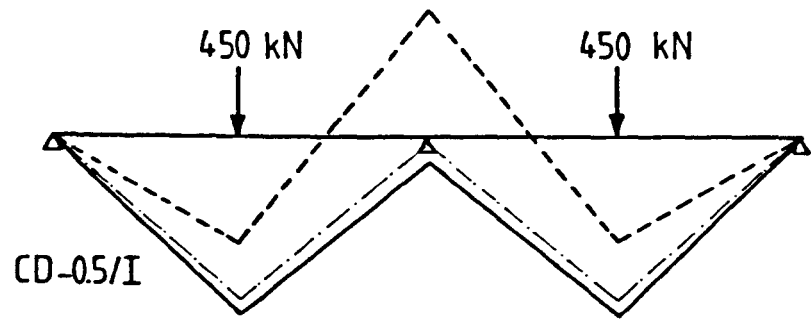
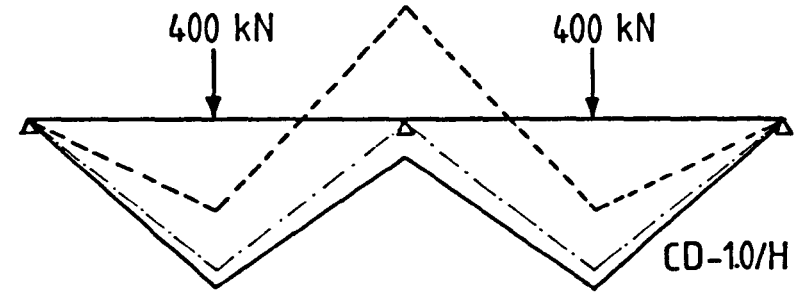
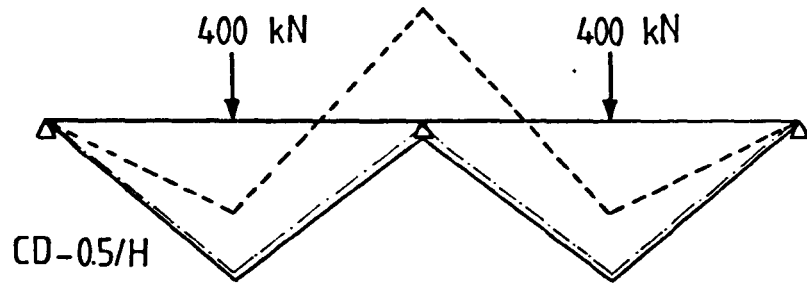


Fig.7.5: contd. Reactions at supports - series CE beams -

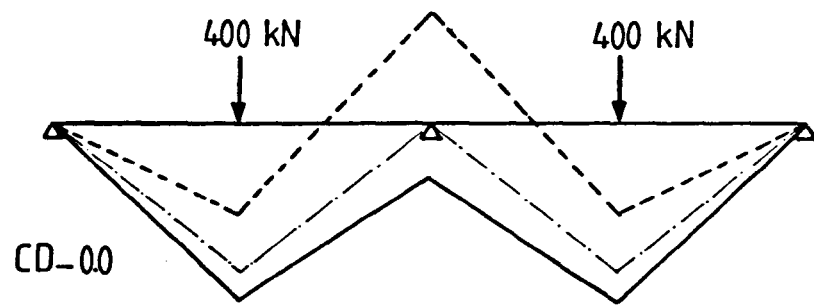


— Measured  
- - - Continuous shallow beams  
- · - single span beams

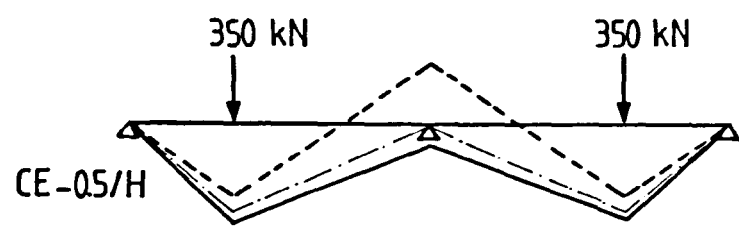
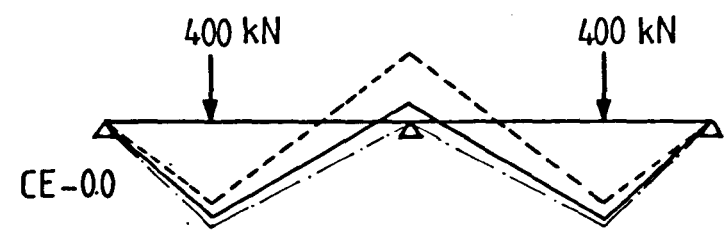
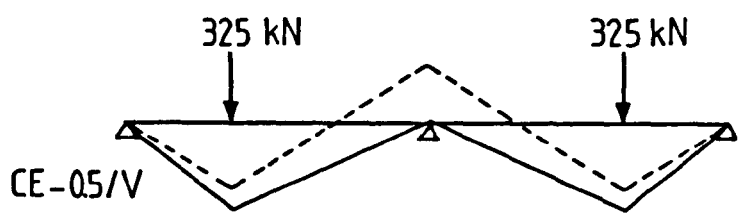
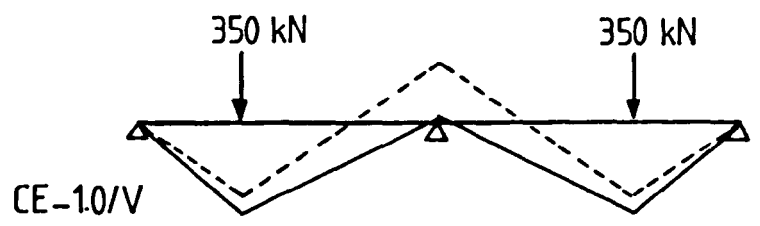


scale: 10mm → 45kN.m

Fig.7.6: Bending moment distribution - continuous deep beams -



— Measured  
 - - - Continuous shallow beams  
 - · - single span beams



- 317 -

scale: 10mm → 45kN.m

Fig.7.6: contd. Bending moment distribution - continuous deep beams -

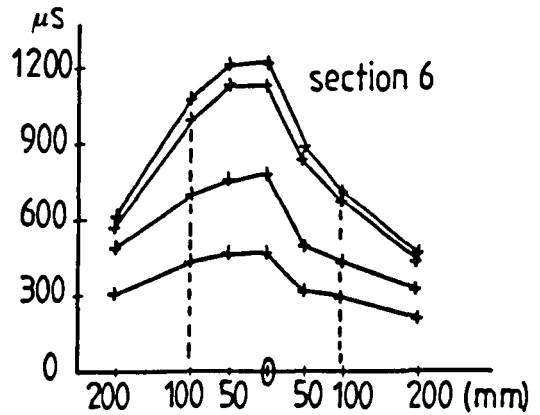
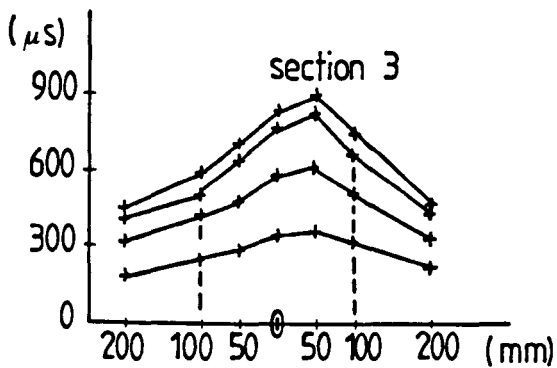
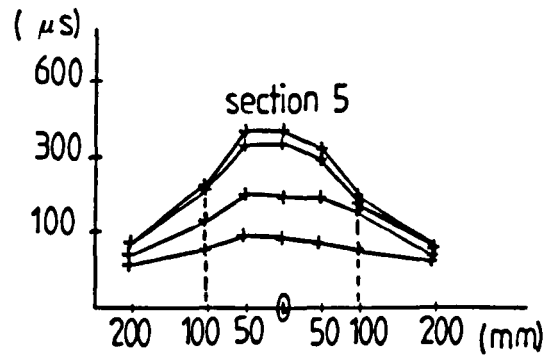
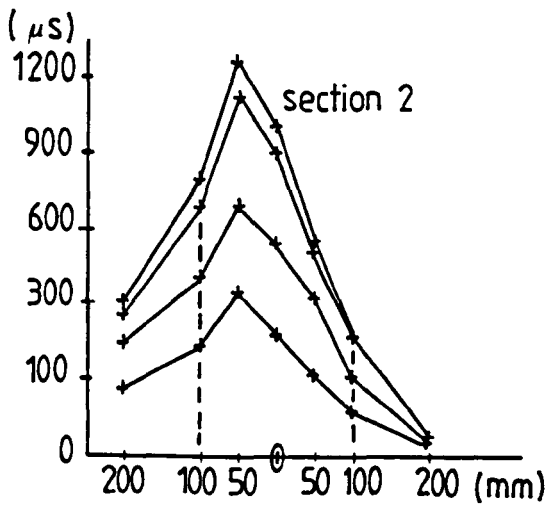
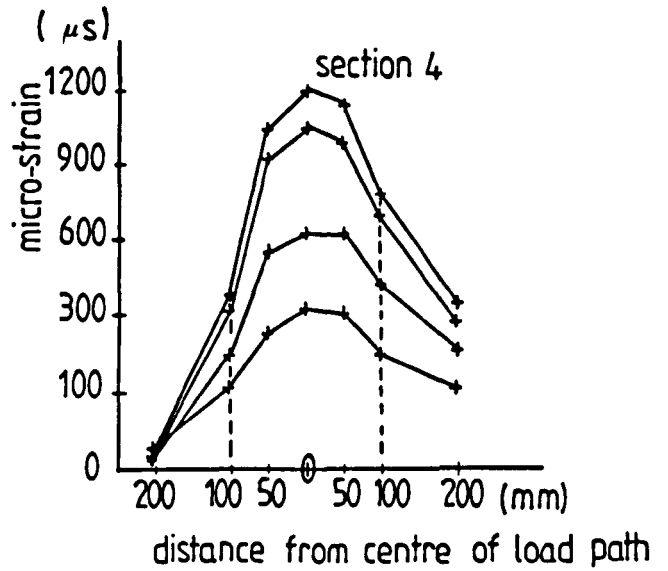
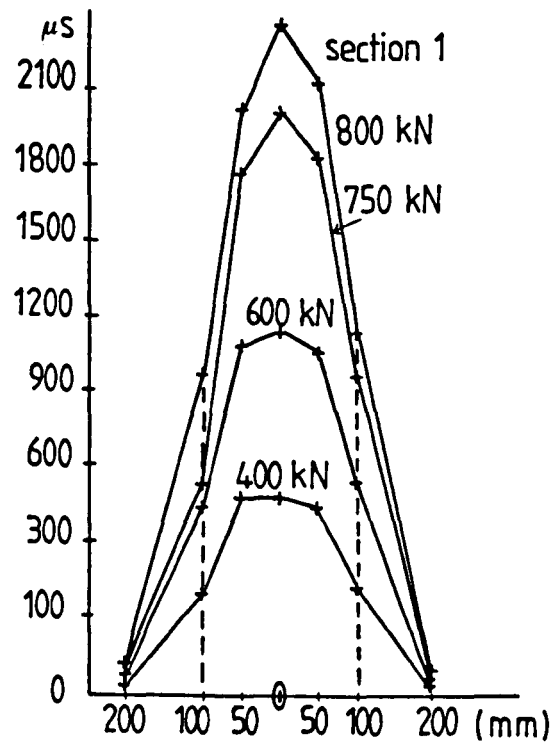


Fig.7.7: Typical compressive strain distribution at sections perpendicular to the load path - beam CD-1.0/1 -

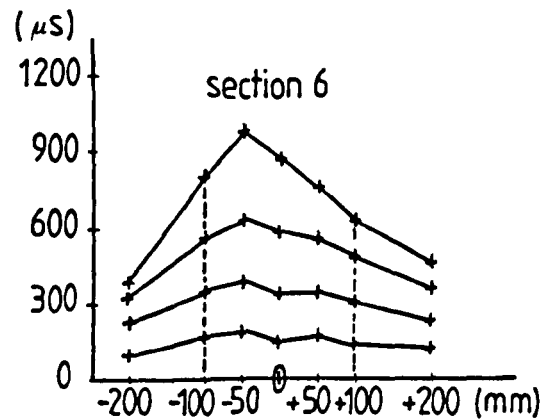
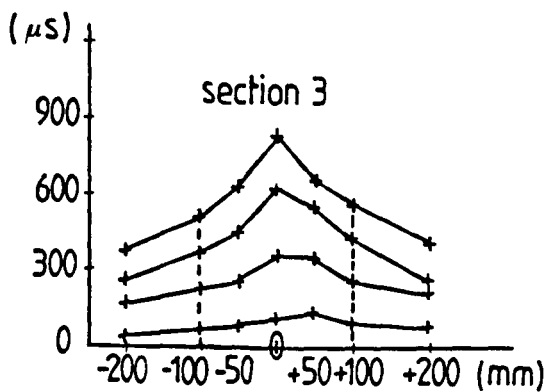
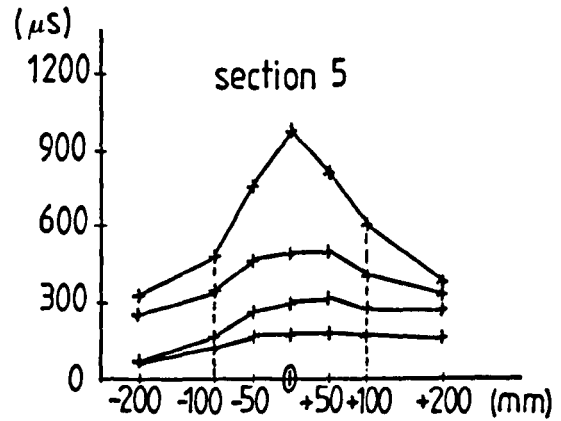
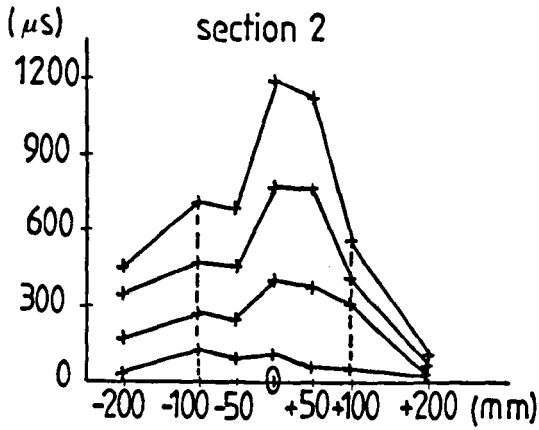
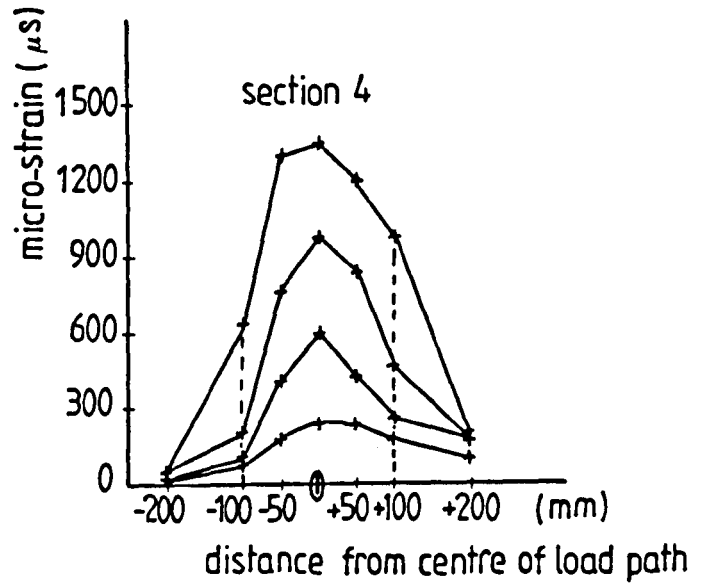
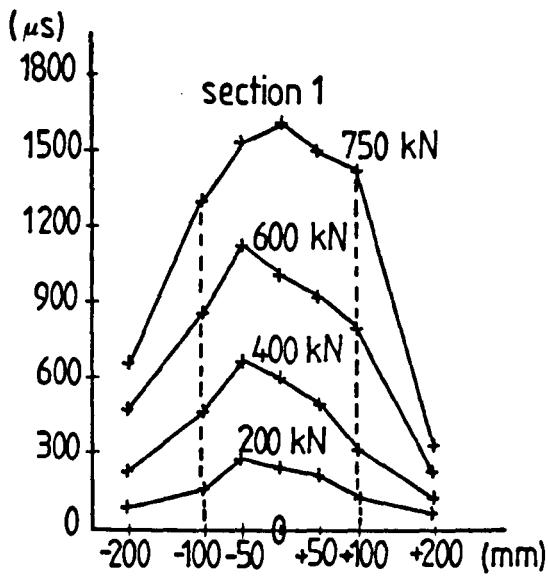
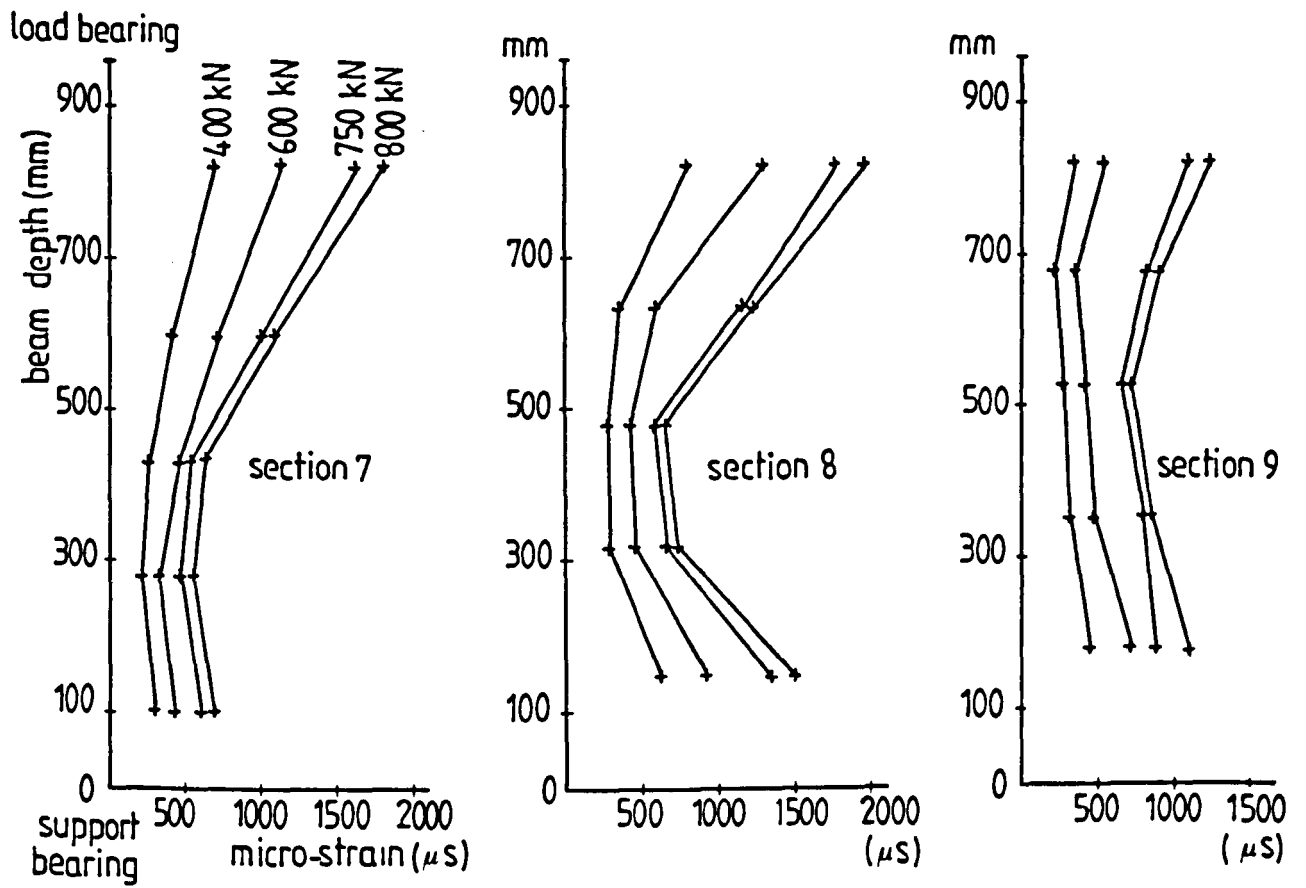
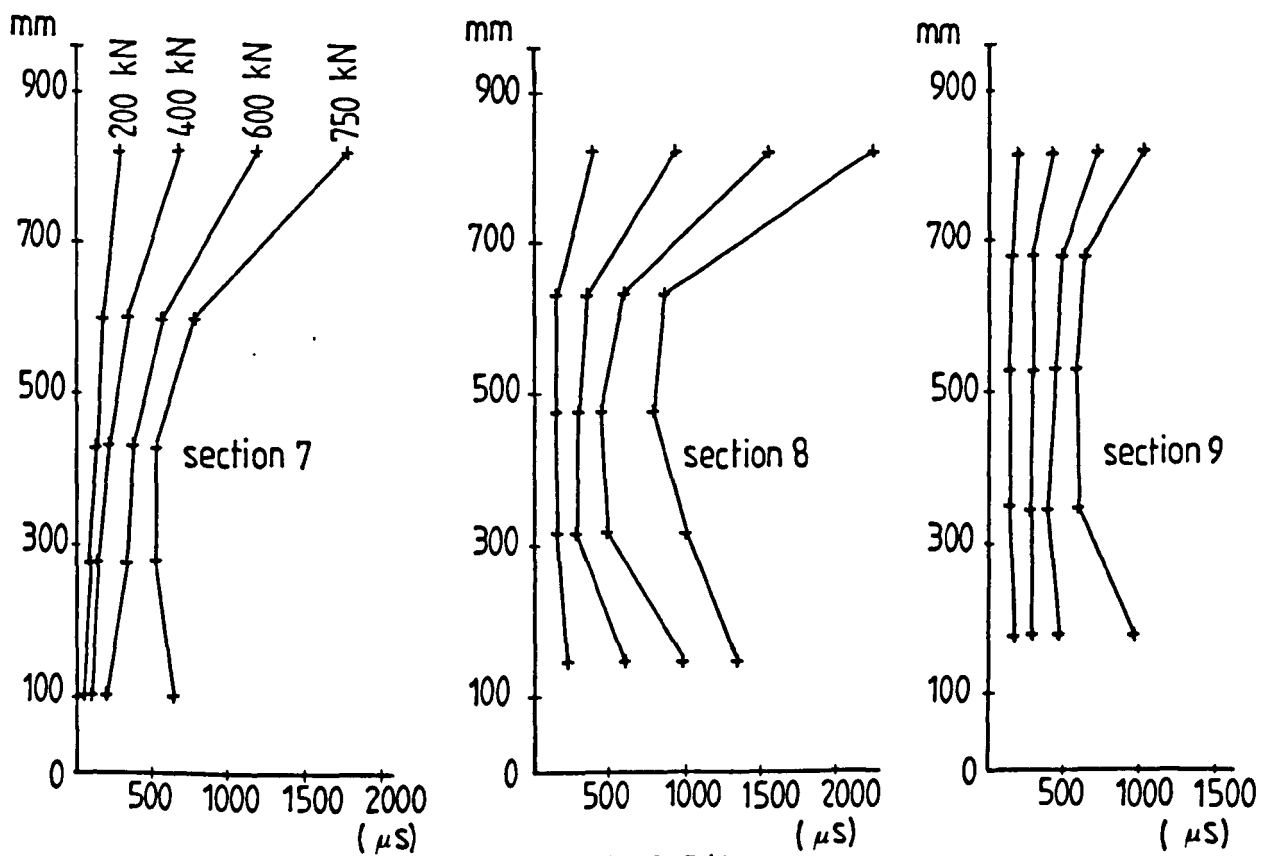


Fig.7.7: contd. Compressive strain distribution at sections perpendicular to the load path - beam CD-0.5/1 -



beam CD-1.0/I



b) beam CD-0.5/I

Fig.7.8: Typical compressive strain distribution along the load path

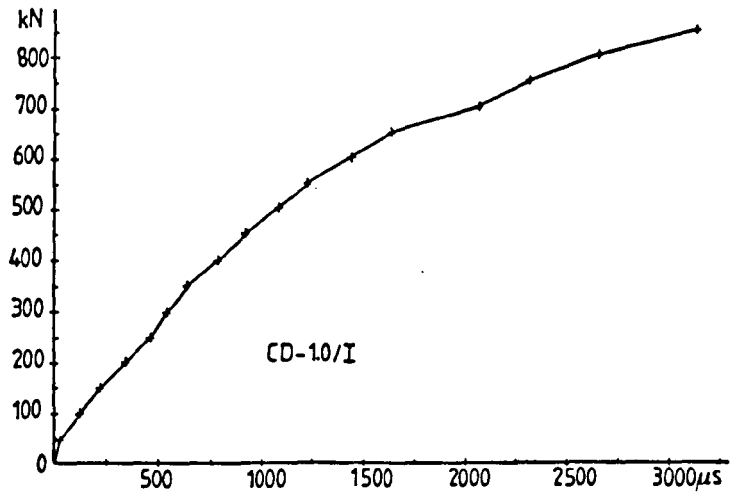
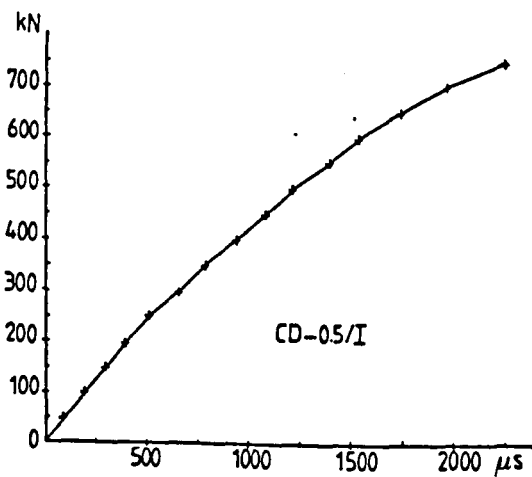
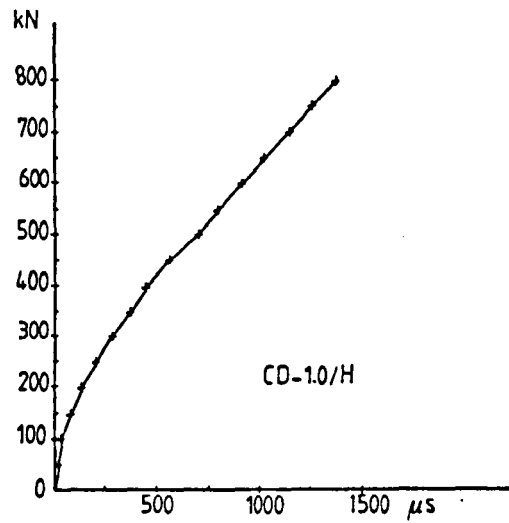
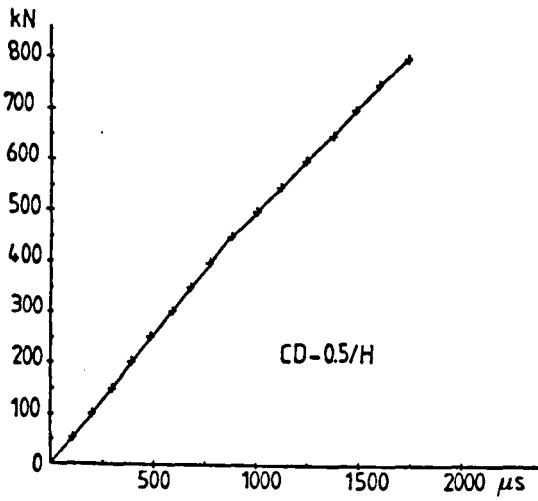
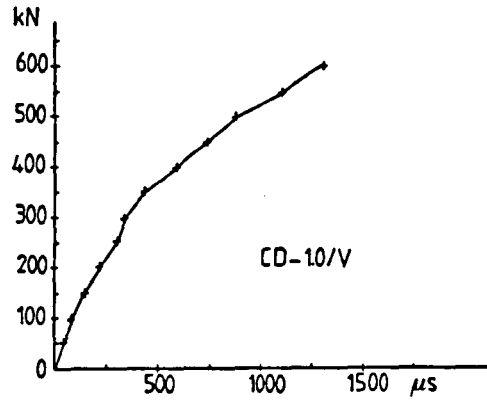
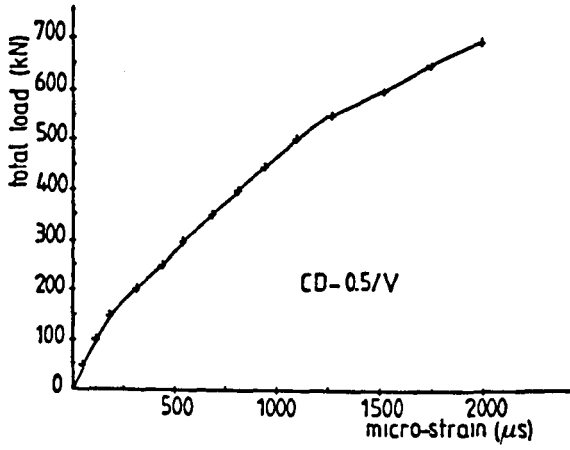


Fig.7.9: Load against maximum compressive strain within the load path

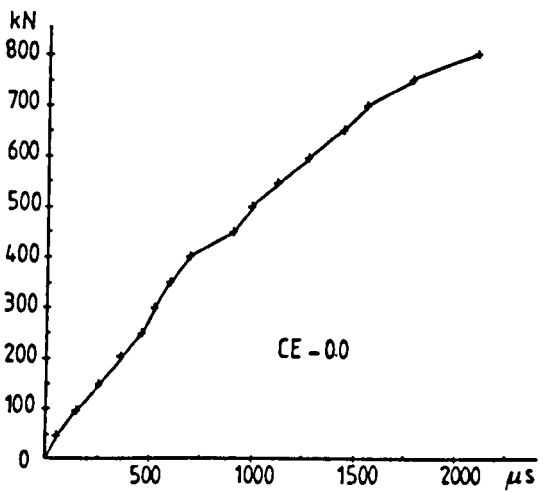
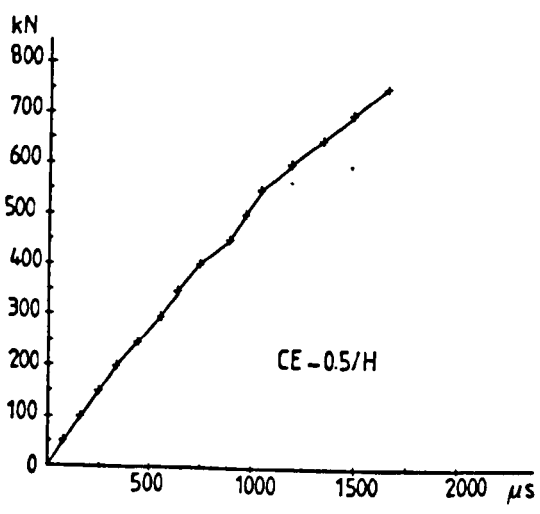
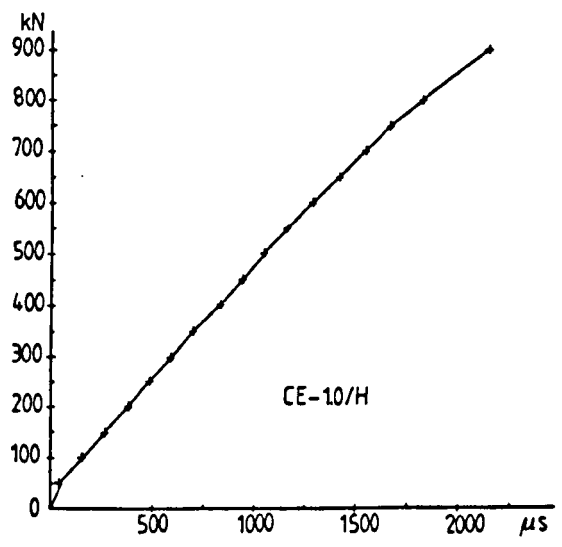
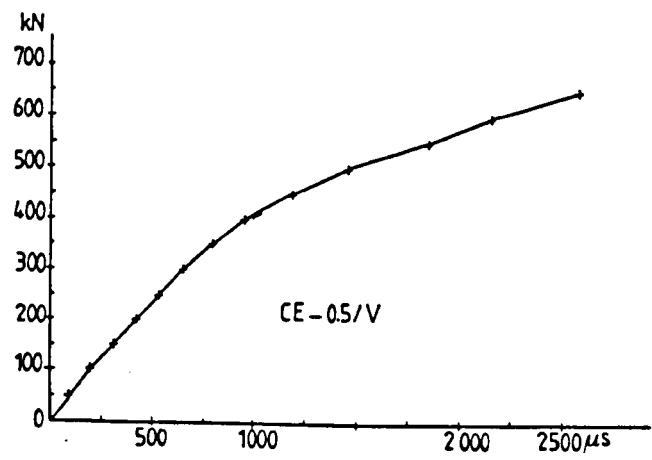
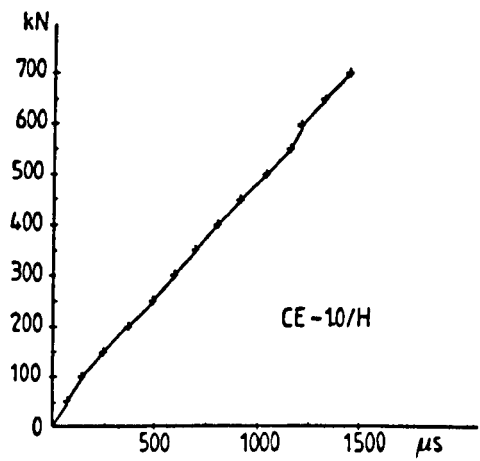
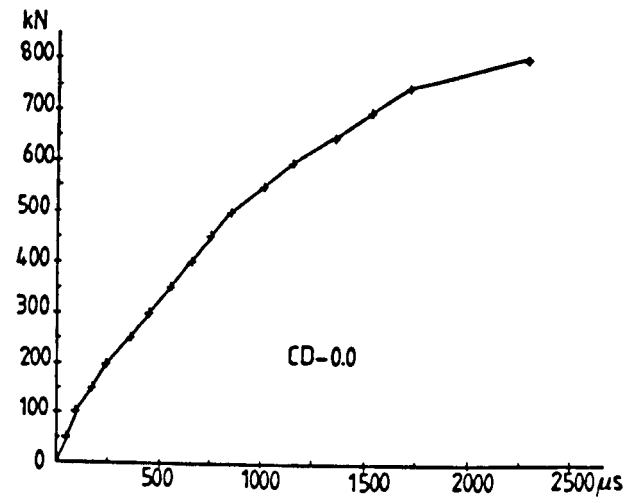


Fig.7.9: contd. Load against maximum compressive strain within the load path

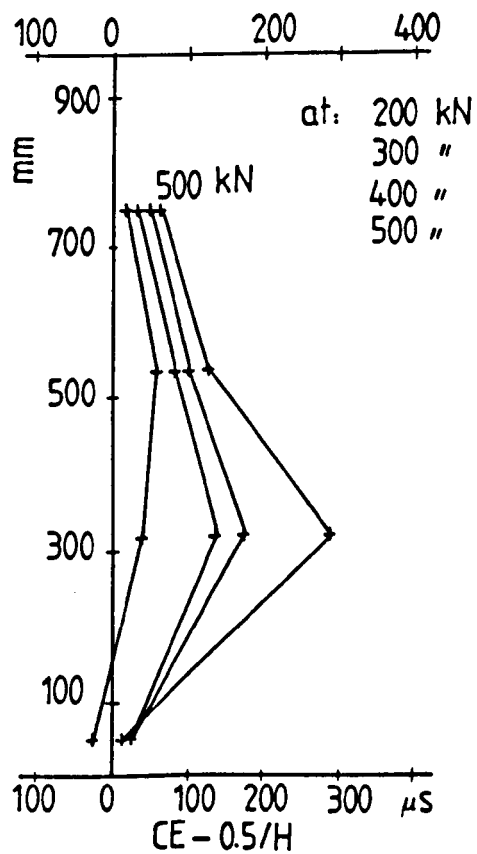
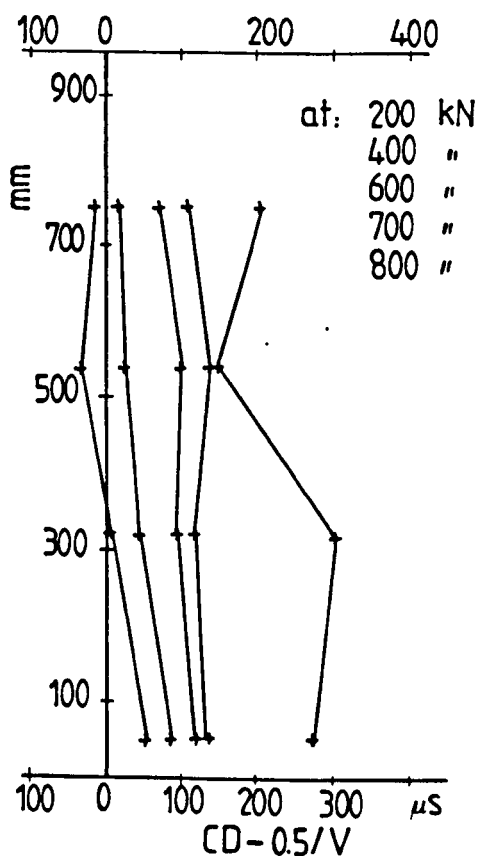
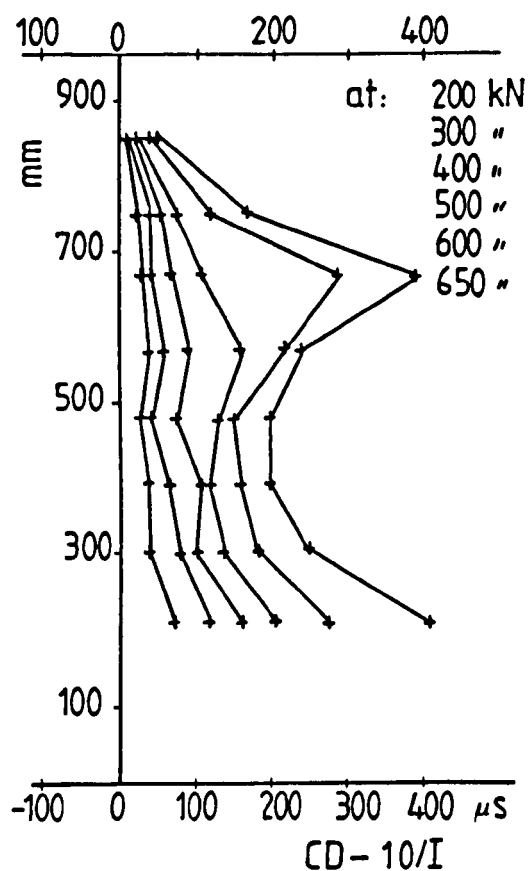
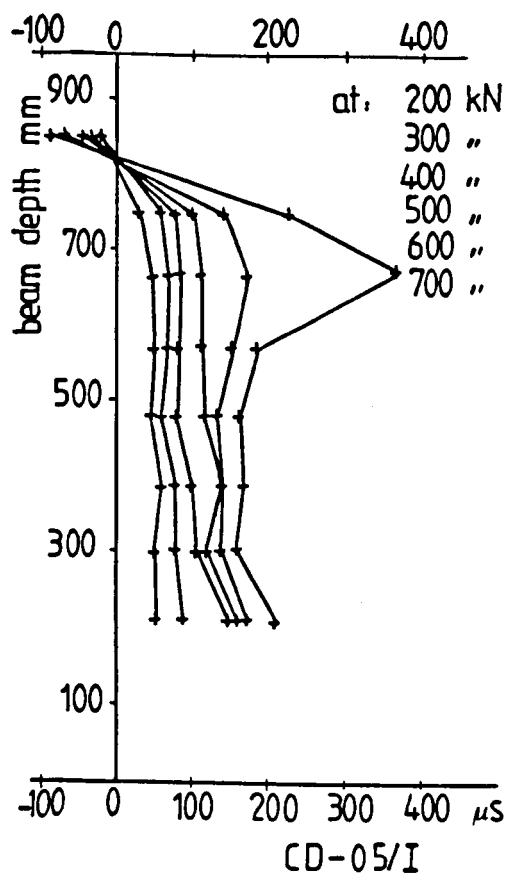
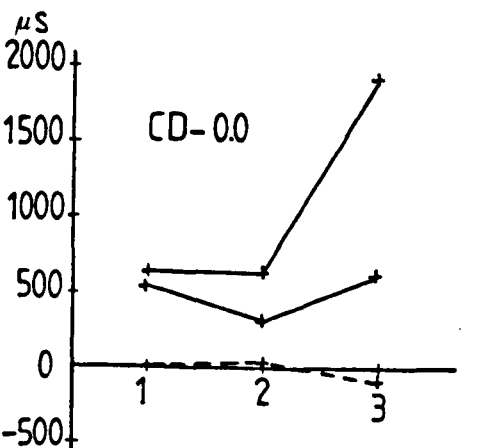
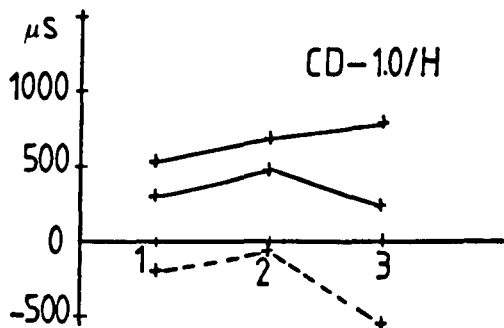
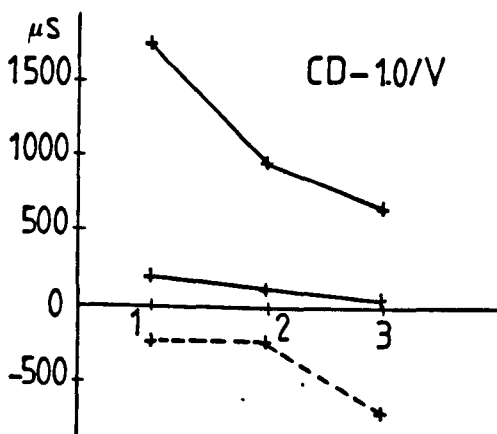
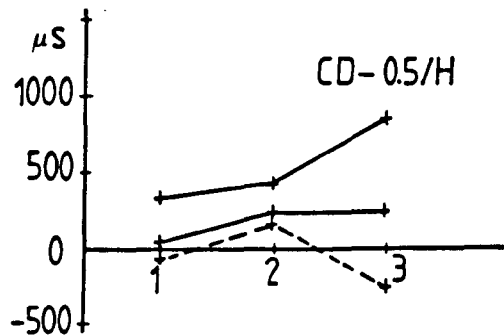
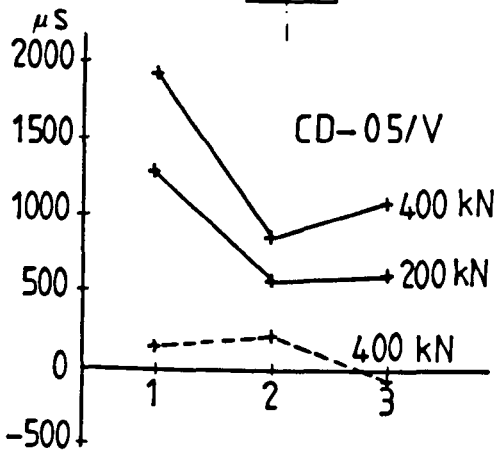
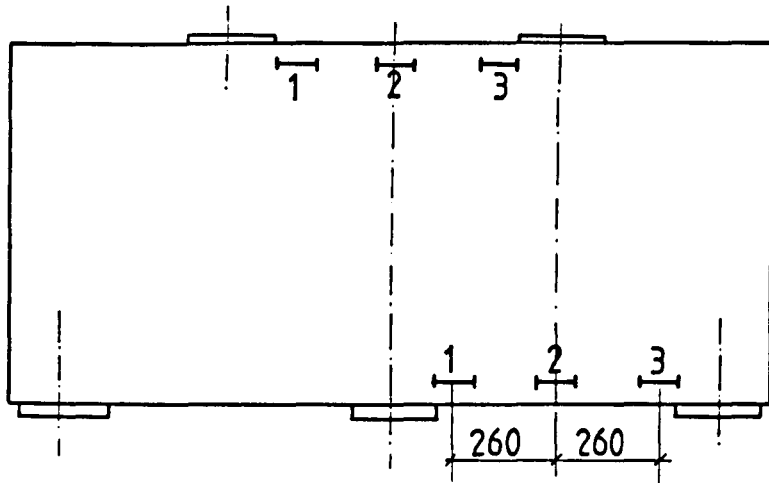


Fig.7.10: Typical tensile strain distribution within the load path before diagonal cracking



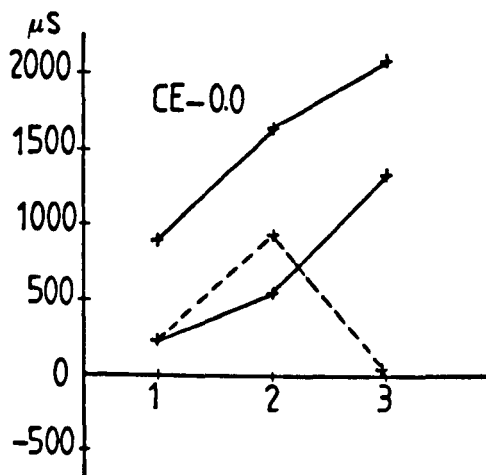
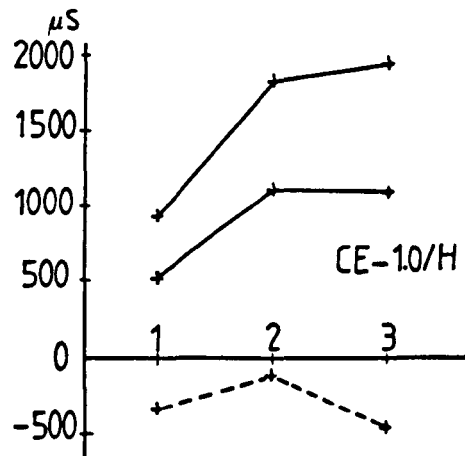
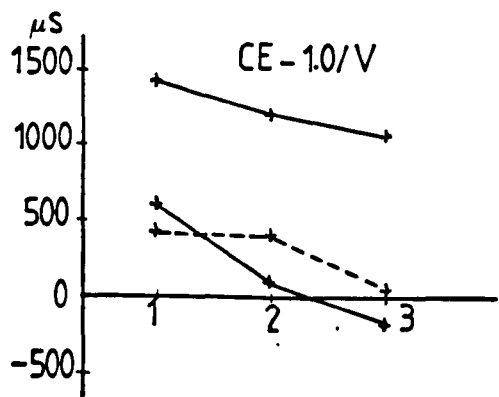
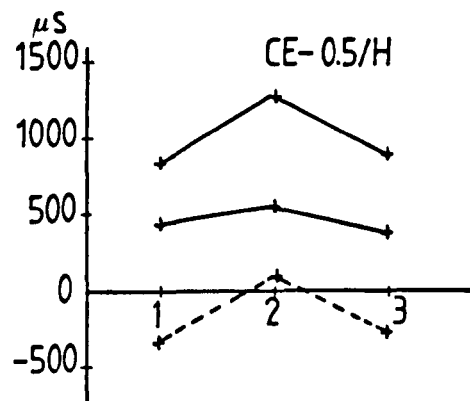
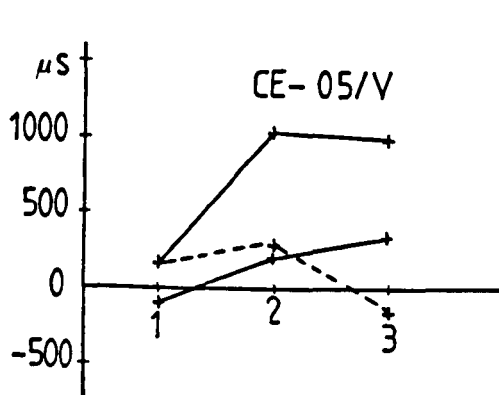
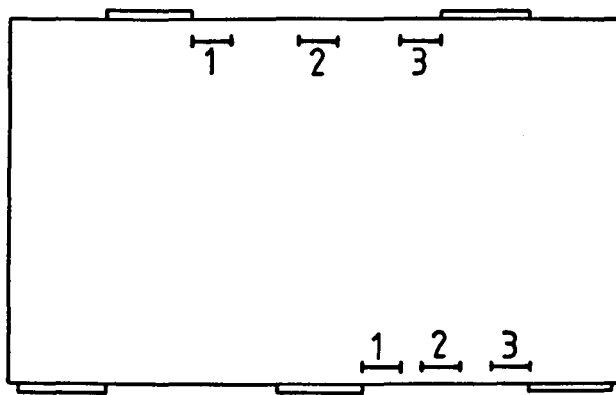
+: tension    -: compression

— : strains at bottom at 200 and 400 kN

- - - : strains at top at 400 kN

series CD beams

Fig.7.11: Strains along the longitudinal reinforcement at bottom and top



+: tension -: compression

—: strains at 400 kN and at or near ultimate at bottom

- - - -: strains at 400 kN at top

series CE beams

Fig.7.11: contd. Strains along the longitudinal reinforcement at bottom and top

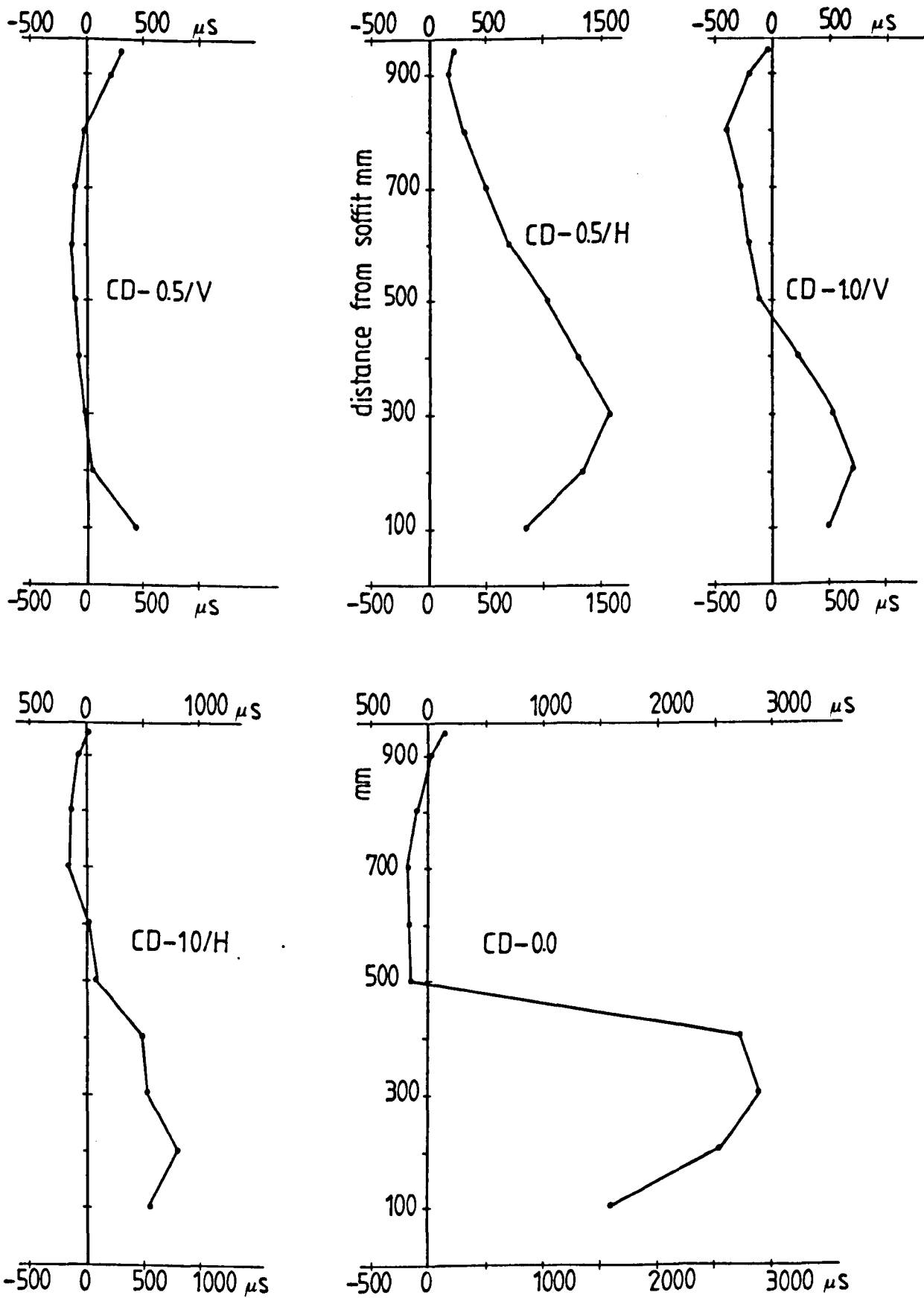


Fig.7.12: Longitudinal strain distribution above interior support at 400 kN - series CD beams -

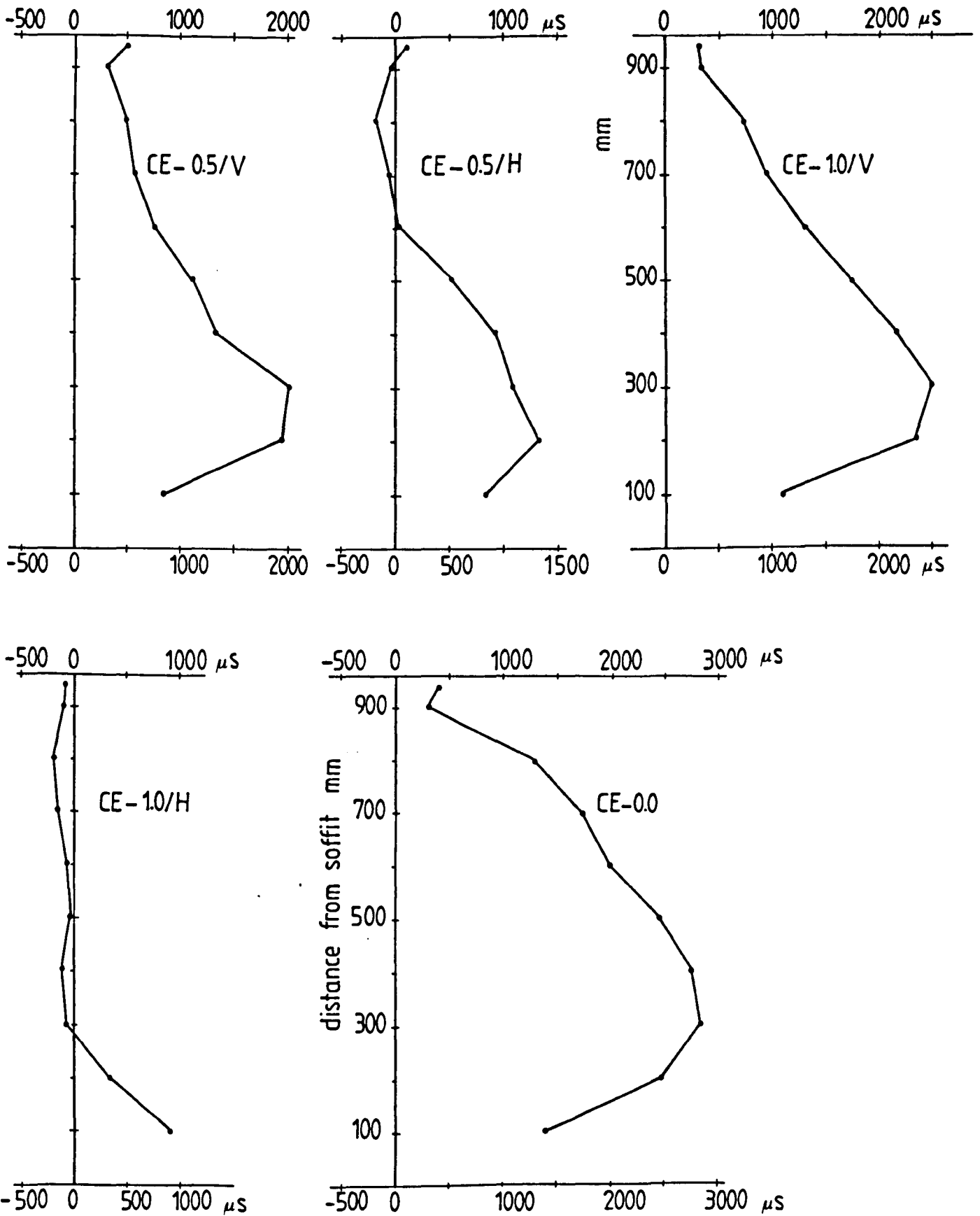
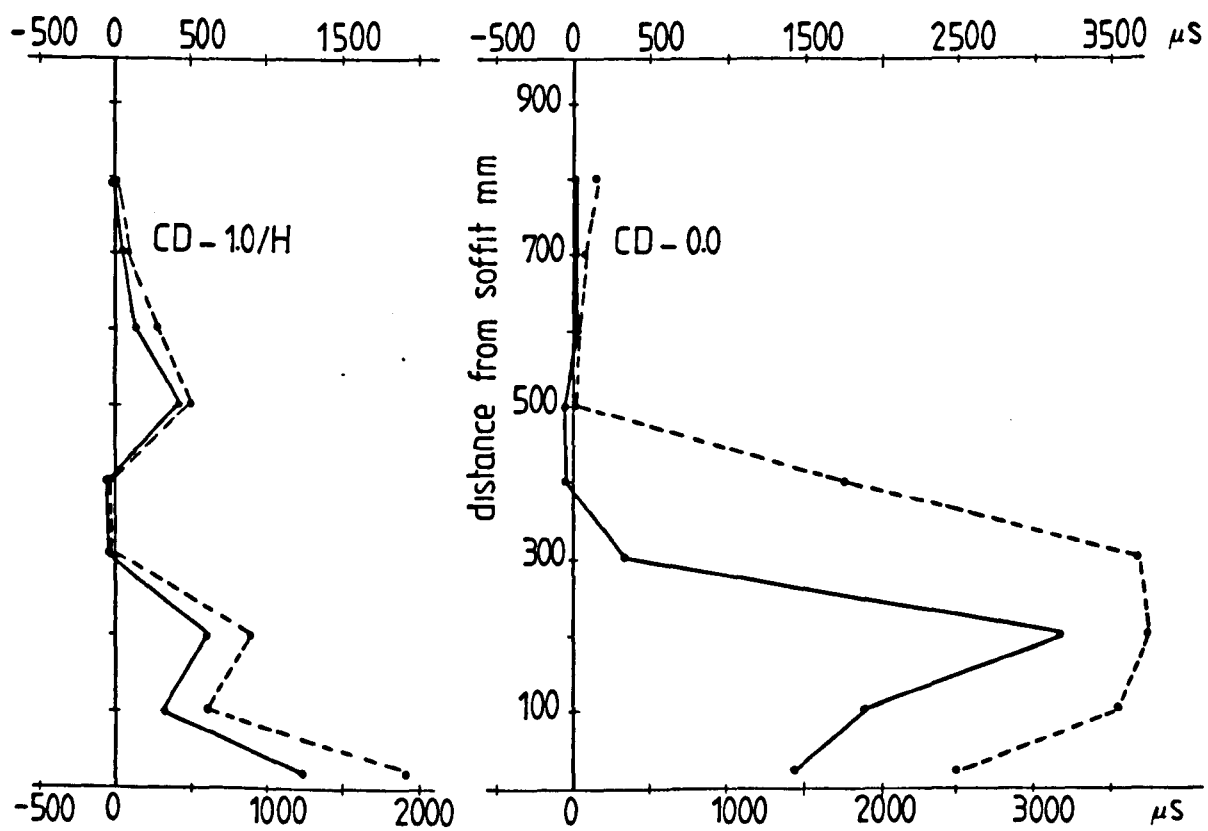
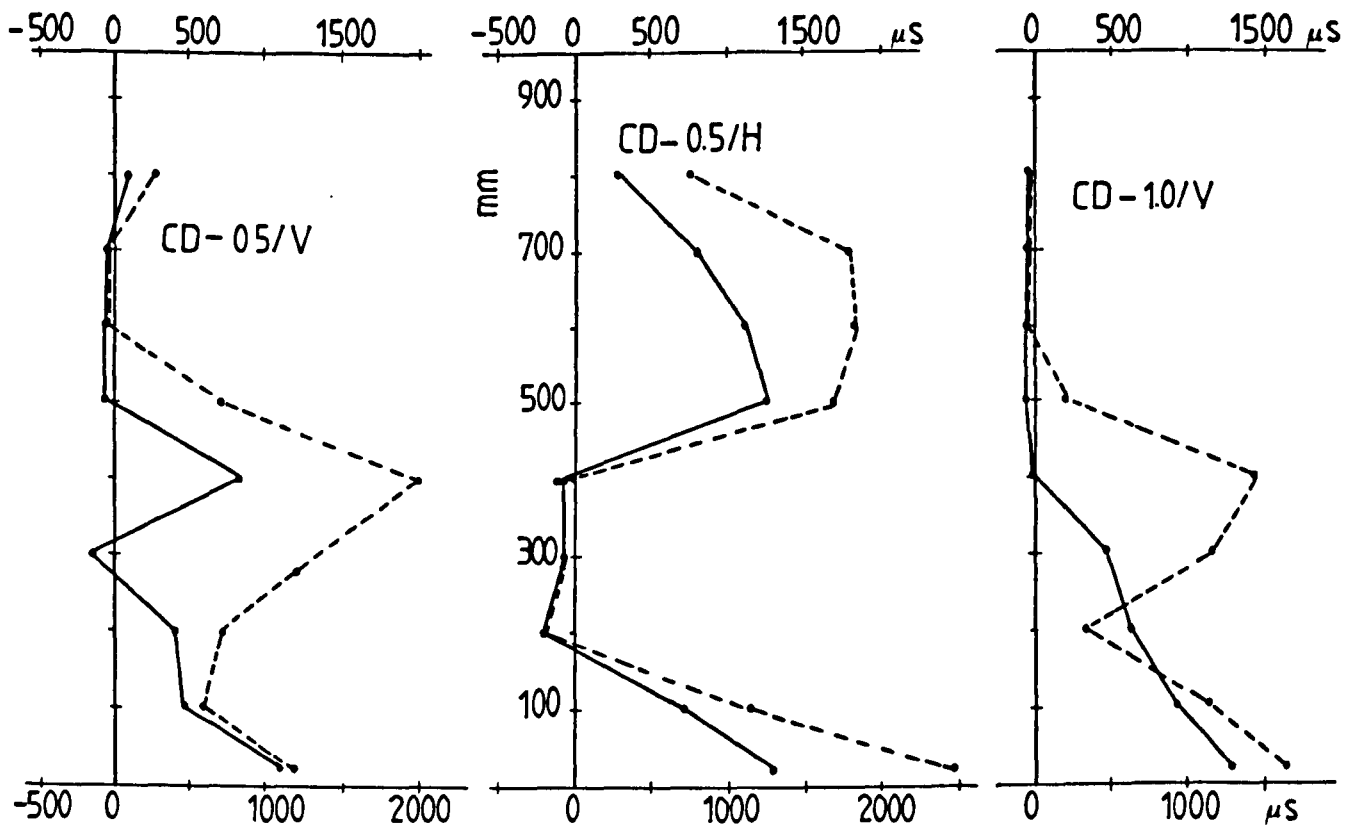
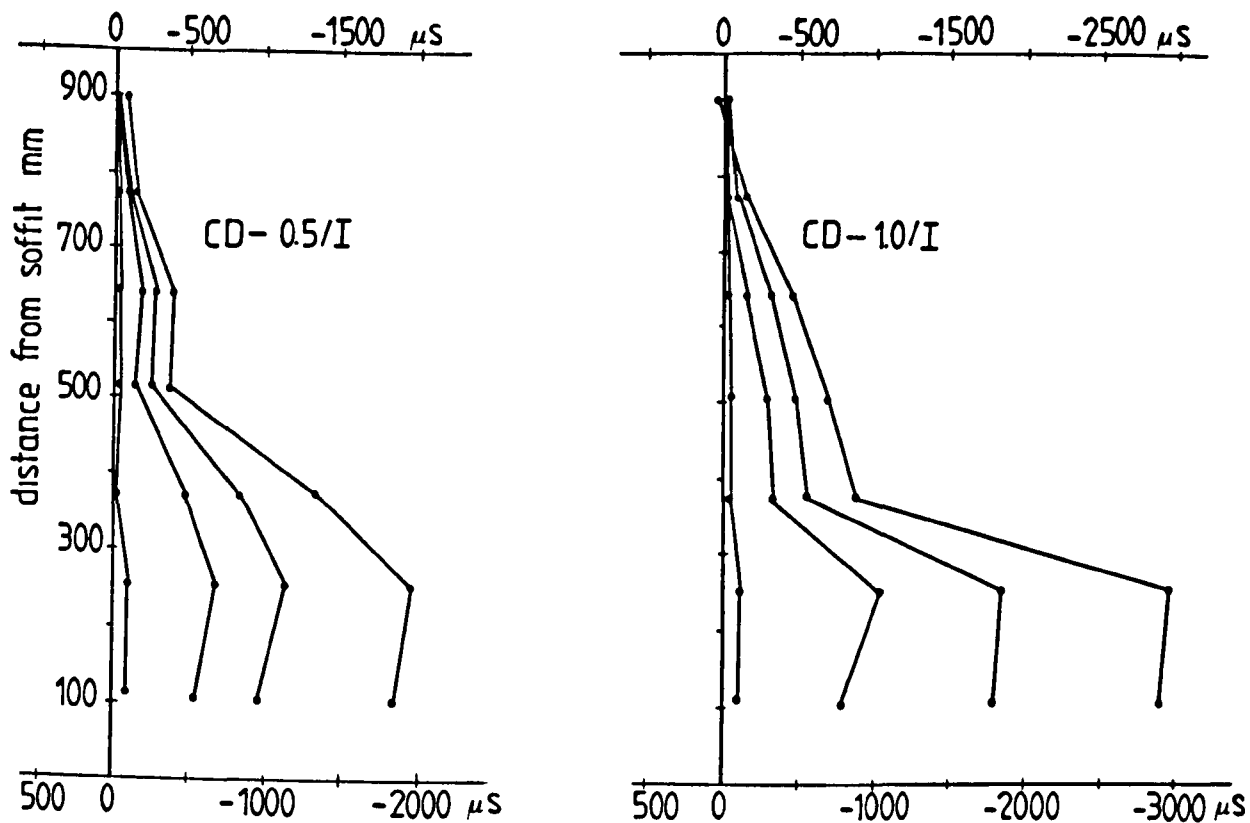


Fig.7.12: contd. Longitudinal strain distribution above interior support at 400 kN - series CE beams -



— at 400 kN  
 - - - at or near ultimate

Fig.7.13: Longitudinal strain distribution at mid-span sections



+ tension - compression

Fig.7.14: Typical vertical strain distribution above interior support

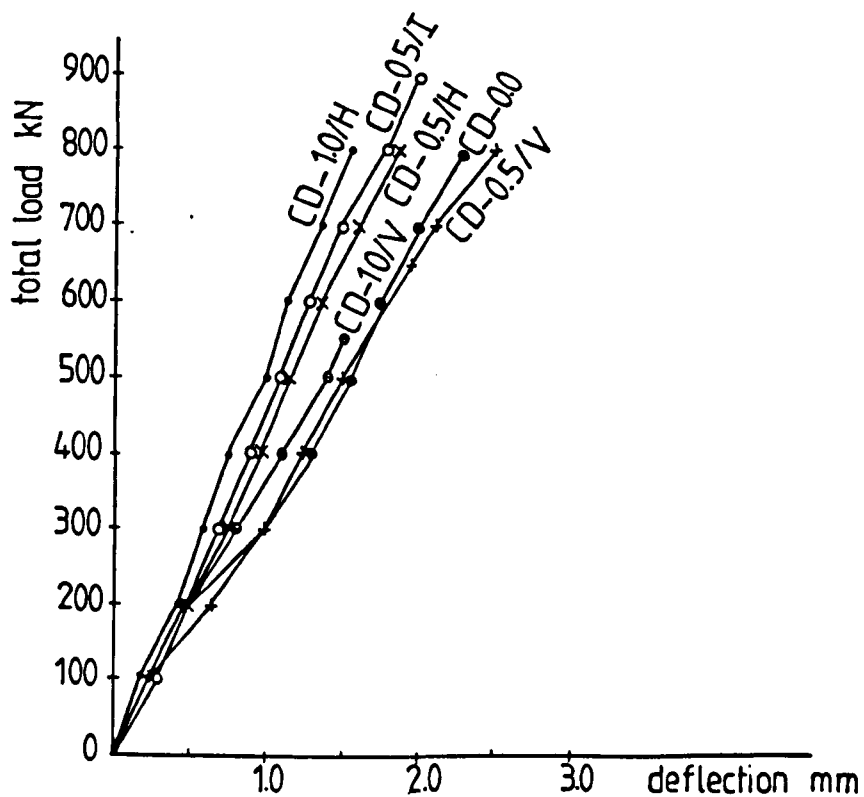


Fig.7.16: Load against deflection curves for continuous deep beams  
- series CD beams -

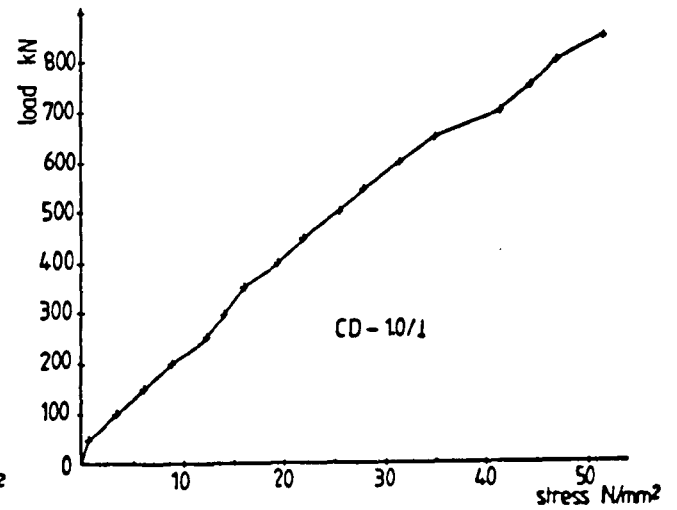
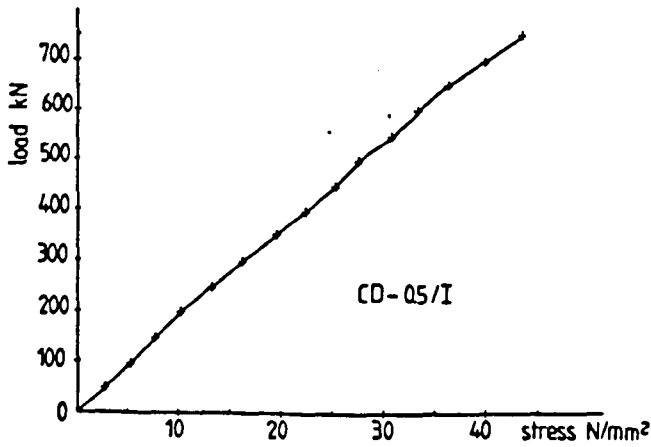
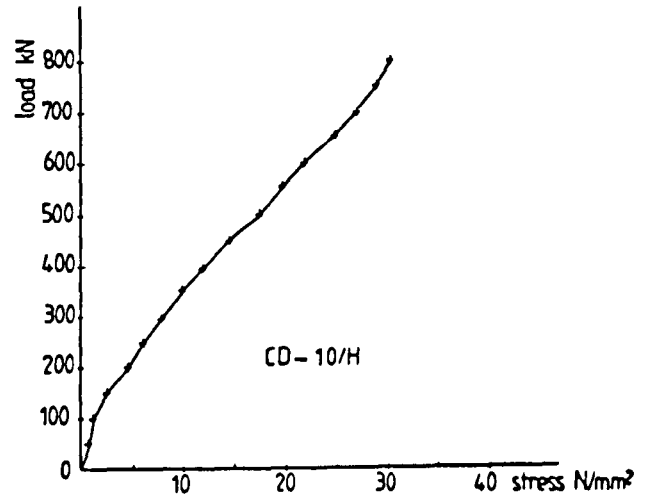
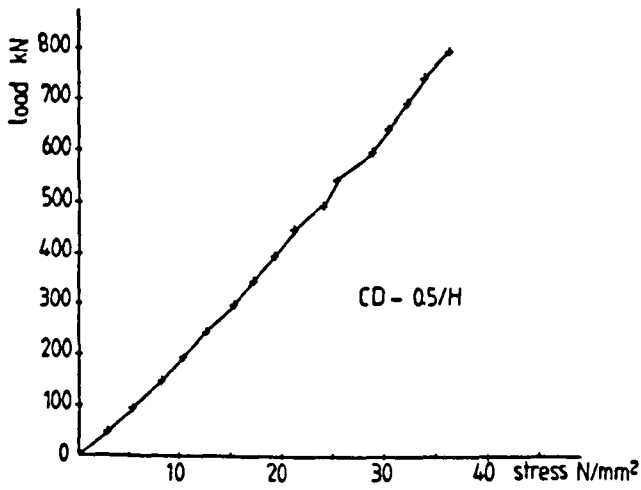
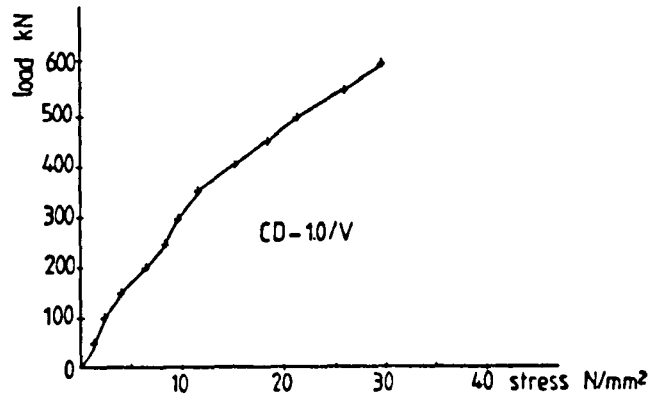
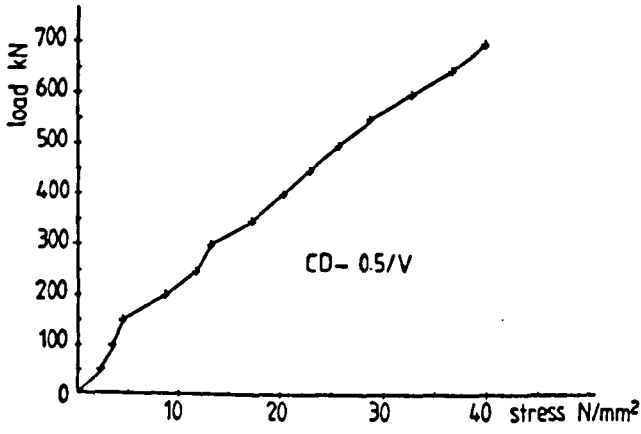


Fig.7.15: Load against maximum compressive stress within the load path

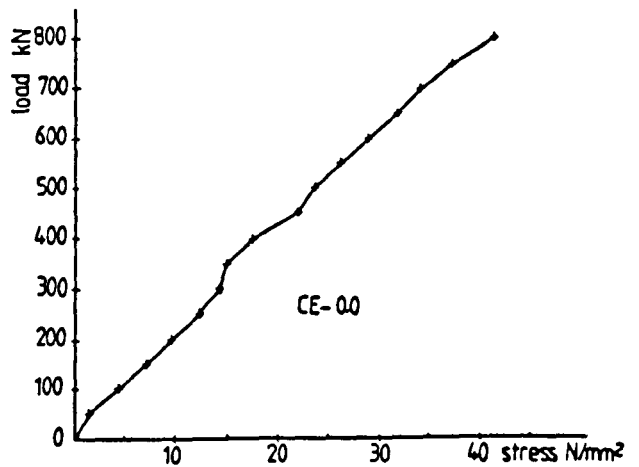
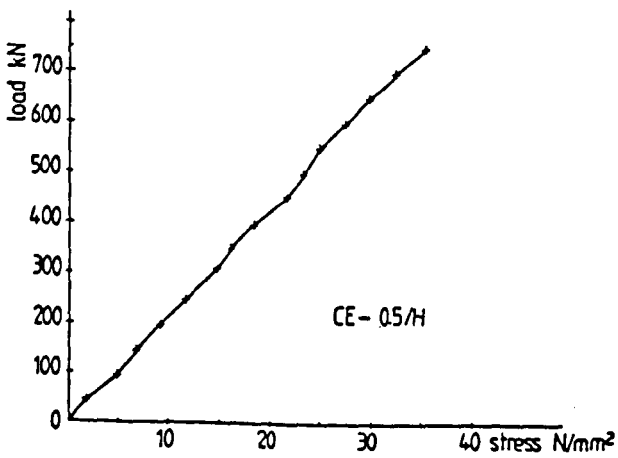
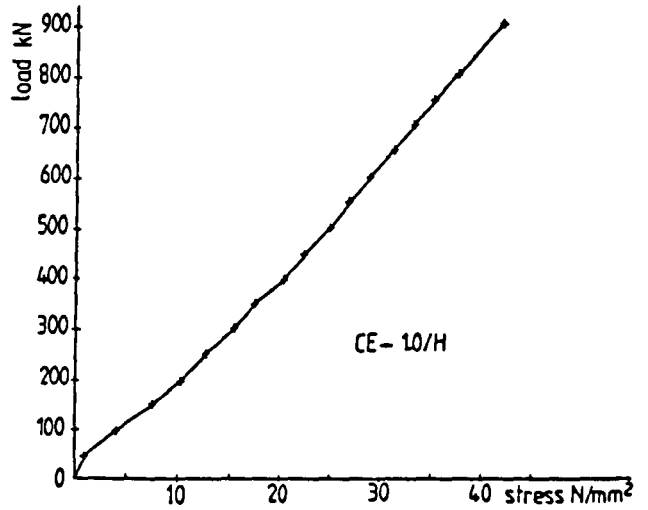
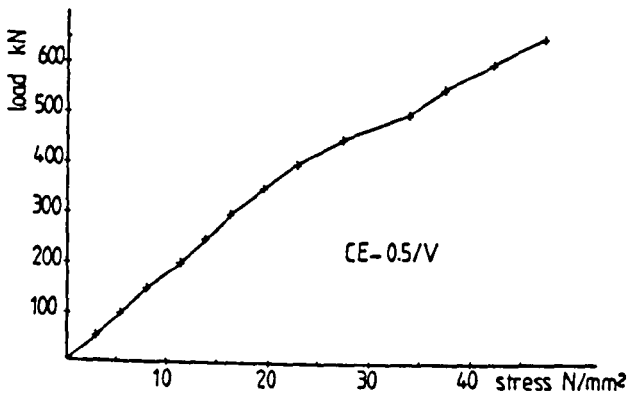
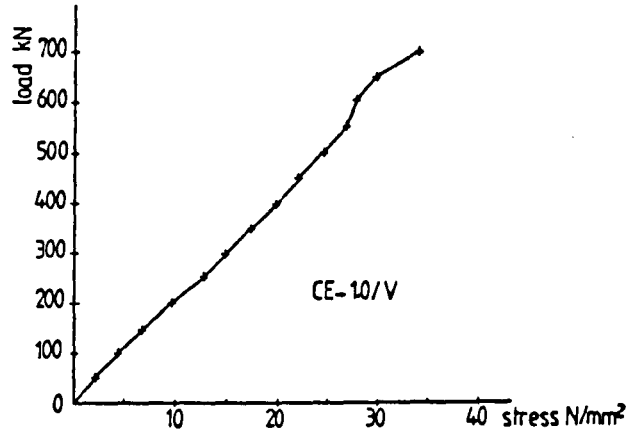
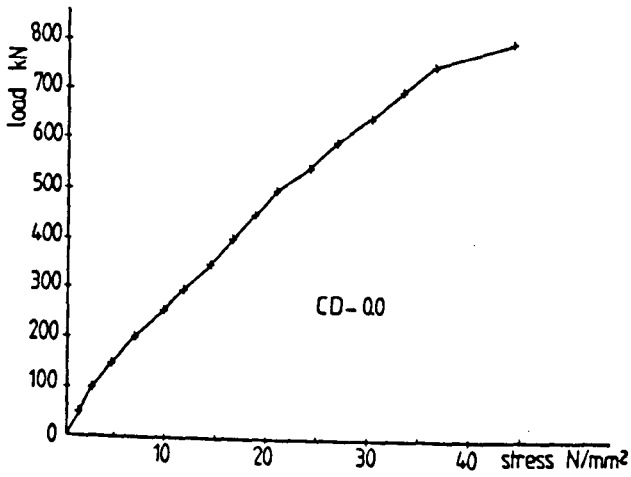


Fig.7.15: contd. Load against maximum compressive stress within the load path

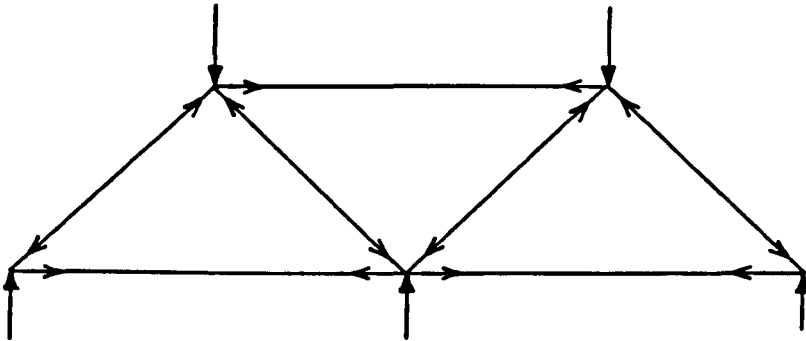


Fig.8.1: Flow of forces in moderately deep continuous beams of Rogowsky et al [96] [97] ( $2 < l/h < 5$ )

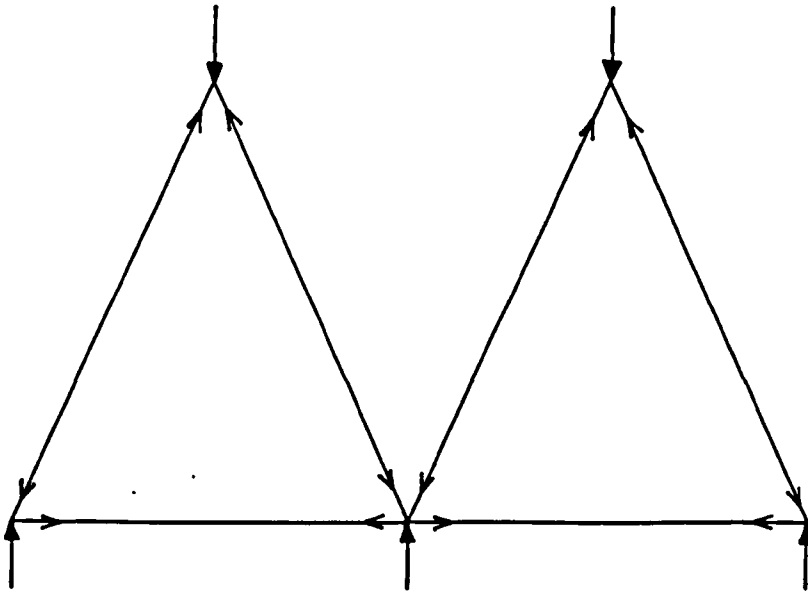


Fig.8.2: Flow of forces in the author's beams ( $L/h < 1$ )

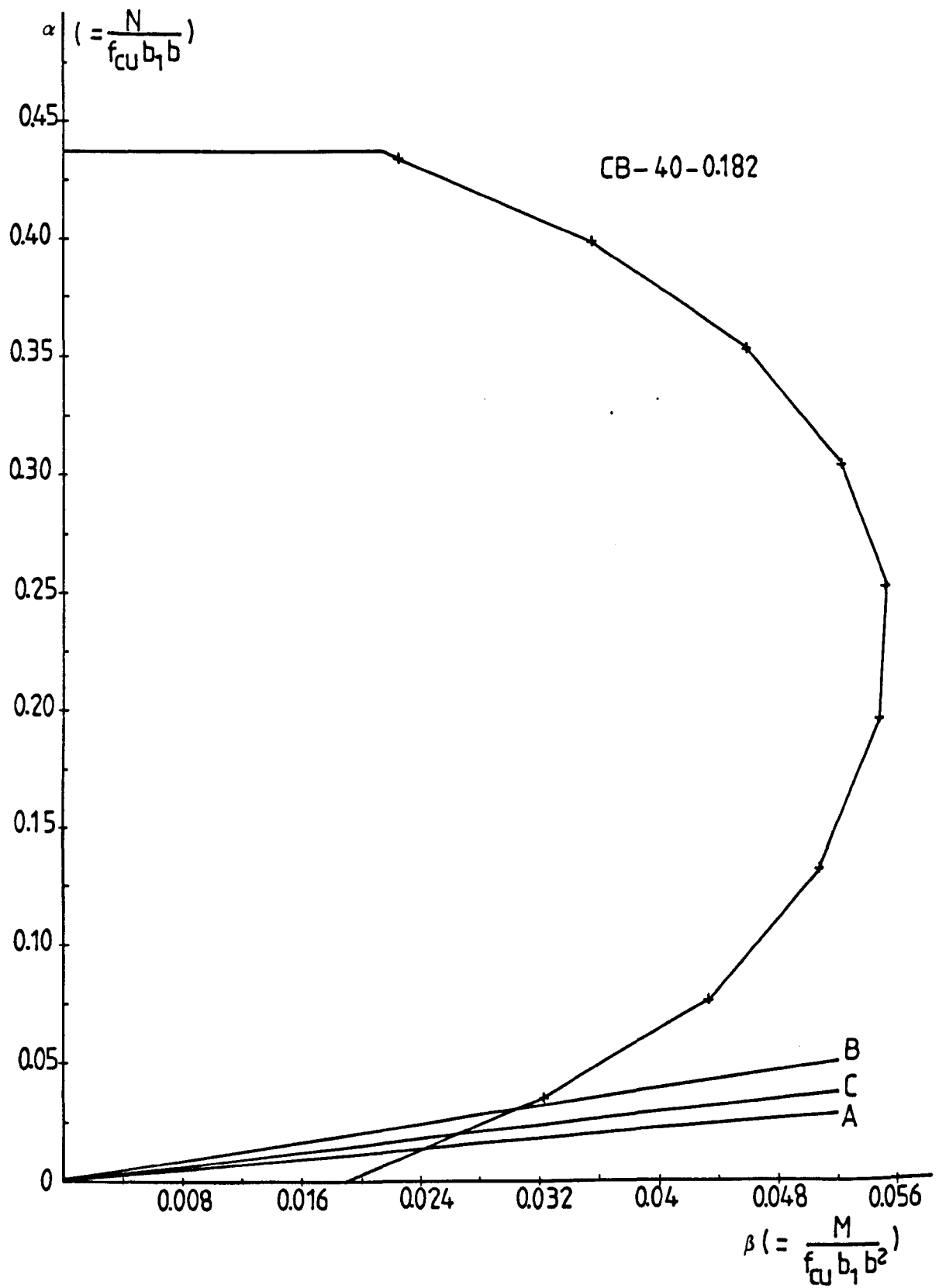


Fig.A.1: Interaction diagram for beam CB-40-0.182

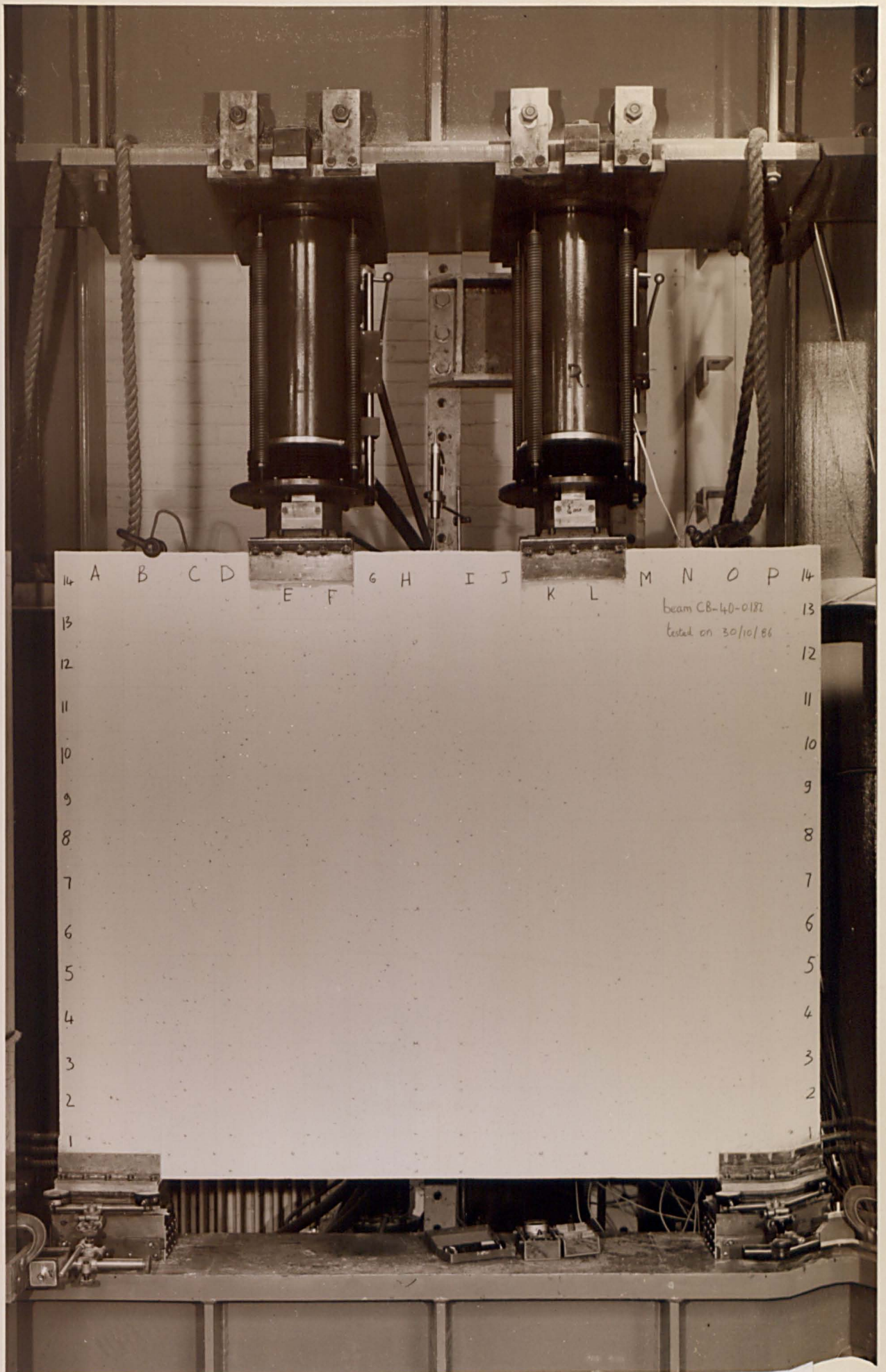


Plate 3.1: Front view of a beam in the testing rig  
 - loading arrangement -

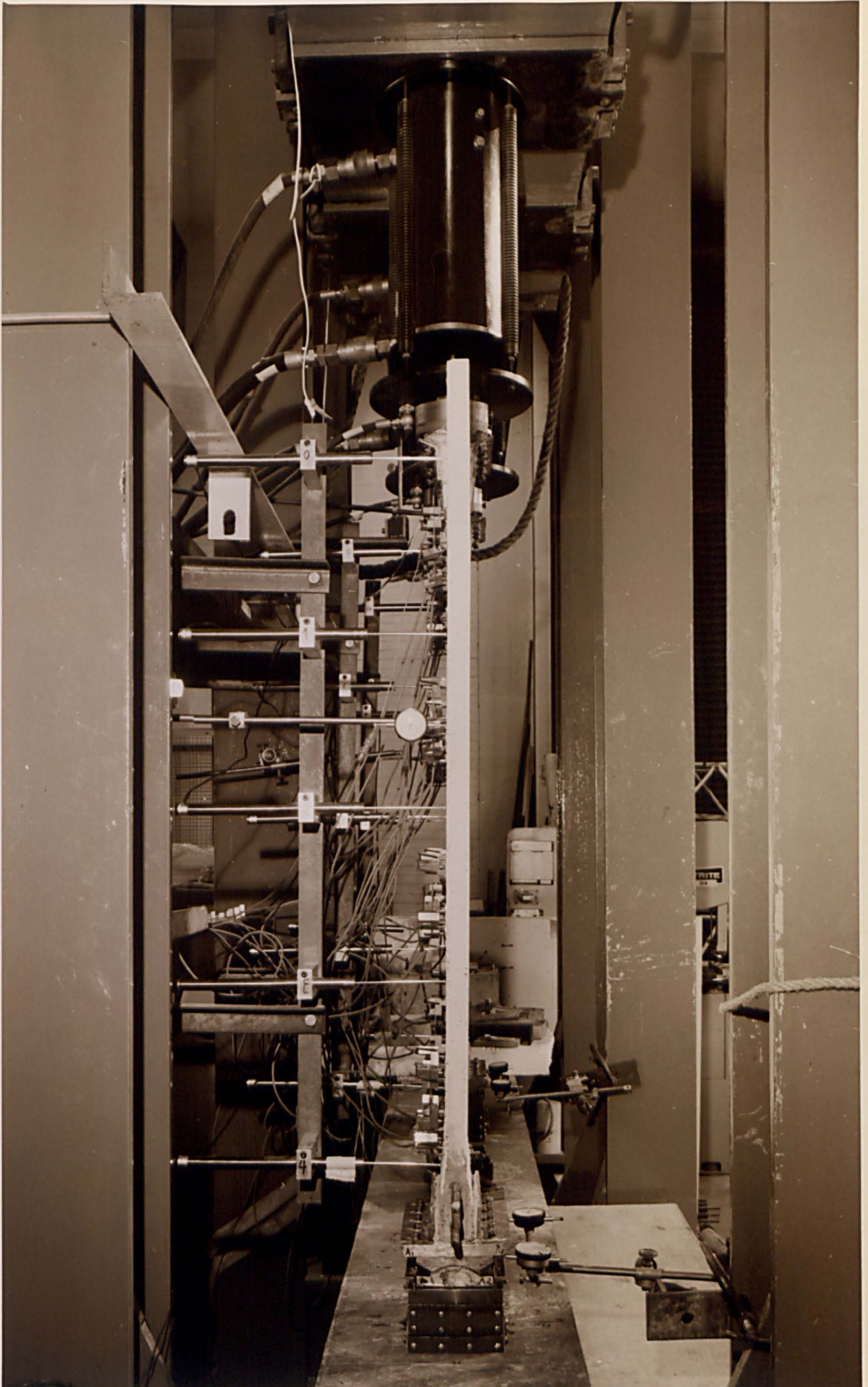


Plate 3.2: Side view of a beam in the testing rig  
- instrumentation on the back -

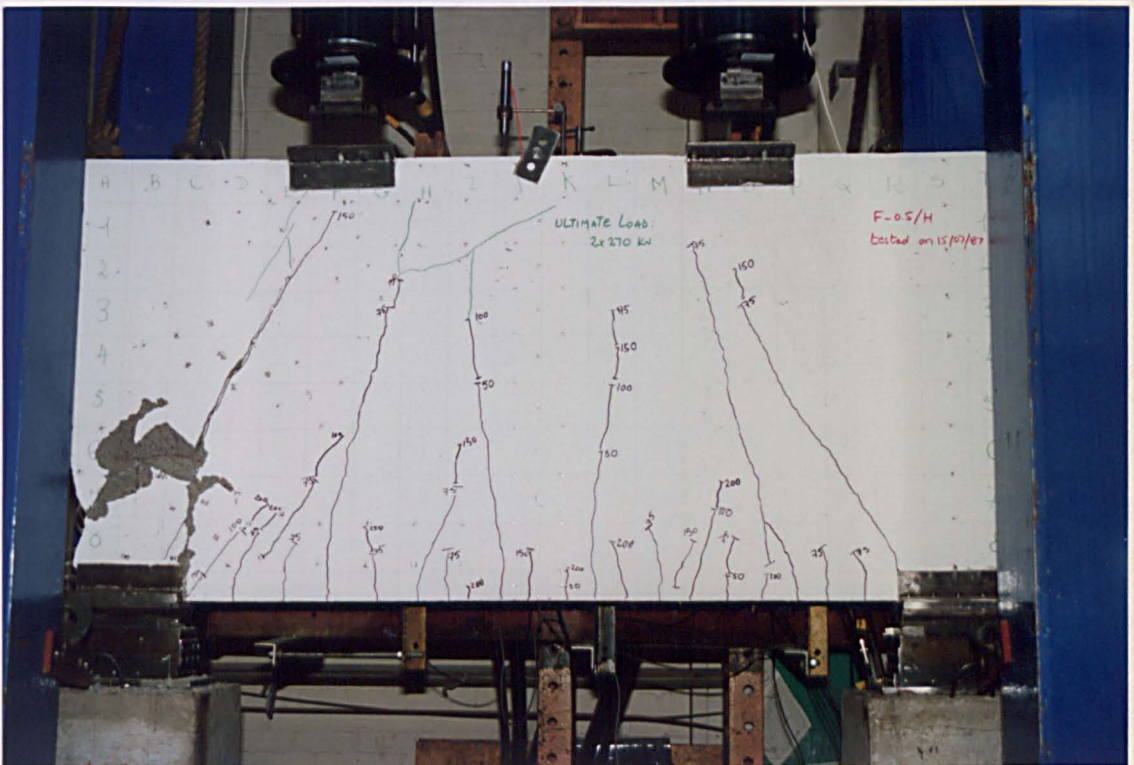
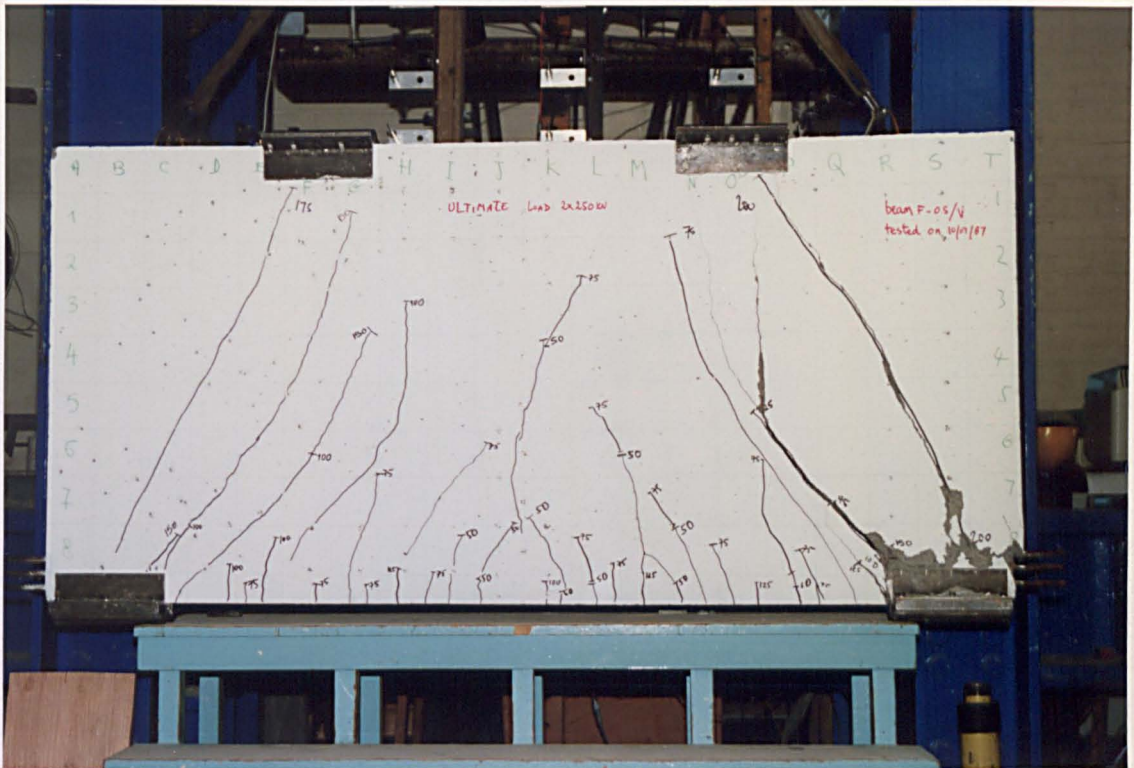
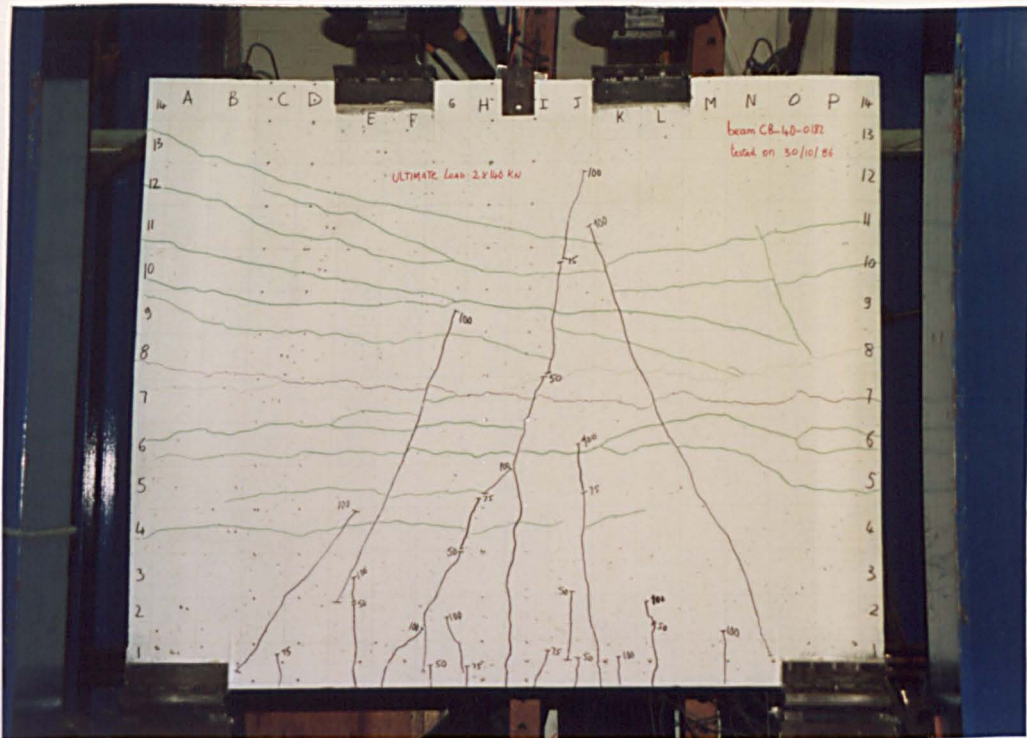
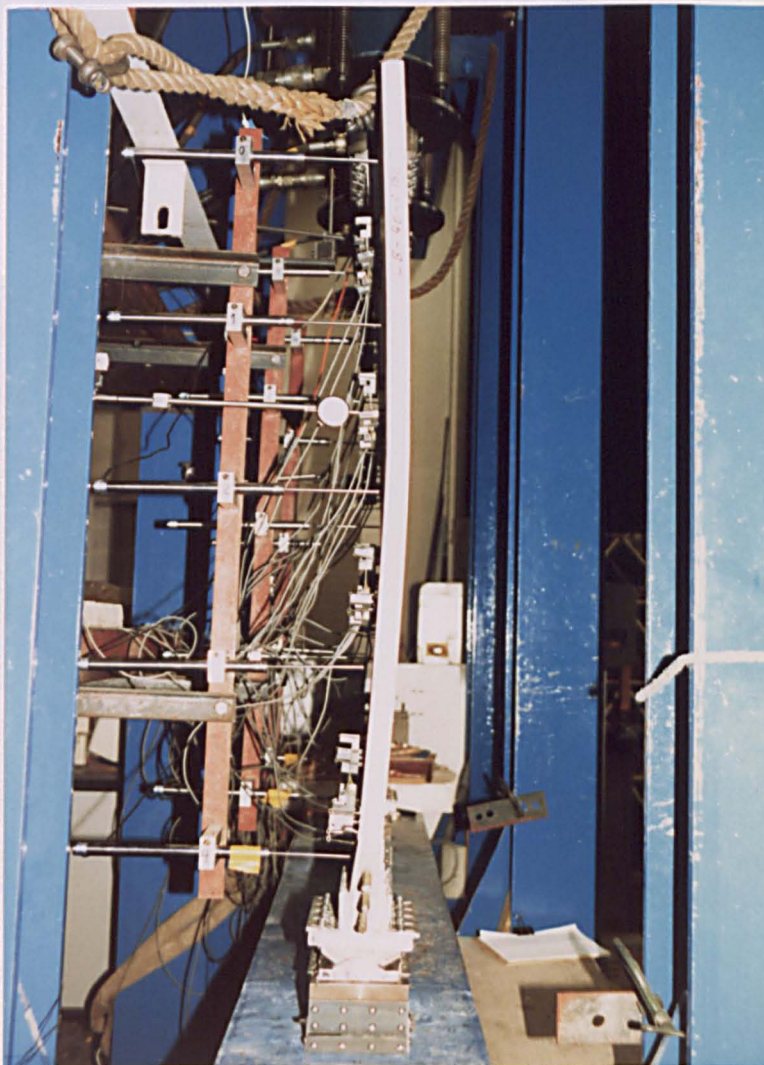


Plate 3.3: Typical shear failure of a deep beam  
 - splitting along a diagonal crack and spalling of concrete -

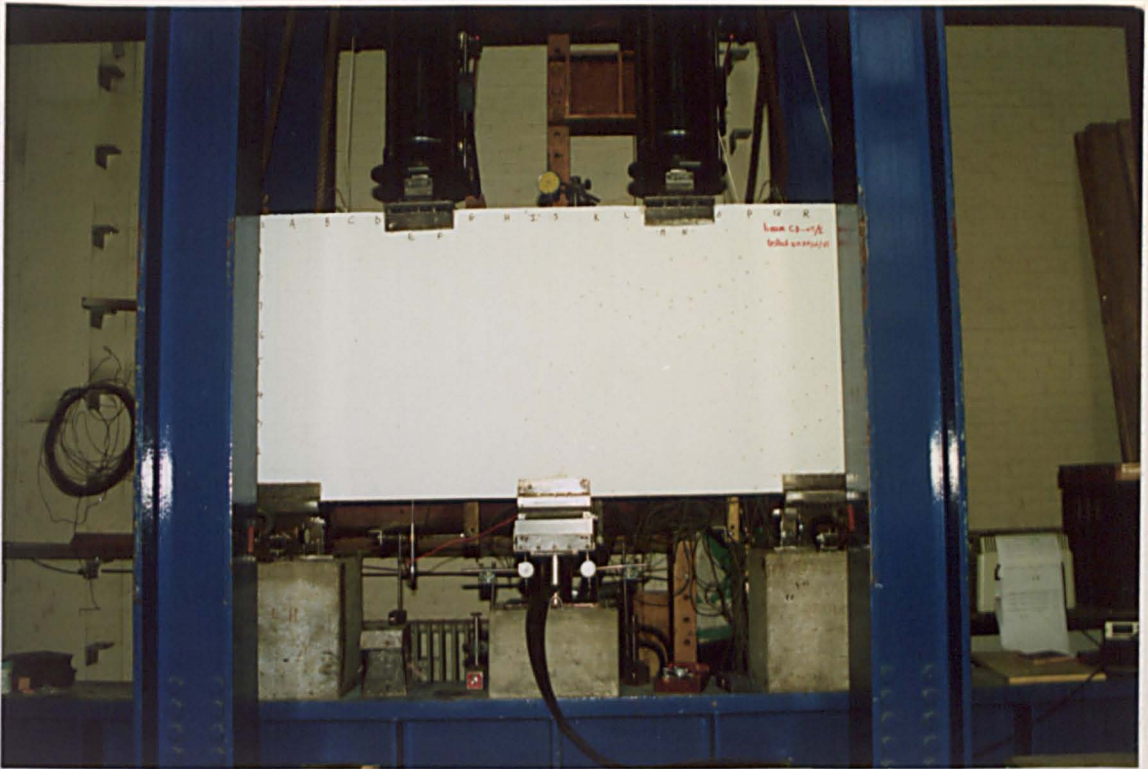


a) front view

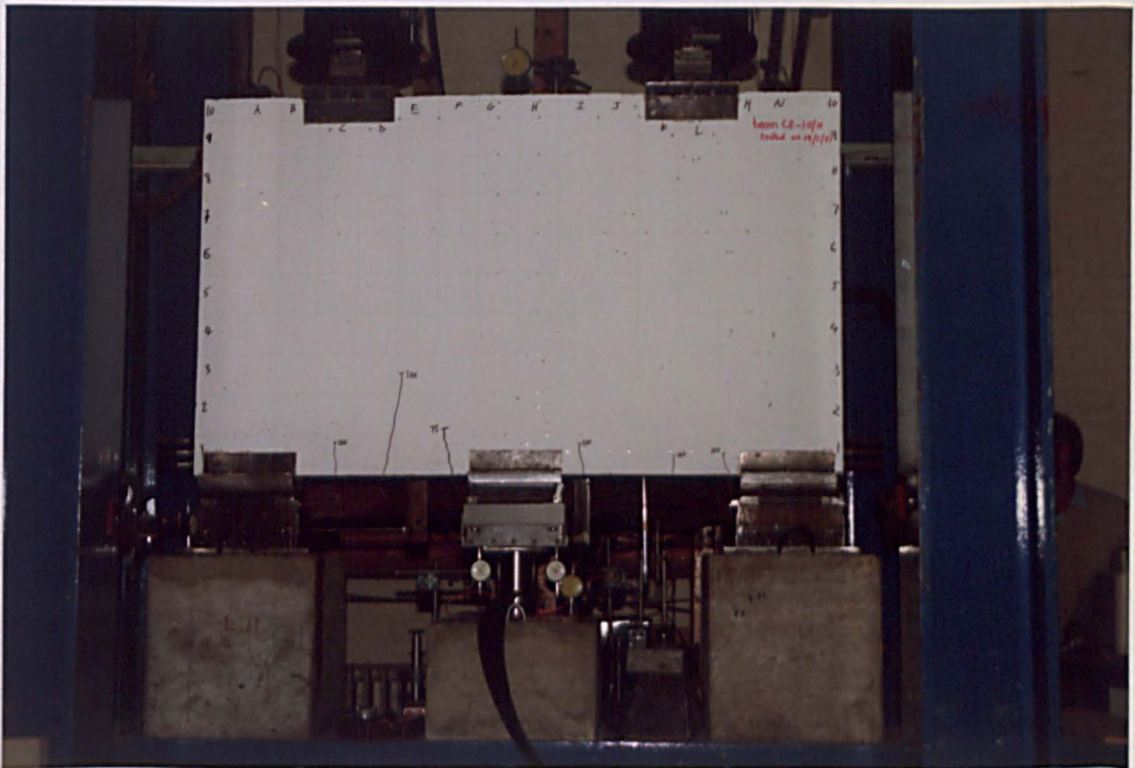


b) side view

Plate 5.1: Typical ductile buckling failure



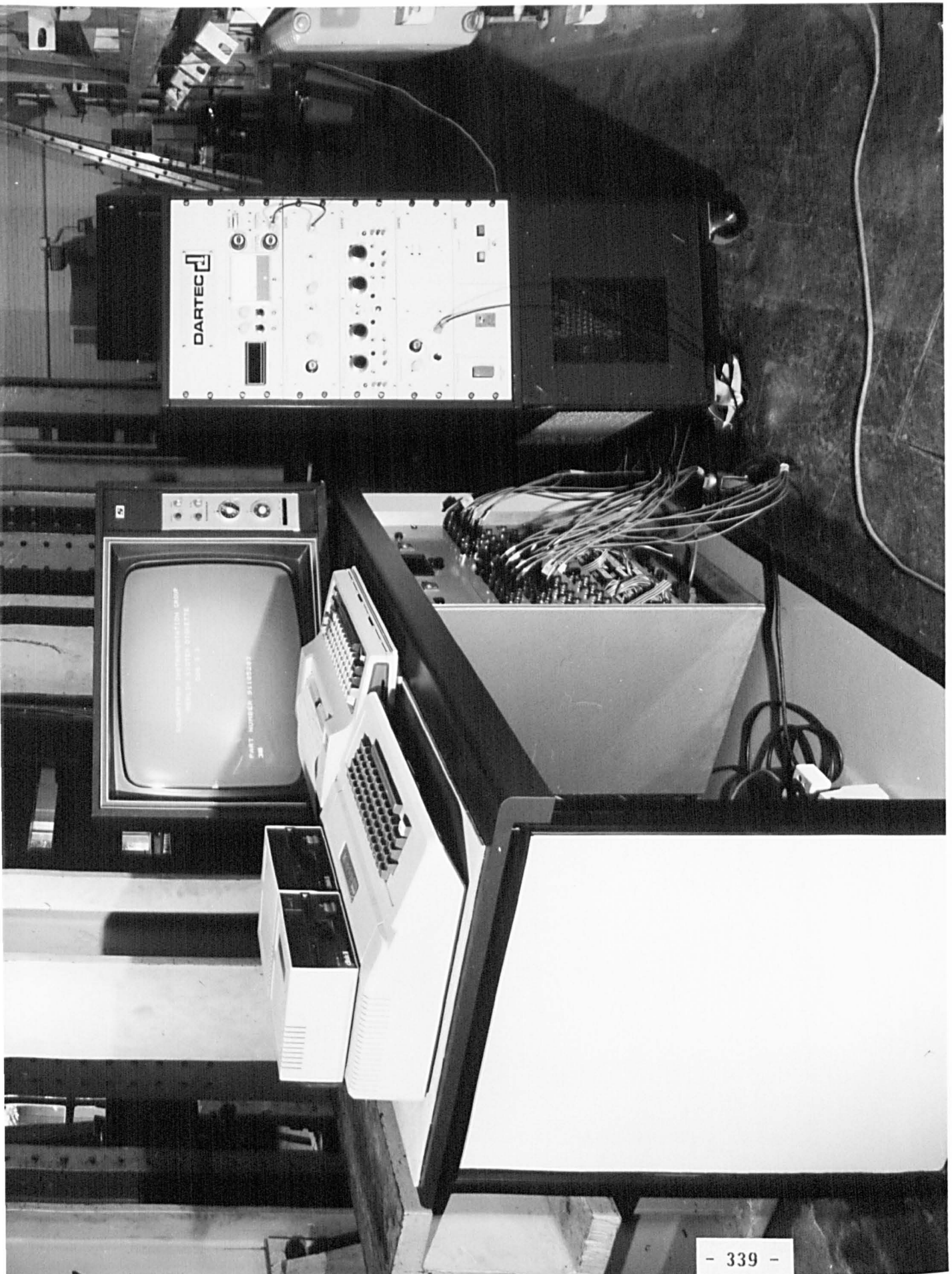
a) series CD beam

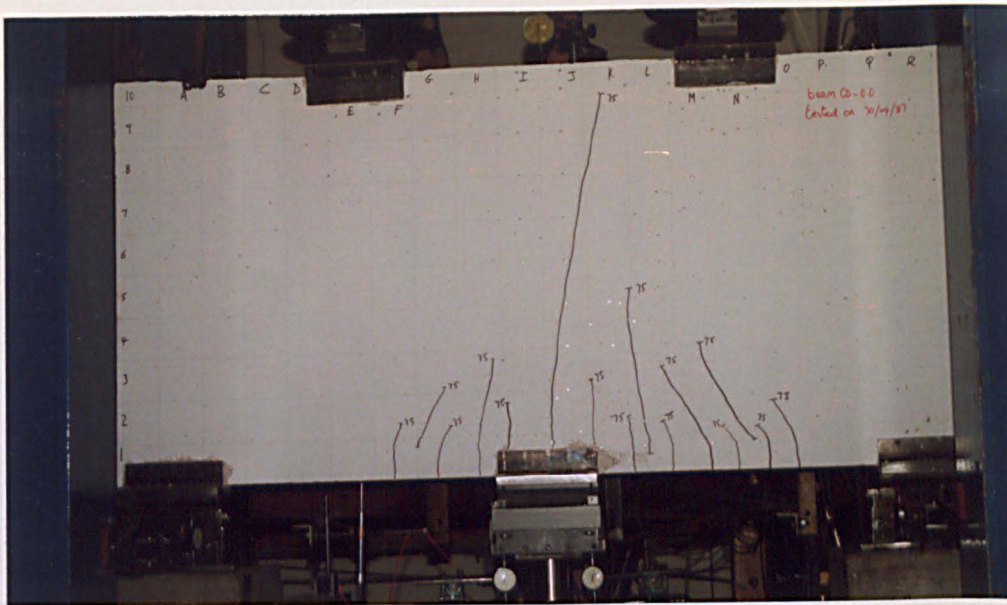


b) series CE beam

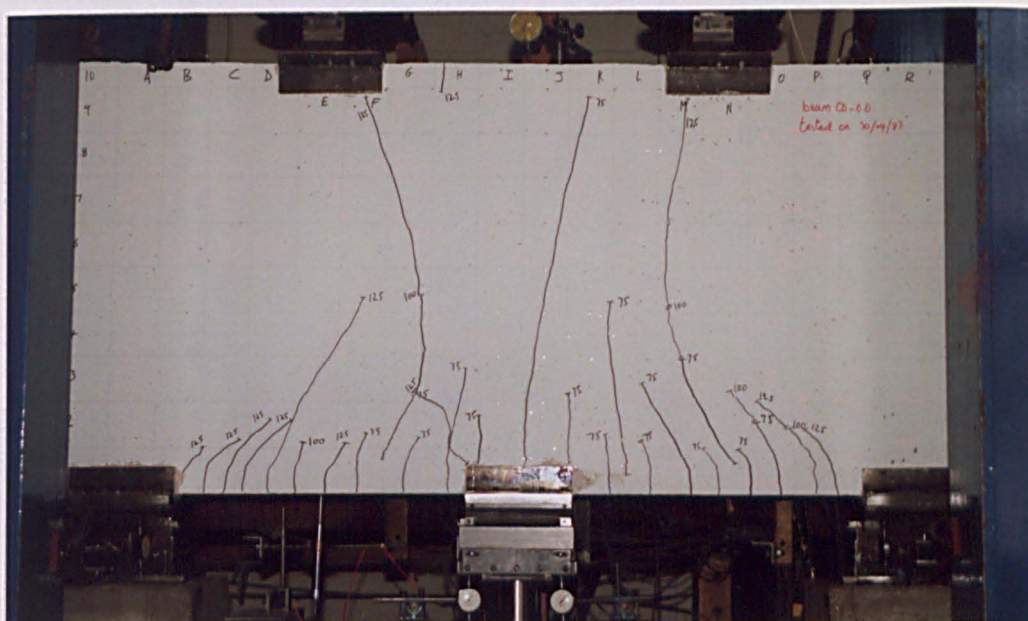
Plate 6.1: Continuous deep beams in the rig ready for testing

Plate 6.2: The data logging system and the load control unit

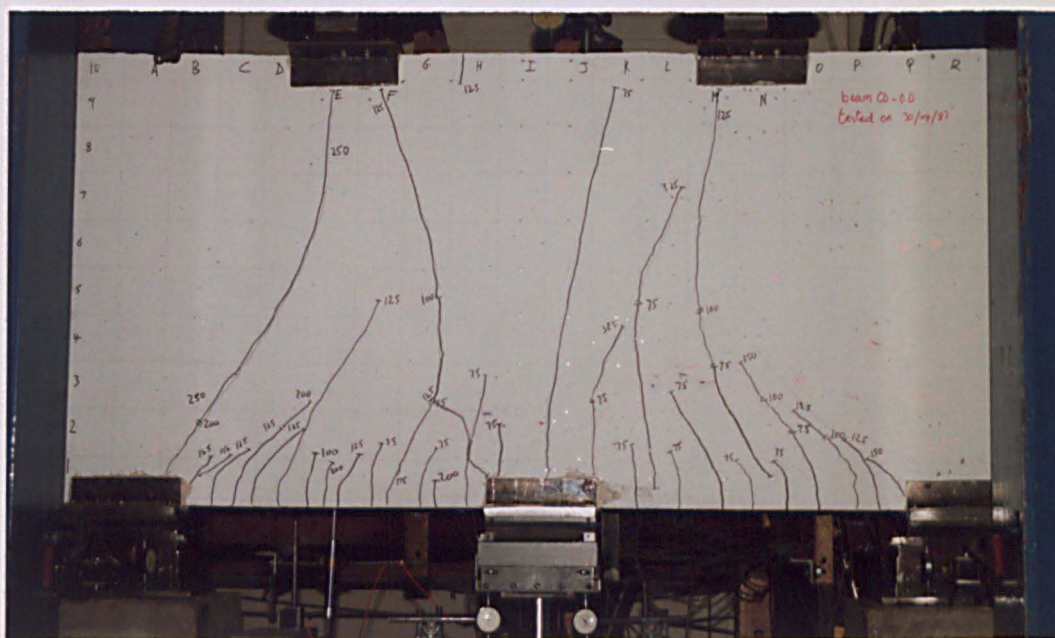




flexural  
cracks

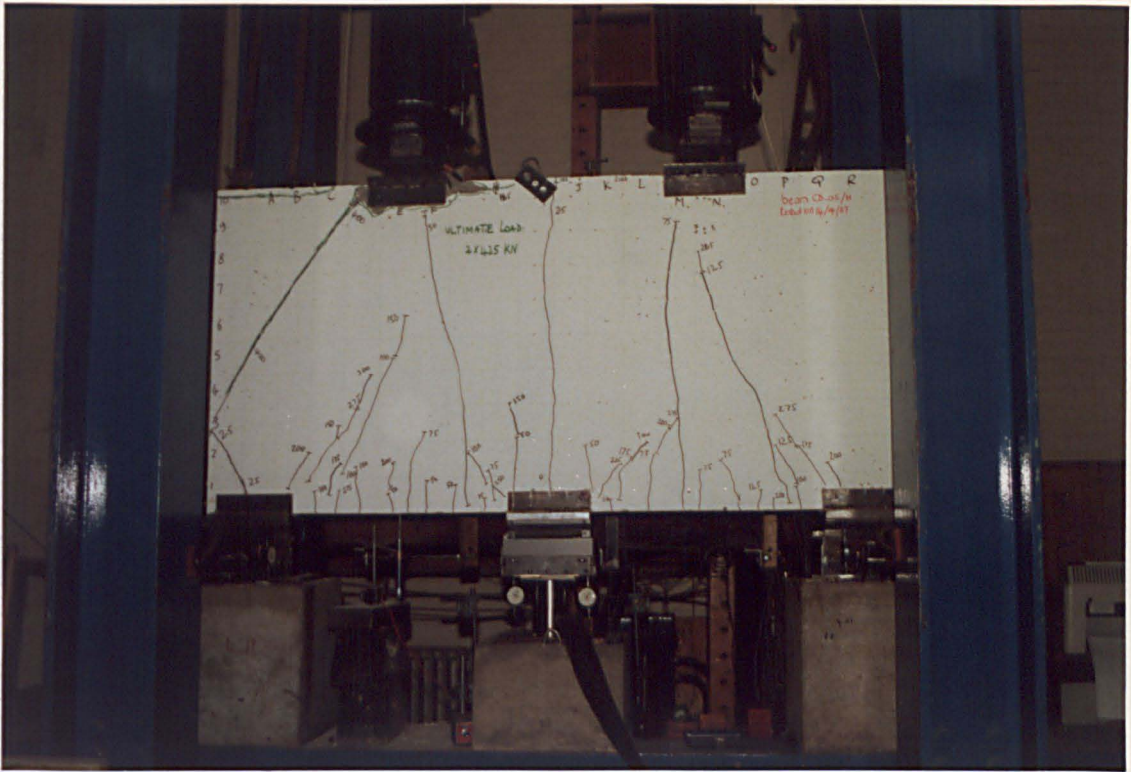


inclined  
cracks

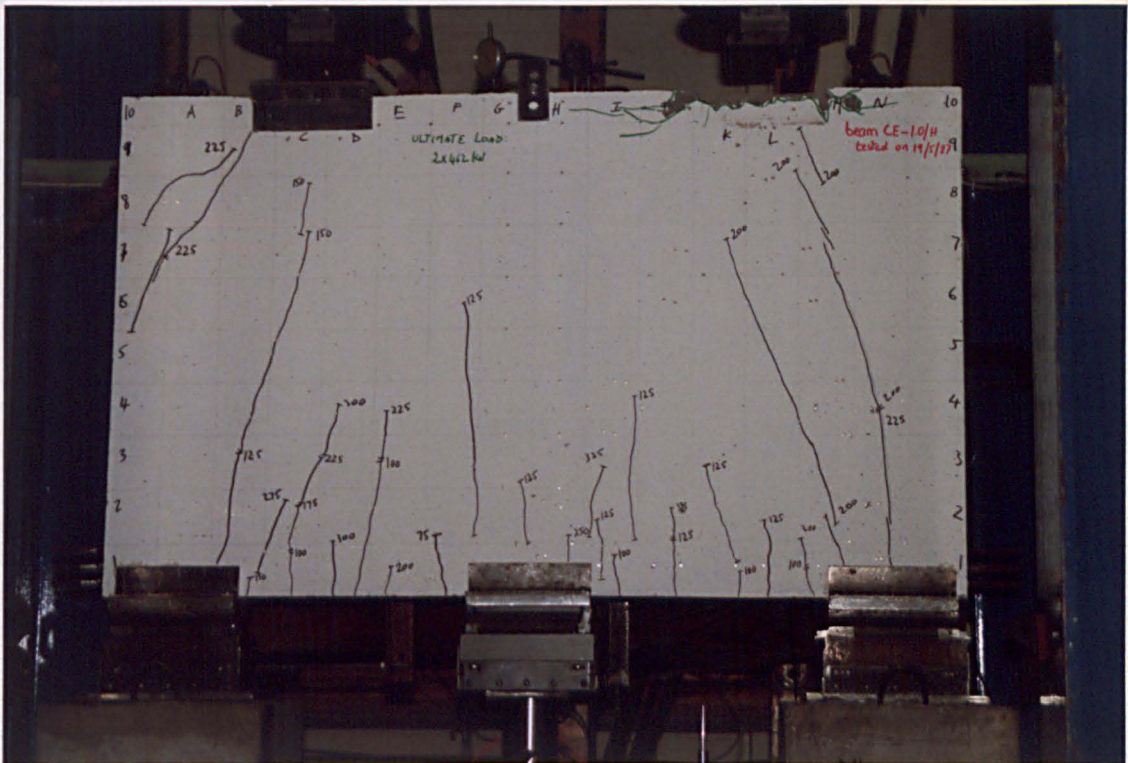


diagonal  
cracks

Plate 7.1: Typical cracks development with load



a) Typical shear-bearing failure (bearing failure precipitated by diagonal cracking)



b) Typical proper bearing failure

Plate 7.2: Types of failure of the continuous deep beams tested